The effect of orifice edge geometry on the discharge of non-Newtonian liquids from a tank

by

Ninelle Samia Mampouya

Dissertation submitted in fulfilment of the requirements for the degree

Master of Engineering: Chemical Engineering

in the

Faculty of Engineering and Built Environment

at the

Cape Peninsula University of Technology

Supervisor: Dr Morakane Khahledi

Co-supervisor: Prof. Veruscha Fester

Bellville Campus

Date of submission: September 2025

Declaration

This dissertation is my work and will be submitted in fulfillment of the requirements for the Master of Engineering degree at the Cape Peninsula University of Technology, Cape Town. The content of this work has not been submitted for any degree or examination at any other tertiary institution.

(Signature) N.S Mampouya

Signed in Cape Town this February 2026

Abstract

The discharge coefficient can be challenging to predict. This is due to many factors, including rheological characteristics of the flow liquid and orifice geometry. Indeed, predicting the orifice discharge can be difficult but can be accomplished experimentally. Flow rates were measured for square bevel back cut angle, chamfer-, quadrant- and short square-edged orifices from the bottom of the tank. The discharge coefficient was determined and related to the Reynolds number for water, different concentrations of glycerine and CMC solutions, and bentonite and kaolin suspensions. The calibrated average C_d values for: square bevel back cut angle edge was 0.6; chamfer-edged 0.88, quadrant-edged 0.84, and short square-edged 0.58 in the turbulent flow regions. The highest Re values for square-edged orifices (short square-edged and square-edged orifice with bevel back cut angle) were 14000 to 23000 whereas for chamfer and quadrant the Re was 14000 to 25000 for all water tests. The rheological parameters of the slurrie liquids were obtained and utilised in the determination of Re values for the different concentrations of the liquids discharged. The Re values for liquids tested; highly viscous Newtonian, Power Law, Herschel Bulkley and Bingham, were 18, 66, 300, and 340.

It was determined that C_d as a function of the Re in the laminar flows were $0.00823Re^{0.39}$, $0.0787Re^{0.40}$, $0.0904Re^{0.39}$, and $0.0923Re^{0.38}$ for highly viscous Newtonian liquids and $0.0009 Re^{0.77}$, $0.0128 Re^{0.71}$, $0.0276 Re^{0.57}$ and $0.0188Re^{0.63}$ for square bevel back cut angle, short square, chamfer- and quadrant-edged orifices, respectively.

The results obtained for all the orifice geometry explored showed that the C_d increased as the Re increased, but from Re of 1000, the C_d increased significantly before decreasing and becoming constant.

This study adds to the empirical data that already exists in the discharge of non-Newtonian liquids from tanks for different edge geometry and confirms that the efficiency of flow in discharging operations is dependent on the edge effect of the orifice flow meter. This will be useful in engineering designs and processes.

Acknowledgements

I would like to extend my thanks and appreciation to:

- Almighty God for granting the opportunity to further my studies and to become the first woman in my family to complete a master‘s degree.
- Cape Peninsula University of Technology, CPGS, the department of chemical and civil engineering for allowing research that adheres to national and international research regulations.
- To the Flow Process Research Centre for giving me access to their Labs even during University recess.
- My surpervisors, Prof. Veruscha Fester and Dr Khahledi for their guidance, patience, moral support and time.
- Dr Khahledi for her technical support and overseering of the experimental set-up.
- Prof. Haldenwang and Dr Ntamba for their hasty feedback after reviewing this paper from as early as proposal level.
- Miss Sharon Legodi for her technical and moral support.
- Dr Tshilumbu for his assistance with overseeing the rheology tests and making sure that testing equipment was handled with care.
- To Mr Sutherland for assisting with data capturing device set-up.
- My mother, Miss Prisca Samba Déstinée for her spiritual, moral, and financial support, and my sister, Miss Mischca Nganga Tshicaya Samba for her words of encouragement.
- My aunt Mrs Bernadette Samba for her guidance, words of encouragement, and moral support.
- Mr Patrick Kaja for his moral support and words of encouragement.

TABLE OF CONTENTS

List of Figures

Aucune entrée de table d'illustration n'a été trouvée.

List of Tables

Nomenclature

Symbol	Description	Unit
A	Cross section Area of the tank	m^2
A_o	Cross section Area of orifice	m^2
H	Height of liquid in tank	m
Q_1& Q_2	Volumetric flowrate	m^3/s
n	Flow behaviour index	-
K	Consistency coefficient	-
V_1 & V_2	Flow velocity at the orifice and tank	m/s
g	Gravitational Acceleration	m/s^2
Re_{MR}	Metzner and Reed Reynolds number	-
Re	Reynolds number	-
Re_2	Slatter's Re number	-
C_d	Discharge coefficient	-
C_o	Discharge coefficient at the orifice	-
C_{dE}	Discharge coefficient experimental	-
C_{dTh}	Discharge coefficient theoretical	-

Greek symbols

Symbol	Description	Unit
ρ	Density	Kg/m^3
β	Beta	-
μ	Viscosity of the fluid	Pa.s
$\dot{\gamma}$	Shear rate	s^{-1}
τ	Shear stress	Pa
τ_y	Yield stress	$N.m^{-2}$

Terms and concepts

Term	**Explanation**
Aspect ratio	The ratio between the width and height of an orifice opening.
Coefficient of discharge or discharge coefficient	The ratio between the actual flow discharge and the theoretical flow discharge.
Fluid	This is said to represent a liquid or gas.
Laminar flow	The flow of a viscous fluid in which the fluid moves in parallel layers. Each layer has a constant velocity at the same time moves in motion relative to its neighboring layers.
Orifice	A device that appears as thin plate with a hole or aperture opening and it is utilised to measure how quickly a fluid flows through it
Newtonian liquids	Any liquid or gas that has a direct proportional relationship between shear stress and shear rate.
Non-Newtonian liquids	Any liquid that does not have a direct proportional relationship between shear stress and shear rate.
Rheology	Study of the deformation and flow of materials.
Reynolds number (Re)	The ratio of inertial to viscous forces
Turbulent flow	The fluid undergoes irregular fluctuations or mixing owing to inertial forces dominating viscous forces.
Weir orifice	A notch cut to discharge liquids, a notch in a dam to discharge water or to measure water flow.
Viscosity	The ability of a liquid to resist flow.
Yield stress	The stress that is exerted on a material just before it begins to deform

CHAPTER ONE: INTRODUCTION

1.1 Background and motivation

It is most desired in all processing industries to have optimal flow of discharge in a short time. Processing industries such as the chemical, food, waste water, and pharmaceuticals utilise tank discharge operation. These operations require correct prediction and determination of the discharge coefficient for an optimal and efficient process. Discharge of liquids in tanks face two challenges that can slow down or optimize the discharging, transferring or disposal of liquids. When the discharge coefficient is too low this may results in major flow restrictions or losses and when the discharge coefficient is too high, the actual flow rate is higher than expected. Therefore, accurate loss coefficient data is essential for efficient design as well as understanding the role of the orifice and the hydraulic design of the process.

Orifice flow rates for non-Newtonian liquids are not easily predicted but can be accomplished experimentally. This prediction assists in the determination of the orifice discharge coefficient (Teoman et al., 2022). It is discussed by Laera et al. (2007) that rheological properties can be determined through viscometry or rheometry, where the relationship between shear stress and shear rate will assist in establishing a parameter such as yield stress (τ_y), consistency coefficient (K), and flow behaviour index (n) (Haldenwang et al., 2012). According to Adam et al. (2016), the orifice geometries can be characterised by the orifice diameter ratio, the orifice thickness ratio, and the inner orifice thickness ratio and sharp- edge angle. The effect of orifice edge geometry has been studied in tanks by Spaur (2011) and Alwan et al. (2020) to evaluate tank discharge for Newtonian liquids. The orifice geometries used were mainly square and sharp edge. Marcinkowski and Dziubinski (2004) and Dziubinski and Marcinkowski (2006) mentioned that, whereas these edges display similar discharge characteristics, the effect of edge geometry is only noticeable when there is a variation in length to diameter (L/d) of the orifices. Abdalla Alajmi et al. (2019) conducted experimental research to establish theoretical values of discharge coefficients of orifices: borda, short-tubed, and sharp-edged. They focused on the flow and pressure loss behaviour of both nozzles and orifices in fluid system in a tank, but not for non-Newtonian liquids. The discharge of non-Newtonian liquids through orifices from tanks has been studied by Mohajane (2020), Khahledi et al. (2020), Khahledi et al. (2019), and Dziubiński and Marcinkowski (2006), where the C_d is calculated utilising the area of tank and orifice, height and drainage time.

1.2 Research problem

There has not been any study on the effect of varying edge geometry such as square-edged with bevel angle, square-edged with back cut, chamfer-edged- and quadrant edged orifices for flow measurements of non-Newtonian liquids from tanks.

1.3 Research question

What effect will different orifice geometries have on Newtonian and non-Newtonian liquids discharging from tank?

1.4 Aim and objective

Aim:

The aim of this study is to determine the effect of orifice edge geometry (square bevel back cut angle, short square, chamfer- and quadrant-edged orifices) of the discharge on Newtonian and non- Newtonian liquids from tanks.

Objective:

To determine the;

- Flow rate and determine the Cd for square bevel back cut angle, chamfer, quadrant and short square edge orifice attached to the bottom of a rectangular tank. For water, glycerine carboxymethyl cellulose (CMC), bentonite and kaolin.
- Rheology of the Newtonian and non-Newtonian liquids and calculate the relevant Reynolds number.
- Relationship between the discharge coefficient and the Reynolds number for square bevel back cut angle, chamfer, quadrant and short square edge orifices for Newtonian; water and glycerine solution, and for non-Newtonian liquids: carboxymethyl cellulose (CMC), bentonite and kaolin suspensions.

1.5 Context of work

This research falls within the discipline of Civil and Chemical Engineering as this study will be useful in engineering designs and processes.

1.6 Significance

The research will be significant to all industries that deal with processing, storing and transportation of non-Newtonian liquids. The Cd values that resulted from this experimental work, will broaden the range of C_d and Re data for square-edged orifice with back bevel angle, short square-edged orifices, chamfer-edged orifices, and quadrant-edged orifices for Newtonian (water and glycerine at different concentrations) and non-Newtonian liquids **(**Carboxymethyl cellulose (CMC) solution, bentonite and kaolin suspensions**)** (Khahledi et al., 2019; 2020; Mohajane, 2020).

1.7 Delineation

In this study, the flow measurement of Newtonian and non-Newtonian slurries was discharged through square-edged orifices with back bevel angle, short square-edged orifices, chamfer-edged orifices, chamfer-edged orifice, and quadrant-edged orifices (Zakariya, 2017). Circular orifices were used but not any other shapes. Sharp and long-crested orifices were not used.

1.8 Methodology

All experimental work was conducted in the slurry and rheology laboratory at the Flow Process and Rheology Centre (FPRC). The research methodology is explained, and the experimental set-up and apparatus are listed in detail along with their functions.

- The flow instrumentations, the process of mixing the raw material into flow liquids are highlighted and the experimental rig is described.
- The experiments are designed to be safe and in accordance with the FPRC laboratory inductions and laboratory rules; safety aspects and procedures are conducted yearly before entering the laboratory. All equipment was calibrated using water, slurries were prepared and rheological parameters were determined and the discharge tests were conducted.

1.9 Organisation of the dissertation

Chapter Two: Literature review

Literature was reviewed to demonstrate the need for this type of study and the outcome of previous research surounding similar work. This section explains key concepts that are major contributors to achieving the objectives of the study. Concepts such as orifice, orifice geometry, discharge coefficient, Reynolds number (Re) are discussed. Newtonian and non-Newtonian liquids, and flow behaviours in tank discharge are reviewed in this chapter.

Chapter Three: Research methodology

Chapter three explains the research methodology utilised to conduct the experimental work. This section presents the method, procedures and experimental set-up used for data collection, data capturing and data analysis.

Chapter Four: Results and analysis

This chapter presents the results, in a form of tabulated data and graphical diagrams for C_d versus and Re values for Newtonian and non-Newtonian liquids tested. The results of the experimental research are presented.

Chapter Five: Discussion of results

The results are discussed and the relevant arguments are put forward pertaining to the study at hand.

Chapter Six: Conclusion and Recommendation

The findings are concluded and recommendations are suggested.

CHAPTER 2: LITERATURE REVIEW

2.1 Introduction

The literature review on the investigation of how orifice geometry affects non-Newtonian liquids discharge from a tank is presented in this work. Orifice discharge is a concept that has been studied for years, but the dynamics surrounding the prediction of flow has become a subject in many science and engineering fields. This chapter will provide a review on the discharge of Newtonian liquids through different orifice edge geometries from a tank.

2.2 Orifice

The term orifice is commonly referred to as an opening or a hole through which fluids (liquid or gas) pass. The hole can be machined or already existing, and the hole may have various aspect ratios, diameters, edge geometries, and/or shapes. The device can be inserted into any shape, size, and orientation of conduit (Swamee & Swamee, 2010). An orifice device or meter is meant to measure flow by restricting flow at the orifice point. As the fluid passes through the orifice, a pressure difference is produced across the hole and maximises flow. To characterise the flow of fluid through an orifice, the discharge coefficient is determined for accurate measurement of flow (Reader-Harris, 2015;Tukiman et al.,2017; Yau et al.,2017; Babu et al .,2018 and Tomaszewski et al.,2020; Vemulapalli and Venkata,2021)

2.2.1 An orifice meter and plate

An orifice is used to describe an opening or aperture and the term meter is any apparatus automatically measuring the quantity of something passing through it. There is a difference between orifice plate and orifice flow meter. The orifice plate is a device (with the material of manufacturing varying, i.e., it can be made of stainless steel or polyvinyl chlorine plastic material) with a hole machined or already existing, and the hole may have various aspect ratios, diameters, edge geometries and or shapes (Swarmee, 2010; Reader-Harris, 2015). In a pipe setting, the device is mounted between two pairs of flanges in a straight arrangement of smooth pipes (ESDU, 2007; Ntamba, 2011).

The orifice device has been utilised to measure flow rates in pipe and in tanks. The discharge coefficient evaluated as result of the flow measurements depends on the orifice geometry and/or aspect ratio. Khahledi et al.,(2019); Mohajane et al., (2019); Khahledi et al., (2020);

Mohajane,(2020) conducted where the ,effect of aspect ratio on the discharge of Newtonian and non-Newtonian liquids from a tank was studied.

2.2.2 Orifice geometry

An orifice is an opening categorised depending on the upstream and downstream surface profile of that application (Bohr, 2004).Selecting the optimal orifice plate geometry for a specific application is of interest. (Sanghani et al., 2016) of accurate measurement of flow.

2.2.3 Orifice edge geometry

According to the ESDU, (2007) : the inlet mouth of the orifice can have an entry edge profile (square, knife, beveled, rounded with edge radius, r, quadrant, chamfered edge or an exit edge profile (square, squared back cut or back bevel with beveled angle φ). Figure 2.1 illustrates different orifice geometry plates. In this research, the orifice geometry with entrance and exit edge was considered. Figure 2.1 shows the flow direction of orifices with different edge geometries.

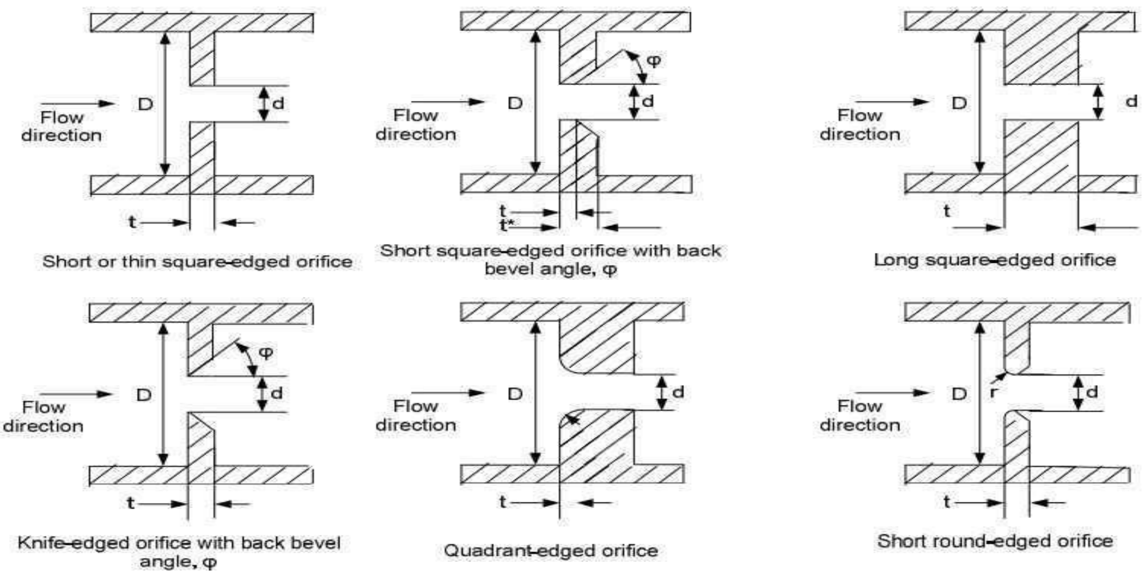

Figure 2.1: Direction of flow in different orifices: square, knife, beveled, rounded with edge radius, r, quadrant, square, squared back cut or back bevel with beveled angle φ (ESDU, 2007)

2.2.4 Categorisation of orifice plates

According to the ESDU (2007) short orifices have L/d ratio that is less than 0.75 and the L/d ratio of long orifices is greater than 1. Orifices can be categorised based on their geometry and length. The length can range from 0.1–4.27m. According to Davis (1952), the C_d values can range between 0.62 and 0.98 for different lengths and geometries. It is also mentioned by Sanghani et al. (2016) that sharp-edged orifices are classified as sharp-edged when the orifice length is less than or equal to 2mm. If the orifice length exceeds 2mm, the orifice is said to be a chamfer-edged orifice.

2.2.5 Common orifice edge geometries

Orifice-edge geometry can be classified into two different categories: sharp-edge geometry and rounded-edge geometry.

In sharp-edged orifices:

2.2.5.1 At the throat of the orifice diameter, it is notable that the radius is smaller.

2.2.5.2 Low viscosity fluids are usually discharged and/or clean fluids, gas, liquid, and steam (Ahmed et al.,2016 and Tomaszewski et al., 2020).

In rounded-edged orifices:

2.2.5.3 The radius is closer in magnitude to the throat diameter.

2.2.5.4 It is used for specific applications to prevent erosion.

2.2.5.5 It improves flow characteristics for viscous liquids and liquids with solid particles

2.2.5.6 In the turbulent regimes standard C_d value for chamfer and rounded/quadrant-edged is in the range of = 0.8–0.85 (Baillio,2003).

Casey (2017) found that rounded-edged orifices resulted in an onset of cavitation inside the throat of the orifice plate, and the flow remained single-phase until it exited. Their study aimed to characterise the pressure difference across the orifice and the discharge coefficient. They examined cavitation effects on the flow using a rounded-edged orifice plate under high flow conditions. It was noted that the discharge coefficient (C_d) for rounded-edged orifices was independent of the Reynolds number (Re) for values above 10^5. It was then concluded that the pressure differential range influencing the orifice plate's discharge coefficient depends solely on the orifice geometry and not on the Reynolds number.

Table 2.1 shows the C_d performance of a sharp-edged and a rounded-edged orifice. The C_d values in the table are taken from Davis (1952). The coefficient of contraction and coefficient of a control valve that is fully opened is also included to emphasize the orifice geometry effect on the overall discharge coefficient performance of the orifice plates (Teoman et al.,2022)

Table 2.1 Theoretical coefficients of sharp edge and rounded edge orifices (Dally et al., 1993; Davis, 1952)

	Sharp edge	**Rounded edge**
d 		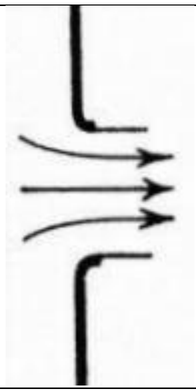
C_d	0,61	0,98
Cc	0,62	1,00
Cv	0,98	0,98

Linfield (2000) studied the discharge coefficient experimentally, based on a partial blowout of a pressurised vessel through a short pipe ending with wall angle and orifice-edged rounding. It was evident that small changes in the edge geometry have a large effect on the discharge coefficient and this effect increases with increase in wall angle. It is discussed by Linfield (2000) that the orifices with inlet corner rounding resulted in a higher discharge coefficient as there is a reduction in the separation of liquids at the upstream inlet edge (Adam .,2016; Abdelrahman and Mobasher 2021) . Cao et al. (2023) conducted research on the mechanical energy loss and Rayleigh-Taylor instability in the free discharge of vertical sharp-edged and wedged-shaped orifices. In the representation of their data they evaluated C_o vs Re and $C_o$vs h.They focused on the influence of orifice geometry and the liquid depth in a tank and the liquid of discharge was water. As part of their analysis thin- walled and thick -walled orifice was utilised. It was determined that thin-walled orifices produced high energy loss and this was due to the influence of air trapped inside the annulus area of the orifice during the discharging process. In summary it was concluded that liquid passing through an orifice increases the C_o from thin-wall to thick-walled orifices (Cao et al,.2022)

Bordoloi and Longmire (2018) conducted an investigation where, the local velocity variations for the drop fluid moving through an orifice were evaluated to study the effect of edge geometry and surface wettability of rounded edge orifice and sharp-edge orifice. It was determined that the rounded-edged orifice demonstrated behaviours of no contact between the orifice fluid drop and the orifice surface. However the the sharp-edged orifice promotes liquid contact, this in turn changes the near-surface flow field as well as the orifice fluid drop. Silicon oil and glycerine solutions were utilised as testing liquids.

Figure 2.2 describes the different flow meters and their applications. Flow meters are separated into quality measurement and flow measurement. Our study is focused on flow measurement flow meters, particularly orifice plates. Flow nozzle and venture tubes were not tested. Thin concentric, quadrant and conic plates are the types of orifice that were tested in the study. Flow meters consist of two parts: the primary element which has direct contact with the fluid in the form of interaction, and then transmitting the interaction phenomena into a signal, then ultimately into volumetric flow (Panda et al,.2022). This study consists of both parts.

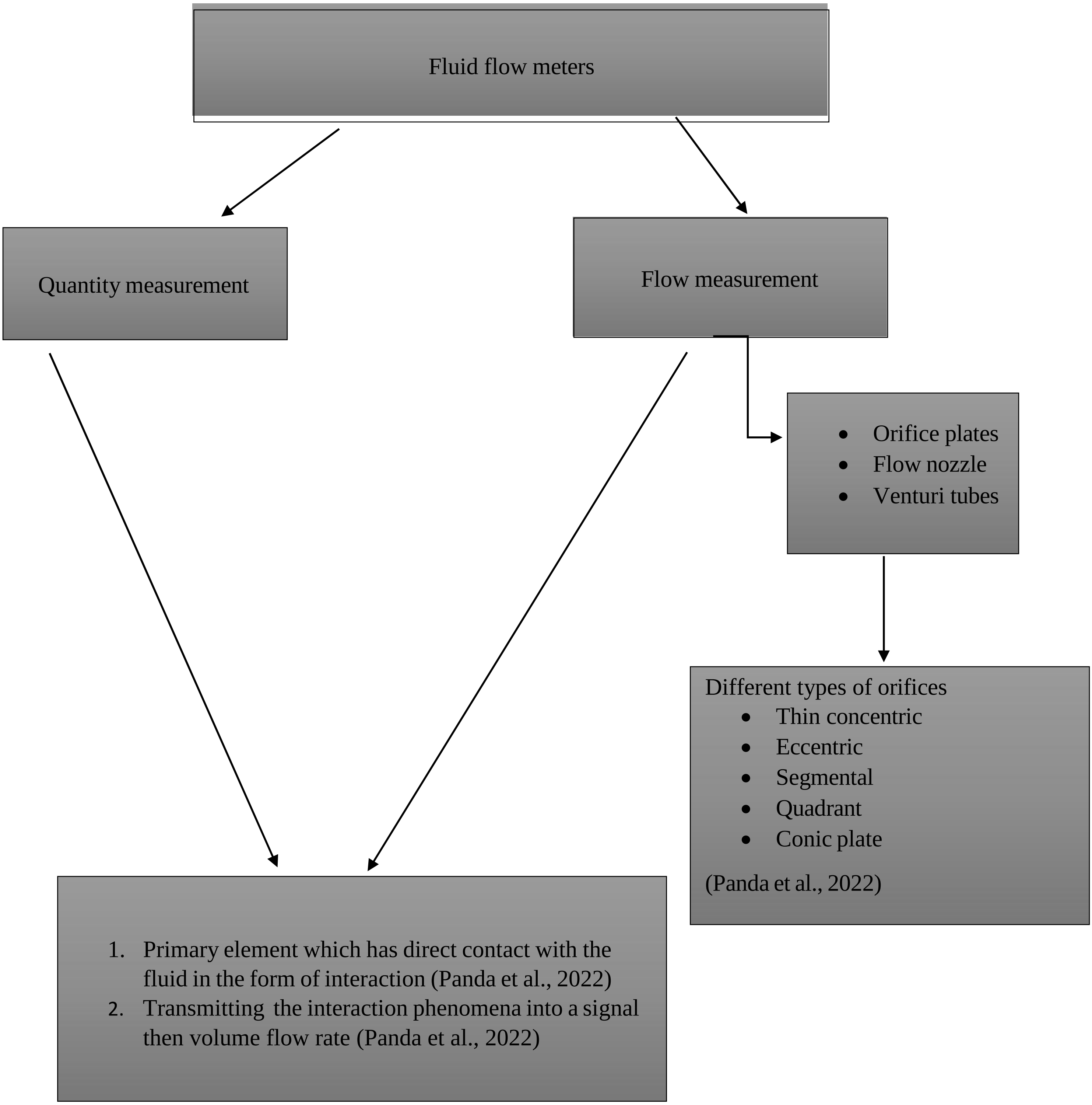

Figure 2.2: Fluid flow meters ECS transaction

(Panda et al., 2022; Reader-Harris.,2015 and Swamee.,2010)

2.3 Types of orifices

Figure 2.3 depicts an illustration from Singh et al. (2009) which shows the different types of orifices. This illustration is intended to showcase what the types of orifices mentioned in Figure 2.3 look like in a systemic drawing of the front and the side. Figure 2.4 is included as a continuation of Figure 2.3 and Figure 2.4 is aimed to demonstrate the difference between an orifice plate and orifice flow meter, where the edge geometry would be visible.

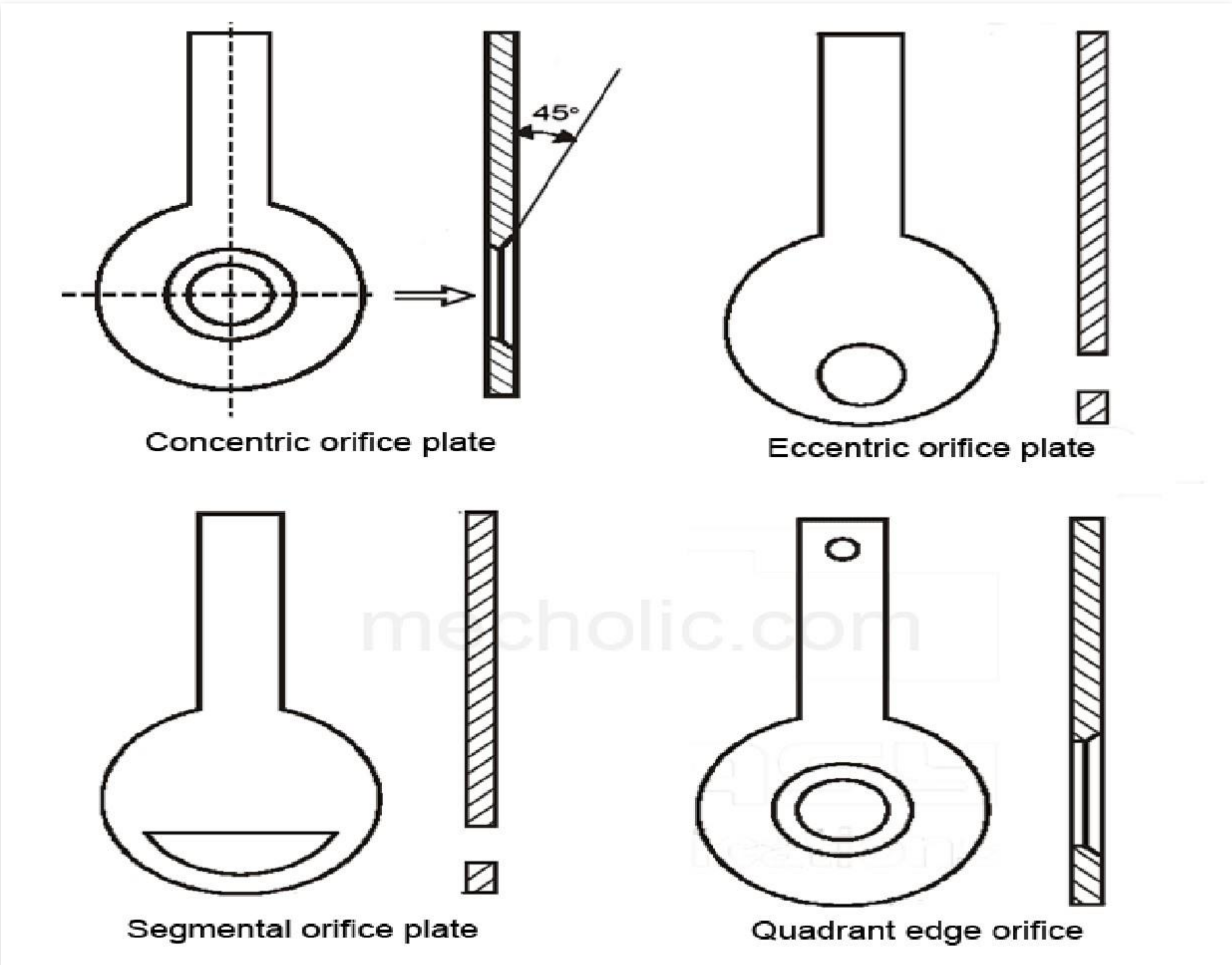

Figure 2.3: Types of orifice plates (Singh et al., 2009).

2.4 Flow through an orifice

Liquid flowing through an orifice will possess a certain velocity and pressure. As the liquid approaches the orifice plate, flow accelerates and converges through the opening, which leads to a formation jet downstream. At the downstream of the entry edge, contraction occurs to a minimum cross-sectional area of the jet. This is due to the radial velocity component. The minimum cross-sectional area is also referred to as the vena contracta (ESDU, 2007 and Tukiman et al ,.2017). The orifice meter is renowned for its efficiency in the determination of the discharge coefficient for flow, whether single or multiple flow (Babu et al., 2018 ;Tomaszewski et al.,2020 and Panda et al., 2022).

2.4.1 Characteristics that affect flow rate measurements through an orifice plate

The following characteristic influence flow through an orifice flow meter:

2.4.1.1 Orifice edge geometry

2.4.1.2 Orifice bore diameter (d) to tank diameter (D) or the ratio (β) of orifice bore diameter

(d) to pipe diameter (D)

2.4.1.3 Orifice thickness (t) to bore diameter (d) (ESDU, 2007).

Figure 2.4 shows different common edge geometry. The plates can be flat and thin with an inside and outside diameter (diameter ratio) that is in proportion to the pipe and differential pressure that is proportional to the flow rate. According to the (ESDU, 2007) and International Organization for Standardization (ISO 5167–1 2003): ―The orifice plate stimulates a change in the energy to form a reduction in the static pressure and an increase in the velocity at the orifice point‖

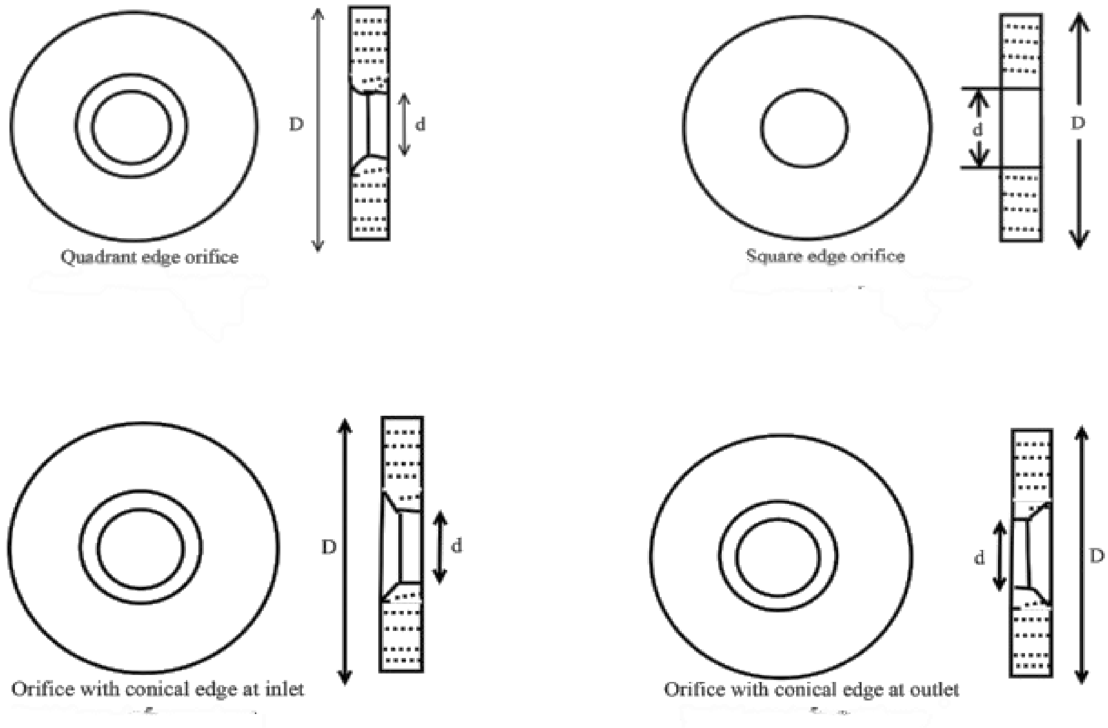

Figure 2.4: Systemic illustrations of different orifice edge geometries

(Vemulapalli & Venkata, 2022)

Abdelrahman and Mobasher (2021) evaluated the effect of orifice thickness on different orifice shapes. Circular, square, equilateral triangular and rectangular with orifice diameters: 35, 40, 45 and 50 cm. It was found that the thickness of the orifice did influence the C_d. The C_d gradually decreases when t/d (orifice thickness/orifice equivalent diameter) increases.

Nasiruddin and Singh (2021) conducted a study on the performance of an innovation design modification of an orifice meter. The orifice modification is accomplished by changing the surface topology to curvature on both sides of the orifice plate. Kim and Park (2019) found that the more round the nozzle orifice inlet is, the more smoothly the fluid flows through the orifice. There is an influence in the variation of flow and this is observed at the formation of the vena contracta, caused by the difference in orifice inlet shapes. Elsaey et al. (2014) conducted research where CFD simulations of fractal orifices of different geometries were used for flow measurement improvements in pipes. Significant effects were observed on the flow mixing properties downstream of the pipe owing to their orifice shape. Sanghani et al. (2016) investigated orifice geometry of six different geometries: square-edged, square-edged with 45°backcut, sharp-edged, streamlined, inclined approach and quadrant-edged with same diameter ratio and thickness in a CFD (computational fluid dynamic) approach (Davoudi and

Mahdi,2021). A comparison of orifice geometry was made for pressure drop, and water was the working medium. It was determined that the minimum pressure drop occurred in the streamline approach and the maximum pressure drop occurred in the square-edged with 45°back cut (Sanghani et al. ,2016 and Panda et al,.2022)

Panda et al. (2022) utilised, numerical and experimental analysis to determine pressure drop and the discharge coefficient on a variation of geometrical and flow parameters. This research focused on the size of the wellhead chokes, and the different range of flow rates and fluid properties. The accuracy of the predicted experimental data on the tested correlations were developed on two-phase flow and its thermodynamic properties on the geometrical shape of wellhead choke size on the upstream flow pressure.

According to Simpson and Ranade (2018), an orifice sharpness, no matter how insignificant the rounding at the edge of the orifice might be, can change the flow fields drastically. Casey (2017) discussed that the C_d obtained for a rounded-edged orifice was independent of the Re number for values above 10^5. According to Flachskampf et al. (1990), evaluating the discharge in terms of the eccentricity difference, circular and elliptic, they found no appreciable change in discharge coefficient. However when the area is augmented, the discharge coefficient shows an encouraging increase. It was stated by Frachskampf et al. (1990) that having an orifice with a nozzle-like narrowing inlet, which was constructed on the atrial side of the orifice, improves the discharge coefficient. C_d values ranged from 0.675–0.93 for nozzle-like inlet and the C_d increased between 0.81 and 0.93 for the round orifice.

2.5 Application of orifice plates

Many industries deal with fluid flow dynamics, from construction to food technology to pharmaceuticals to oil and gas, to mention a few. There are numerous metering applications like storing, transporting, transferring decanting draining and pumping (Morrison et al., 1990). McNally, (2010) explains that, an orifice flow meter is important in measuring bulk flow as it:

- Reduce the flow in the line.
- Dissipate energy in flood conduits and
- Dissipate energy in slurry flow applications

2.5.1 Advantages and disadvantages of orifice plate usage

The orifice is a popular device known as an instrument for mass flow estimation but also possesses significant benefits.

Advantages :

Morrison et al.,(1990), stated that the orifice flow meter is :

1. simple to construct,
2. inexpensive i.e. it's affordable in most cases
3. there is no to little moving parts when inserted to pipes or tanks and they can be manufactured from large to small sizes.

Disadvantages:

- Subject to corrosion, which may be responsible for bring about inaccuracies in flow rate (of about 2%–3%)
- Consistency can be affected by change in viscosity and temperature.

2.5.2 The Cd in relation to the edge geometry

Ahmed and Ghanem (2020) evaluated,the discharge coefficient of a square-edged concentric orifice at low Reynolds number. They were able to find that there are significant variations in the Cd in relation to the Reynolds number. Leading to investigation of viscous liquids flowing through a square-edged aperture with concentric features with the aid of a computer model.The Re number in the laminar flow regions went up to 250.

There has been work done by a number of authors (Ahmed & Ghanem, 2020; Abd et al., 2019; Sanghani et al., 2016; Tharakan & Rafeeque, 2016; Hollingshead et al., 2011) where the orifice geometry is tested, for both Newtonian and non-Newtonian liquids. The geometries were usually sharp-edged orifices, square-edged orifices, in a pipe installation or att

Table 2.2: Discharge of Newtonian and non-Newtonian liquids through different orifice geometry in pipes and in tanks.

References	Orifice geometry tested	Attachment : Pipe or Tank	β	Fluid type	Investigated method	Representation of C_d	C_d values obtained	Re range
Ahmed et al. (2020)	Square-edged concentric orifice	Pipe	$0.2 \le \beta \le 0.8$	Viscous incompressible liquid	Computational fluid dynamics	Graph : C_d vs Re	0.68	$0 \le Re \ge 250$
Abd et al. (2019)	Sharp-edged	Pipe	0.5,0.6,0.65,0.75,& 0.85	Water	Experimental investigation	Graph : C_d vs Re	0.6-0.85	$Re < 900$
Tharakan and Rafeeque (2016)	Sharp-edged	Cylindrical tank	-	Water	Experimental investigation	Graph : C_d vs Re	0,67	$Re < 62\,500$
Reader-Harris et al. (2012)	Sharp-edged	Pipe	0.2,0.4,0.6,&0.75	Nitrogen at 63 bars (gas)	Computational fluid dynamics	Graph: C_d vs (10^6)	0.63	100000000

						/(ReD)$^{0.5}$		
Chowdhury and Fester (2012)	Long square-edged	Pipe	0.36,0.4,0.5&0.7	Viscous liquids	Experimental investigation	Graph : Kor vs Re	-	$1 \leq Re \leq 100\,000$
Hollingshead etal. (2011)	Sharp edge	Pipe	Venturi:0.24& 0.66 Orifice:0.5,0.6,0.65 &0.7 V-Cone:0.66,0.69&0.82 Wedge: 0.50 &0.61	Viscous liquids: Heavy oils	Computational fluid dynamics	Graph : C_d vs Re	~0.96	$Re \leq 20\,000$
Ntamba (2011)	Short square-edged orifices	Straight line pipe	0.2,0.3,0.57&0.7	Viscous liquids	Experimental investigation	C_d vs Re	0.63-0.72	>3 500
Spaur (2011)	Square edge	Tank	-	Water	Experimental investigation	C_d vs Re	0.625	6.80000
Ramamoorthy and Seetharamaiah (1965)	Quadrant edge	Pipe: D & D/2	0.22,0.40,0.50,0.60 &0.63	Water	Experimental investigation	C_d vs kL	0.77-0.92	150 000

Johansen (1930)	Sharp-edged and beveled 45°orifices	Vertical pipe orifice immersed in tank	0.2,0.4,0.59&0.79	Water	Experimental investigation	C_d vs Re	0.608	25000

2.6 Fluid classification

According to (Chhabra, 2010;Chhabra & Richardson 2008) fluids can be classified either according to their response to the externally applied pressure or to the effects caused under the action of shear stress. It was discussed by Chhabra (2010), that the characteristics of non-Newtonian liquids have the following flow behaviours: shear-thinning, shear-thickening, visco-plastic, time-dependent and visco-elastic behaviours under appropriate circumstances. Materials such as foams, suspensions, polymer solutions and melts are representative examples of different non-Newtonian liquids. Newtonian liquids are characterised by a linear relationship between the shear stress and the shear rate of a liquid on a flow curve. Liquids can be Newtonian or non-Newtonian (Adam et al.,2016 ; Babu et al .,2018; Tomaszewski et atl.,2020 and Davoudi and Mahdi, 2021).They are classified accordingly based on rheological characteristics. It is further demonstrated by Chhabra and Richardson (2008), and Chhabra (2010),that Newtonian fluids (liquids and gases) exhibit a constant viscosity, that is, to indicate that a plot can be sketched of, shear stress versus shear rate at a given temperature, and a constant slope that is independent of shear rate can be observed. According to Chhabra and Richardson (2008), and Chhabra (2010), gases can only exhibit Newtonian behaviour at low molecular weight solutions, and Non-Newtonian liquids cannot obey Newtonian linear relationship trends. However, solutions with a higher molecular weight, such as polymer melts and polymer solutions slurries, and paste, are typical examples of non-Newtonian liquids (Chhabra, 2010; Chhabra & Richardson 2008).

Water is a Newtonian liquid and results in turbulent regime when flowing through orifices. Non-Newtonian, highly viscous, time-dependent liquids (carboxymethyl cellulose, bentonite and kaolin slurry mixtures) at different concentrations provide a wider range of data in the laminar regimes. By measuring the discharge coefficient through orifices of varying geometries a wider range of data can be obtained for laminar regimes.

Newtonian liquids in the laminar flow regime, showcase the following traits: the relationship between all the total stresses is equal to the product of the viscosity of the shear rate of the fluid. Chhabra and Richardson (2008) stated that, the equation is observed of shear forces exerted on the liquid per unit area and the shear rate is the change in velocity with the force applied normally to the x-axis. Equation 2.1 expresses this relationship mathematically.

$$\frac{F}{A} = \tau_{yx} = \mu\left(-\frac{dvx}{dy}\right) = \mu\dot{\gamma}_{yx} \qquad \text{Equation 2.1}$$

The subscript at τ and $\dot{\gamma}$ describe the direction normal to the shear force (Chhabra & Richardson, 2008). The constant of proportionality is known as the coefficient of dynamic viscosity (μ). In Figure 2.5 it is noticeable that the higher the viscosity of the liquid, the steeper the slope of the linear, as the liquid‘s viscosity increases. According to Lui (2003), this reduces the liquid‘s ability to flow.

Figure 2.5 is a flow curve that shows the relationship between shear stress and shear rate. The relationship is proportiona and it produces a linear curve. Newtonian liquids shown on the rheogram indicate the viscosity in the slope of a straight line.

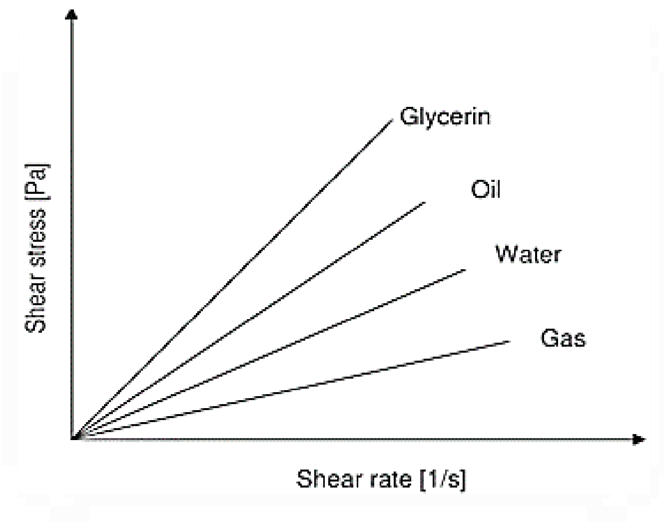

Figure 2.5: A flow curve of Newtonian liquids

(Lui, 2003)

Liquids: Newtonian and non-Newtonian

A range of non-Newtonian liquids (Power Law, Bingham and Herschel-Bulkley models) have been explored and tested, and the rheological parameters of these liquids obtained (Ntamba, 2011; Khahledi et al., 2020; Mohajane et al, 2019).

- **Shear-thinning pseudoplastic model**

According to Chhabra and Richardson (2008), for a liquid to be classified as a shear thinning liquid or a pseudoplastic liquid, the liquid has to show that has an apparent viscosity (shearstress/shear rate) which decreases with increasing shear rate. This means that the slope of the

curve becomes smaller as the shear rate increases. Shear thinning liquids use the Power Law model and the following equation:

$$\tau_{yx} = (\dot{\gamma}_{yx})^{n} \quad \text{Equation 2.2}$$

For the Power Law model, the apparent viscosity of the liquids becomes:

$$\mu = \frac{\tau_{yx}}{\dot{\gamma}} = k\,(\dot{\gamma})^{n-1} \quad \text{Equation 2.3}$$

Where n:

- If the liquid exhibits shear thinning behaviour; $n < 1$
- If the liquid exhibits shear thickening behaviour; $n > 1$
- If the liquid exhibits Newtonian behaviour; $n = 1$ (Chhabra and Richardson, 2008).

Liquid consistency coefficients (k) and flow behaviour indices are curve-fitting parameters. In the case of a shear thinning liquid, (n) may have a value between 0 and 1.The degree of shear thinning is dependent on the value of (n); the smaller the value of (n), the greater the degree of shear thinning. For shear thickening, on the other hand, (n) greater than 1 and further from 1 means a higher degree of shear thickening (Chhabra & Richardson, 2008).

- **Viscoplastic liquids**

Viscoplastic liquid behaviour has a yield stress. Yield stress is one of the characteristics that exists to categorise viscoplastic fluid behaviour. For the liquid to flow, it must be deformed by overcoming the yield stress. This material deforms elastically only when the external stress applied is less than the yield stress. The relationship of the curve may be linear or non-linear, but it must not pass the graph origin (Chhabra & Richardson, 2008).

- **Bingham plastic models**

Bingham plastic liquids are characterised by having a constant viscosity and yield stress (Chhabra & Richardson, 2008). Bingham plastic models are described in Equation 2.4:

$\boldsymbol{\tau} = \boldsymbol{\tau}_{\boldsymbol{O}+k}\,\dot{\boldsymbol{\gamma}}$ Equation 2.4

- **Herschel-Bulkley model**

A Herschel-Bulkley liquid is a non-Newtonian liquid where the relationship is described by the three flow parameters: the consistency index (k), the flow behaviour index (n), and the yield stress $(\boldsymbol{\tau}_{\boldsymbol{O}})$**.** The model incorporates yield stress and Power Law model (Chhabra & Richardson, 2008). Equation 2.5 is as follows

$\boldsymbol{\tau} = \boldsymbol{\tau}_{\boldsymbol{O}} + (\dot{\boldsymbol{\gamma}}\,)$ Equation 2.5

Where:

$\boldsymbol{\tau}$ = Shear stress

$\boldsymbol{\tau}_{\mathbf{O}}$ = Yield stress

$\dot{\boldsymbol{\gamma}}$ = Shear rate

K = Consistency index

n = Flow behaviour index

Figure 2.6 is a representation of different flow curves of time-independent liquids.The diagram classifies the different types of liquids along with their respective flow curves. Shear stress vs shear rate flow curves result in the following catagories; Bingham plastic, pseudoplastic, yield pseudoplastic, dilatant and yield dilatant for time-independent liquids.

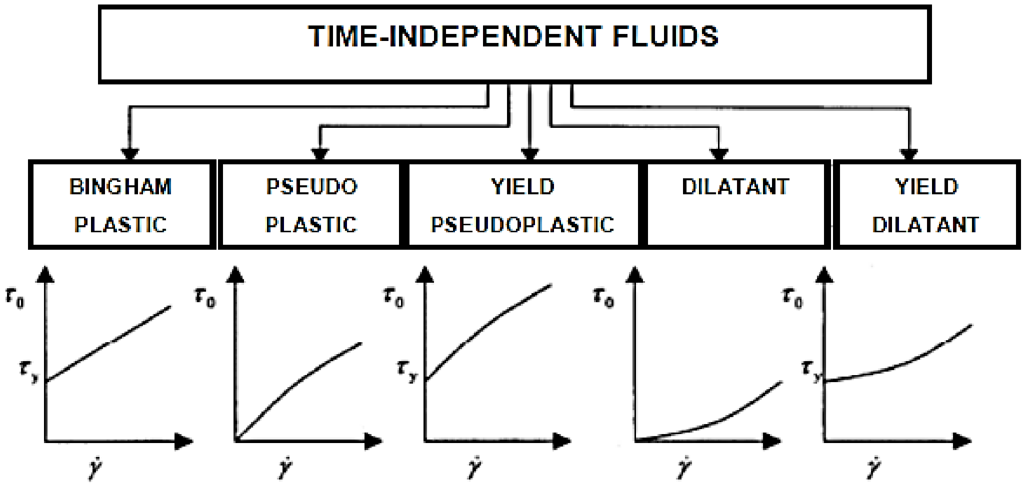

Figure 2.6: Rheogram of time-independent liquids

(Paterson & Cooke, 1999)

- **Shear-thickening or dilatant behaviours flow model**

Shear thickening liquids show similar characteristics as pseudoplastic liquids as they also have no yield stress. But their apparent viscosity does increase with increasing shear rate, making them thicken or dilatant as shear rate and apparent viscosity increase together (Chhabra and Richardson, 2008).

- **Viscosity**

Bird (2002) explains that viscosity is internal friction; it is the resistance of a material to shear and deform. For example, water will flow easily as it has a low viscosity which is equal to $1(\mu = 0.01\ Pa.)$ while honey is thick and has higher resistance to flow, making it a viscous material (viscosity is all the way up to, $\mu = 23.40$ Pa. s). Viscosity describes the material's internal resistance and is evaluated to measure liquid (fluid) friction. It is also proportional to the shearing stress and shearing rate in steady state flow. Shear stress versus shear rate gives a relationship that classifies different types of liquids.
Equation 2.6 relates shear stress (τ) to the shear rate ($\dot{\gamma}$) and denotes the rate at which the liquid is being deformed

$$\boldsymbol{\tau} = (\dot{\boldsymbol{\gamma}}) \qquad \text{Equation (2.6)}$$

The viscosity constant is denoted by (μ) for each liquid and has a particular value at a given temperature. Liquids that obey a linear relationship of shear stress versus shear rate are called Newtonian liquids (Chhabra, 2010).

As indicated by Chhabra and Richardson (2008), Equation 2.7 is the linear relationship of applied shear stress to the rate at which the liquid is being deformed. In short, total stresses are equivalent to the product of viscosity and the shear rate of the liquid.

Mathamatically, the equation is according to Chhabra and Richardson (2008) and Chhabra (2010); where shear force is equal to the force exterted on the liquid per unit area and the shear rate is the change in velocity with respect to the force applied to the normal x-axis.

$$\boldsymbol{\sigma_{yx}} = \frac{\boldsymbol{F}}{\boldsymbol{A}} = \boldsymbol{\eta}\dot{\boldsymbol{\gamma}}_{\boldsymbol{yx}} \qquad \text{Equation (2.7)}$$

The apparent viscosity of fluids is expressed as follows:

$$\mu = \frac{\tau}{\frac{dv}{dz}} \quad \text{Equation (2.8)}$$

The apparent viscosity for psuedoplastic and dilatant fluids are as follows:

$$\mu = \frac{K(\frac{dv}{dz})^{\wedge}n}{\frac{dv}{dz}} = K\left(\frac{dv}{dz}\right)^{n-1} \quad \text{Equation (2.9)}$$

- **Yield stress**

Kazemain et al. (2012) stated that yield stress is when there is enough shear stress being applied to the material to break the link between particles. Yield stress can be described by the presence of different forces, capillary, flocculation, colloidal, van der Waal and electrostatic forces. According to Kazemain et al. (2012), flocculation and colloidal forces are the most common as they result in a link between particles. Kazemain et al. (2012) explans that this is due to the weak interaction that is as a result of a small amount of shear force applied to the material, which is just enough to start the flow. Beaupré et al. (2004) explain that yield stress is evident when there is enough shear applied for the liquid to flow.

2.7 Discharge coefficient (C_d)

The coefficient of discharge or orifice discharge (C_d) is vital in the design of orifice flow meters, presuming that all other flow characteristics around the orifice and discharging liquid are known (Sahin & Ceyhan, 1996). In terms of orifice flow meters, ESDU (2007) defines the discharge coefficient through an orifice as the ratio between the actual flow rate (Q_{Actual}) and the highest theoretical flow rate ($Q_{Theoretical}$).

$$C_d = \frac{QActual}{QTheoretical} \quad \text{Equation (2.10}$$

The orifice discharge (C_d) as well as the Re values are tabulated and plotted, not only to showcase the relationship between liquid head and Re but to communicate under what regime (laminar, transition or turbulent) the liquid falls when compared from highly viscous to less viscous (water) liquid. The effect of orifice edge (chamfer, quadrant and square, short and bevel back) were explored by means of C_d determination with Re. Newtonian (water and glycerine) and non-Newtonian (carboxyl methyl cellulose, bentonite and kaolin) liquids were used.

Tank liquid discharge has no pressure drop, as depicted in literature pertaining to piping systems, and the vena contracta effect is aided by the gravitational pull downwards vertically. The influence of orifice edge on the discharge coefficient for Newtonian and non-Newtonian liquids has not been explored. The pressure drops across a pipe attached to an orifice flow meter with the edge effect having been done for rounded edge, square-edged orifices and/or sharp edge (Ntamba, 2011).

Table 2.3, showcases the different orifice geometries with their particular findings over at least three decays in literature. It shows that the there is a scarcity of orifice geometry evaluation in tank discharge for viscous liquids.

Table 2.3: Discharge of Newtonian and non-Newtonian liquids through different orifice geometry in pipes

The symbol _E‘ denotes the experimental study

_SCMC‘ – Sodium carboxylicmethyl cellulose and _CFD‘ – Computational fluid dyamics

Author	Geometry	Orifice diameter (mm)	Testing rig	β	Discharge coefficient C_d	Testing liquid	Technique	Re range	Data representation format	Findings
Hobbs and Humphrey (1990)	Sharp edge (Measuring sharpness of the edge)	Bore diameter 120mm 180 mm 225mm	Pipe	0.4, 0.6 and 0.75	0.604-0.0608	Water	E	$5*10^5$	C_d vs Re	It was determined that there was a gradual increase in C_d value as the radius of the sharpness of the edge increased
Arun et al. (2010)	Different edge pipe	50mm 100mm 200mm	Pipe	• 0.4 • 0.6 • 0.8	0.75 0.85 0.90	SCMC	CFD	100–100000	C_d vs Re	The C_d is also influence by the density of the liquids.
Author	Geometry	L /D	Testing rig	β	Discharge coefficient C_d	Testing liquid	Technique	Re range	Data representation format	Finding

Metwally (2014)	Short tube	L= 0.25–1	Pipe	0.6–0.9	0.65–0.98	Viscous liquid	CFD	500–2 000	C_d vs L/d and C_d vs L/d	The vortices generated because of rounding edge orifice largely impact the C_d .
Casey (2017)	Rounded edged	2.5	Pipe	Not provided	0.84–0.93	Water	E	*10^5	C_d vs Re	It was found that there was no significant rise or drop in C_d for the selected range of Re number
Simpson and Ranade (2018)	Rounded edge and sharp edge	L/d:0–5	Pipe	Orifice thickness		Viscous liquid	CFD: Simulated in terms of velocity and pressure gradient vapour volume fraction and turbulent quantities	-	C_d vs L/d and C_d vs P_1/P_2	At a higher Re fluctuation is experienced in the flow.

Likitha et al. (2018)	Short square-edged Long square-edged Knife-edged orifice with back bevel		Pipe	0.3 and 0.5	0.3: C_d = 0.67 0.5: C_d = 0.65	Newtonian fluid: Turbulent flow	CFD	10 000 0–1 000 000	C_d vs Re	Cd remained constant at 0.67 for β of 0.3 but was not constant at 0.65 β of 0.5
Nasiruddin and Singh (2021)	Curverture	10	Pipe	0.4–0.8	0.66–0.98	-	Computer fluid dynamic experimental	10^3-to-10^6	C_d vs Re	It was found that providing curvatures on orifices improves the performance, particularly on both sides of the orifice. When the curves are on the upstream face of the orifice the performance improved significantly.

2.7.1 Orifice geometry effect

The discharging aperture size, shape, aspect ratio, edge sharpness, angle and/or geometry as well as rheological properties of the liquids are major contributors to predicting the discharge (Assran & Mohamed, 2022). The influence of orifice geometry cannot be discussed without emphasing how the discharge coefficient is impacted when the orifice geometrical characteristics are varied. Geometric characteristics are orifice shape and diameter ratio in pipe orifice installation. The discharge coefficient is influenced by many factors, all quite similar to factors that influence orifice flow efficiency: edge sharpness, fluid properties, flow condictions, Reyolds number and the shape and diameter ratio of the orifice. The effect on flow of geometrical characteristics such as orifice shape, diameter ratio as well as the aspect ratio L/d has been measured by Chowdhury and Fester (2012), Ntamba (2011), and Khahledi et al. (2020).

Dittmann et al. (2003) investigated the discharge behaviour of short orifices with chamfered and radiused inlet geometry in pipes. They were able to discuss the discharge behaviour of rotating systems of orifices with different geometry. It was determined that the discharge coefficient remains nearly constant for low velocity ratios.

Kabir (2004) studied the flow of Newtonian (water) and non-Newtonian liquids (polyacrylamide and polyacrylamide solutions). The non-Newtonian liquids all demonstated Power Law flow behaviour. The experimental investigation took place in an open channel obstructed at the entrance, where the position of the obstruction could result in a flow that is reversed, forward or stagnant. The obstruction geometries were semicircle, triangle circle and different shapes of rectangule. It was mentioned by Kabir (2004) that the size and shape of the obstruction geometry inside and around the test were some of the parameters that influenced the flow. It was also discussed that the influence of different shapes and sizes of obstruction geometry was more pronounced at the entrance and exit edge of the obstruction plates.

Frachskampf et al. (1990) measured the eccentricity of orifices to analyse the orifice geometry. They discussed that the higher the eccentricity the lower the C_d for the same diameter. They also mentioned that the reason was that the flow contractions by themselves could not be responsible for decreasing the C_d when there was a change in orifice geometry. Teoman et al.

(2022) stated in their research that the discharge coefficient is strongly affected by the orifice geometry and the liquid rheological characteristics.

Prohaska (2008) conducted research where the author evaluated the discharge of flow passing through a circular orifice fitted into a thin-walled vertical rise pipe. The orifice had a curved surface at the edge. The author was able to determine that, as the discharge coefficient increased, the head valves decreased. It was also found that, for a given orifice size, as the orifice height above the tank floor was increased, so the discharge coefficient decreased. This might have been as a result of suppression of the flow entering the orifice at lower heights. Arun et al. (2010) studied the effect of beta ratio and pipe diameter on the discharge coefficient of an orifice meter for Re numbers ranging from 100–100 000 using simulations (computer fluid dynamic analysis). It was determined that the C_d decreases with the increase of pipe diameter for constant beta ratio, and that a variation in density influenced the C_d.

According to Abd et al. (2019), the orifice discharge coefficient reduces with increasing Reynolds numbers, particularly in the turbulent regimes. Hence, geometric parameters have to be properly designed to achieve the desired objectives. Linfield (2000), studied the discharge coefficient experimentally, based on a partial blowout of a pressurised vessel through a short pipe ending with a wall angle and orifice-edged rounding. It was evident that small changes in the edge geometry have a large effect on the discharge coefficient and this effect increases with the increase in wall angle. It is discussed by Linfield (2000) that orifices with an inlet corner rounding have a higher discharge coefficient as there is a reduction in the separation of liquids at the upstream inlet edge.

2.8 Effect of edge on discharge of Newtonian and non-Newtonian liquids in a pipe system

Studies on the effect of orifice edge geometry on the discharge of non-Newtonian liquids have been conducted by a few researchers in pipes. Sections 2.81 and 2.82 discuss previous literature pertaining to the discharge of non-Newtonian liquids in pipes where the effect of orifice edge geometry was studied.

2.8.1 Flow through edge orifice for non-Newtonian liquids in a pipe system

Kiaoulias et al. (2019) conducted research where varying dimensions and inlet geometries were evaluated. The study investigated the inlet geometry effect of single circular orifices with liquid injector pressure drop and jet breakup length. Different orifice diameters and length-to-diameter ratios were used. The geometries of the orifices were chamfered and sharp-edged.

The relationship between discharge coefficient (C_d) vs Reynolds number (Re) resulted in a parabolic trend, regardless of orifice dimensions.

The discharge coefficient as a function of the Reynolds number was studied but for orifice pipe attachment in the discharge of viscous liquids.

2.8.2 Flow through square-edged orifice for non-Newtonian liquids in a pipe system

Non-Newtonian liquids flowing through a square-edged orifce in pipe system is demonstrated by Chowdhury (2010), and Ntamba (2011). In the laminar flow, the C_d data was presented as a function of Re_{Mr}. in water to showcase turbulent flows for different diameter ratios.

Ntamba (2011) used non-Newtonian liquids with the following concentrations: CMC (4%–8 % w/w); bentonite (6%–9% w/w), and kaolin (4%–24% v/v).

In Table 2.4, a tabulation is displayed of short square-edged orifices of different beta ratios tested by Ntamba (2011) for the purpose of showcasing the generalised C_d range for a short square-edged orifice.

Table 2.4: A tabulation of the Reynolds number in relation to different beta ratios obtained for a short square-edged orifice (Ntamba,2011)

β	0.2	0.3	0.57	0.7
Re	500	1 000	3 500	6 000
Cd	0.72	0.67	0.63	0.68

Figure 2.7 shows non-Newtonian and Newtonian liquids tested by Chowdhury (2010) for an in-pipe system, both flange and D & D/2 tapping. A square-edged long orifice of β=0.5, 0.7 and 0.36 was used but only β=0.5 and β=0.7 are plotted and discussed in this section as the aspect ratio (t/d) = 5 for both orifices, whereas for β=0.36, the aspect ratio (t/d) = 4. The loss coefficient (C_{or}) was determined in the laminar flow for the non-Newtonian liquids and the C_{or} was represented as a function of Re_{MR}^{-1}. The correlations were $1500Re_{MR}^{-1}$ and $3000Re_{MR}^{-1}$

respectively for β=0.5 and β=0.7. Turbulent flow resulted in C_d values ranging from 0.79 to 0.83. It is noticeable that the C_d increases with the increase in the Re until a C_d value of 0.79 is reached before gradually becoming constant.

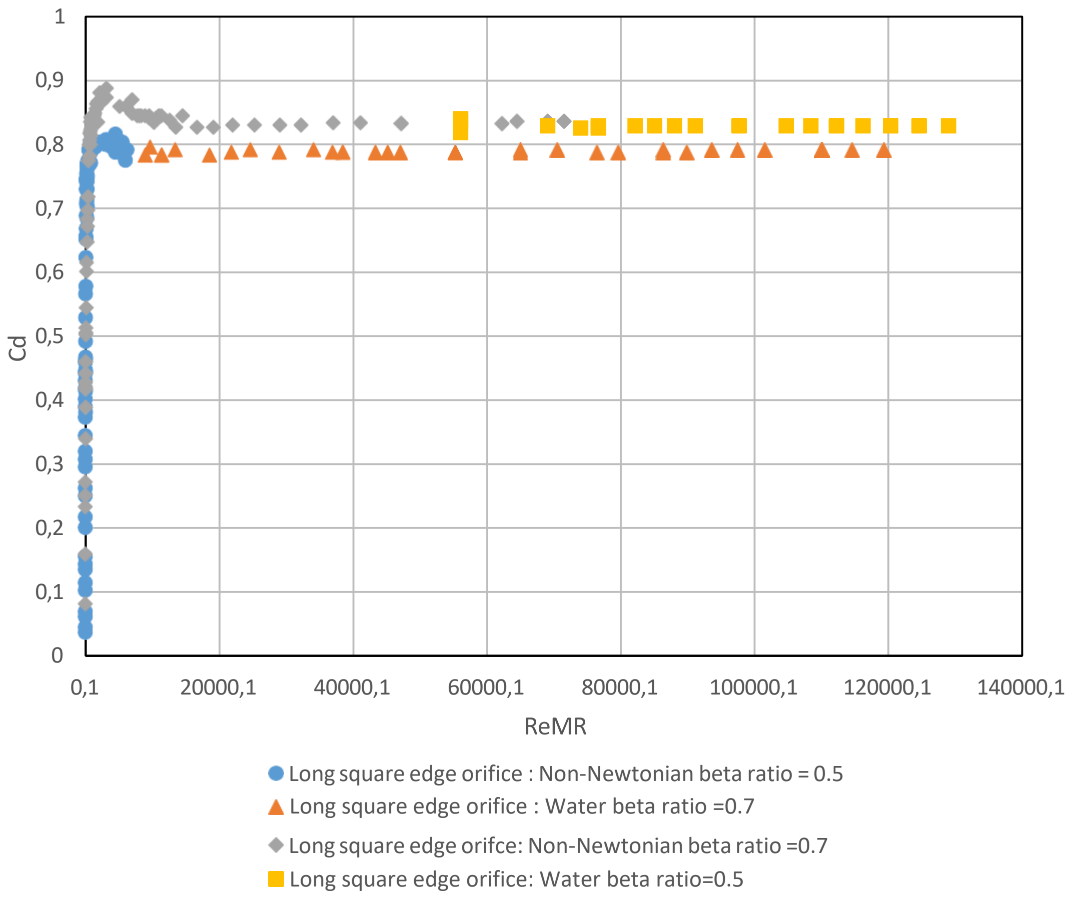

Figure 2.7: C_d vs Re_{MR} for flange and D & D/2 of β=0.05 and t/d= 5 long square-edged orifice for non-Newtonian liquids in pipe system (Chowdhurry, 2010)

Hollingshed et al. (2011) conducted research where the discharge of performance of a venturi, concentrated orifice V-cone and wedge flow meter were evaluated. The study was more focused on low Reynolds numbers in connection with pipeline transportation of viscous fluids. Testing took place for both laminar and turbulent flow conditions.

Figure 2.8 is an illustration to show how the C_d values of different flow meters with geometries of orifice, a venturi, wedge and V-cone are influenced by the Re.
It was mentioned by Hollingshead et al. (2011) that a correction factor was incorporated into calculating the discharge to achieving the flow curves, as demonstrated in Figure 2.7. It is clear

in the illustration that the C_d versus Re relationship is at its peak when the Reynolds number Re= 100. Moving into the turbulent flow, the flow starts gradually to become constant from Re≥ 10 000. The relationship between C_d versus Re becomes constant the higher the Re is.

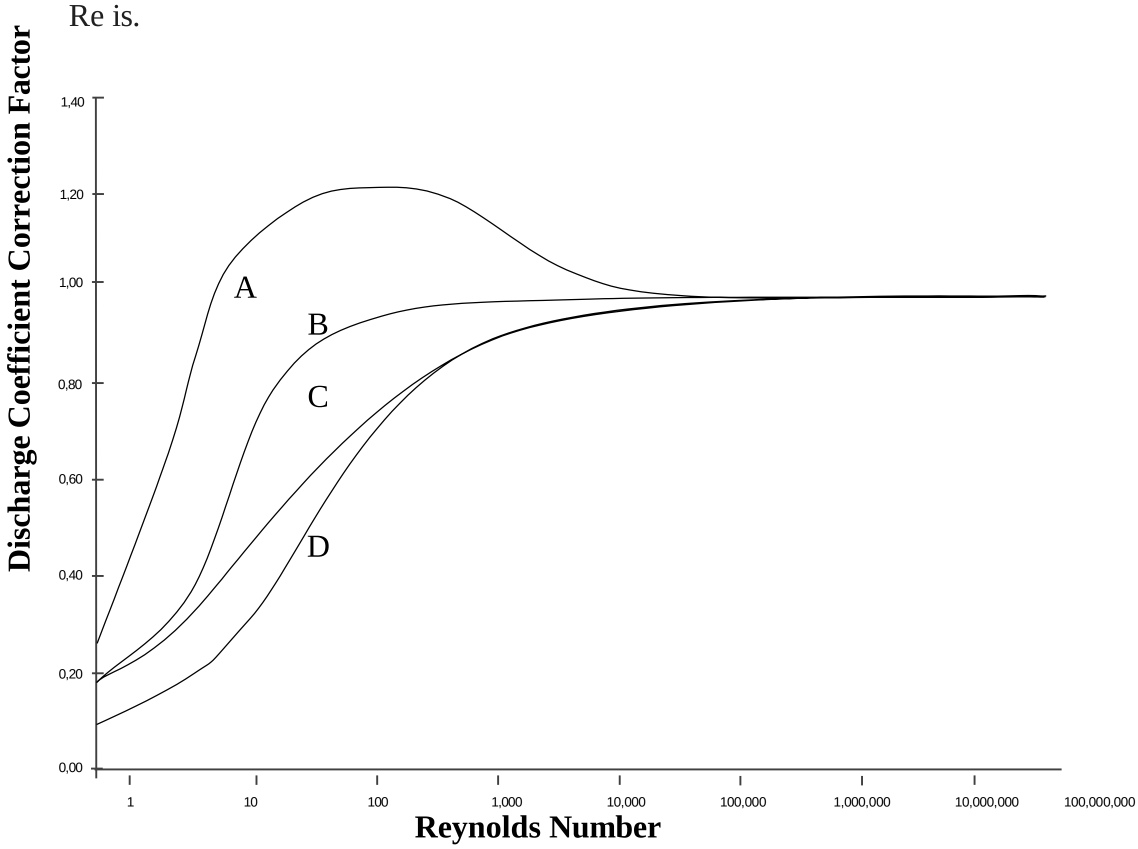

Figure 2.8: C_d vs Re for the discharge performance of a venturi(A), orifice (B),V-cone(C) and wedge(D) flow meters for viscous liquids in a pipe system (Hollingshead et al ., 2011)

According to Likitha et al. (2018), the value of the Re for a particular pipe flow can be decreased by decreasing the velocity or by increasing the viscosity of the working fluid. Reynolds number (Re) can be increased by decreasing the viscosity of the discharging liquids. For better management of fluids in pipes, an orifice is installed as a flow meter. The discharge coefficient is determined to relate the flow rate to differential pressures across the pipe.

Figure 2.9 depicts a graphical illustration that has been re-plotted to show the C_d obtained for short square-edged orifice with back bevel angle of beta values 0.3 and 0.5. The purpose of discussing this illustration in research conducted by Likitha et al. (2018) is to show the general C_d values available in literature for a square-edged orifice with bevel back cut angle. The liquid being discharged in Figure 2.9 is water and the Re values range from 10 000-to-1 000 000. The C_d values become constant at 0.67 for $\beta = 0.3$, whereas for β = 0.5 the C_d values only become constant at 0.65. The generalised C_d value for a square-edged orifice with bevel back cut angle can range between 0.65 and 0.67 for Newtonian liquids that are not viscous.

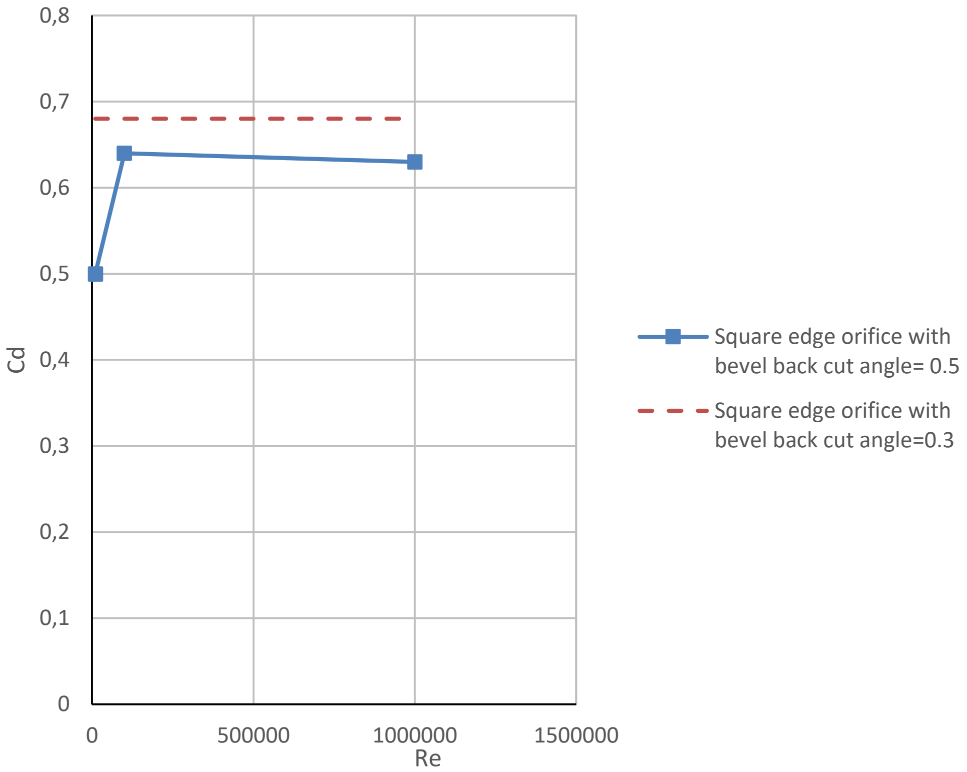

Figure 2.9: C_d vs Re for short square-edged orifices with back bevel angle beta values 0.3 and 0.5 (Likitha et al.,2018)

2.9 Reynolds number

Flow regimes are classified by the determination of Re. According to Coulson and Richardson (2019), Re is based on the velocity of the liquid, the diameter of the orifice, and the density of the liquid divided by the viscosity of the liquid.

Reynolds number, used to describe flow regime of liquids is characterised by Equation 2.11

$$Re = \frac{\rho d V_2}{\mu} \qquad \text{Equation (2.11)}$$

According to Slatter and Lazarus (1993), the Reynolds number (Re_2) which they proposed for Herschel-Bulkley and Bingham model liquids as Re_2 is illustrated in Equation 2.12 and will be used to determine Re for non-Newtonian liquids.Equation (2.12)

$$Re_2 = -\frac{8\rho(V2)^2}{\tau_y * k\left(\frac{8V_2}{d}\right)^n} \qquad \text{Equation (2.12)}$$

Cd computation can be referred to as the coefficient of determination in regression analysis. Where the uncertainty propagation is a method to estimate the accuracy of results.

2.10 Flow through an orifice from a tank

In surge tanks head losses are extreme owing to the impact of the orifice edge causing mass oscillation from a closing downstream discharge control. The introduction of an orifice-edged geometry can also bring about asymmetrical behaviour in the heads losses experienced in surge tanks.

Torricelli (1643) initiated the theoretical approach to the discharge in tanks by developing the kinetics of water jets, based on Galileo's projectile movement, leading to the development of Equation 2.13. This formula enables the calculation of the velocity Equation 2.14 of the liquid stream under the influence of gravity (g). The stream exits the vessel through a small hole in the wall, and from there, —the distance to the free water surface is H_1 (Bird, 2002; Wilkes, 1999; De Nevers & Wilcox, 1991). This eliminates the friction loss of the vena contracta and the tank. The liquid jet narrows some distance downstream of the orifice and is also dependent on the turbulent flow. The C_d takes into account these influences; for Reynolds numbers greater than 10 000, it is typically 0.61; however, it can also occasionally range from 0.60–0.64 (Bos, 1989; Wilkes, 1999). Equations for Bernoulli and continuity are commonly applied when flow passes through a tank that has an orifice located at the bottom or side. At the top of the tank the velocity is $V_1$and at the bottom of the tank the velocity is V_2. Since the head rises with increasing tank length, when the tank is positioned vertically, the head is estimated from the liquid surface to the end of the exit tank (Wilkes, 1999). There is gravitational release of water from a tank into the atmosphere, where H_2 is the overall head above the orifice.

$V_2 = \sqrt{2gh}$ Equation (2.13)

$V_1 = V_2$ Equation (2.14)

Figure 2.10 is an illustration showing an orifice fitted at the bottom of a tank. This is a gravitational discharge where water flows freely through a flooded sharp-edged orifice plate. The liquid (water) is drained from height (H_1) to height (H_2) at a constant atmospheric pressure.

(Pa). (D) is the diameter of the tank; passing through (d) is the diameter of the orifice with moderate speed. (I) the centre of the tank and exact middle point where the orifice is inserted.

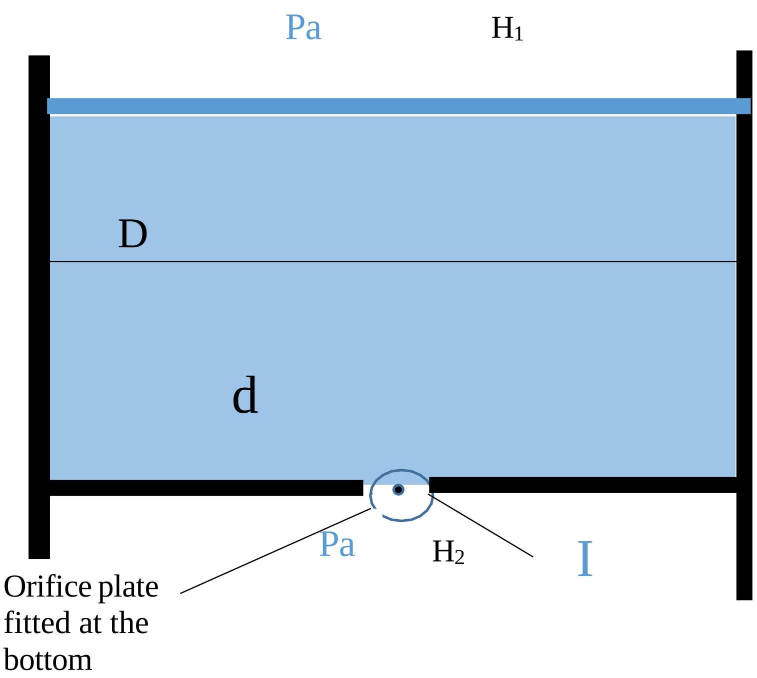

Figure 2.10: Discharge of water from a tank through an orifice

(Spencer, 2013)

2.11 Effect of orifice

2.11.1 Orifice edge effect: tanks

Bordoloi and Longmire (2018) conducted an investigation into the local velocity variations for drop moving through an orifice to evaluate the effect of edge geometry and surface wettability of rounded edged orifices and sharp-edged orifices:

A rectangualar tank with a cross-sectional area of 255mm × 255mm and height of 280mm. It was supported by a steel frame and filled with liquid to the height of 160mm. A rectangular plate (254mm × 230 mm × 2mm) was placed with a circular orifice at its centre and was suspended horizontially at a height of 120 mm below the free surface. The gravitational potential energy of the drop was redistributed into kinetic energy for the liquids and the surface deformation energy of the drop was tracked through various stages of the drop's motion through the orifice (rounded edge or sharp edge). Re (Reynolds number) and we (Weber number) were determined and calculated based on the drop terminal velocity (U_t).

2.11.2 Effect of orifice on the discharge of liquids (Newtonians and non-Newtonian) from tanks

Khahledi et al. (2019) mentioned that, for Newtonian liquids, the Re values for square orifices was less than the Re values for circular orifices in the laminar region. But there was no significant difference in the Re and average C_d values in the turbulent region for both Newtonian and non-Newtonian liquids. Mohajane (2020) and Mohajane et al. (2019) determined that, for the turbulent flow of Newtonian liquids, such as water and glycerine, the averaged C_d values were 0.60, 0.59, 0.80 and 0.78 for orifices with L/d rations of 0.05, 1, 3, and 5, respectively. Non-Newtonian liquids, such as carboxymethyl cellulose (CMC) solution, kaolin and bentonite suspensions resulted in average C_d values of 0.62, 0.59, 0.78 and 0.74 for orifices of L/d ratios of 0.05, 1, 3, and 5, respectively. Hence, the flow of Newtonian and non-Newtonian liquids is affected by different L/d ratios of the orifices.

2.12 Previous research on the different types of edge geometry

Hobbs and Humphrey (1990) evaluated the C_d values for different orifice edge radii in pipe systems for Newtonian liquids. It was determined that there was a gradual increase of C_d as the radius of the sharp edge increased. Ntamba and Mulumba (2011) mentioned that flow in the laminar conditions have given a limited range of data for short square-edged orifices for the discharge coefficient in pipes. According to Teoman et al. (2022), the discharge coefficient is strongly affected by the orifice geometry. Abdalla Alajmi et al. (2019) conducted experimental research to establish theoretical values of discharge coefficient of Borda, short-tubed and sharp-edged orifices. It was determined that the difference in error between the theoretical $C_{d\ Th}$ values and experimental $C_{d\ E}$ values was found to be higher for the Borda geometry than for the short-tubed and sharp-edged. The short-tubed produced the lowest error percentage. The experimental study was a comparison between experimental results and theoretical predictions of the discharge coefficient and the Borda orifice geometry produced the lowest $C_{d\ Th}$ value of 0.51 but produced the highest $C_{d\ E}$ value of 0.726. Sharp-edged orifices produced $C_{d\ Th}$ value of 0.62 and $C_{d\ E}$ value of 0. 688. For the flow and pressure loss behaviour of nozzles and orifices in fluid systems in a tank, the C_d is calculated utilising the area of the tank and orifice, height and drainage time.

Prohaska (2008) Conducted research where the researcher evaluated the discharge of flow passing through a circular orifice cut into a thin-wall from a vertical rise pipe. Experimental work was analysed and plotted; the discharge coefficient (C_d) was plotted vs the head (h/d). What was evident in the characteristics of the plots was that, for a given orifice size, the C_d increases as the h/d decreases. The researchers were able to determine that, as the discharge coefficient increased, the head values decreased. It was also found that, for a given orifice size, as the orifice height above the tank floor was increased, so the discharge coefficient decreased.The author added that this might have been as a result of suppression of the flow entering the orifice at lower heights.

Figure 2.11 is a systemic drawing of a quadrant-edged orifice: it is an orifice with an edge that is shaped like a nozzle, where the radius is equal to the thickness of the orifice plate (Ramamoorthy & Seetharamaiah, 1965).

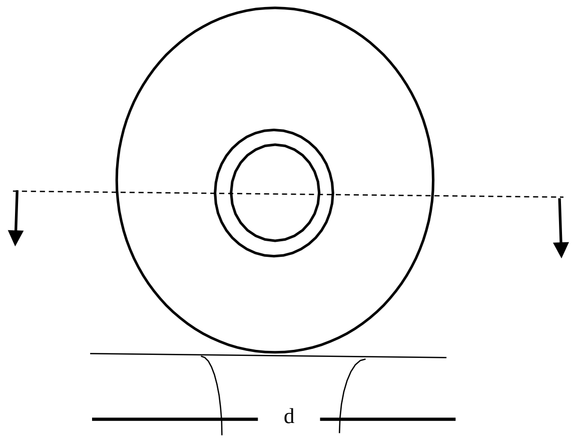

Figure 2.11: Quadrant-edged orifice upward and sideward view

(Ramamoorthy & Seetharamaiah, 1965)

The C_d is an essential factor in evaluating the nozzle efficiency. Nozzle geometry consists of converging angle and throat length. The nozzle profile can affect flow characteristics both outside and inside the nozzle (Jiang et al., 2022). It was determined by Jiang et al. (2022) that the greater the converging angle, the more severe the fluctuation that is noticed and the higher the flow speed. Quadrant-edged and conic orifice plates are used for high viscous fluids or low Re flows.

Different dimensionless parameters have been utilised to quantify the mechanical energy losses that occur during the discharge of viscous liquids through orifices. C_d,K_{or} triangular, square and/or Eu are some of the parameters most explored. From this it is seen that the discharge flow rate can be controlled by a gravitational or differential pressure process. Casey (2017) conducted a research study to characterise the pressure difference across the orifice and the discharge coefficient to determine the effect of cavitation on the instrument of flow. The pressure drop across the orifice plate geometry and flow rate were measured. It was also discussed that the C_d obtained for rounded-edged orifices was independent of the Re number for values above 10^5. A pressure differential was obtained of 2500 psig across the orifice geometry.

Simpson and Ranade (2018) discussed the modelling of hydrodynamic cavitation with orifices, focusing on the influence of different orifice designs on the importance and influence of the orifice sharpness and the effect of a rounding at the edge of the orifice, which can change the flow fields drastically.

Muñoz-Díaz et al. (2012) conducted a numerical analysis on an orifice flow meter with an abrupt contraction. It was concluded that the orifice flow meter performance is improved when modifications are introduction. Modifications such as testing of different orifice geometry, aspect ratio, different orifice shapes and testing orifice edge sharpness. Nasiruddin and Singh (2021) conducted a study on the performance evaluation of an innovation design modification of an orifice meter. The author explains that the orifice modification is accomplished by changing the surface topology to curvature on both sides of the orifice plate, particularly where the orifice performance was evaluated upon modification. Performance evaluation was achieved through computer fluid dynamics where the discharge coefficient and standard deviation was measured.

Nasiruddin and Singh (2021) explain that in all three principal flow meters were utilised and had the same diameter and a $\beta = 0.6$. The newly modified orifice had a radius of curvature 7.07mm, a V-cone flow meter with a fore vertex with an angle of 75°, and a reference orifice of $\beta = 0.6$ were compared.

Discharge coefficients with Reynolds number were determined for:

- $\beta = 0.6$ with a curvature of 7.07mm resulted in a mean C_d value of 0.808
- V-cone flowmeter for $\beta = 0.6$ resulted in a mean C_d value of 0.7561.
- Reference orifice of $\beta = 0.6$ resulted in a mean C_d value of 0.6628 (Nasiruddin and Singh 2021)

Nasiruddin and Singh (2021) utilised different radius curvatures (0, 5, 6, 7.07, 8, 9, and 11.18) of $\beta = 0.6$ and tested the standard deviation with mean C_d value which ranged from 0.66–0.98 with radius curvatures 5 and 6 being 0.98 and 0.87 as the highest. It was mentioned by the authors that, the curvature can be designed on the entrance of the orifice opeing or on the exit opening of the orifice. It was observed that the mean C_d values were much more interesting when the curvature was on the entrance than on the exit opening of the orifice.

Sanghani et al. (2016) conducted research on orifice geometry of six different geometries: square-edged, square-edged with 45°backcut, sharp-edged, streamline approach, inclined approach and quadrant-edged with the same diameter ratio and thickness used in a CFD (computational fluid dynamic) approach. A comparison of orifice geometry was made for pressure drop, and water was the working medium. It was determined that the minimum pressure drop occurred in the streamline-approach and maximum pressure drop occurred in the square-edge with 45°back cut.

Spaur (2011) conducted research investigating the discharge coefficient for irregular orifices. It was determined that irregular orifice plates resulted in a higher discharge coefficient across the orifice, resulting in higher flow rates. Their experiment was in a pipe system and water was tested. It was also stated that non-Newtonian liquids are known to have complex rheological properties. This makes drainage of these liquids from tanks complicated.

Table 2.5 shows the discharge coefficient of both Newtonian and non-Newtonian liquids through different orifice geometries from tanks only. In tank discharge, where the orifice-edge geometry is being evaluated, Newtonian liquids are used in most cases as a discharging liquid. In the cases were non-Newtonian liquids are incorporated, the discharging liquid is usually carboxymethyl cellulose (CMC) in solution. The discharge coefficient for sharp-edged, sharp-crested and square-edged have been observed by Dziubinski and Marcinkowski (2006) Khahledi et al. (2020) and Mohajane et al. (2019).

Table 2.5: Discharge of Newtonian and non-Newtonian liquids through different orifice geometries in tanks

Author and year	Liquid	Discharge	Orifice geometry	L/d	Discharge coefficient
Dziubinski and Marcinkowski (2006)	Newtonian: Water	Gravitational: tank	Sharp-edge circular orifice	-	C_d =0.62
Alajmi et al. (2019)	Newtonian: Water	Vertical tank fluid system	Sharp-edged	-	CdTh= 0.62 Cd_E =0.688
Alwan et al.(2020)	Newtonian: Water	Rectangul ar sharp- crested orifice	Orifice	-	C_d= 0.605-0.618
Khahledi et al (2020)	Water and glycerine	Rectangular tank, orificnt at the bottom in the centre of tank	Circular Square Triangle	-	C_d= 0.64.

Author and year	Non-Newtonian liquids	Discharge	Orifice geometry	L/d ratios	Discharge coefficient
Dzuibinski and Marcinskowski (2006)	Non-Newtonian: CMC	Cylindrical tank	Aspect ratio of various orifices	0 0.35 0.5 0.75 1 5	C_d= 0.468 C_d= 0.505 C_d= 0.49 C_d= 0.477 C_d= 0.506 C_d= 0.483
Khahledi et al., (2020)	Non-Newtonian : CMC , Kaolin and Bentonite	Rectangular tank	Aspect ratio of circular, square and triangular sharp-crested orifices	-	C_d= 0.61
Mohajane (2020); Mohajane et al. (2019)	Non-Newtonian: CMC , kaolin and bentonite	Rectangular tank	Aspect ratio of circular sharp-crested orifices	0.05 1 3 5	C_d= 0.62 C_d= 0.59 C_d= 0.78 C_d= 0.74

2.12 Conclusion

The literature reviewed pertained mostly to flow in pipes where Newtonian and non-Newtonian liquids were discharged through orifices of different geometry. In tanks, the orifice edge geometry effect was not explored for non-Newtonian liquids although the effect of aspect ratio and orifice shape was explored.

The literature available is predominantly about orifice attachments to pipes, where dimensionless parameters such as pressure loss, discharge coefficient and Euler number qualify the mechanical energy losses during the discharge of non-Newtonian (complex) fluids (Teoman et al., 2021). Dziubinski and Marcinkowski (2006) proposed equations describing discharge coefficient as a function of the Reynolds number and orifice geometry for Newtonian and non-Newtonian liquids. This research is aimed at assisting in further understanding the effect of orifice geometry and the influence of rheological properties on the flow, utilising different outlet orifice geometries for the discharge of non-Newtonian liquids through a tank. There are studies that have explored the effect of orifice edge on the discharge of liquids, Newtonian and non-Newtonian, in pipe settings (Abdalla Alajmi et al., 2019; Ramamurthi & Nandakumar, 1999; Ntamba, 2011; Hobbs & Humphrey, 1990) but not for tanks.

There is a scarcity of available literature showing the effect of orifice geometry on the discharge of non-Newtonian liquids. Attempts have been made to express loss coefficients in terms of discharge coefficients as they hold true for Reynolds number when utilising water as a flowing fluid. The loss coefficient can be related to the discharge coefficient in equations that hold good in practical ranges of Reynolds number (Ramamoorthy & Seetharamaiah, 1965). Likitha et al. (2018) stated that, to understand the discharge coefficient for concentric orifice meters with varying Re, multiple models were created using the CFD software. They were able to generate various models for each concentric orifice meter. These models were analysed to determine the effect of different shapes of orifice plates and beta values on the C_d.

Hobbs and Humphrey (1990) evaluated the edge radius of sharp edge orifice in pipes. It was determined that there was gradual increase in C_d value as the radius of the sharp edge increased. Spaur (2011) suggested that uncertainties still exist about the flow behaviour of liquids at the entrance region of the orifice. Non-Newtonian liquids are known to have complex rheological properties. This makes drainage of these liquids from tanks complicated. Khahledi et al. (2019) concluded that there was an effect of viscosity and yield stress for the flow of the non-

Newtonian liquids through orifices from tanks. Khahledi et al. (2020) determined that the average C_d values for orifices (circular, square and triangular) in the turbulent region was approximately the same. Mohajane (2020), and Mohajane et al. (2019) showcased that the flow of Newtonian and non-Newtonian liquids is affected by different L/d ratios of the orifices. It was evident that, for non-Newtonian liquids, this effect is more significant in the laminar regions. In the laminar regions, C_d values were dependent on the Re and in the turbulent regions the flow trend differed from one L/d to another. Assran and Mohamed (2022) discussed that orifice effect on discharge rate is more pronounced if the orifice diameter, shape, edge of orifice opening, thickness of orifice plate or liquid type are varied.

It was determined by Abd et al. (2019) that the relationship between C_d vs Re for the different β, it was noticed that as the C_d values increased as higher β utilised in the experiments. It was noticed that, for higher Re, C_d is almost completely constant. This behaviour was concluded to be as a result of the effect of the orifice plate on the velocity inside the pipe. It was stated by Hollingshead et al. (2011) that low Re resulted in laminar flow regions and larger C_d values, for the reason that the orifice plate does not affect the velocity associated with the flow passing through the orifice meter. Frachskampf et al. (1990) noticed that, when an orifice has a nozzle-like shape at the edge, the flow experiences a gradual narrowing at the inlet and later the flow is on the atrial side of the orifice. This, in turn, results in an improvement in the discharge coefficient.

The discharge behaviour of short orifices was investigated where the inlet geometry was selected either to be radiused or chamfered. It is discussed by Dittmann et al. (2003) that radiusing the inlet edge of an orifice increased the discharge coefficient.

However, there is limited research about the effect of orifice geometry on the discharge coefficient of non-Newtonian liquids, particularly from tanks. There is a scarcity in comparative studies for different edge geometries, be it inlet edge or outlet orifice edge. The discharge coefficient for viscous materials passing through square, chamfered or quadrant-edged orifices attached to a discharging tank is lacking. This research was initiated with the objective of evaluating the discharge coefficient with different orifice edge geometries: square, short and bevel back as well as chamfer-edged and quadrant-edged (orifice with a conical looking nozzle outlet). The discharge of these four different edge orifice geometries was determined utilising non-Newtonian liquids that exhibited the pseudoplastic Power Law, Herschel-Bulkley and Bingham plastic rheological characteristics, in accordance with the work of Ntamba (2011), Chowdhury (2012), Khahledi et al. (2020), and Mohjane,et al. (2020).

CHAPTER 3 RESEARCH METHODOLOGY

3.1 Introduction

This study was conducted at the Flow Process and Rheology Centre, located at the District Six campus of the Cape Peninsula University of Technology in Cape Town, South Africa. In this chapter, the method of investigation and apparatus used to determine the discharge coefficient data for different edge geometries (chamfer edge, quadrant-edged, short square-edged, and square-edged bevel back) are described. A detailed presentation of the experimental rig is provided, along with an explanation of the data collection technique.

Water was used as a solute in the mixing process for all percentage volume concentrations of kaolin suspensions, bentonite suspensions, CMC solutions, and glycerine solutions.

It was established that the discharge coefficient can be compared to the Reynolds number for the edge chamfered, quadrant-edged, short square-edged, square-edged, orifice with bevel back.

The tests involved water, glycerine solutions, percentage volume concentrations of kaolin suspensions, percentage mass concentrations of bentonite suspensions, and percentage mass concentrations of CMC.

This chapter describes the experimental work conducted, including the test rig, experimental layout, instrumentation, material tested, calibration, different edge geometries, flow rate measurements, and rheometry.

The experimental work conducted is outlined in this chapter as follows: an explanation of the test rig, the layout of the experiments, instrumentation, the material utilised for testing, and the calibration process. The different orifices edge geometries, flow rate measurements and rheometry.

3.2 Experimental test rig

Four polyvinyl chloride (PVC) orifices of different edge geometry: square-edged, chamfer-edged, quadrant-edged and short square-edged bevel back were utilised for empirical experimental study of the discharge of glycerine solutions and water and CMC solutions, kaolin and bentonite solutions liquids from a tank. A rectangular tank of L×b×h (400×400×600) mm was used with a load cell attached to the tank by steel frames to measure the discharge rate.

This was achieved by converting the voltage to weight from which the liquid height could be calculated as a function of time and height. A graph of time versus height was produced, and a second order polynomial was fitted to the data, which resulted in a slope of $\frac{dh}{dt}$. The derivative was utilised in the determination of the discharge coefficient (C_d) and the Reynold's number(Re). This was achieved by obtaining the discharge rate (ϑ) which was a product of the area of the orifice and the velocity of the discharging liquid.

The discharge coefficient accounts for losses and inefficiencies in the flow system through orifices, nozzles and valves. Non-Newtonian liquids are complex liquids as they have viscosity and yield stress variations which result in flow characteristics that differ significantly. The discharge coefficient quantifies these rheological properties that affect the flow rate and pressure losses in practical applications.

Rheological characterisation was carried out with the aid of a Paar Physica MCR 300 rheometer. The configurations used incorporated cup and bob, having a 1mm gap, and shear rate range of 0–1000s^{-1}. Non-Newtonian liquids require rheological studies to determine their flow behaviour. This is achieved through evaluating viscosity versus shear rate, and shear stress versus shear rate utilising a rheometer..

Figure 3.1 showcases the research work place and the instrumentation utilized to carry out the experiments.

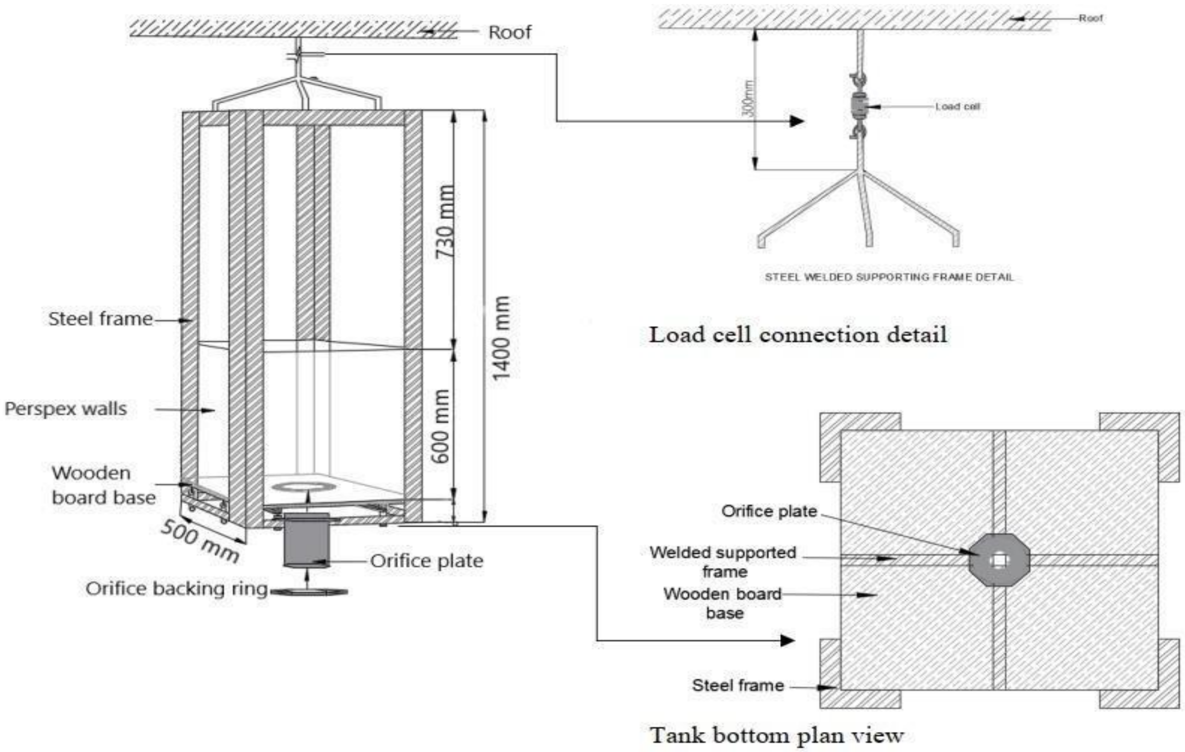

Figure 3.1 A: Test rig

(Khahledi et al., 2019)

The image below is an P&ID drawing of the experiment test rig

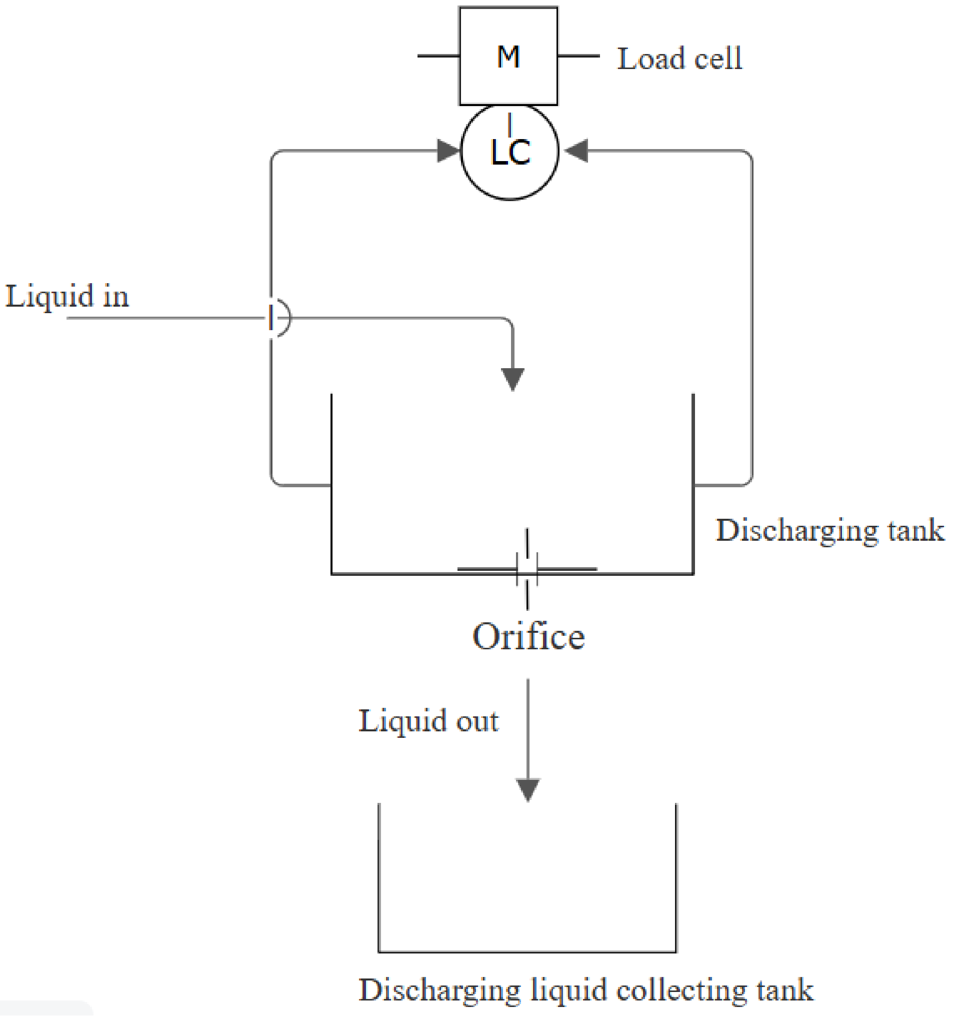

.

Figure 3.1 B: P&ID image of the experimental test rig

3.3 Experimental design

A rectangular tank was positioned vertically where the liquid was poured from the top and discharged from the bottom through the orifice. The tank was connected to a load cell, attached to a suspended weighbridge. The load cell was used to measure the volumetric mass over time and the orifices were fitted flush with the inside surfaces of the tank. The slurry mixtures, such as the glycerine solution, carboxymethyl cellulose solution, and the bentonite and kaolin suspensions were tested. The glycerine was mixed with water for different concentrations into a glycerine solution. Carboxymethyl cellulose, bentonite and kaolin were mixed manually with water, since they are powders, before being transferred to the discharging tank.

3.4 Orifice geometry edge used in the study and the material tested

Table 3.1 explains the different orifices; the diameter and thickness including the different material of testing utilised in the study.

An 8mm diameter was chosen as diameter smaller than 8 mm does not allow adequate flow for the orifice edge geometry to be properly examined With larger diameters the vena contracta effect would have been less pronounced reducing relative blockage; shortening separation and reattachment lengths. The gap filled here would be that the turbulent flow region the Re is between 5000 -10000and in the laminar to transition flow region Re can be found between 100-1000 for an 8mm diameter orifice.

Table 3.1: The orifice geometry edge, the diameter, the thickness and the material utilised for testing

Orifice geometry edge	D_{OR} (mm)	t / d (mm)	Discharging liquids
Chamfer-edged Quadrant-edged Short square-edged Square edge with bevel back	8	8	Water, glycerine and CMC mixture(solution), kaolin and bentonite suspensions

3.5 Instrumentation

This section presents all the instruments used to collect data.

3.5.1 Orifice geometry edge

Four different edge geometry orifices: chamfer edge, short square-edged, quadrant-edged and square-edgde with bevel back were used, as shown in Figure 3.2. The orifices were made of grey polyvinyl chlorine material, manufactured to have the same diameter and thickness, that is, no L/d variation for all the orifices. The only variation is in terms of the orifice exit opening, which is made deliberately different with the aim to measure the effect of orifice edge geometry on flow being discharged.

The chamfered and quadrant edge orifices, have a smooth entry which reduces flow disturbances and energy losses and increase Cd values up to 0.9. Higher Cd results in a more efficient flow measurement process. Whereas square edge orifices resulted in abrupt flow separation causing turbulence and lower Cd values up to 0.6.

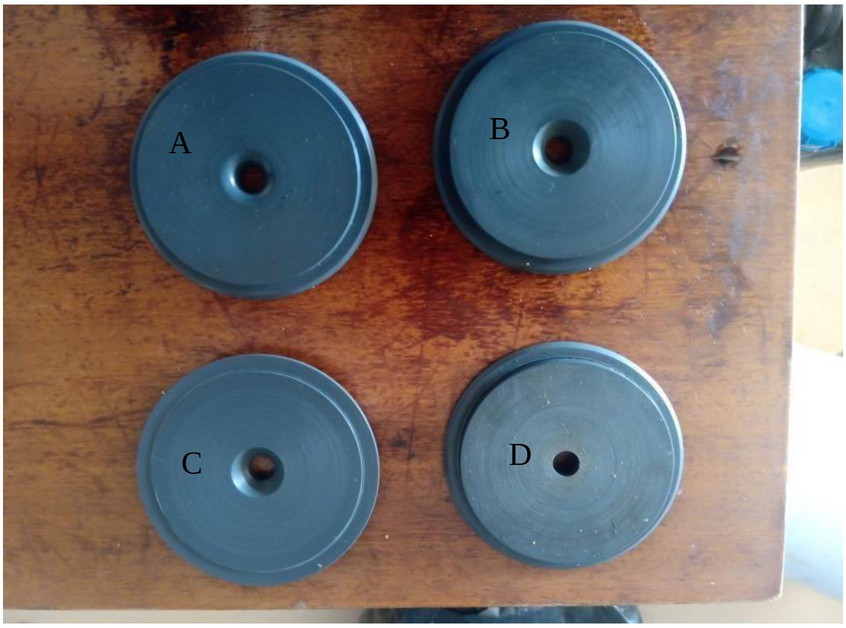

Figure 3.2: Orifice geometry edge: Quadrant-edged (A), Chamfer-edged (B), square-edged with bevel backcut angle (C) and short square-edged (D)

3.5.2 Edge orifice geometry tested

Presented below are the different edge orifices that were used. Figure 3.3 to Figure 3.6 illustrate the systematic diagrams of square-edge orifice with back bevel angle, short square-edge orifice, chamfer-edge orifice, chamfer-edge orifice, and quadrant-edged orifice that were used.

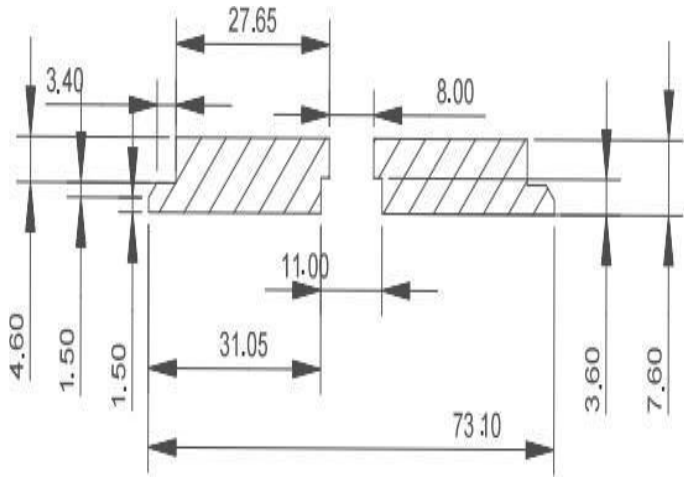

Figure 3.3: Square-edged orifice

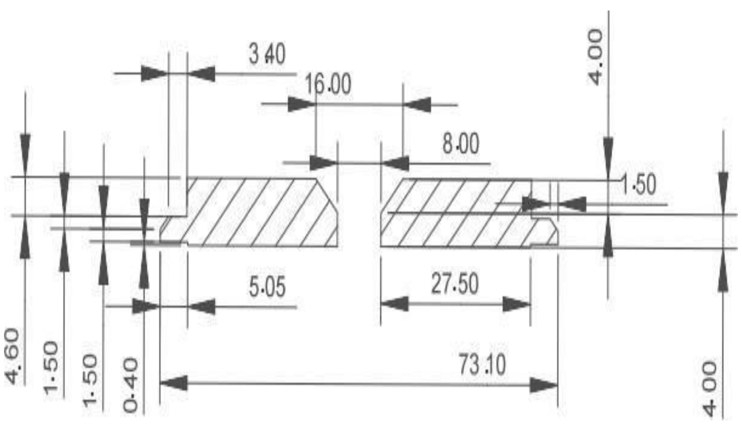

Figure 3.4: Chamfer-edged orifice

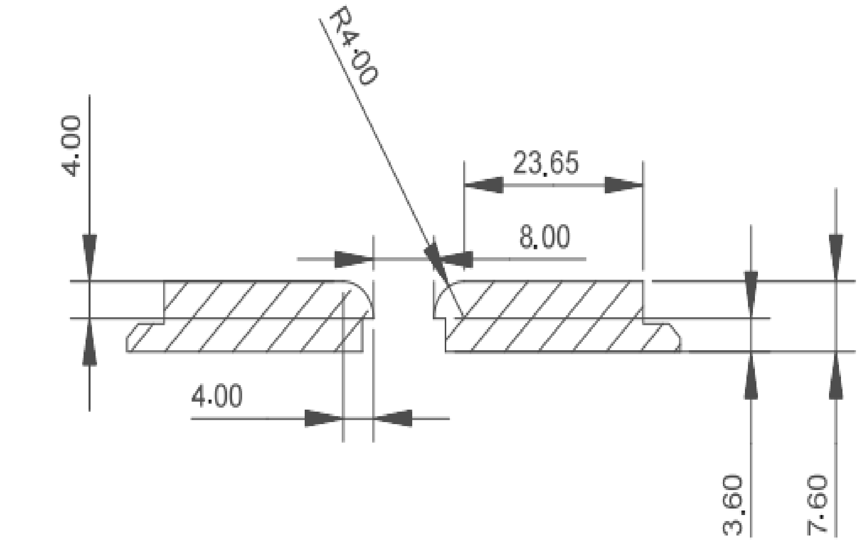

Figure 3.5: Quadrant-edged orifice

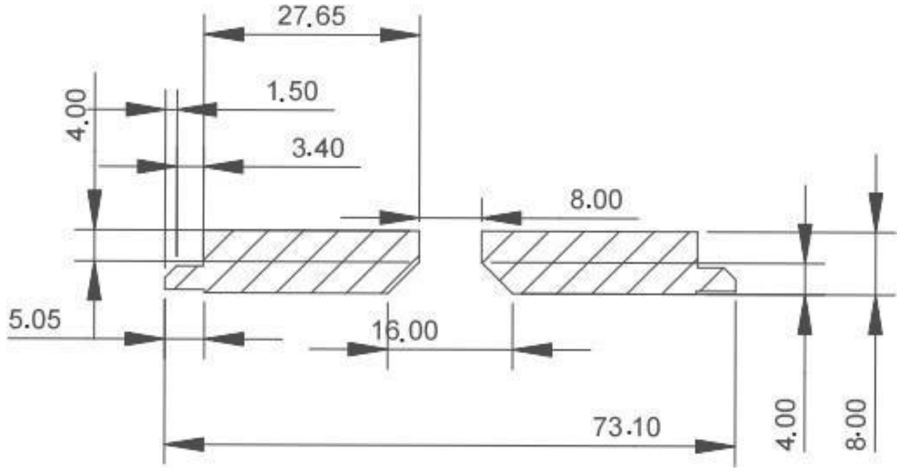

Figure 3.6: Short square-edged orifice with back bevel angle

3.5.3 Discharge tank

One batch of testing liquid was prepared from the highest concentration and later diluted to the desired concentration moving from laminar to turbulent flow. The orifices are lined up in the order that they will be tested beforehand, testing is conducted simultaneously to the rheological testing of the liquid. The liquids were prepared in batches and one batch was utilised for testing for all orifices per experimental set-up. Orifices were tested systematically one after the other and each run the tank is filled to the same height.

Figure 3.7 and Figure 3.8 show the discharge tank made of plexi transparent glass with measuring tapes running vertically from top to bottom of the tank. The orifice is situated at the centre in an upwards direction at the bottom of the tank. For each run, the tank is discharged to the point that a vortex is evident. Upon observation, the test is stopped and a different orifice edge geometry is inserted; the tank is refilled, and the discharging process is started all over again.

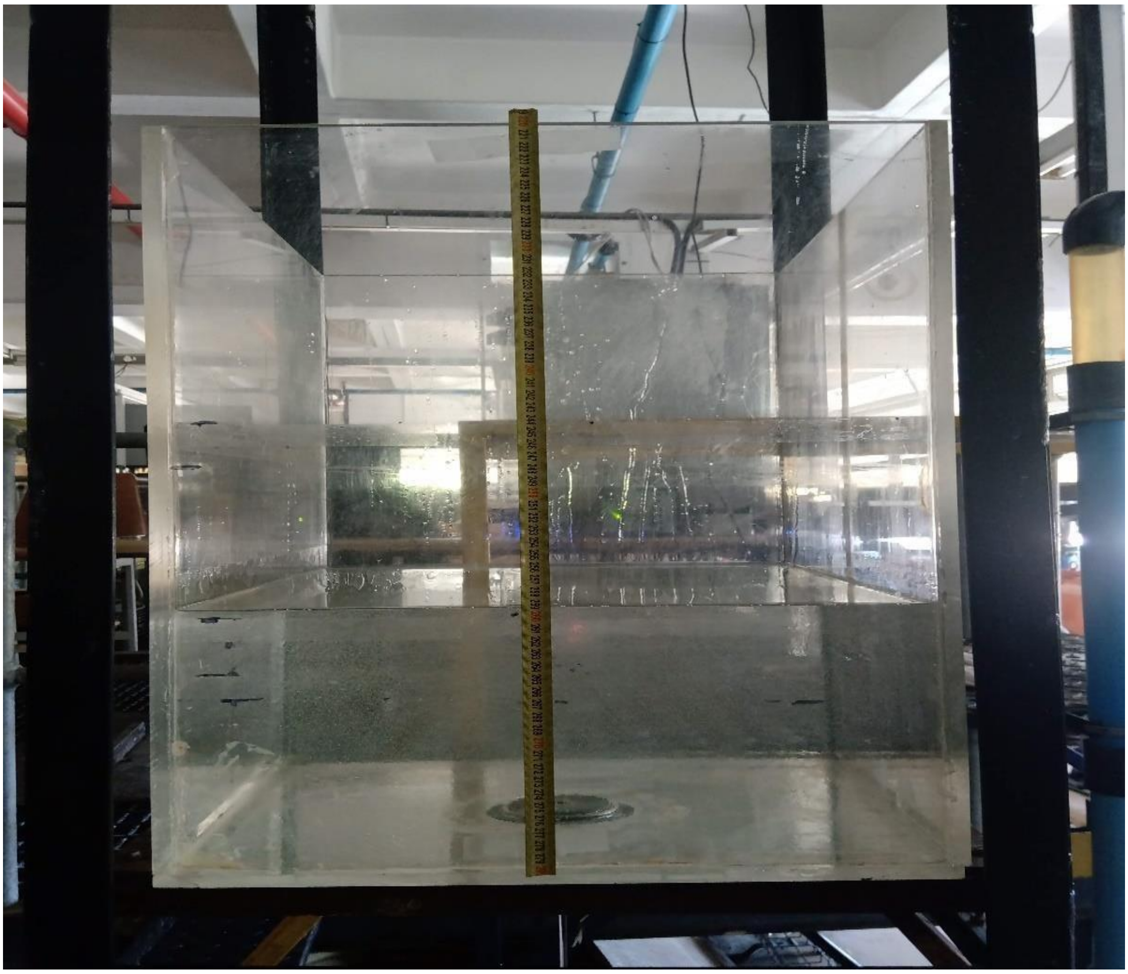

Figure 3.7: Discharge tank with glycerine solution

Figure 3.8: Orifice attached to the base center of the tank discharging glycerine solution

3.5.4 Orifice locating and relocating ring

Fixed at the base of the tank is a locating and relocating ring, which is used to keep the orifice in place and is employed to secure the orifice to the tank. This was vital as there was pressure build-up from the liquid in the tank. The process of incorporating a locating or relocating ring was mainly to secure the orifice and prevent it from falling out, regardless of the pressure of the liquid inside the tank. The liquid is only being discharged at the orifice opening. As shown in Figure 3.9 the orifice backing ring is sealed and attached to the orifice and tank while the liquid is being discharged.

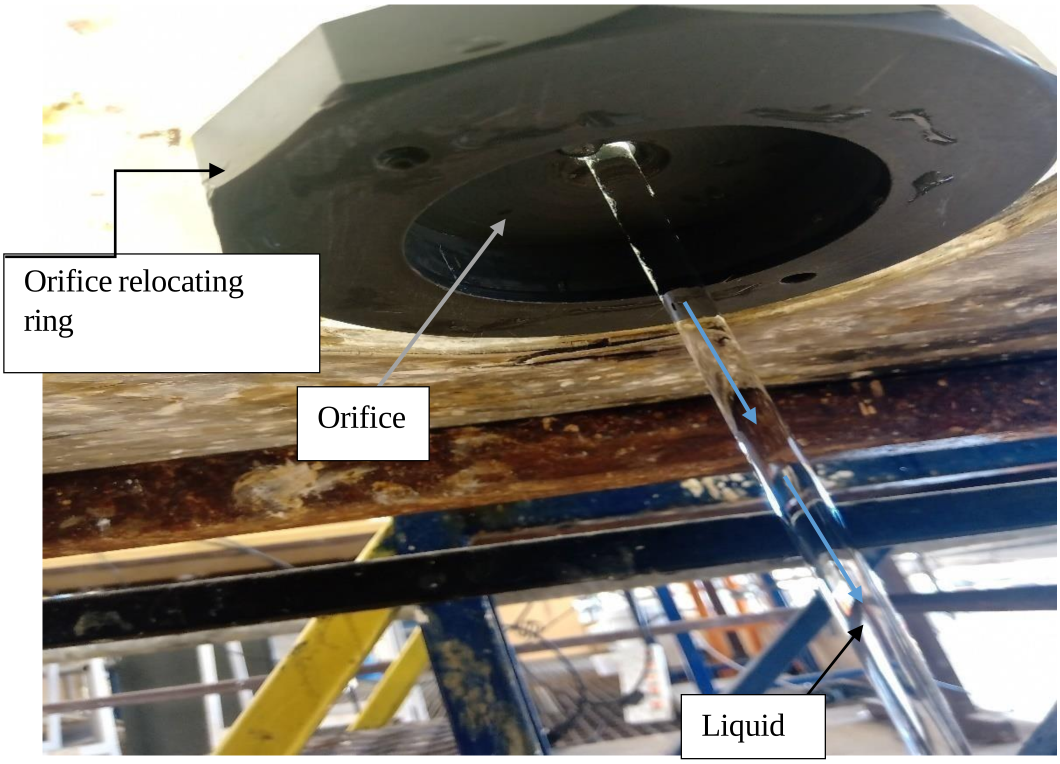

Figure 3.9: An image of the orifice backing ring attached to the orifice and the tank

3.5.5 Camera and tripod

A camera mounted on a tripod was placed away from the tank to capture the motion of the liquid discharging. To calculate the volumetric flow rate discharged, the number of frames extracted from the top to the bottom of the tank was based on how much liquid could flow from one height to the other.The KMPlayer software was utilised to analyse the videos recorded. The frames extracted were utilized to determine the time required for liquid to move from one point to the other and the volume discharged per measured time.

3.5.6 Computer

The computer displayed in Figure 3.9 was situated in the laboratory and was utilised for recording reading from the data acquisition system (DAQ). The DAQ system is connected to the computer and software was installed in the computer to capture the volumetric weight as the height changed according to the ellipse time for the discharging process. As a result, the raw data is used to aid in the determination of the volumetric flow rate through the orifice.

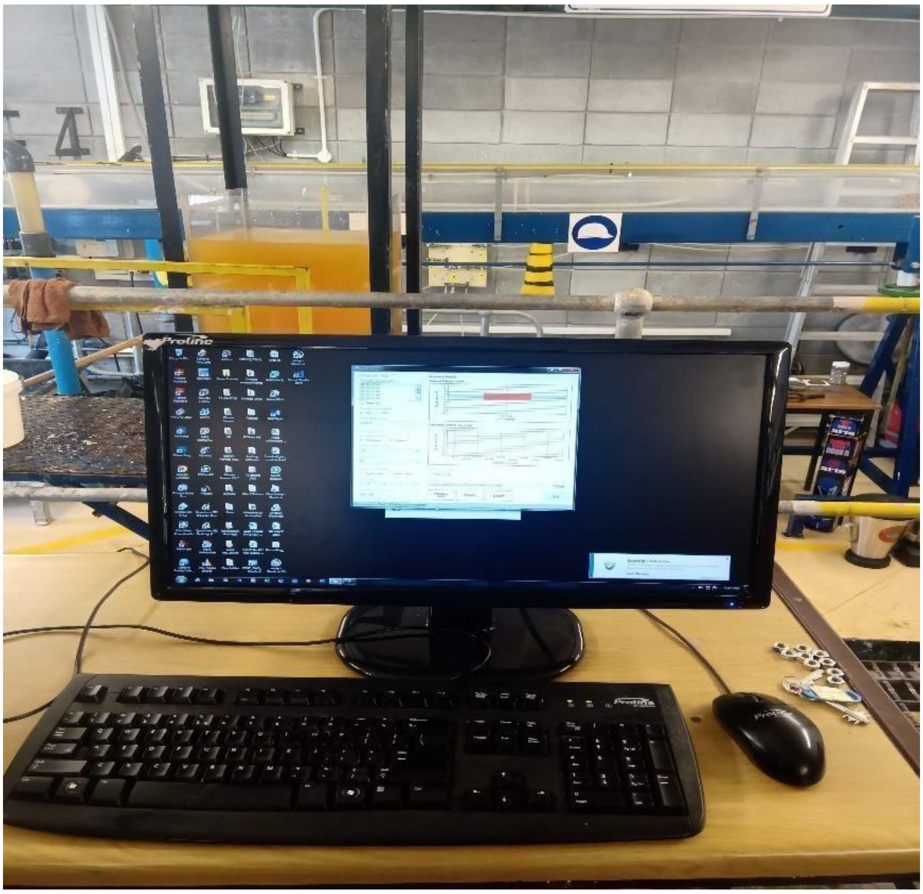

Figure 3.10: The computer connected to the DAQ system

3.5.7 Load cell

By using the load cell, we were able to monitor the change in liquid mass over time as it exits the tank through the orifice. A stainless steel load cell (type _S' multipurpose universal load cell, model 9363) was mounted and utilised to measure the flow as the discharging process took place.

The advantages of utilising load cells are that they measure weight directly and provides an accurate to weight measurement of the tank or discharging vessel in comparison to a flow meter which measures at a flow point upstream. The camera-based method adds visual monitoring components; this can altogether serve as a non- contact measurement and verification. The limitations with load cells are factors such as vibration and temperature can impact load cell accuracy if not properly managed. Camera-based method tend to be costly initially due to combination of hardware.

Figure 3.11 is an image of the loadcell suspended in the air at the research laboratory.

Figure 3.11: Load cell

3.5.8 Data acquisition

The data acquisition system incorporated a power supply and an amplifier.

Figure 3.12 shows the data acquisition NI USB 6001. Using USB, the signal was transported from the NI USB 6001 to the computer and later transferred into the Excel spreadsheet..

Figure 3.12: Data acquisition system

3.5.9 Measuring tape

The height was determined by using the measuring tape.

3.5.10 Balance

The relative density tests involved measuring the test material samples using a top pan balance.

3.6 Material tested

The turbulent regions were defined for Newtonian liquids by running tests where the testing liquid is water, as well as for calibrating the orifices. For laminar regions glycerine solutions were carried out at various concentrations. Carboxymethylcellulose (CMC) solutions of various concentrations and a variety of rheological values for non-Newtonian liquids were obtained by preparing and testing suspensions of bentonite and kaolin. Note was taken when determining rheological parameters that CMC is pseudoplastic liquid, kaolin is a Herschel- Bulkley liquid and bentonite is a Bingham liquid.

3.6.1 Preparation of slurry

The slurry preparation had to be conducted in advance as the materials selected for the study were powder. The slurry make-up involved mixing the powdery materials with water in calculated ratios to obtain a slurry.

Slurry preparation calculations were as follows:

1. Volume of the tank to be used to conduct the experiment must be calculated.
2. Calculate the mass of powder based on % v/v for kaolin

$$\% \frac{V}{V} = \frac{\textit{Volume of dry solids}}{\textit{Volume of total mix}} \times 2.65 \times 100 \qquad \textbf{Equation 3.1}$$

For Bentonite and CMC, the mass of powder based on % w/w was calculated

$$\% \frac{W}{W} = \frac{\textit{Mass of dry solids}}{\textit{Mass of total mix}} \times 100 \qquad \textbf{Equation 3.2}$$

3. Manually mix the powder by pouring in the required amount together with the measured quantity of water and leave the mixture for five days with constant stirring on a daily basis to avoid lumps.

3.6.2 Water

Water was used to calibrate the equipment. It was used for making up the slurries, solutions (glycerine and CMC) and suspensions (kaolin and bentonite). Water was used for relative density determination to make up the samples to facilitate the density determination. The slurries were diluted to different concentrations.

3.6.3 Glycerine

Six 25L of pure canned glycerine was purchased, kept sealed and stored at room temperature prior to experimental work. The glycerine was diluted to 90%, 85%, 76%, 60%, and 47% solutions.

Glycerine is transparent in colour, odourless and highly viscous and it is used in cosmetics as a primary material in moisturisers for skin and hair hydration. Glycerine is water absorbent; it was diluted to different concentrations corresponding from laminar to turbulent and, right after mixing, could be poured into the discharging tank for immediate testing.

3.6.4 Carboxymethyl cellulose (CMC)

Water and CMC were combined to form a solution, which was then diluted to various amounts. Five days were spent mixing to fully hydrate the mixture before testing. To prevent lumps, mixing was done every day until testing.

.

3.6.5 Kaolin

Kaolin powder was mixed with water and left for three days for complete hydration before testing and to obtain a suspension that was later diluted to the different concentrations. The suspension was also mixed daily to avoid lumps.

3.6.6 Bentonite

Bentonite powder was mixed with water and, to achieve the suspension, was allowed to stand for five days during which time daily mixing took place. A suspension was obtained and later diluted to achieve different concentrations.

3.7 Calibration

Experimental equipment required calibration. Water was used as a calibration liquid. Calibration was conducted of the load cell and orifice.

3.7.1 Loadcell calibration

Data acquired from the transducer load cell were used to calculate parameters such as time, height, volume, velocity and flowrate. The load cell was used to measure the voltage against time during the discharge of liquids from a tank. The velocity at the orifice was determined through the continuity equation. In nutshell for every liquid and orifice geometry, the correction between the C_d and Re was established.

The following was implemented in order to calibrate the loadcell:

1. Water was weighed in buckets of known mass on a scale.
2. After manually filling the tank with water, the voltage output was noted
3. Water quantity had to be added to cause an increase in the voltage and this too was recorded. A frequency was selected on the NI-DAQmx software of 60 Hz for the load cell to transmit signals (Khahledi et al., 2019; Khahledi et al., 2020; Mohajane, 2020).

The following was the calibrating process:

- Switch on the computer, and connect the DAQ into the USB port of the machine.
- Launch the NI –DAQmx application, then select channel Dev/10. The purpose of this channel is to record the voltage generated within the loadcell.

- The frequency should be maintained at of 60 Hz for the signal to be sent to the transducer.
- Monitor and record the voltage induced by the loadcell for at least one minute prior to loading any liquids into the tank.
- Close the orifice hole with a plug (which is attached to a long string for ease of removal once the tank is filled) and pour 10 L water into the tank. After a minute or so the system would have stabilised. Run the programme once more and each time water is added to the tank, measure and record the voltage induced by the loadcel.
- The procedure is to be repeated until the tank is filled up.
- Plot a voltage versus weight graph to find the linear relationship‘s slope intercept.

There was a relationship between the weight of the liquid in the tank and the voltage and this is demonstrated through a linear regression graph. Figure 3.13 shows a linear weight-voltage for the calibration of the loadcell.

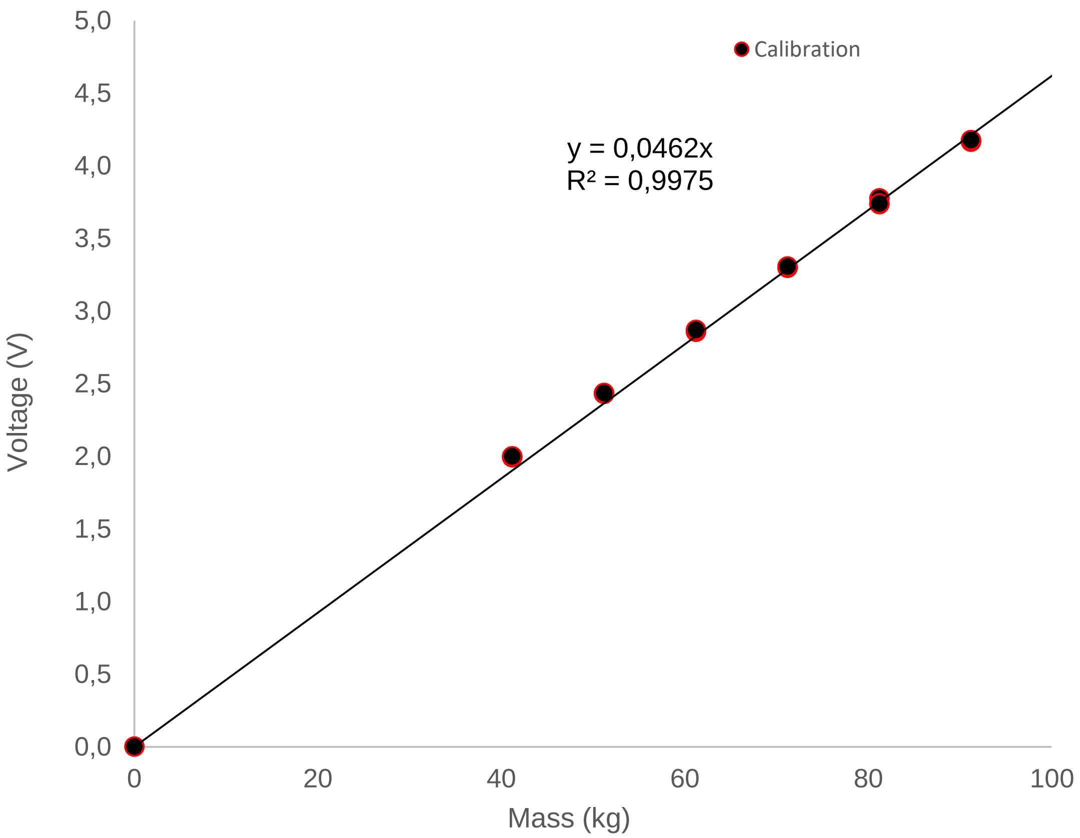

Figure 3.13: Load cell calibration

3.7.2 Orifice calibration

To determine whether the orifices being utilised are correctly constructed and manufactured, a calibration process was carried out.

The orifice calibration procedure:

- Place the orifice at the bottom of the tank, making it level with the inside.
- Manually fill the tank with water and close the orifice with a plug.
- Allow the tank to stabilize for a moment; then turn on the computer and begin the DAU program..
- The DAU should have the Dev/10 channel selected to capture the voltage induced on the loadcell.
- Pick the 60Hz frequency that the load cell uses to monitor the change in mass over time as the water flows from the tank.
- Pull the plug simultaneously to stop the flow at the aperture and allow the water to exit the tank through it. In order to record the data as the water is being released from the tank, simultaneously press start on the program.
- Stand ready to press the Stop button on the programme as the water in the tank reaches vortexes.
- Repeat the same procedures for all the orifices.

Figure 3.14 show the results for orifice calibration of the chamfer-edged orifice, quadrant-edged orifice, short square-edged orifice and square-edged orifice with bevel back.

The influence of the edge geometry on the flow was observed by plotting the acquired Cd values against the Re. The avearge C_d values for square edged orifice was 0.58, and for the square edge orifice with bevel back cut it was 0.60. The average C_d values from chamfer and quadrant were between 0.80 and 0.90. Section B of the appendices contains the orifice calibration for each test.

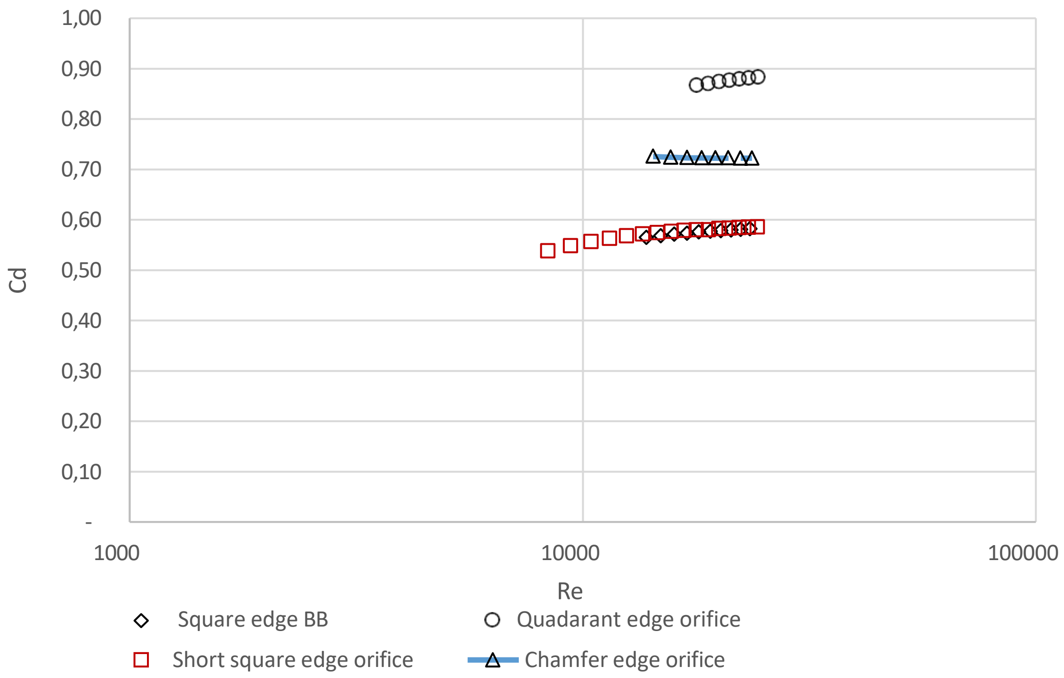

Figure 3.14: The different orifice edge geometry orifice water calibration

Table 3.2 shows the comparison between the reference average C_d values and the compatibility between load cell and camera results for chamfer-edged, quadrant-edged, short square-edged and square-edged with bevel angle and back cut.

Table 3.2: The compatibility average C_d values for the load cell and camera and a comparison between the references C_d values available in literature

Orifice edge geometry tested	Reference/Standard Cd values	Load cell Average Cd values	Camera method Average Cd values
Chamfer-edged	0.83–0.85	0.80	0.73
Quadrant-edged	0.60–0.80	0.84	0.79
Short square-edged	0.60–0.85	0.58	0.63
Square-edged with bevel back cut	0.60–0.85	0.60	0.58

3.8 Flow rate measurements

Flow rate measurements were obtained utilising the equipments in 3.8.1

3.8.1 Equipment used for flow rate measurements

1. Test materials.
2. Load cell
3. Four different edge geometry orifices
4. Data acquisition unit (DAU)
5. Tank

The procedure followed was:

- Ensure that the DAU is connected to the computer and the program is initialised.
- Ensure the opening of the orifice is blocked with a plug..
- Fill the tank with the liquid and allow it to settle..
- Choose the Dev/10 channel.
- Pick a frequency that is 60 Hz.
- Simultaneously, pull the plug from the orifice opening and press the Start button to run the programme.
- The flow of liquids will transmit a signal to the computer which is in the form of a voltage.
- The recorded mass of the liquid passing through the orifice was utilized to determine the flow rate and velocity of liquids exiting the tank. All of this will be used to calculate the C_d and Re.
- The procedure is repeated for various concentrations for each orifice edge geometry.

3.8.2 Equipment used for flow rate measurements for calibration purposes

1. Water
2. Camera and tripod
3. Computer with KMPlayer software
4. Tank and orifice inserted at the bottom

The procedure followed was:

- Place measuring tapes on the side of the tank.

- Use a plug to block the opening of the orifice.
- Fill the tank with the liquid and let it settle.
- Film and capture the video once the liquid in the tank has stabilised.
- To start the program, simultaneously remove the plug from the orifice opening and press the Start button.
- After the filming is finished, use KMPlayer software to extract the frames.
- Record the time it takes for the liquid to reach each planned level in the tank while it flows out of the tank.
- In order to decrease the percentage of errors and obtain an average time, the process must be repeated at least three times.

In Figure 3.15, the compatibility between the load cell and camera method is suggested for chamfer-edged orifice. The individual curves; square bevel with back cut angle, short square and quadrant-edged orifices are found in the appendices FC1-FC3.

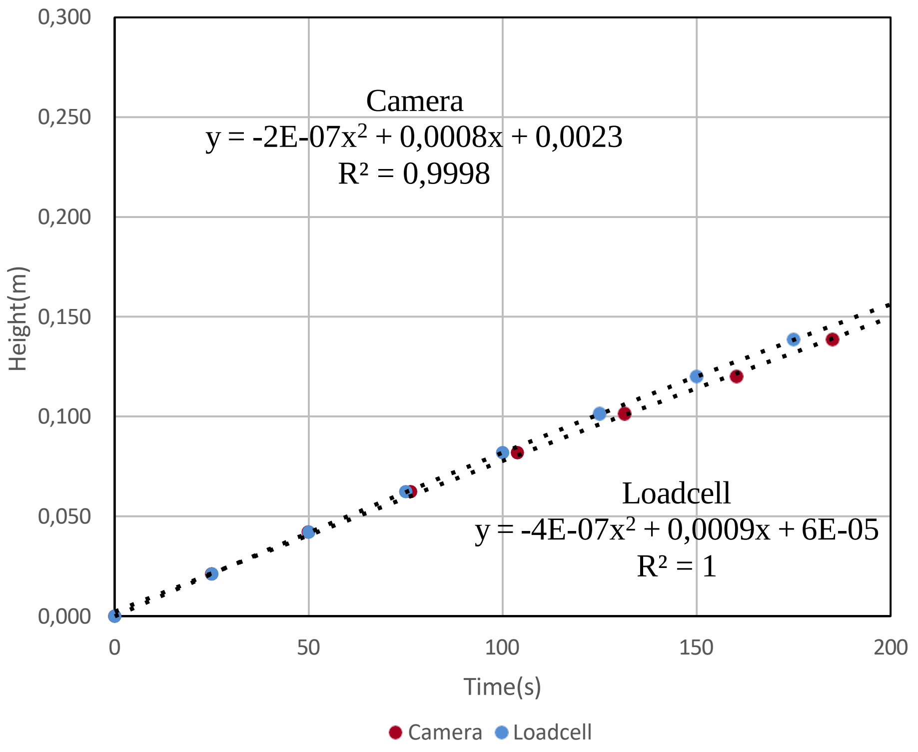

Figure 3.15: Compatibility between load cell and camera for chamfer edge orifice

3.8.3 Data analysis, collection and tools

- By converting the voltage to weight, liquid height was calculated based on time and height. A time vs height graph was created, as shown in Figure 3.15.

- The data was fitted with a second-order polynomial and its slope was determined to be dh/dt. The velocity is influenced by the height of the liquid at the top of the orifice. The mass flow rate was determined by calculating its derivative. The C_d values were calculated according to Equation 3.3 which is a replica of Equation 2.10 expressed in more detail. Equation 3.4 is produced from cross mutiplication of Equation 3.3.

$$C_d = \frac{Q}{A_o\sqrt{2gh}} \quad \text{Equation (3.3)}$$

$$Q = C_d \times A_2\sqrt{2gh} \quad \text{Equation (3.4)}$$

The Reynolds number, used to describe the flow regime of Newtonian liquids, is characterised by Equation 2.11.

$$Re = \frac{\rho d V_2}{\mu} \quad \text{Equation (2.11)}$$

The Reynolds number (Re2) proposed by Slatter and Lazarus (1993),for non-Newtonian liquids :Power law, Herschel-Bulkley and Bingham model liquids as Re2 is illustrated in Equation 2.12 in chapter 2, was utilized to determine Re for non-Newtonian liquids in chapter 3.

The traditional Re assumes a constant viscosity for Newtonian liquids, whereas the non-Newtonian Re does not have a constant viscosity as there are shearing forces that are exerted on the liquid to flow, Re for non-Newtonian liquids utilized is Re_2 as it incorporates non-Newtonian liquids parameters.

$$Re_2 = \frac{8\rho V^2{}_2}{\tau_y * k\left(\frac{8V_2}{d}\right)^n} \quad \text{Equation (2.12)}$$

ρ -Density of the liquid

τ_y -Yield stress of the liquid

d - Diameter of the orifice

V_2 - Velocity at the exit point

K -Consistency index

n- Flow behaviour index

The density of the liquids was determined through the relative density determination explained under sub heading 3.9.1. The yield stress, consistency and flow behavior index are rheological parameters of the non-Newtonian liquids and they were determined through rheological characterisation of the liquid this is further explained under heading 3.9.2. The diameter of all the orifices; chamfer, quadrant ,short square and square bevel back cut edge orifices are kept at 0.008m and the velocity at the orifice is determine from equation 2.13 on page 29.

In Figure 3.16, calibration methods used for compatibility to show the change in height as time increased for the load cell method. The graph showed a polynomial trend where the value for R^2 =1 meaning regression prediction perfectly fits the data for all orifices. All orifices produced the same trend and the individual curves; square bevel with back cut angle, short square, chamfer edge and quadrant-edged orifices are combined in Figure 3.16.
Appendices section c.

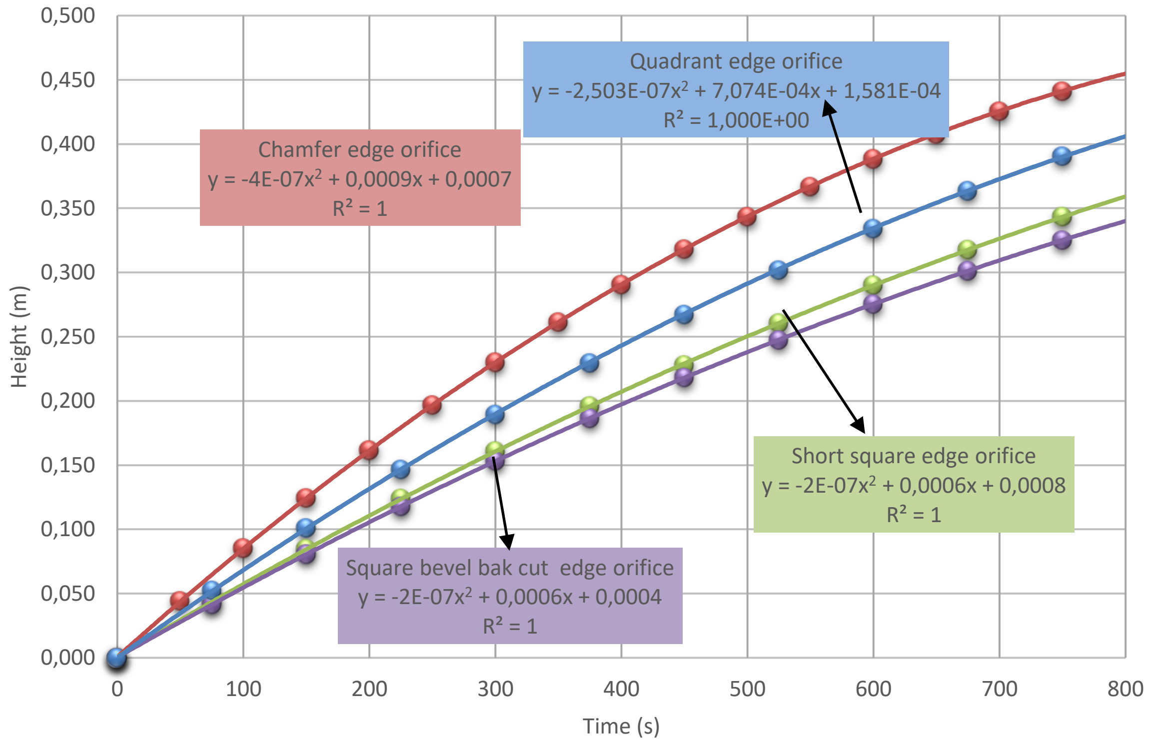

Figure 3.16: Time vs height polynomial graph for short square, square edge, bevel back cut edge orifice and chamfer- and quadrant-edged orifices

3.9 Rheometry

The rheometer device is utilised to the rheological characteristics of viscous liquids. To operate the rheometer efficiently parameters such as temperature, at each point, pre-shearing rate and duration of measurement should be known. For viscous materials that display liquid-like qualities a rotational rheometer is used. An MCR300 paar-physica rheometer and measuring geometry of CC 27 consisting of a cylindrical cup and bob was utilised in this study.

The measuring data spreadsheet for CC 27 are as follows:

- As a result of the orifice shear rate limitations below 100 l/s, throughout the flow rate experiment, the temperature was maintained consistent with the slurry‘s temperature.
- The gap was 1mm, the shear rate range was 0.01-1000 l/s for Newtonian and Power Law liquids. The shear rate range was 100-1000l/s for Herschel-Bulkley and Bingham plastic liquid. The data fitting with Herschel-Bulkley models was used to fit kaolin data, and Bingham plastic models for bentonite suspensions, and, Power Law model for CMC solution.

Data collection

Data collection involved relative density calculations to determine the density of the liquids. Excel spreadsheets were utilised to calculate velocity from the mass of liquid being discharged and from the height difference in the tank together with the liquid flow rate, viscosity, liquid consistency index, flow behaviour index and yield stress.

Figure 3.17 shows the cylindrical cup with a sandblasted bob measuring the geometry that was utilised for this study. Figure 3.18 shows the MCR300 paar-physica rheometer used to conduct rheological measurements.

Figure 3.17: Cup and bob

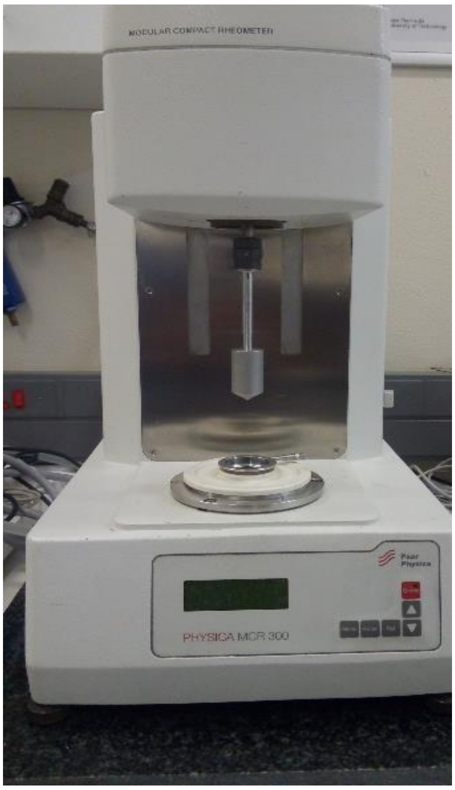

Figure 3.18: MCR300 paar-phyisca rational rheometry

3.9.1 Relative density (RD) determination

The apparatus used in the determination of the relative density.

Apparatus required for RD testing:

- Three volumetric flasks
- Sampled slurry for testing
- Thermometers to record the temperature of the water and slurry

- Top pan balance
- Clean water and water bottle.

Relative density testing procedure :

- Take the temperature of the slurry and clean water and record, taking note that the temperature difference of the slurry and water should be 1%. If not, try to get the temperature of the water closer to that of the slurry for better accuracy.
- Clean three 250 ml volumetric flasks and dry them.
- Label the flasks and weigh them using the top pan balance.
- Record the masses of the empty flasks as (M_1)
- Fill the empty flasks halfway with the testing slurry
- Weigh the flasks and record the masses as (M_2)
- With the flasks still half filled with testing slurry, add water to each flask and fill to the meniscus, making sure all material in the flask is well mixed and homogeneous
- Weigh the three flask and record the masses as (M_3)
- Throw out all the mixture in the flasks, clean the flasks (making sure no residue of the mixture is left in the flasks), and dry the flasks.
- Fill the flasks with clean water from the water bottle of known temperature
- Fill each flask with water to the meniscus
- Take note to dry the flasks again (so as not to influence the weight of the water in the flask)
- Weigh the three flask and record the masses as (M_4)

M_1= Mass of empty volumetric flask (bottle)

M_2 = Mass of bottle + mass of slurry

M_3 = Mass of bottle and mass of slurry+ water

M_4 = Mass of bottle + water

After recording (M_1–M_4), the relative density was calculated using

$$\boldsymbol{RD} = \frac{\textit{Mass of liquid}}{\textit{Mass of equal volume of water}} = \frac{M2-M1}{M4-M1-M3+M2} \qquad \text{Equation 3.8}$$

3.9.2 Flow curves of the liquids

Once the testing materials are mixed and become slurries, rheological characterisation of the slurries were made per sample of the different concentrations. The prepared material were rheologically characterised by using the following

- Various concentrations glycerine solutions: Newtonian models
- Various concentrations CMC solutions: Power Law
- Various concentrations kaolin suspensions: Heschel-Bulkley
- Various concentrations bentonite suspensions: Bingham plastic

The rheological properties of kaolin and bentonite exhibit thixotropy flow behaviour and yield stress that depend on the solid content.Kaolin and bentonite exhibit shear thinning behaviour this causes them to resist flow until a certain stress is applied.CMC has lower to almost little yield stress which entails that CMC has less pronounced shear thinning.

In the case of non-Newtonian liquids viscosity is both shear rate and temperature-dependent, as temperature increases the viscosity for non-Newtonian liquids decreases which implies that the flow will change and effect the discharge coefficient. Non-Newtonian characteristics such as shear thinning or shear thickening can be enhanced or diminished by temperature changes and this can affect the flow resistance and C_d. Temperature variations influence the C_d. In the case of viscous Newtonian liquids and Newtonian liquids this effect is evident by the change in viscosity and related flow properties which affects the velocity profile, fluid resistance and flow regimes.

Figures 3.19, 3.20, 3.21, and 3.22 are shear diagrams of shear rate versus shear stress. Figure 3.19 depicts 100% glycerine curve that shows a linear regression graph as it is a Newtonian liquid. Figure 3.20 is a kaolin 19% v/v shear diagram showcasing non-Newtonian flow pattern and using Heschel-Bulky model for rheological characterisation. Figure 3.21 is a CMC 6.6% w/w shear diagram demonstrating non-Newtonian flow pattern and using Power Law model for rheological characterisation. Figure 22 is a bentonite 6% w/w shear diagram showcasing non-Newtonian flow pattern and using Bingham plastic model for rheological characterisation as this model better describes the behaviour of the liquid where the flow behaviour index (n) is 1. Parameters such as flow behaviour index, fluid consistency coefficient and the yield stress were calculated from the shear stresses and shear rates from the shear diagrams.

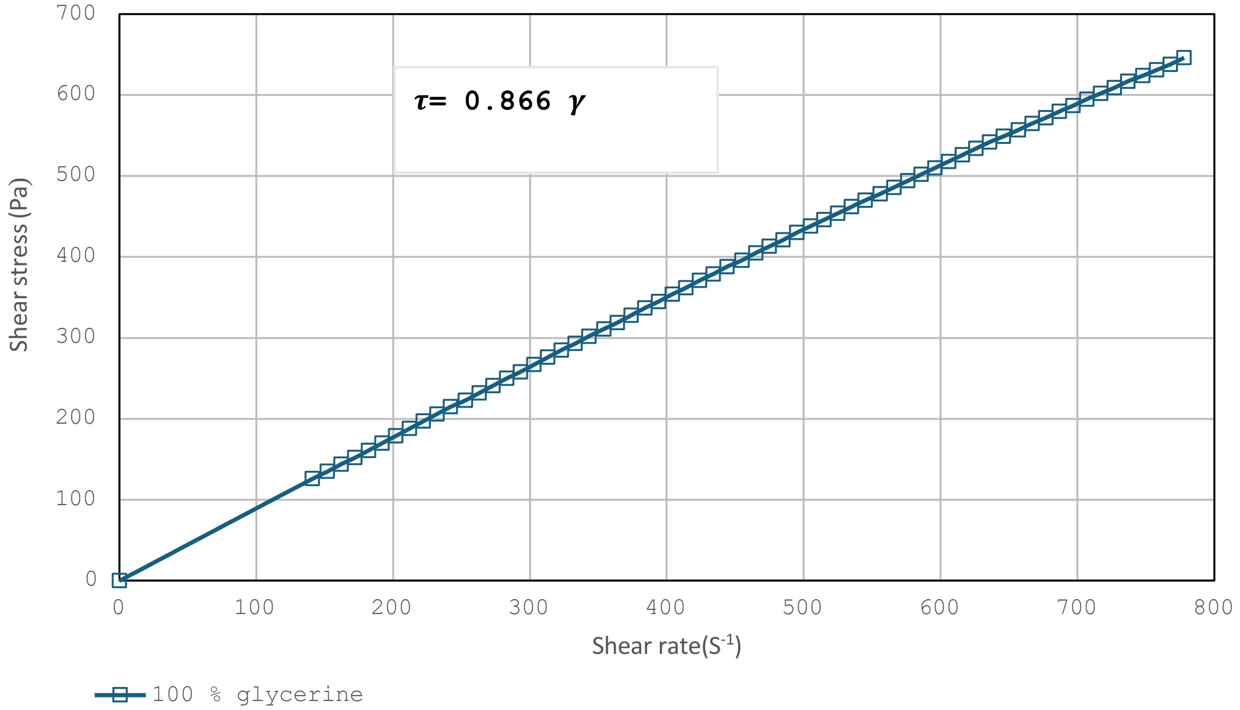

Figure 3.19: Flow curve 100% glycerine

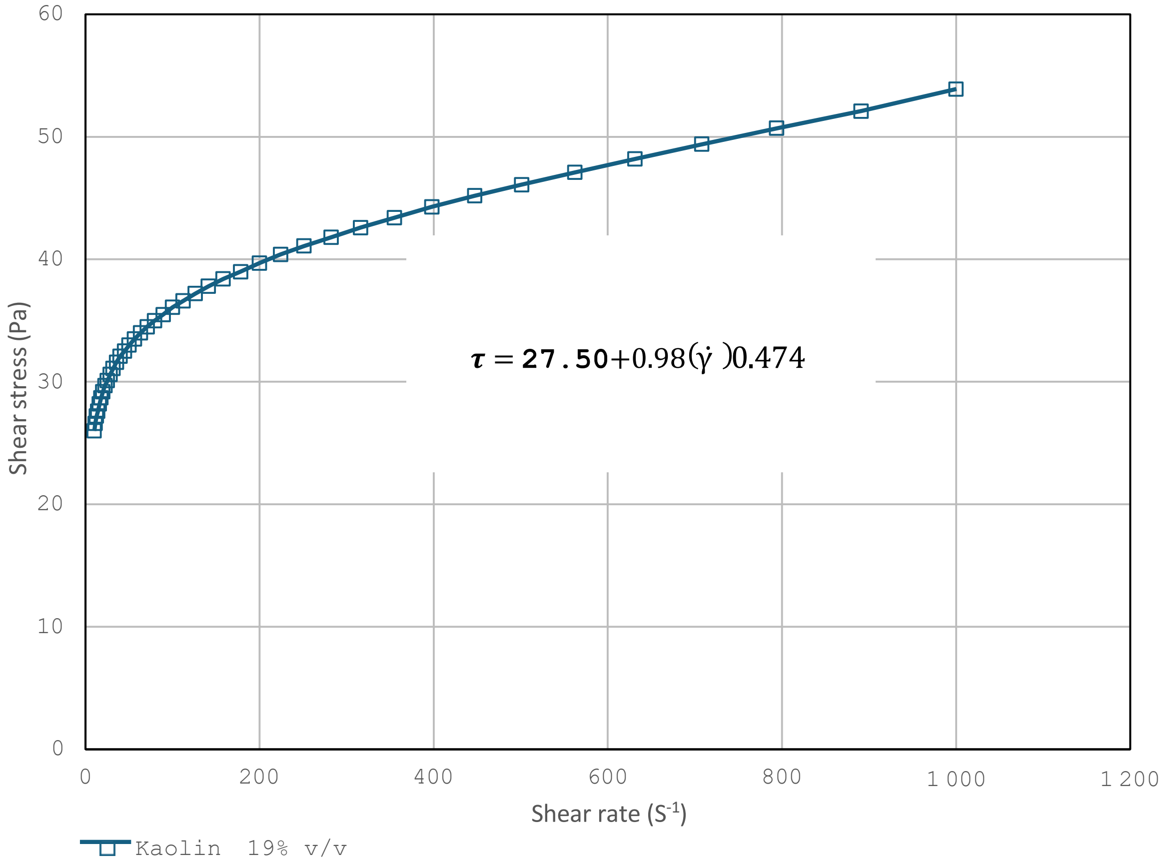

Figure 3.20: Flow curve kaolin 19 % v/ v

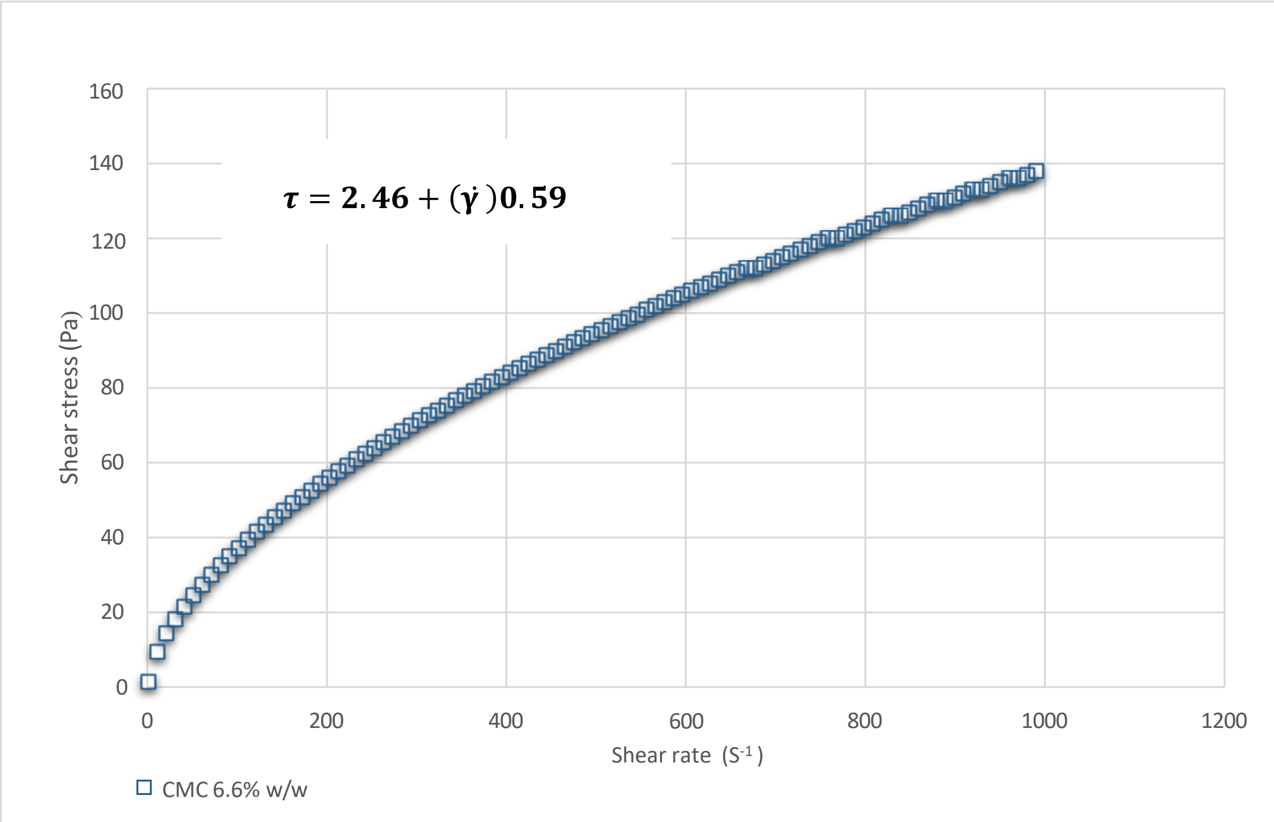

Figure 3.21: Flow curve of CMC 6.6% w/w

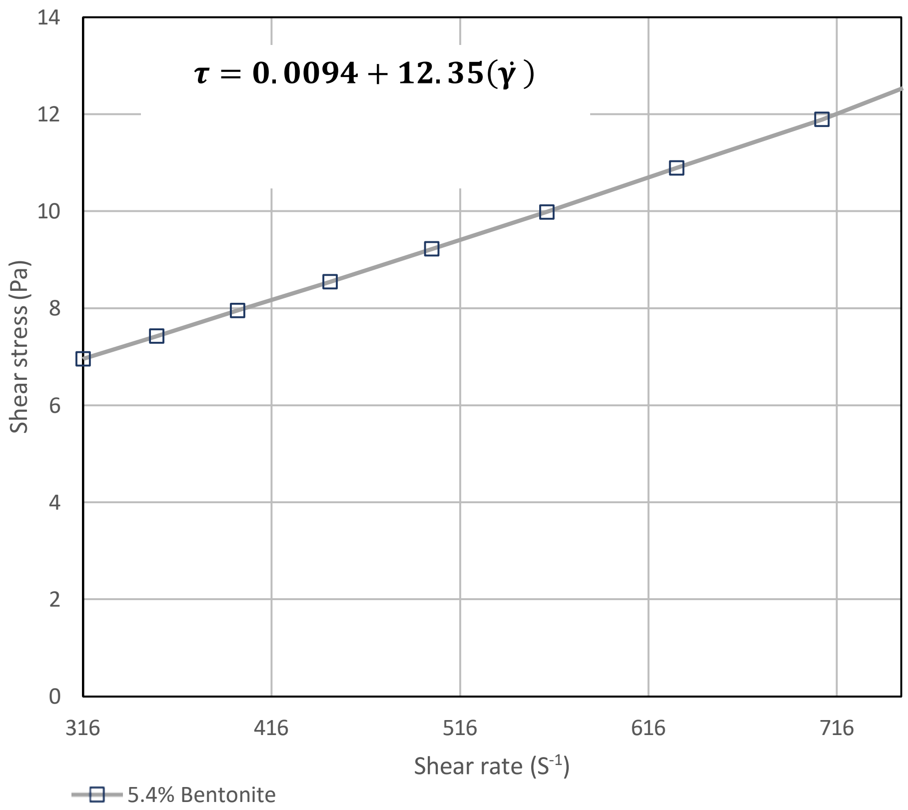

Figure 3.22: Flow curve of 6% w/w bentonite

3.10 Experimental errors

According to Bezinger and Aksay (1999), three types of errors can exist in experimental work. They are gross errors, systematic errors and random errors. Hence, it is of the utmost importance to be aware of these errors. Although, in almost all experimental study procedures protocols are put in place to limit or to keep errors as minimal as possible, complete accuracy is not ever attained.

1. **Gross errors**

   Gross errors are due to blunders, usually caused by equipment failure or by power failure. Gross errors result in the immediate rejection of measurement (Bezinger & Aksay, 1999).

2. **Systematic errors**

   Systematic errors are due to constant bias in experimental measurement and these errors are usually caused by known conditions (Bezinger & Aksay, 1999), such as natural, instrumental and/or operator.

   - Instrumental, e.g., calibration not being done or done incorrectly, utilising flasks that are not graduated.
   - Natural, e.g., not considering temperatures, pressures and humidity level.
   - Operator or laboratory operator, e.g., poor sight, incorrect reading of measurement, not repeating experiment for precision and not cleaning equipment after use to avoid contamination in future use (Barry, 1991)

3. **Random errors**

   Random errors are errors that are due to inconsistencies in readings, which may occur by repeating measurements not taken in the same way, minor variations in readings being overlooked and carried over and, in the end, following no systematic trend (Bezinger & Aksay, 1999; Barry, 1991).

Uncertainty analysis

The camera, fixed on the tripod and situated 1.47 meters from the tank, captured the water flowing out through the orifice. The number of frames taken to track the fluid's movement from one location to another was employed to determine the displacement height. For every decrease in the water level, the height difference measured was 0.01; thus, the parallax error from the captured camera frames for each height was computed using a trigonometric tangent formula. Each recorded height had a deviation of ± 0.39 degrees.

$$\tan^{-1} = \left[\frac{\text{height difference}}{\text{distance from camera to tank}}\right]$$

$$\tan^{-1} = \left[\frac{0.01}{1.47}\right]$$

$= 0.39^{0}$

Therefore, each measurement that was read by frames was out by ± 0.39°.

Figure 3.23: Presented in this figure is the standard/reference C_d values, load cell C_d values and the camera method C_d values. This is to show how the standard Cd value can be compared to the data in this study and determine the error of the data to the standardized C_d values

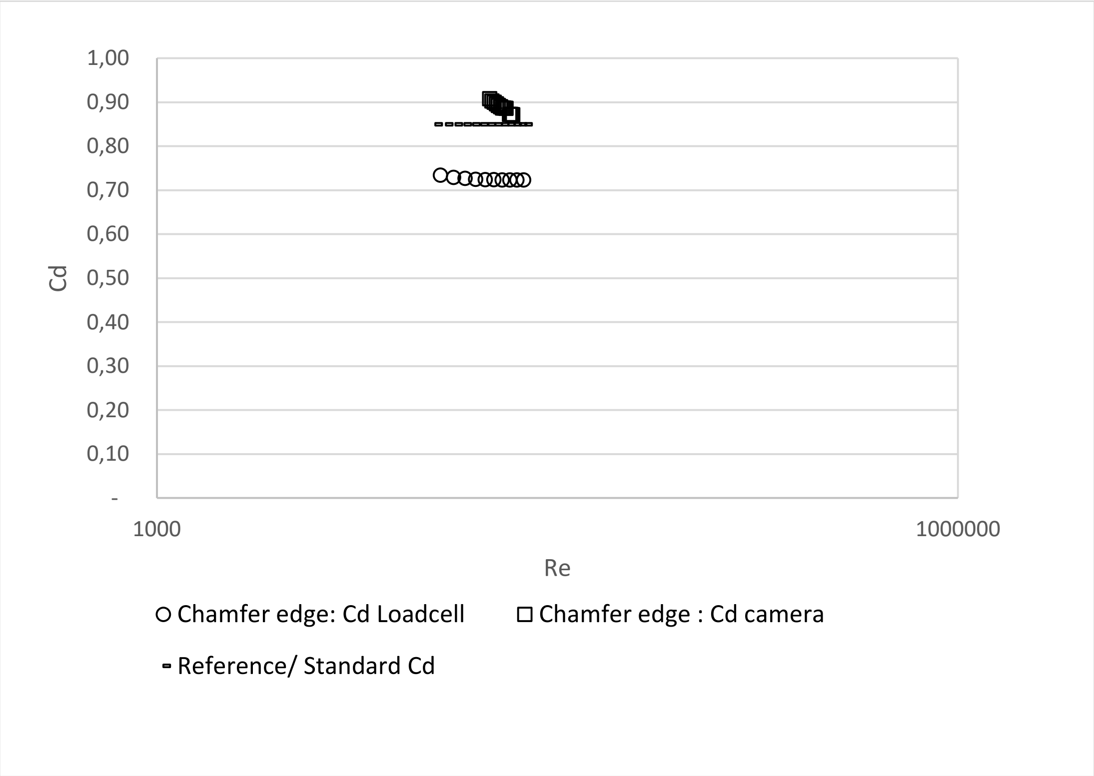

Figure 3.23: Chamfer standard/reference C_d values, load cell C_d values and the camera method C_d values.

The error (E) is determined by subtracting the $C_{d\ Av}$ determined through the camera(C) from the standard / referenced Cd value and (S)dividing by the sum.

∴ E =(S-C)/S

Under calibration the standard/ value are plotted showing the deviation of the results from the standard values. The error is at 0.14,under heading 3.72 on page 58 table 3.2 presents the ranges of the standard/reference C_d values, load cell C_d values and the camera method C_d values.

Table 3.3:The error % for each orifice tetsed

Orifice edge	Error
Chamfer	0,14
Quadrant	0.06
Short square	0.05
Square edge bevel back cut	0.045

3.11 Conclusion

The flow process research centre laboratory (slurry lab) was utilised to conduct all the experimental work. The testing equipment was the tank rig. Testing procedures, equipment and material utilised for this study were described.

The orifices used for the study of different edge geometries were chamfer-edged, short square-edges, quadrant-edged and square-edge dwith bevel back. The average C_d values for the different edge geometry were 0.85 for chamfer-edged and quadrant-edged, 0.58 for short square-edged, and 0.60 for square-edged with bevel back.

A MCR300 paar-physica rheometer was used to measure the rheological properties of all the slurries made for the study. The slurries were composed of various concentrations of glycerine and CMC solutions, kaolin and bentonite suspensions. Procedures used in obtaining rheological parameters were discussed.

CHAPTER 4 RESULTS AND ANALYSIS

4.1 Introduction

This chapter presents the experimental results and analysis. The goal was to measure the flow rate and determine the discharge coefficient of various Newtonian and non-Newtonian liquids flowing from a tank through orifices with different exit edge geometries.

The findings include measurements of density, rheology, and flow rate. Water tests were conducted to calibrate the equipment. As reported by Khahledi et al. (2019), Khahledi et al. (2020), and Mohajane (2020), they followed a specific procedure for assessing their orifices: for each edge geometry of the orifice, the Reynolds number was determined based on the flow velocity, flow rate, orifice diameter, and rheological properties. The study examined three flow regimes: laminar, the transition from laminar to turbulent, and fully turbulent flow.

The results were as follows:

- Relative density determinations and rheological characteristics of Newtonian and non-Newtonian liquids.
- Presentation of C_d vs Re plots for chamfer-edged, quadrant-edged, short square-edged, and square-edged with bevel back.

Table 4.1 illustrates the rheological characteristics of Newtonian and non-Newtonian materials used in the testing.

4.2 Rheological characteristics

The rheological parameters of the liquids tested are provided in Table 4.1

Table 4.1: The rheological characteristics of liquids tested

Liquids	Con.	Density	Temperature	μ			Shear rate (γ)
	%	kg/m^3	℃	Pa.s			s^{-1}
		Newtonian					
Glycerine	100	1276	24.5	0.867			322.01–1181.31
	96	1248	19	0.153			280.48–1102.52
	93	1241	18	0.138			255.09–1134.08
	90	1234	25	0.077			1083.60–1908.89
	85	1200	23	0.055			966.15–1771.49
	76	1202	14	0.022			1028.56–1955.69
	47	1136	21	0.0073			4.26*10^–12–8.33*10^–12
	37	1130	21	0.005			4.04*10^–12–7.51*10^–12
		Non-Newtonian					
				Rheological properties			
				k	n	τy	Shear rate range
CMC w/w				Pa.s^n		Pa	s^{-1}
	6.6	1037	17	2.406	0.593	-	1106.07 – 2023.87
	5.9	1033	17	0.932	0.662	-	1226.57 – 2063.86
	4.8	1027	17	0.172	0.831	-	882.83 – 1767.73
	3.8	1021	17	0.0587	0.859	-	837.09 – 1946.17
	2.4	1014	17	0.013	0.944	-	940.36 – 1946.78
Kaolin v/v							
	19	1310	17	1.295	0.440	26.291	1162.73 – 2149.71
	15	1246	17	0.133	0.664	12.845	1095.04 – 2217.80
	12	1193	16	0,055	0.731	0.55	1071.19 – 2318.11

	9	1149	16	0.013	0.885	2.435	1162.73 – 2149.71
Bentonite w/w							
	6	1037	20	0.0172	1	7.040	942.37 – 1271.88
	5.4	1033	20	0.013	1	2.827	949.39–1908.71
	3.6	1022	20	0.007	1	0.186	898.28–1920.35

4.2.1. Newtonian liquid: Glycerine

In this experiment, Newtonian liquids used were water and glycerine. The rheological properties for glycerine at concentrations from 100% to 37% are shown in a flow curve in Figure 4.1. The graph displays a shear rate versus shear stress plot: shear stress increases linearly with shear rate, with the slope representing viscosity. A higher viscosity results in a steeper slope. The shear rate ranged from 0.01 to 1,000 s-1. It is important to note that viscosity was measured at the test temperature.

$\tau=\mu\,\dot{\gamma}$ Equation (2.6)

Figure 4.1 presents flow curves obtained in the determination of rheological parameters of glycerine solutions.

Flow curve: Glycerine solutions at different concentrations (100– 37) %

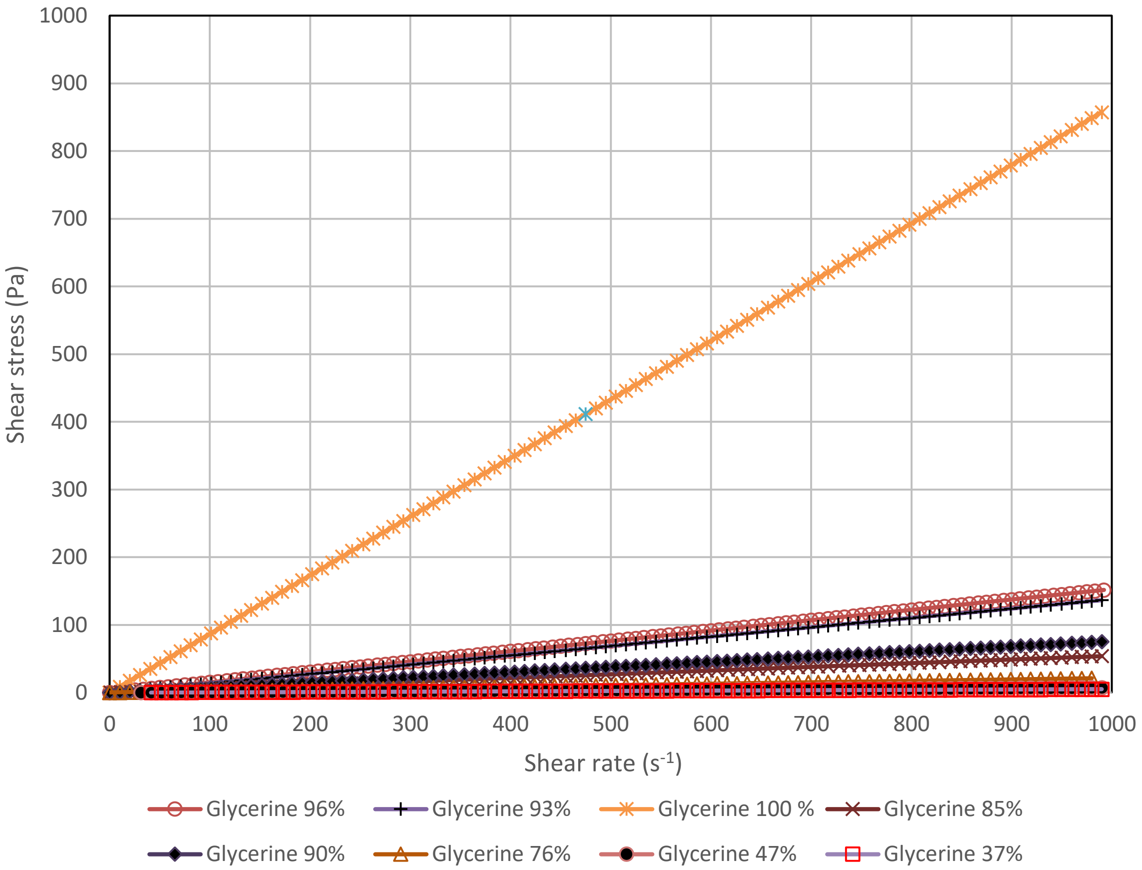

Figure 4.1: Flow curves for glycerine

4.2.2 Non-Newtonian liquid: CMC

CMC solutions were prepared and tested. Concentrations ranging from 6.6 to 2.4 were tested. A pseudo shear curve for CMC concentration by mass were 6.6%, 5.9%, 4.8%, 3.8%, and 2.4 % . This is presented in Figure 4.2

Pseudoplastic liquids have an apparent viscosity, and this apparent viscosity decreases with increasing shear rate. It is observed in Figure 4.2 that the slope of the curve becomes smaller as the shear rate increases. Shear-thinning liquids use the Power Law model, and the following equation is applicable:

$$\tau = K(\dot{\boldsymbol{\gamma}})^n \qquad \text{Equation (2.2)}$$

The shear stress (τ) is equal to the consistency index (K) multiplied by the shear rate ($\dot{\gamma}$) to the power of (n) flow behaviour index

A non-linear relationship is observed, and this is due to the shear thinning behaviour that the liquid undergoes; The (n) at 2.4% is approximately equal to 1(n $\neq$ 1 for pseudoplastic liquids, as the viscosity of these liquids tends to decrease with increasing shear rate; when n=1, the liquid behaves like a Newtonian liquid, i.e., the viscosity of the liquid remains constant.

Figure 4.2 demonstrates shear thinning behaviour and the shear rate range was from 0.01–1000 s^{-1}.

Flow curve: CMC solutions at different concentrations (6.6 – 2.4) %

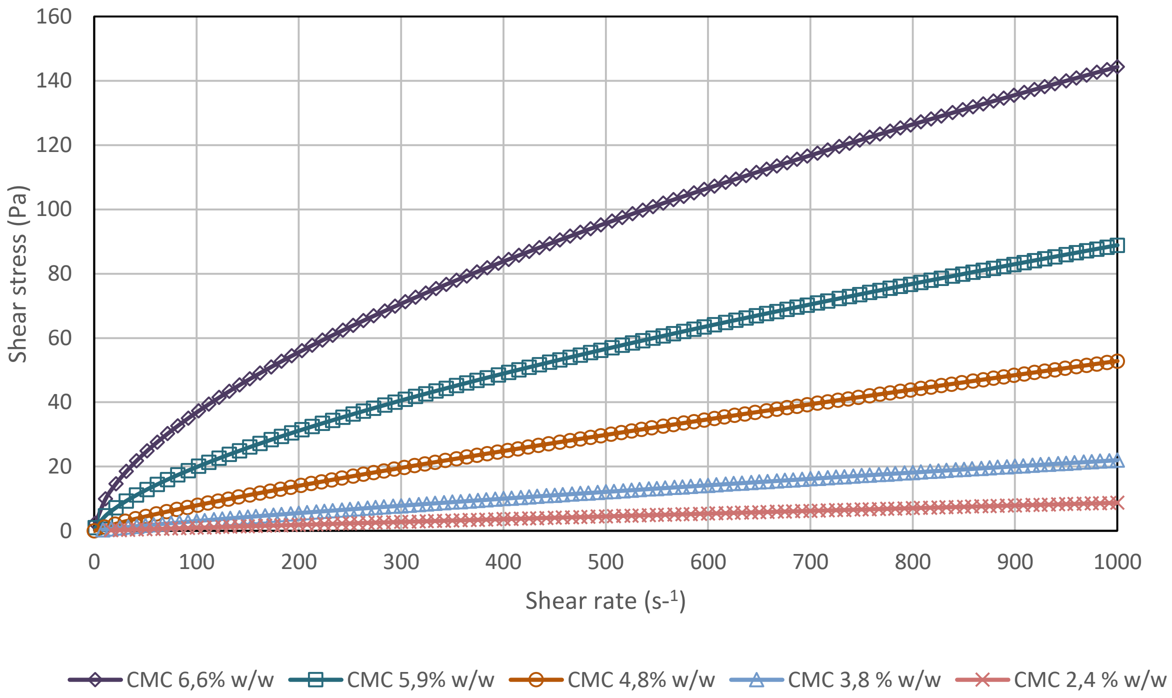

Figure 4.2: Pseudo shear curve fitting for CMC solutions

4.2.3 Non-Newtonian liquid: Kaolin

Kaolin suspensions were prepared and tested separately in four concentrations. Figure 4.3. Showcases the pseudo shear diagram for 19%, 15%, 12% and 9%.

Equation 2.5 was applied in the determination of rheological parameters for kaolin suspensions.

$$\tau = \tau y + K(\dot{\gamma})^n \qquad \text{Equation (2.5)}$$

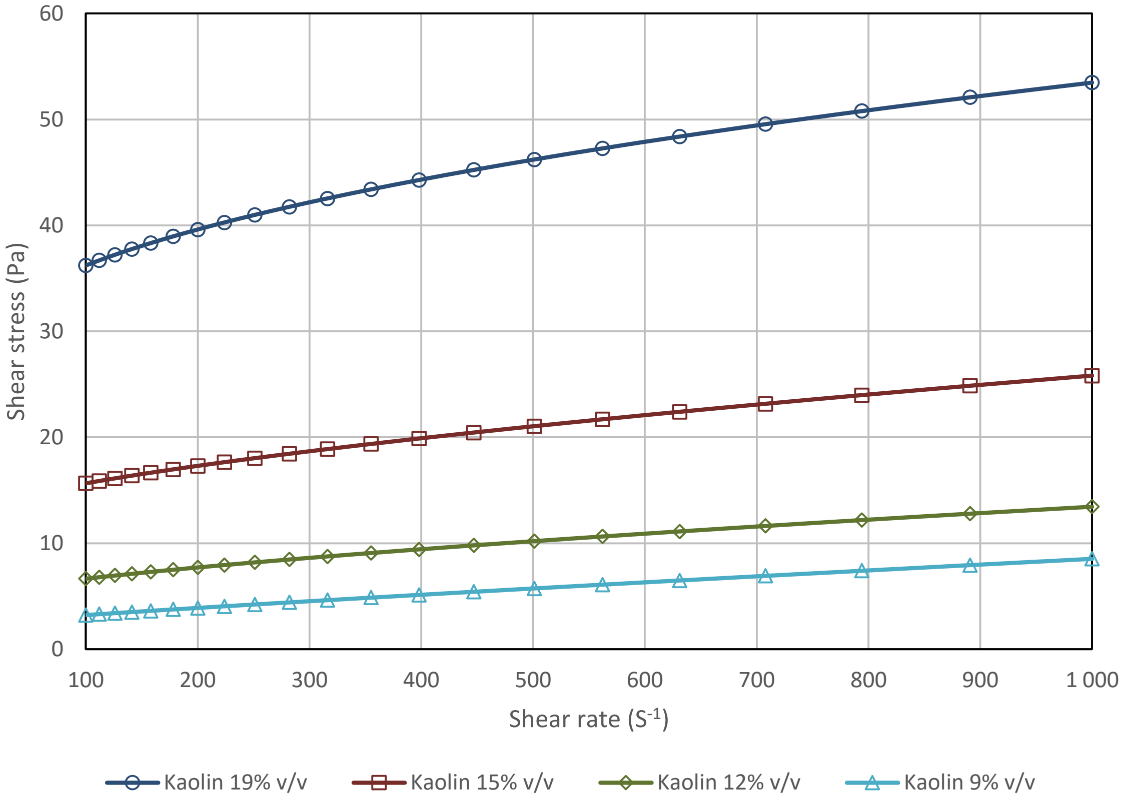

Figure 4.3: Pseudo shear diagram for kaolin suspension

4.2.4 Bentonite

Three bentonite concentrations were prepared and tested 6%, 5.4% and 3.6% (w/w) and Figure 4.4 illustrates the pseudo shear diagram. It was noticed that, for the bentonite and kaolin suspensions, the shear rate range was from 100–1000 s^{-1} because results lower than 100 S^{-1} were not stable.

Bingham plastic equation was utilised for bentonite suspensions in Equation 2.4.

$\tau = \tau y + (\dot{\gamma})$ Equation (2.4)

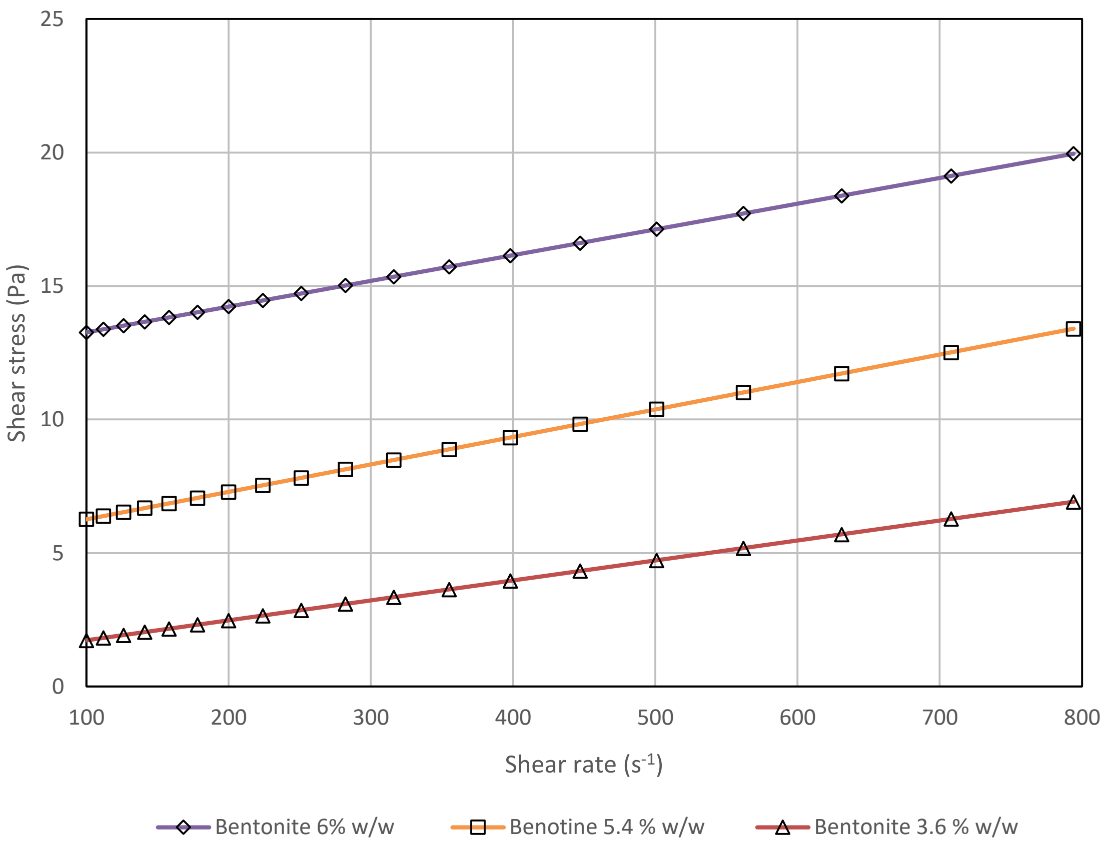

Figure 4.4: Bentonite pseudo shear curves

4.3 C_d vs Re plots for chamfer, quadrant, short square, and square bevel back cut edge orifices.

This section involves graphical representation of the C_d and Re values obtained for glycerine and CMC solutions, inclusive of kaolin and bentonite suspensions. The Re ranges in the laminar, transition and turbulent flow regions are tabulated in Table 4.2 and 4.3 for chamfer- and quadrant edge orifices.

Table 4.2: Flow region for chamfer-edge orifice (Re and Re_2)

Chamfer - edged orifice	Flow region	Glycerine	CMC	Kaolin	Bentonite
	Laminar	$21 < Re < 100$	$100 < Re_2 < 300$	$300 < Re_2 < 800$	$500 < Re_2 < 1000$
	Transition	$100 < Re < 2000$	$300 < Re_2 < 2000$	$800 < Re_2 < 2000$	$1000 < Re_2 < 2000$
	Turbulent	$24000 < Re$	$7000 < Re_2$	$2300 < Re_2$	$4200 < Re_2$

Table 4.3: Flow region for quadrant edge orifice (Re and Re_2)

Quadrant - edged orifice	Flow region	Glycerine	CMC	Kaolin	Bentonite
	Laminar	$19 < Re < 100$	$100 < Re_2 < 300$	$300 < Re_2 < 800$	$500 < Re_2 < 1000$
	Transition	$100 < Re < 2000$	$300 < Re_2 < 2000$	$800 < Re_2 < 2000$	$1000 < Re_2 < 2000$
	Turbulent	$24000 < Re$	$7000 < Re_2$	$2300 < Re_2$	$4200 < Re_2$

Figures 4.5 to 4.8 are C_d vs Re curves for all tested liquids (Newtonian and non- Newtonian: Power Law, Herschel Bulkley and Bingham plastic) combined for each orifice: chamfer, quadrant, short square and square bevel back cut edge orifices. The curves demonstrate for each edge the diferent flow regions at different concentrations of the liquids tested.

Figure 4.6 shows the curves produced from the chamfer edges orifice for concentrations tested for 100%–37 % glycerine, 5.9 % CMC, 19% kaolin, and 3.6 % bentonite.

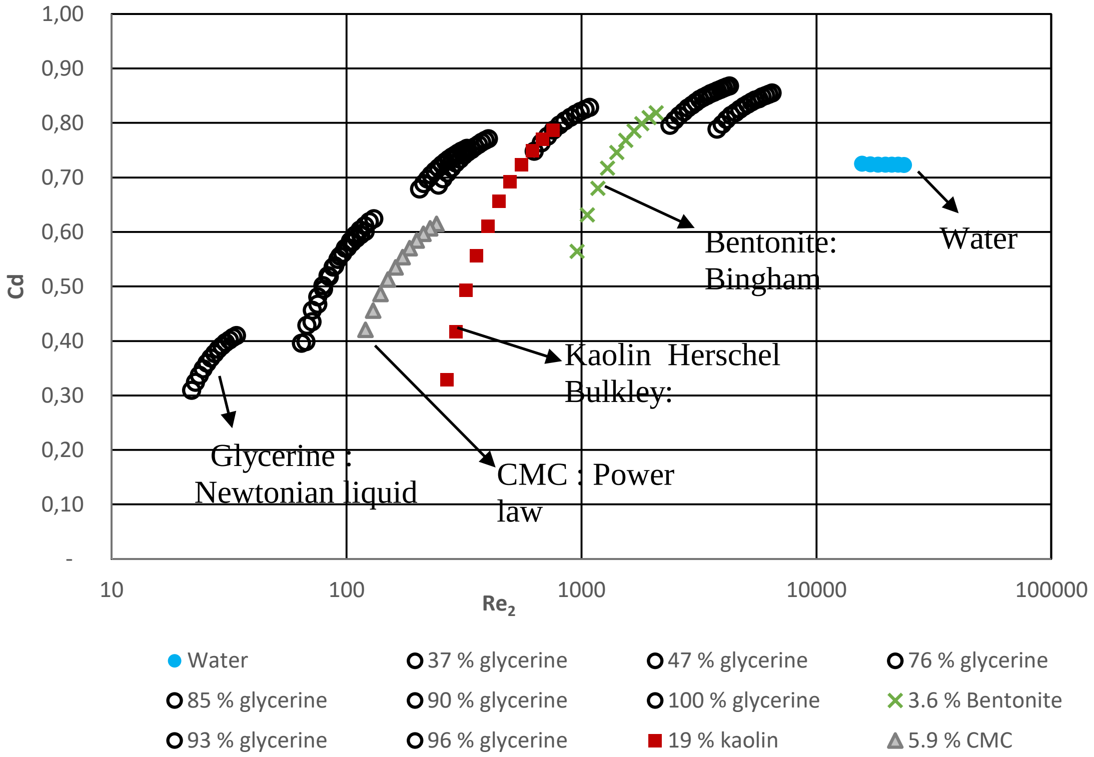

Figure 4.5: Coefficient of discharge vs Reynolds number for glycerine: Newtonian; CMC: Power Law; kaolin: Hershel Bulkley and bentonite: Bingham plastic for chamfer edged orifice

Figure 4.6 shows the curves produced from the quadrant edges orifice for concentrations tested for 100–37 % glycerine, 5.9 % CMC, 19% kaolin, and 3.6 % bentonite.

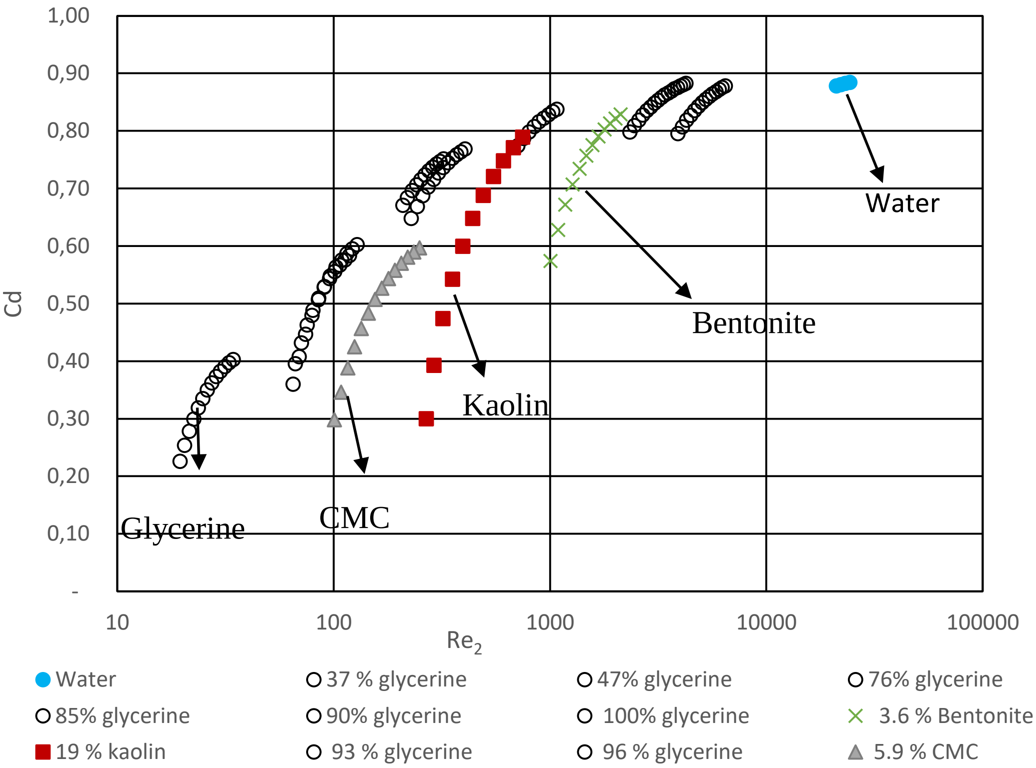

Figure 4.6: Coefficient of discharge vs Reynolds number for glycerine: Newtonian; CMC: Power Law; kaolin: Hershel Bulkley and bentonite: Bingham plastic for quadrant-edged orifice

Table 4.4 and Table 4.5 show the Re ranges for short square and square with bevel back cut for all tested liquids: Newtonian and non-Newtonian: Power Law, Herschel Bulkley and Bingham plastic (Glycerine, CMC, kaolin and bentonite) Glycerine: Re; 20,100 and 24,000, CMC: Re_2; 100 and 300 kaolin: Re_2; 300 and 700 and bentonite: Re_2; 500, for laminar, transition and turbulent, respectively.

Table 4.4: Flow region for short square-edged orifice (Re and Re_2)

Short square-edged orifice	Flow region	Glycerine	CMC	Kaolin	Bentonite
	Laminar	$20 < Re < 100$	$100 < Re_2 < 200$	$300 < Re_2 < 800$	$700 < Re_2 < 1000$
	Transition	$100 < Re < 2000$	$200 < Re_2 < 2000$	$800 < Re_2 < 2000$	$1000 < Re_2 < 2000$
	Turbulent	$24000 < Re$	$7000 < Re_2$	$2300 < Re_2$	$4200 < Re_2$

Table 4.5: Flow region for square orifice with bevel back cut (Re and Re_2)

Square belvel back cut orifice	Flow region	Glycerine	CMC	Kaolin	Bentonite
	Laminar	$20 < Re < 100$	$100 < Re_2 < 200$	$300 < Re_2 < 800$	$700 < Re_2 < 1000$
	Transition	$100 < Re < 2000$	$200 < Re_2 < 2000$	$800 < Re_2 < 2000$	$1000 < Re_2 < 2000$
	Turbulent	$24000 < Re$	$7000 < Re_2$	$2300 < Re_2$	$4200 < Re_2$

Figure 4.7 shows the curves produced from the short square edges orifice for concentrations tested of 100–37 % glycerine, 5.9 % CMC, 19% kaolin, and 3.6 % bentonite.

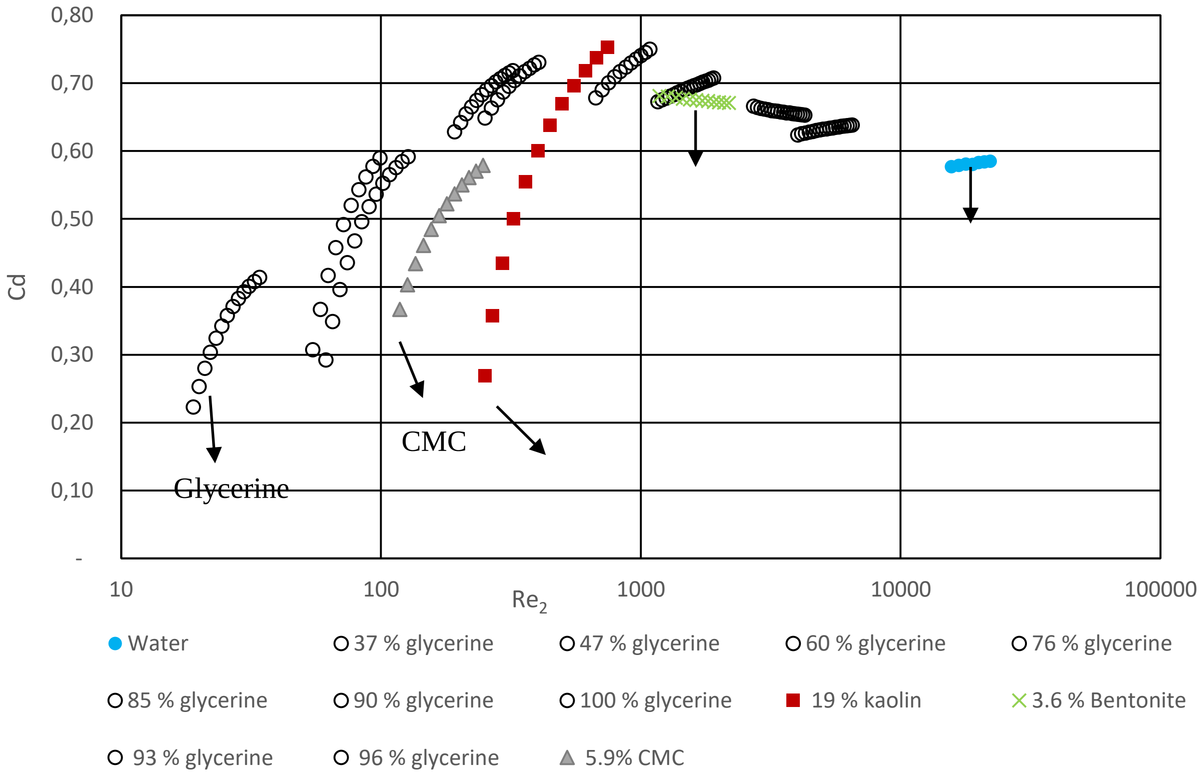

Figure 4.7: Coefficient of discharge vs Reynolds number for glycerine: Newtonian; CMC: Power Law; kaolin: Hershel Bulkley and bentonite: Bingham plastic for short square-edged orifice

Figure 4.8 shows the curves produced from the square bevel back cut edges orifice for concentrations tested of 100–37 % glycerine, 5.9 % CMC, 19% kaolin, and 3.6 % bentonite

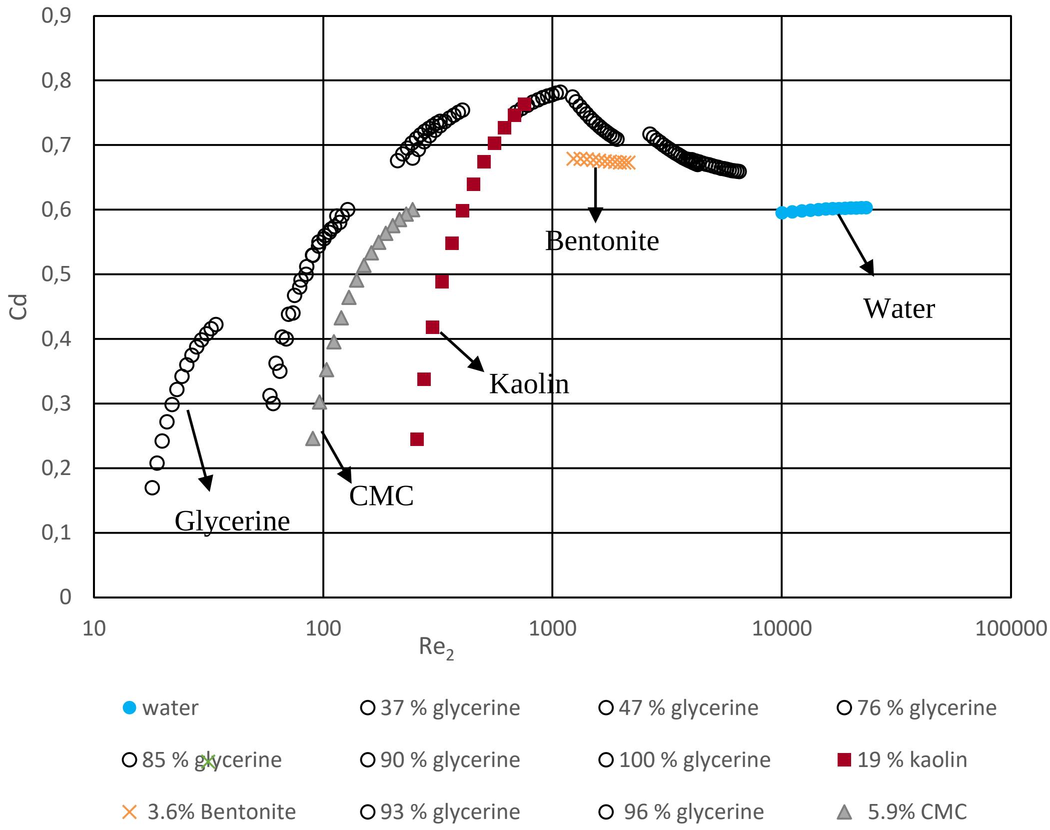

Figure 4.8: Coefficient of discharge vs Reynolds number for glycerine: Newtonian; CMC: Power Law; kaolin: Hershel Bulkley and bentonite: Bingham plastic for quare orifice with bevel back edge

4.4 C_d vs Re plotted with tested liquids both Newtonian and non-Newtonian

4.4.1 Chamfer-edged orifice

Chamfer-edged can be discussed along with a circular orifice as it exhibits certain traits that are common. The geometry is noticed and more defined at the edge, which is more like a funnel and the liquid being discharged is initially observed to show traits of a vena-contracta before smooth flow is observed. An average C_d value of 0.88 is observed in Figure 4.9.

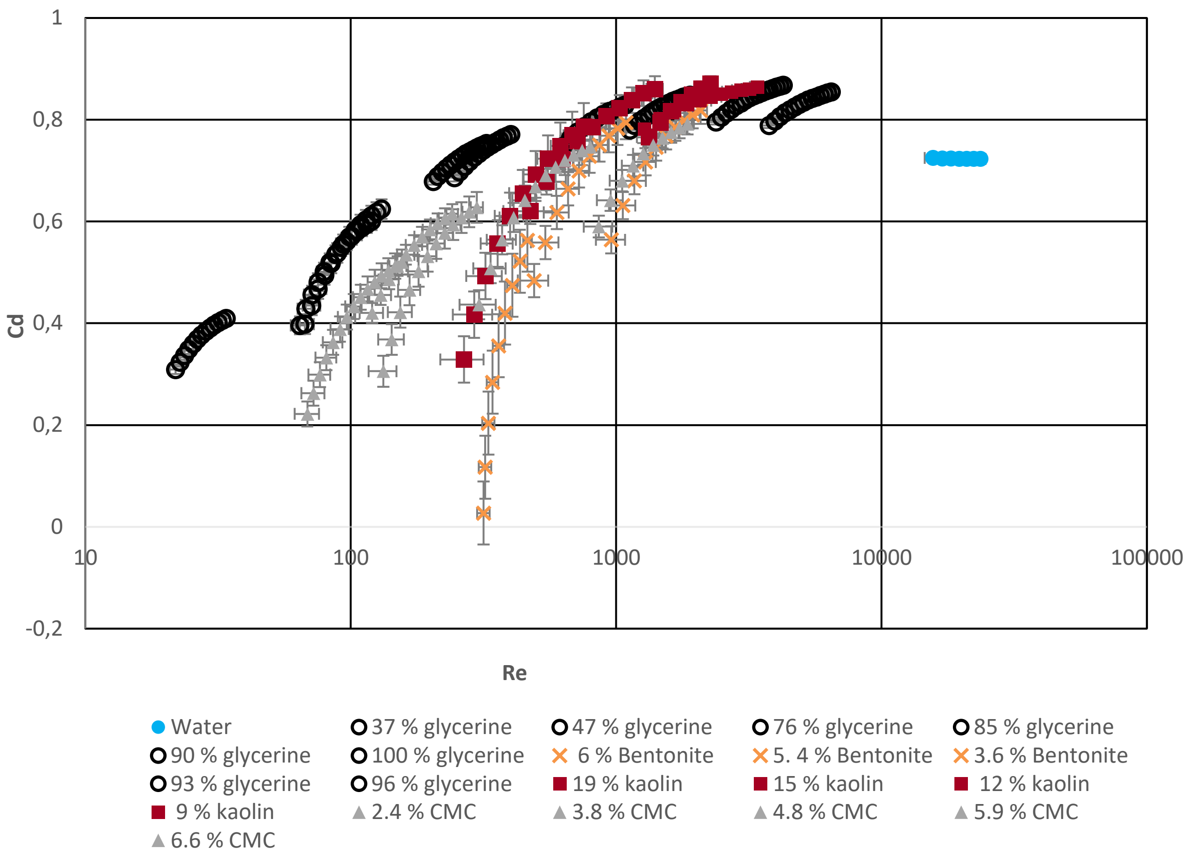

Figure 4.9: C_d vs Re plotted with tested liquids; Newtonian and non-Newtonian liquids chamfer- edged

4.4.2 Quadrant-edged orifice

Figure 4.10 showcases the findings for quadrant edge orifice upon discharging of Newtonian and non-Newtonian liquids. The C_d to Re relationship is not that different from the chamfer edged orifice. C_d values increase with the increase in Re values and gradually become constant as the flow becomes turbulent. An average Cd value of 0.90 is observed from Figure 4.10.

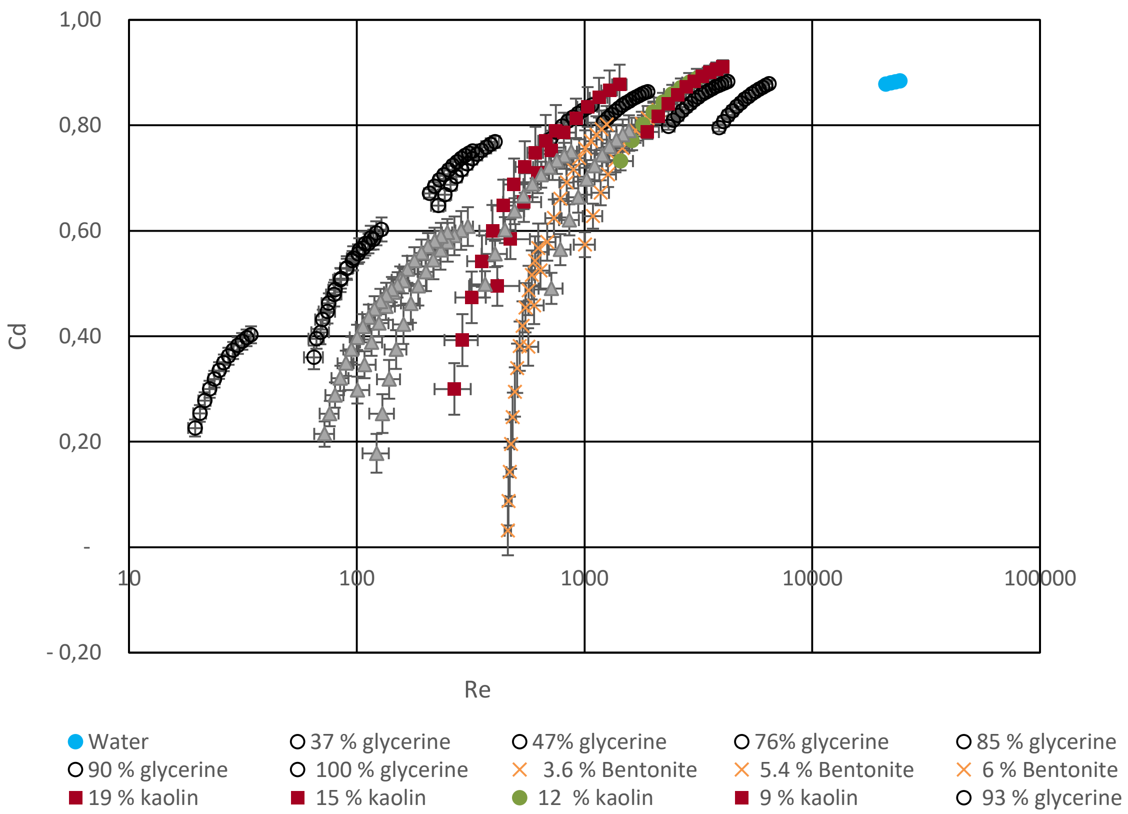

Figure 4.10: C_d vs Re plotted with tested liquids; Newtonian and non-Newtonian liquids quadrant-edged

4.4.3 Short square-edged orifice

Figure 4.11 displays all the C_d vs Re values for both Newtonian and non-Newtonian liquids. It can be observed in Figure 4.12 that short square-edged orifice results in a C_d value of 0.78 in the transition regions for kaolin as the highest discharge and a C_d value of 0.59–0.61 for water.

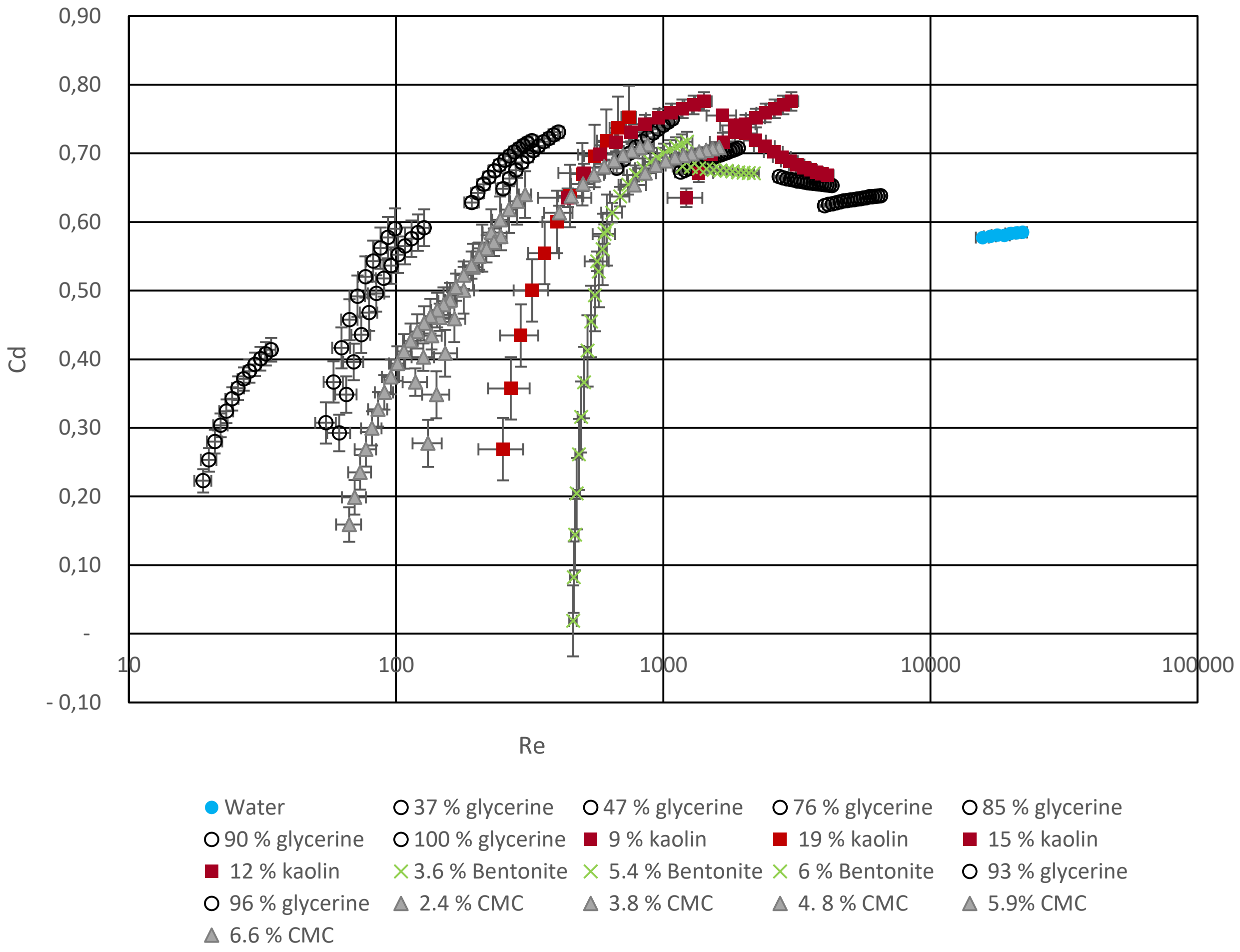

Figure 4.11: C_d vs Re plotted with tested liquids; Newtonian and non-Newtonian liquids short square-edged orifice

4.4.4 Square orifice with bevel back edge

Figure 4.12 displays, that from the transition to turbulent flow regions of non-Newtonian liquids (CMC, kaolin and bentonite), there was an interesting observation made at Re = 1000 Where the C_d values ranging from 0.62–0.81 are clustered altogether, the highest C_d that square with bevel back cut produced was 0.81 and this is noticed to be for 12% kaolin. The C_d value for water is constant at 0.61.

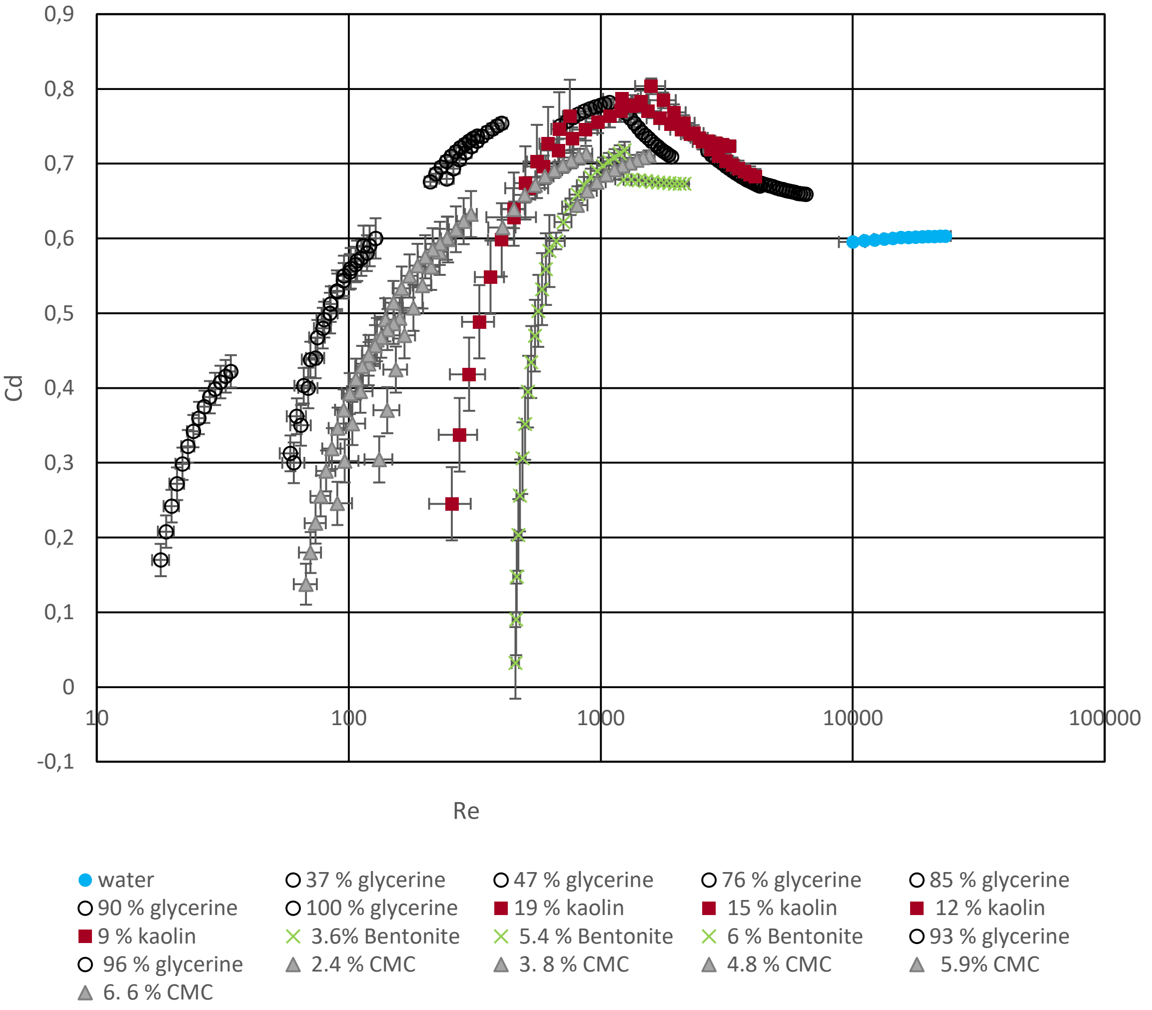

Figure 4.12: C_d vs Re plotted with tested liquids; Newtonian and non-Newtonian liquids square orifice with bevel back edge

It was observed that the influence of the orifice edge experience a separation and reattachment of the liquid before and after at the orifice area. The sharpness of the orifice edge directly effects the location, size and intensity of the vena contracta and the extent of the flow separation. As when the liquid is approaching the orifice the streamlines must curve inwards to pass through the opening of the orifice

Figure 4. 13 demonstrates the ratio of the area of the jet at the vena contracta to the area of the orifice opening. It quantifies how much the flow cross-section contracts.Separation /reattachment is the flow behaviours around the vena contracta particularly in sudden suction. occurs at the upstream edge of the contraction where the liquids detaches from the surface forming a recirculation zone.

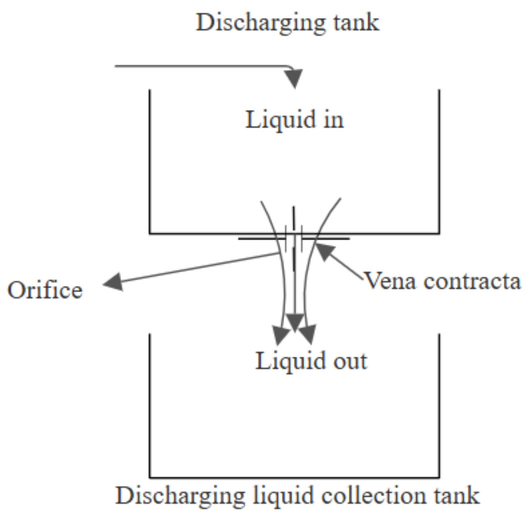

Figure 4.13: The vena contracta in tank discharge

4.5 Conclusion

This chapter presented the results of chamfer-edged orifice, quadrant-edged orifice, short square-edged orifice and square-edged with bevel back discharge coefficients for various concentrations of Newtonian and non-Newtonian liquids. Rheological characteristics (shear stresses and shear rate from the shear diagram) were demonstrated to determine rheological parameters (viscosity, flow behaviour index, fluid consistency and yield stress) to be able to calculate the appreciated Re of the slurry passing the orifice.

Flow regions for each orifice edge geometry, rheological properties, Power Law pseudoplastic and yield pseudoplastic modules were utilised to characterise these liquids. Measuring flow rates of Newtonian and non-Newtonian liquids required rheological parameters and this was possible using the rheometer. The C_d values in relation to the Reynolds numbers were determined and the relationship showed traits whereby as the Re values increased, the $C_d$values altogether increased from laminar to transition. As the liquids become less and less viscous where Re values are between 2500 and 3000 the C_d value gradually become constant for all the edges. Wheras the plateauing of C_d values in turbulence flow suggest that the flow is stable with reliable discharge behavior and informs the design choice to favour turbulent flow conditions for better orifice performance and measurement.

In short, the ratio of the area of the jet at the vena contracta to the area of the orifice opening quantifies how much the flow cross-section contracts. This in turn results in a separation /reattachment flow behaviour around the vena contracta at the upstream edge of the contraction where the liquids detaches from the surface and forms a recirculation zone.

CHAPTER 5 DISCUSSION OF RESULTS

5.1 Introduction

This section discusses the results produced in Chapter 4, the data evaluated, and the aim and objectives. The objective of this study is to measure the effect of orifice geometry for flow of Newtonian and non-Newtonian liquids and to determine the relationship between discharge coefficients and the Re of viscous Newtonian and non-Newtonian liquids.

Discharge coefficients of four different orifice geometries: a set of square-edged orifices, short square-edged orifice and square-edged with bevel back cut angle orifice together with a quadrant-edged orifice and a chamfered edge orifice were evaluated. The water results compared with studies conducted by Khahledi et al. (2019; 2020), Mohajane (2020) and Dziubinski and Marcinkowski (2006).

The following are highlighted in this discussion:

- Calibrated results of water
- The effect of orifice geometry on the discharge coefficient for all tested liquids
- The discharge coefficient as a function of the Re for Newtonian and non-Newtonian liquids discharging from a tank for the following orifice edge geometries: chamfer-edged, quadrant-edged, short square-edged and square-edged with bevel angle with back cut.

5.2 Calibration results

Figure 5.1 shows the calibration results for each orifice geometry (chamfered edge, quadrant-edged, short square-edged and square-edged with bevel back cut angle) related to the generalised or standard c_d values in literature. Water results of Dziubinski and Marcinkowski (2006) for sharp edge geometry orifices; of Khahledi et al. (2020) for sharp crested square shape and circular shape and standard c_d value for sharp edge orifice are presented in the figure inclusive of the water results for the current study.

Figure 5.1 demonstrates that the C_d values for square edge orifices are in accordance with literature, and that chamfer- and quadrant- edged orifices show C_d values that are more or less similar.The reference to C_d values are to comfirm and show how minimal the error margins are.

The discharge coefficient of an orifice indicates the efficiency of the flowmeter (orifice). Standard values or reference values exist for orifices, particularly for water. However, the variation is that C_d values of orifices are attributed to geometerical parameters of the orifice which, in turn, impact the flow of liquids being discharged. This is evident in the results in Figure 5.1.

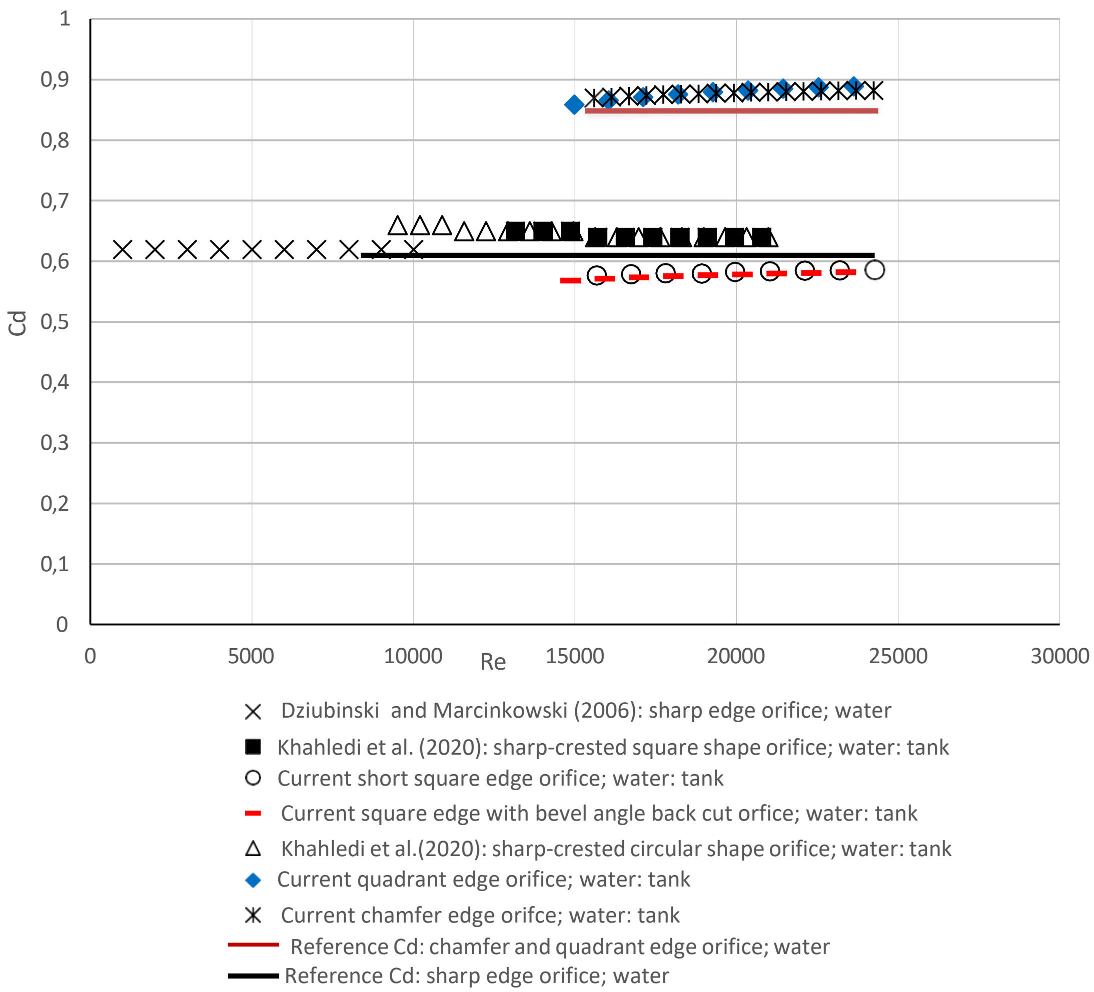

Figure 5.1: C_d vs Re curves for water discharge: the current study, reference and work conducted by Khahledi et al. (2020) and Dziubinski and Marcinkowski (2006) for different edge orifices

5.2.1 Standard C_d values discussed alongside with the C_d values of current study

Table 5.1 shows the C_d values and the Re range and/region for orifices of common diameter (8mm) and common discharge operation (tank) for sharp edge by Dziubinski and

Marcinkowski (2006) and sharp crested square and circular shape by Khahledi et al. (2020). Square-edged with bevel back cut angle are compared with the standard (square) sharp edge C_d values.

The standard C_d values available in literature for chamfer-edged and quadrant-edged are included together in the table, along with water C_d values of the current study of chamfer-edged and quadrant-edged orifices.

The average discharge coefficient (C_d) values available in literature of water results by Dziubinski and Marcinkowski (2006) for sharp edge geometry orifices give the average C_d value= 0.62. The standard C_d value for sharp edge orifice geometry in literature are from 0.6–0.80. These C_d values are compared to water results obtained for each orifice geometry in the current study for square-edged orifices, inclusive of water tests obtained from Khahledi et al. (2020). The standard C_d value for chamfer and rounded/quadrant-edged is in the range of = 0.8–0.85 in the turbulent regimes (Baillio,2003) . In the current study, chamfer-edged geometry average C_d value = 0.88 and for quadrant-edged geometry the average C_d value = 0.84. However, the current study of short square-edged and square-edged with bevel angle back cut produced the average C_d value = 0.57–0.60

Table 5.1: C_d values and Re ranges: water for previous study and the current study

Study conducted by	Orifice geometry	Discharge operation	Diameter	Liquid	C_d value	Re range
Dziubinski and Marcinkowski (2006)	Sharp-edged	Tank	8mm	Water	0.62	1 000–10 000
Khahledi et al. (2020)	Sharp-crested: Square shape & circular	Tank	8mm	Water	0.64	10 882–20 979
Standard	Sharp edge	-	-	Water	0,60	Turbulent
Current study	Short square-edged and square-edged with bevel angle back cut	Tank	8mm	Water	0,57-0.60	14 860–23 379

Standard	Chamfer-and/ rounded edge	-	-	Water	0,85	Turbulent
Study conducted by	Orifice geometry	Discharge operation	Diameter	Liquid	Cd value	Re range
	(quadrant edge)					
Current study	Chamfer- and quadrant-edged	Tank	8mm	Water	0.82 and 0.88	14 980–24 243

There is still a gap in terms of data in the laminar flow regions for orifice edge goemetries such as chamfer, quadrant, short square and square bevel back cut edge, particularly in tanks. This research was initiated with the objective of evaluating the discharge coefficient with different edge orifice geometries : square short and bevel back as well as chamfer-edged (orifice with an edge that is at angle of 45°) and quadrant-edgde (orifice with a conical looking nozzle outlet). The discharge of these four different edge orifice geometries was determined utilising non-Newtonian liquids that exhibited the pseudoplastic Power Law, Herschel Bulkley and Bingham plastic rheological characteristic.

5.3 The effect of orifice geometry

The effect of orifice edge geometry on the discharge of highly viscous Newtonian liquids such as glycerine was evaluated. The glycerine diluted in to different concentrations of glycerol made the influence of edge geometry more visible at Re $>$ 400.

5.3.1 Effect of orifice geometry on Newtonian liquid: Glycerine solutions

In Figure 5.2, The effect of orifice edge geometry is demonstated for all tested orifices: chamfer, quadrant, short square and square bevel back cut edge orifice. The liquid of discharging is a highly viscous Newtonian liquid; glycerine and the soluions are of different concentrates ranging from 100% to 37%. It is noticed that the orifices show the same flow trend when discharging glycerine solution showed distinctive flow trends. Each orifice is observed and it is noticed that the chamfer and quadrant edge orifice portrait similar flow trends and resulted in higher C_d values for Re> 1000.

At the Reynold's numbers between 17< Re> 400 the C_d vs Re curves show logarthimic trend. It is only between Reynold's numbers ranging from 600< Re> 1000 that the chamfer and quadrant edge orifices begin to show more or less the same C_d values and the C_d values incease as the Re values increase. Whereas short square and square bevel back cut edge orifices not only shows similar traits but results in lower C_d values as the the liquid becomes less and less viscous and it can be speculated that the C_d values gradually become constant the higher the Re values.

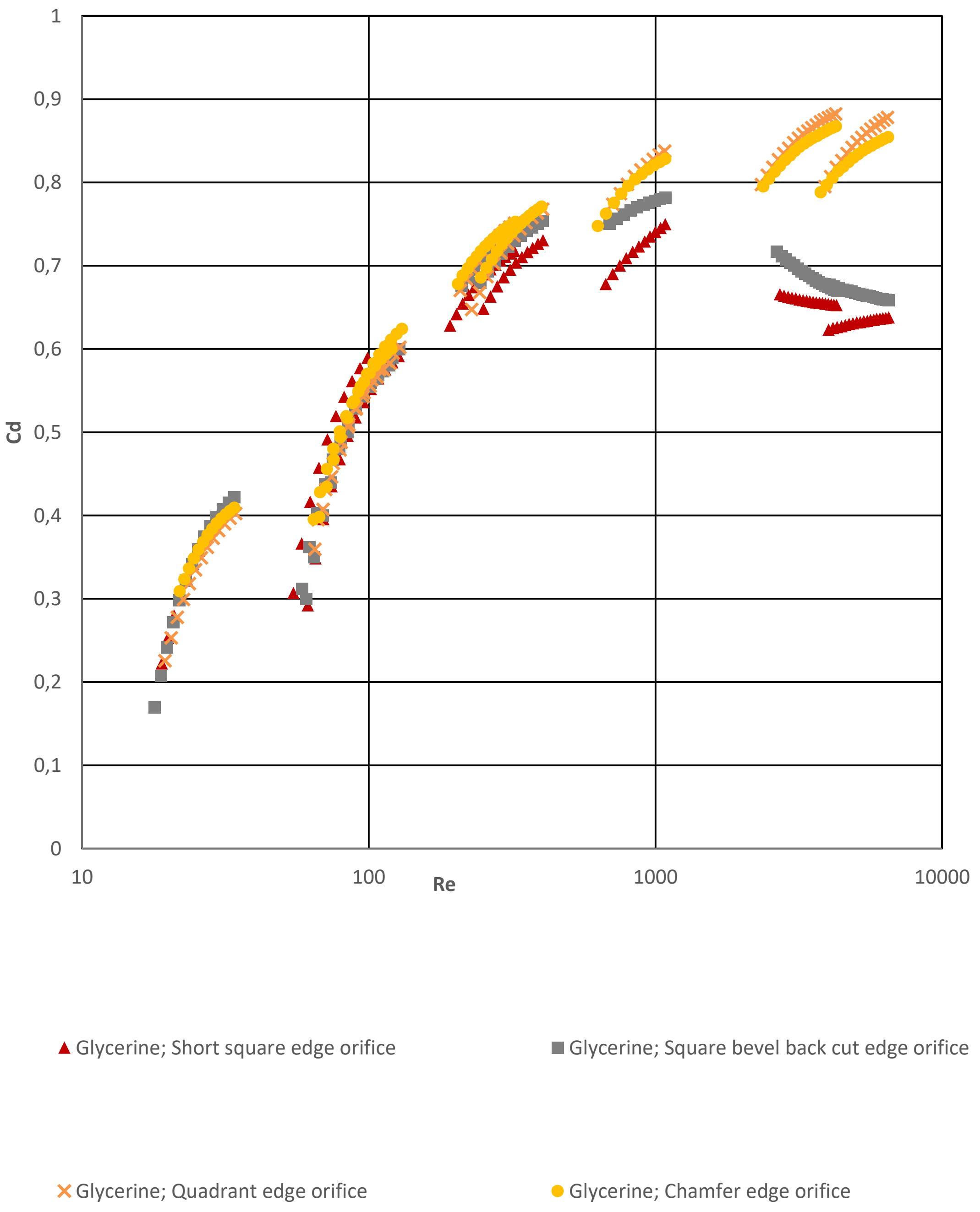

Figure 5.2: C_d vs Re for chamfer, quadrant,short square and square bevel back cut edge orifices discharging Newtonian liquids: glycerine solution from a in tank

5.4 Effect of orifice geometry: All liquids tested (Newtonian and non-Newtonian liquids)

The results obtained for the discharge of Newtonian liquids, particularly in the turbulent regions of water showed that the C_d values start off by being inconsistent before becoming constant. The C_d values are not that far from the values observed in literature. Care was taken not to compare, as the methodology was not the same in most of the cases. The effect of orifice geometry is not actually concerned with the shape of the orifice but more with the edge shape or outer edging shape of the orifice. Khahledi et al. (2020) have studied the effect of orifice shape (circular, square and triangular) on the discharge of Newtonian and non-Newtonian liquids from a tank. The authors conclude in the discussion that, for equal hydraulic diameters, there was no significant difference in the C_d values. For higher concentration liquids such as non-Newtonian and highly viscous liquids like glycerine, the orifice shape does not have an effect.

For the current research, we see that there is an effect. Figure 5.3 is an illustration of the chamfer-edged orifice, where it is noticed that, between Re of 100 and 3400 is where non-Newtonian liquids accumulate. The results obtained for all the orifice geometry explored showed that the C_d increased as the Re increased but from Re of 1000 the C_d increased significantly before decreasing and becoming constant as the Re got higher.

Table 5.2 is an overview of the C_d value obtained for all the liquids tested. In this table all three regions are examined and the C_d value ranges are presented. The orifices are discussed in two parts: the chamfer-edged and quadrant-edged are discussed together, since they demonstrated similar traits in their flow behaviours. This may be because they both have the appearance of a nozzle at the edge, even though the quadrant-edged has a more rounded edge appearance. In the laminar regions their C_d values ranged between 0.3 and 0.5 for glycerine solutions with concentrations of 100, 96, 93, 90, 85, 75, 47 and 37, respectively. Short square-edged and square-edged with bevel back cut angle: their C_d values ranged between 0.3 and 0.4 for glycerine solutions of concentrations of 100, 96, 93, 90, 85, 75, 47 and 37, respctively. Chamfer and quadrant-edged resulted in C_d values ranged between 0.2 and 0.5 for CMC solutions with concentrations of 6.6, 5.9, 4.8, 3.8, and 2.4, respectively. Short square-edgde and square-edged with bevel back cut angle resulted in C_d values ranged from 0.2–0.5 for CMC solutions with concentrations of 6.6, 5.9, 4.8, 3.8, and 2.4, respectively. Chamfer and quadrant-edged resulted in C_d values ranged between 0.6 and 0.8 for Kaolin suspensions of 19, 15, 12, and 9 concentrations. Short square-edged and square-edged with bevel back cut angle resulted in C_d

values ranged from 0.5–0.7 for Kaolin suspensions of 19, 15, 12, and 9 concentrations. Chamfer and quadrant-edged resulted in C_d values ranged between 0.3 and 0.7 for Bentonite suspensions of 6, 5.4, and 3.6 concentrations. Short square-edged and square-edged with bevel back cut angle resulted in C_d values ranged from 0.3–0.7 for Bentonite suspensions of 6, 5.4, and 3.6 concentrations. This was repeated for the transition and turbulent regions for glycerine and CMC solution excluding kaolin and bentonite suspensions. It was determined that all the orifice geometry tested the Re for Newtonian, power-law, Herschel-Bulkley and Bingham were $18< Re <20$, $65< Re <80$, $100< Re <300$ and $180< Re <340$.This variation is due to the rheological properties of each liquid.

Table 5.2: Three flow regions were examined: laminar, transition and turbulent

In the laminar flow region
• Chamfer- and quadrant-edge orifices resulted in C_d values of 0.3–0.5 for glycerine solutions. Short square-edged and square-edged with bevel back orifices resulted in C_d values of 0.3–0.4 for glycerine solutions.
• Chamfer- and quadrant-edged orifices resulted in C_d values of 0.2–0.5 for CMC solutions. Short square-edged and square-edged with bevel back orifices resulted in C_d values of 0.2–0.5 for CMC solutions.
• Chamfer- and quadrant-edged orifices resulted in C_d values of 0.6–0.8 for kaolin suspensions. Short square edge and square edge with bevel back orifices resulted in C_d values of 0.5–0.7 for kaolin suspensions.
• Chamfer- and quadrant-edged orifices resulted in C_d values of 0.3-0.7 for Bentonite suspensions. Short square edge and square edge with bevel back orifices resulted in C_d values of 0.3-0.7 for Bentonite suspensions.
In the transition flow region
• Chamfer and quadrant-edged orifices resulted in C_d values of 0.7–0.8 for glycerine solutions. Short square-edged and square-edged with bevel back orifices resulted in C_d values of 0.7–0.77 for glycerine solutions.
• Chamfer- and quadrant edge orifices resulted in C_d values of 0.5–0.7 for CMC solutions. Short square-edged and square-edged with bevel back orifices resulted in C_d values of 0.50-0.69 for CMC solutions.

• Chamfer and quadrant edge orifices resulted in Cd values of 0.87 for kaolin suspensions. Short square-edged and square-edged with bevel back orifices resulted in C_d values of 0.73 for kaolin suspensions.
Bentonite and kaolin suspensions were limited to laminar and transition flow regions as the study was aimed at determining the effect of orifice edge geometry on the discharge of non-Newtonian liquids.
In the turbulent flow region
• Chamfer- and quadrant-edged orifices resulted in C_d values of 0.8 for glycerine solutions. Short square-edged and square-edged with bevel back orifices resulted in C_d values of 0.69 for glycerine solutions.
• Chamfer- and quadrant-edged orifices resulted in C_d values of 0.69–0.75 for CMC solutions. Short square-edged and square-edged with bevel back orifices resulted in C_d values of 0.6–0.7 for CMC solutions. In the turbulent flow region
In the turbulent flow regions, we observed nearly constant C_d values for both short square edge and square edge orifice with bevel back cut. It is also observed from the graphical illustrations that the average C_d values from laminar to turbulent are almost constant. Khahledi et al. (2020) determined that the average C_d values for orifices (circular, square and triangular) in the turbulent region was approximately the same.

5.5 The discharge coefficient as a function of Re for Newtonian and non-Newtonian liquids discharging from a tank for the following orifice edge geometries

5.5.1 Discharge versus Reynolds number: laminar flow relationships

The C_d vs Re laminar flow relationship yielded a y= $0.0904x^{0.3895}$; where y= C_d *and x = Re*. Testing liquids that resulted in laminar to transition region were glycerine and CMC.
∴ $C_d = 0.0904Re^{0.39}$ and the average C_d value in the turbulent flow = 0.61.

Table 5.3 shows laminar flow relation for glycerine as C_d as a function of the Re number and the different Re ranges for each orifice geometry.

The C_d vs Re laminar flow relationship yielded in a y= $0.0276Re^{0.57}$ ∴ for CMC C_d=

$0.0276Re^{0.57}$ and the average C_d value in the turbulent flow was 0.82

Table 5.3: Glycerine laminar discharge correlations for chamfer, quadrant, short square-edged and square-edged with bevel back cut angle

Glycerine			
	Orifice edge	Discharge	Reynolds number
Laminar	Chamfered	$C_d = 0.0904Re^{0.39}$	$18 < Re > 131$
	Quadrant	$C_d = 0.0923Re^{0.38}$	$19 < Re > 129$
	Short square-edged	$C_d = 0.00823Re^{0.39}$	$19 < Re > 128$
	Square-edged with bevel back cut angle	$C_d = 0.0787Re^{0.40}$	$18 < Re > 128$

Table 5.4 shows the Re and C_d for CMC solutions in the laminar flows regions. Quadrant-edged showed a slight increase of Re where the Re range values were between $72 < Re_2 > 307$. The edge effect for all orifices show unique charateristics.

Table 5.4: CMC laminar discharge correlations for chamfer, quadrant, short square-edged and square-edged with bevel back cut angle

CMC			
Laminar	**Orifice edge**	**Discharge**	**Reynolds number**
	Chamfered	$C_d = 0.0276Re^{0.57}$	$68 < Re_2 > 279$
	Quadrant	$C_d = 0.0188Re^{0.63}$	$72 < Re_2 > 307$
	Short square-edged	$C_d = 0.0128Re^{0.71}$	$66 < Re_2 > 246$
	Square-edged with bevel back cut angle	$C_d = 0.00096Re^{0.77}$	$67 < Re_2 > 245$

5.5.2 The discharge coefficient as a function of the Reynolds number

Figure 5.3.and Figure 5.4 show the discharge coefficient (C_d) as a function of the Reynolds number (Re). The orifice geometry can either be sharp or rounded (bell-mouthed). Chamfer-edged orifices and quadrant-edged orifices portray similar flow behaviour for Newtonian, whereas for non-Newtonian liquids some inconsistencies exist. Therefore, it is vital to discuss each orifice edge geometry and their flow characteristics separately.

In Figure 5.2 the flow regions are highlightered to; laminar, transition and turbulent flow for both Newtonian and non-Newtonian. It can be observed from the figure that most of the data is found in the laminar and transition regions.

Figure 5.3 constitutes of three different graphs where chamfer, quadrant, short square and square bevel back cut edge orifices are displayed.The discharge coefficient versus the Reynold‘s number was determined and presented where all the three graphs are visible to show that chamfer and quadrant edge orifices produced much higher values of the C_d throughout the tests particularly from Re = 1000. Whereas short square and square bevel back cut edge orifices produce lower C_d values as the Re continues to increase and once the C_d values reached 0.69 there is a slight decrease before C_d values become constant. For Re < 800 all the orifices show an increase in the C_d values with increasing Re however as the Re continues to increase square edge orifices decrease and become constant. Chamfer and quadrant edge orifices on the other hand are not influenced by the increase in Re as the C_d values continues to increase with increasing Re.

In this figure a combination of the three graphs that discribes the relationship between the discharge coefficient and Reynold's number for only the non-Netoniam liquids is presented .The graphs separate for each liquid for CMC where it was observed that C_d values increase expontentially from 0.2 to 0.6 and the Re vaules of 90 to 245 for all testeed orifices; chamfer, quadrant, short square and square bevel back cut edge orifice were obained. Chamfer edge orifice has the highest C_d in comparison to the rest of the edges with the C_d =0.82 and the lowest being the short square edge orifice with the C_d = 0.59. For kaolin from Re$\leq$ 1000 both chamfer and quadrant edge orifce produce the highest C_d values 0.91. Short square produces a C_d values of 0.78 before decreasing to 0.65 for both short square and square bevel back cut edge orifice and stay constant at C_d values of 0.65. The highest C_d values are obtained from the quadrant edge orifice at 0.88. For bentonite, chamfer and quadrant edge orifice show the same trend with C_d and Re values that increase exponentially until C_d = 0.83. In contrast, short square and square bevel back cut edge orifices remain constant at C_d = 0.68.

A

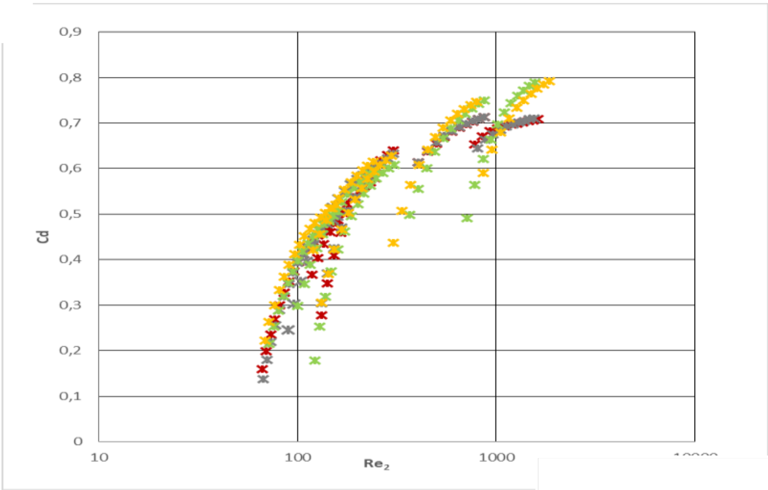

B

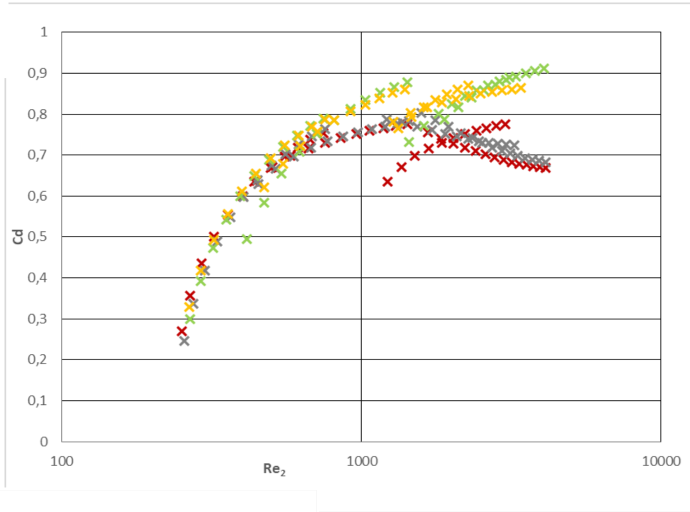

C

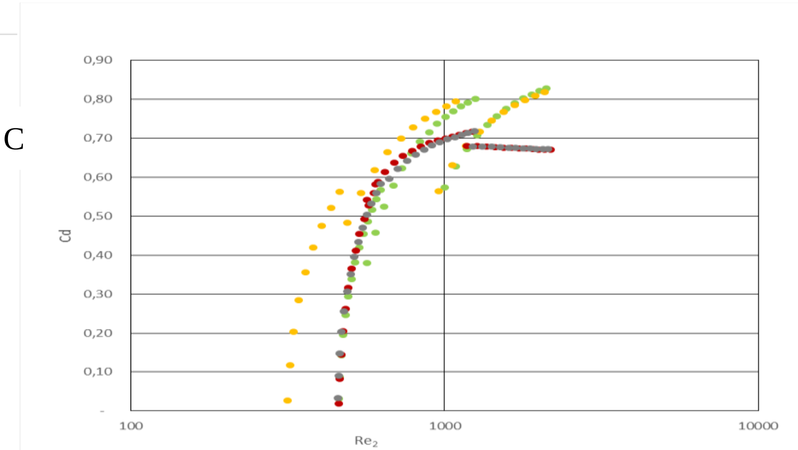

<u>Key</u>

Red - Short square edge
Grey- Square edge bevel back cut edge
Yellow-Chamfer edge
Green- quadrant edge

Figure 5.3: The effect of orifice geometry on the discharge of CMC (A), kaolin (B) and bentonite (C) at different concentrations for all tested orifices

In Table 5.5 illustrates the effect or impact of the orifice edge for the flow of highly viscous Newtonian liquids such as glycerine liquids from a tank. The discharge coefficient as a function of the Re in the laminar regions resulted in a $C_d = 0.0904Re^{0.39}$. Re ranging between $21 < Re < 100$ for the chamfer-edged orifice. And for the quadrant-edged orifice, the discharge as a function of the Re was $C_d = 0.0923Re^{0.38}$ with a Re ranging between $19 < Re < 100$.

The discharge coefficient (C_d) as a function of the Reynolds number (Re) for the chamfer and quadrant-edged orifice shows that there is an effect of orifice edge. Reason being that the C_d values obtained are higher for chamfer and quadrant edges in comparision to the square-edged orifices.

Table 5.5: Flow regions for chamfer and quadrant-edged orifice for all the liquids tested

	Flow region	Glycerine	CMC	Kaolin	Bentonite
Chamfered edge orifice	Laminar	$21 < Re < 100$	$100 < Re_2 < 300$	$300 < Re_2 < 800$	$500 < Re_2 < 1000$
	Transition	$100 < Re < 2000$	$300 < Re_2 < 2000$	$800 < Re_2 < 2000$	$1000 < Re_2 < 2000$
	Turbulent	$24000 < Re$	$7000 < Re_2$	$2300 < Re_2$	
Quadrant - edged orifice	Flow region	Glycerine	CMC	Kaolin	Bentonite
	Laminar	$19 < Re < 100$	$100 < Re_2 < 300$	$300 < Re_2 < 800$	$500 < Re_2 < 1000$
	Transition	$100 < Re < 2000$	$300 < Re_2 < 2000$	$800 < Re_2 < 2000$	$1000 < Re_2 < 2000$
	Turbulent	$24000 < Re$	$7000 < Re_2$	$2300 < Re_2$	

Figure 5.4 is the graph of C_d versus Re_2 for all Newtonian and non-Newtonian liquids tested. This graph represents the set of square-edged orifices tested: short square-edged and square-edged with bevel back cut angle. The set showed similar traits where Re: $800 < Re < 1500$ and is the peak of the transition region and the C_d values ranged from 0.7–0.78. Figure 5.4 is utilised as a reference for the set of square-edged orifices used in the study. Figure 5.4 show that the laminar flows are between Re values of 21 and 100 for chamfer-edged, quadrant-

edged orifice, short square-edged, and square-edged with bevel back cut angle. The transition flows are between Re: 100$< Re <$ 2000 and turbulent from Re: 24000$< Re$.

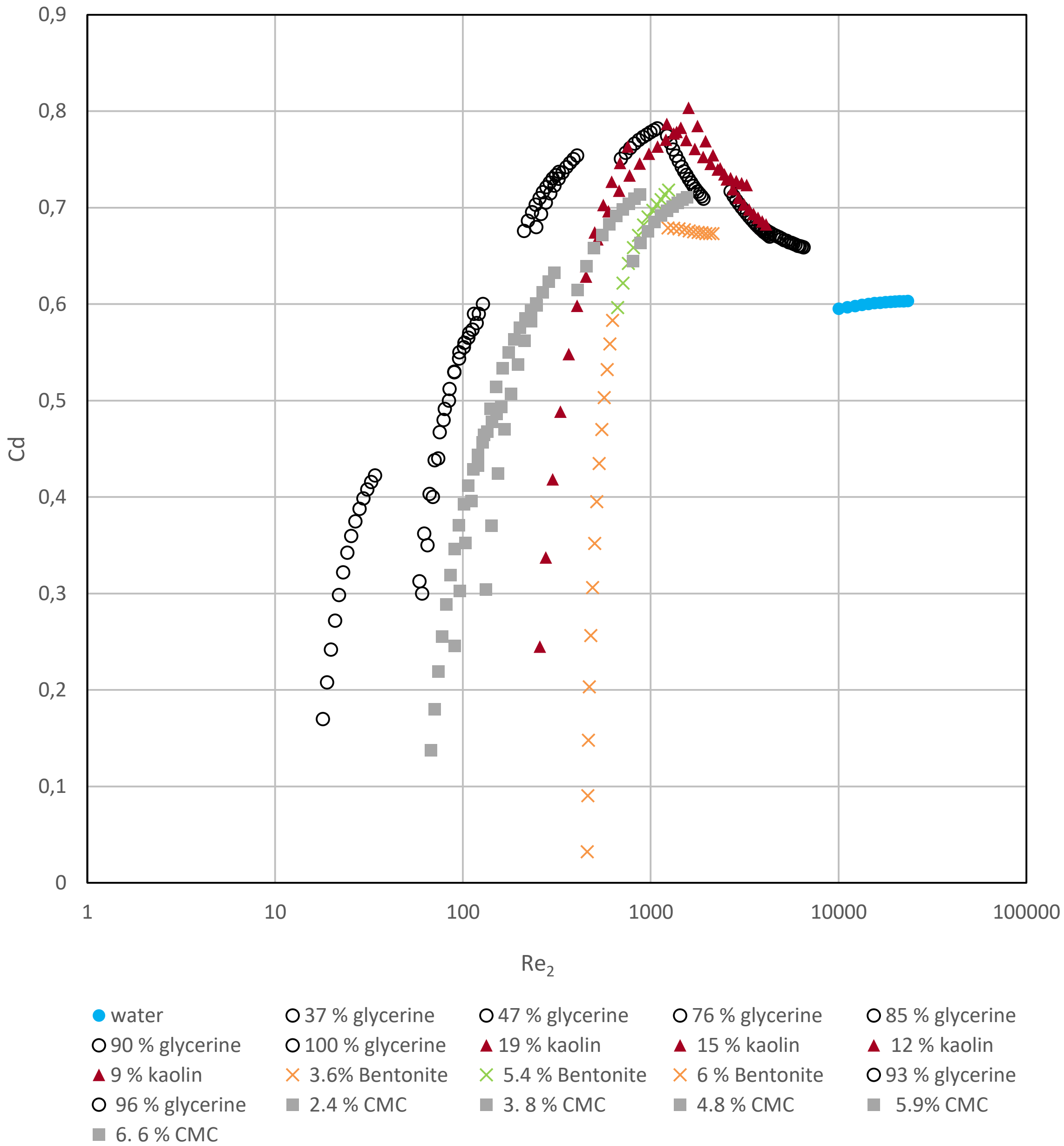

Figure 5.4: The graph shows the effect of orifice geometry on the discharge of Newtonian and non-Newtonian liquids at different concentrations for square-edged and bevel back cut edge orifice

Short square-edged orifice resulted in a correlation of $C_d = 0.00823Re^{0.3897}$ with a Re ranging between 19 $< Re <$ 128. For square-edged with bevel back angle, the discharge coefficient as a function of the Re was $C_d = 0.0787Re^{0.4051}$ with a Re ranging between $18 < Re < 128$.

The square-edged orifices used in this study are short square-edged and square-edged with bevel back cut angle. These orifices are concentric square-edged types of orifices and can be grouped or compared to sharp edge orifices. Short square-edged orifice C_d values reached a peak of 0.77 for kaolin before gradually decreasing to 0.65 for glycerine and staying at 0.70 for CMC and 0.68 bentonite. Square-edged with bevel back cut orifice C_d values reached a peak of 0.78 for kaolin before gradually decreasing to 0.65 for glycerine and staying at 0.71 for CMC and 0.67 bentonite.

Table 5.6 shows the flow regions of chamfer and quadrant-edged for all the liquids tested. It can be observed that from glycerine to bentonite there is a change in the Re this is as a results of the rheological characteristics of each liquid. Bentonite and kaolin suspensions were limited to laminar flow regions to get the desired results and the study was aimed at determining the effect of orifice edge geometry on the discharge of non-Newtonian liquids. Chamfer-edged and quadrant show similar flow characteristic, both having a nozzle-like edge appearance.

The data obtained from this experimental study showed that short square-edged and square-edged with bevel back cut showed more or less identical curves for non-Newtonian and highly viscous liquids. At Re of 2000, the flow starts to become gradually constant after the peak C_d values are reached for both orifices and it can be seen that for less viscous liquids the curves will move more to turbulen regions.

Table 5.6: Flow regions for short square-edged and square-edged with bevel back cut angle orifice for all the liquids tested

Short square-edged orifice	Flow region	Glycerine	CMC	Kaolin	Bentonite
	Laminar	$20 < Re < 100$	$100 < Re_2 < 200$	$300 < Re_2 < 800$	$700 < Re_2 < 1000$
	Transition	$100 < Re < 2000$	$200 < Re_2 < 2000$	$800 < Re_2 < 2000$	$1000 < Re_2 < 2000$
	Turbulent	$24000 < Re$	$7000 < Re_2$	$2300 < Re_2$	
Square bevel back cut edged orifice	Flow region	Glycerine	CMC	Kaolin	Bentonite
	Laminar	$20 < Re < 100$	$100 < Re_2 < 200$	$300 < Re_2 < 800$	$700 < Re_2 < 1000$
	Transition	$100 < Re < 2000$	$200 < Re_2 < 2000$	$800 < Re_2 < 2000$	$1000 < Re_2 < 2000$
	Turbulent	$24000 < Re$	$7000 < Re_2$	$2300 < Re_2$	

It is noticeable from these correlations for the determination of the C_d values in relation to the Re (Reynolds number) of glycerine that the edge effect for chamfer-edged and quadrant is quite similar but short square-edged orifice stands out even though both the square-edged orifices show low discharge coefficient (C_d) correlations.

5.6 Conclusion

The C_d values determined for the square-edged orifice (short square-edged and square-edged with bevel back cut angle) from the calibration results were within the range of the C_d values in reference to Dziubinski and Marcinkowski (2006) for a sharp edge geometry orifice. the C_d values in Khahledi et al. (2020) for sharp-crested circular and square shape orifices in tanks. The sharp edge orifice was compared with the square-edged orifices as they have similar flow characteristics. For the current study, both short square-edged and square-edged with bevel angle back cut produced the average of C_d value = 0.57-0.60. The standard C_d values or reference C_d values of chamfer-edged and rounded (quadrant) edge orifices was also found to be 0.85. It was determined in this study that chamfer-edged geometry resulted in an average C_d value of 0.88 and quadrant-edged geometry an average C_d value = 0.84. It is evident that some discrepancies exist as these are generalised values and the methodologies are different. It is clear that, at this point, the chamfer and quadrant-edged orifices produce higher C_d values for the water results analysis. The square-edged (short square-edged and square-edged with bevel back cut angle) resulted in lower C_d values, both becoming constant at C_d values = 0.61. Short square-edged produce the lowest C_d values = 0.57 and 0.60 respectively. Square-edged with bevel back cut angle C_d values start at 0.59 and 0.61 respectively from laminar to turbulent.

The average C_d values for the different edge geometry were as follows: chamfer-edged was 0.88, short square-edged was 0.58, quadrant-edged was 0.84 and square-edged with bevel back was 0.61 in turbulent regions.

The discharges were C_d value = 0, 62 and C_d value = 0, 64. The Re values for the current study for square-edged orifices (short square-edged and square-edged orifice with bevel back cut angle) was 14860–23379 and for chamfer and quadrant was 14980–24243 for all water tests. In previous studies for in-tank orifices, water discharge for sharp edge orifice found Re values to be 10882–20979.

The effect of orifice geometry on the discharge coefficient for all tested liquids

Non-Newtonian liquids and highly viscous liquids such as glycerine at higher concentrations made up the laminar regions. For all the liquids tested, the viscosity versus shear rate, and shear stress versus shear rate testes results utilising a rheometer were evaluated. Rheological characteristics were determined and parameters such as flow behaviour index, fluid consistency coefficient and the yield stress were calculated from shear diagrams, and the C_d values and correct Re (Reynolds numbers) were determined. It is critical that the discharge coefficient is determined in relation to the Re for each orifice to analysis the flow efficiency for different liquids. The Re values for all liquids tested, Newtonian, Power Law, Herschel-Bulkley and Bingham liquids. Are as follows:

Re = $20<Re<100$ was observed for Newtonian (highly viscous liquid s= glycerine), for Power -Law, the Re $=100<Re_2<200$, for the Herschel-Bulkley, the Re $=300<Re2<800$ and for Bingham liquids the Re $=700<Re_2<1000$ for square-edged orifices, both short square-edged and square-edged with bevel back cut angle. However, for chamfer-edged orifice Re = $21<Re<100$ was observed for Newtonian (highly viscous liquids= Glycerine), for Power Law the Re $=100<Re_2<300$, for the Herschel-Bulkley, the Re $=300<Re_2<800$ and for Bingham liquids, the Re $=500<Re_2<1000$ and Quadrant-edged orifice Re = $19<Re<100$ was observed for Newtonian (highly viscous liquids = glycerine), for Power Law the Re $=100<Re_2<300$, for the Herschel-Bulkley the Re $=300<Re_2<800$ and for Bingham liquids the Re $=500<Re_2<1000$.

The discharge coefficient as a function of Re for Newtonian and non-Newtonian liquids discharging from a tank for the following orifice edge geometries: chamfer-edged, quadrant-edged, short square-edged and square-edged with bevel angle with back cut were obtained.

Newtonian: glycerine

Chamfer-edged orifice: The discharge coefficient as a function of the Re in the laminar regions resulted in $C_d = 0.0904Re^{0.39}$ correlation. Re = 18 . Quadrant-edged orifice: The discharge as a function of the Re was $C_d = 0.0923Re^{0.38}$ with a Re = 19

Short square-edged and square-edged with bevel back cut angle: The square-edged orifice: short square-edged resulted in $C_d = 0.00823Re^{0.39}$ with a Re = 19. Square-edged with bevel back cut angle the discharge coefficient as a function of the Re was $C_d = 0.0787Re^{0.40}$ with a Re = 18

Non-Newtonian: CMC

Chamfer-edged orifice: In the laminar regions resulted in the $C_d = 0.0276\,Re^{0.57}$ and $Re_2 = 68$. Quadrant-edged orifice: The laminar regions resulted in $C_d = 0.0188Re^{0.63}$ and $Re_2 = 72$.

Short square-edged and square-edged with bevel back cut angle: Short square-edged orifice in laminar regions resulted in, $C_d = 0.0128\,Re^{0.71}$ and $Re_2 = 66$ Square-edged with bevel back cut in laminar regions resulted in $C_d = 0.0009\,Re^{0.77}$ the $Re_2 = 67$.

In the case of highly viscous and non-Newtonian liquids the flow at high concentrations remained in the laminar regions and gradually moved to the transition regions at lower concentrations. In the case of Herschel Bulkly and Bingham liquid (kaolin and bentonite) the flow shows slight traits of being in the laminar however rapidly moves to the transition regions for both high and low concentrations. At higher concentrations of (viscous and non-Newtonian) the liquid are more viscous and whereas at lower concentrations the liquids are less viscous.

CHAPTER 6 CONCLUSION AND RECOMMENDATIONS

6.1 Introduction

The discharge through of four different orifice geometries were used to determine C_d-Re relationship for Newtonian and non-Newtonian liquids from a tank. Rheolgical properties were determined for different concentrations of the liquids and the flow rates measured were represented as a function of the liquid flow properties and the Reyonlds number. The following edge geometries were studied:chamfer-edged, quadrant-edged, short square-edged, and square-edged with bevel back cut orifices. This work adds to the extensive studies done on orifices and contributes to the determination of the discharge coeffeicient of different orifice geometries consisting of chamfer-edged, quadrant-edged, short square-edged, and back cut square-edged. This chapter provides a summery of the findings and conclusions, and the contributions and finally the recommendations for further research.

6.2 In summary

Four different edge orifices were manufactured with edges such as chamfer-edged, quadrant-edged, short square-edged and square-edged with bevel back. Non-Newtonian liquids such as different concentrations of CMC (carboxymethly cellulose) solutions, kaolin and bentonite suspensions were used. Newtonian liquids were water and different concentrations of glycerine solutions. The discharge coefficient was determined for each orifice edge geometry and presented in relation to the Reynolds number.

The discharge of these four different edge orifice geometries were:

- The Re values for all the orifice edge geometry tested were for square-edged orifices (short square-edged and square-edged orifices with bevel back cut angle) were 14860–23379 and for chamfer and quadrant were 14980–24243 for all water tests.
- The Re values for all the orifice geometries tested from Newtonian and Power Law, to Herschel-Bulkley and Bingham were 18, 66, 300 and 340, respectively. This is in comparison with experimental data found in previous literature for Newtonian, Power Law, Herschel-Bulkley and Bingham, which were 11, 53, 232 and 330, respectively, according to Khahledi et al. (2020) in their study of sharp-crested orifices (circular, square and triangular) on the discharge of Newtonian and non-Newtonian liquids from a tank.

6.3 Conclusion

The findings in this study comfirm that there is an effect on the discharge when utilising an orifice with a defined edge geometry to discharge Newtonian and non-Newtonian liquids from a tank. It was determined that highly viscous Newtonian liquid; the Re ranges moves from laminar regions starts from Re = 18 to turbulent regions Re ≤ 60000 for less viscous liquids. Whereas for CMC, there is an increase in C_d in relation to Re before becoming stable at the transition regions. Bentonite and kaolin suspensions are dominant in the the transition flow regions for all tested orifice edges. All of this may be attributed to the unique variations in the rheological properties of each liquid.

The discharge efficiency values were determined to be:

- C_d (average)values were: chamfer-edge 0.88; quadrant edge 0.84; short square edge square bevel back cut angle edge 0.61 and 0.58 in the turbulent flow regions
- The discharge coefficient as a function of the Re for glycerine in the laminar regions resulted in $0.00823\ Re^{0.39}$, $0.0787Re^{0.40}$, $0.0904Re^{0.39}$ and $0.0923Re^{0.38}$, and for non-Newtonian liquids 0.0009 $Re^{0.77}$, 0.0128 $Re^{0.71}$, 0.0276 $Re^{0.57}$ and 0.0188$Re^{0.63}$ for square bevel back cut angle, short square, chamfer and quadrant edge orifice,s respectively.

After having tested all these orifices it was observed that the chamfer and quadrant edge orifices produced higher coefficient values in comparison to the square edge orifices (short square and square bevel back cut edge orifices). It can be concluded that the chamfer and quadrant edge orifices are more efficient and better suited in optimising discharge processes.These two orifice edges resulted in higher C_d values be it in the discharge of Newtonian or non- Newtonian liquids overall. The chamfer and quadrant edge orifices both have a funnel-like appearance even though the quadrant edge orifice has a rounded bell mouth-like edge. There is an area one (A1) and area two (A2) at the opening exit side of the orifices and this seemes to be a major contributor for the flow variation in liquid discharge. Therefore the orifice edge geometry has an effect in the discharge of Newtonian and non-Newtonian liquids through orifices from the bottom of the tank.

6.4 Contribution

This experimental study adds to existing data in the laminar flow regions. It extends to the data found in literature for edged orifices such as square, chamfer- and quadrant-edged orifices. The discharge coefficient in relation to the Reynolds number determined for each orifice edge will be beneficial in engineering designs and processes.

6.5 Recommendations

The study covered Newtonian and non-Newtonian liquids, but there is still room for more data. The literature reviewed demonstrated that most of the research conducted was both experimental and numerical, where computational fluid dynamics (CFD) were utilised for the same experiment and the two were compared. This was evident for evaluating orifice geometry effect and their results were in agreement with that in the literature. The research at hand can also undergo a numerical evaluation utilising CFD and being compared with the experimental results in this research can serve as future work.

Some limitations of the study were that the rheological and determination of the liquids characteristics could not be conducted simultaneously as the discharging process took place in a different laboratory .The CFD visualisation to validate separation/reattachment hypotheses and extend to other β and diameters an also be recommended in future studies.

Recommend the CFD visualisation to validate separation/reattachment hypotheses and extend to other β and diameters.

REFERENCES

Abd, H.M., Alomar, O.R. & Mohamed, I.A., 2019. Effects of varying orifice diameter and Reynolds number on discharge coefficient and wall pressure, *Flow Measurement and Instrumentation, 65*:219–226.

Abdalla Alajmi, S.S.A., Alkhudhari, M., Alqaffas, J., Carrasco, Z., Payan, J., Pasamba, M., Zirakian, T. & Boyajian, D., 2019. *A civil engineering senior design research effort to ascertain discharge coefficients of different orifice geometries*. David Publishing www.davidpublisher.com, 13:204-208.

Abdelrahman, A.M. & Mobasher, A.M. 2021. Effect of varying orifice thickness on the discharge. *Engineering Research Journal (Shoubra*), *1*(48): 148–163.

Adam, N.J., Cesare, G. De & Schleiss, A.J., 2016. Experimental assessment of head losses through elliptical and sharp-edged orifices. In *Proc. of the 4th IAHR Europe Congress* (p. 165).

Adam, N.J., De Cesare, G., Schleiss, A.J., Richard, S. and Muench-Alligné, C., 2016, November. Head loss coefficient through sharp-edged orifices. In *IOP Conference Series: Earth and Environmental Science*, *49*(6): 062009. IOP Publishing.

Ahmed, E.N. & Ghanem, A.A., 2020. A novel comprehensive correlation for discharge coefficient of square-edged concentric orifice plate at low Reynolds numbers. *Flow Measurement and Instrumentation*, *73* :101751.

Alwan, H.H., Saleh, L.A., Al-Mohammed, F.M. & Abdulredha, M.A.J.J., 2020. Experimental prediction of the discharge coefficients for rectangular weir with bottom orifices. *Journal of Engineering Science and Technology*, *15*(5) :3265-3280.

Arun, N., Malavarayan, S. & Kaushik, M., 2010. CFD analysis on discharge coefficient during non-Newtonian flows through orifice meter. *International Journal of Engineering Science and Technology*, *2*(7) :3151-3164.

Assran, M.H. & Mohamed, H.I., 2022. *Effect of orifice-meter shape on discharge coefficient and head loss through it.* https://doi.org/10.21203/rs.3.rs-1741688/v1

Barry, B.A., 1991. *Construction measurements* (Vol. 50). John Wiley & Sons.

Babu, K.M., Gowda, C.G. and Ranjith, K., 2018, June. Numerical study on performance characteristics of multihole orifice plate. In *IOP Conference Series: Materials Science and Engineering* (Vol. 376, No. 1, p. 012032). IOP Publishing

Baillio,PA,. 2003. *True sharp edge orifices*. Bird precision data shee

Bhattarai, B. and Priezjev, N.V., 2018. Wetting properties of structured interfaces composed of surface-attached spherical nanoparticles. *Computational Materials Science*, *143*, pp.497-504.

Beaupré, D., Chapdelaine, F., Domone, P., Koehler, E., Shen, L., Sonebi, M., Struble, L., Tepke, D., Wallevik, J.E. & Wallevik, O., 2004. *Comparison of concrete rheometers: International tests at MB* (Cleveland OH, USA) in May 2003.National Institute of Standards and Technology. https://discovery.ucl.ac.uk/id/eprint/11096/1/11096.pdf

Bezinger, J.B. & Aksay, I.A., 1999. Notes on data analysis. *Chemical Engineering*, 346: 08544-5263.

Bird, R.B., 2002. *Transport phenomena*. New York, NY: Wiley.

Bordoloi, A.D. & Longmire, E.K. 2018. Local velocity variations for a drop moving through an orifice: effects of edge geometry and surface wettability. *Physical Review Fluids*, *3*(12):1–34.

Cao, R., Zhong, F., Liu, Y., Duan, A., Mei, X. &Gong, R., 2023. Mechanical energy loss and Rayleigh-Taylor instability in free discharge of vertical sharp-edged orifices. *Chemical Engineering Research and Design*, *190*, 282-295.

Casey, T.C., 2017. The design, experimentation, and characterization of a high-pressure round-edged orifice plate test facility (Doctoral dissertation, Johns Hopkins University).

Chhabra, R.P., 2010. Non-Newtonian fluids: an introduction. *Rheology of complex fluids:* 1–33.

Chowdhury, M.R. & Fester, V.G., 2012. Chemical engineering research and design modeling pressure losses for Newtonian and non-Newtonian laminar and turbulent flow in long square edged orifices. *Chemical Engineering Research and Design*, *90*(7): 863–869. http://dx.doi.org/10.1016/j.cherd.2011.11.001.

Chowdhury, M.R., 2010. *Determination of pressure loss and discharge coefficients for non-Newtonian fluids in long square-edged orifices* (Doctoral dissertation).

Chhabra, R.P. & Richardson, J.F., 2008. Non-Newtonian fluid behaviour. *Non-Newtonian flow and applied rheology*, Elsevier: 1–55.

Chhabra, R.P., 2010. Non-Newtonian fluids: an introduction. *Rheology of complex fluids*, Springer Nature: 3–34.

Dally, J.W., Riley, W.F. & McConnell, K.G., 1993. *Instrumentation for engineering measurements* (Vol. 576). New York, NY: Wiley.

Davoudi, M.R. and Mahdi, M., 2021. Experimental and numerical investigation of geometric effect on cavitation flow through orifice. *Mechanics & Industry*, *22*, p.31.

Davis, C.V., 1952. *Handbook of applied hydraulics.* New York, NY: McGraw-Hill.

De Nevers, N. & Silcox, G.D., 1991. *Fluid mechanics for chemical engineers*. New York, NY: McGraw-Hill.

Dittmann, M., Dullenkopf, K. & Wittig, S., 2003, January. Discharge coefficients of rotating short orifices with radiused and chamfered inlets. In *Turbo Expo: Power for Land, Sea, and Air* (Vol. 36886, pp. 1001-1009).

Dziubinski, M. & Marcinkowski, A. 2006. Discharge of Newtonian and non-Newtonian liquids from tanks. Institution of Chemical Engineering. *Chemical Engineering for Research and Design*, *84*(A12) :1191-1198.

ESDU, 2007. Incompressible flow through orifice plates – a review of the data in the literature. Engineering Science Data Unit. https://www.esdu.com/cgi-bin/ps.pl?t=doc&p=esdu_tn07007b

Elsaey, A., Abou El-Azm Aly, A. & Fuoad, M. 2014. CFD simulation of fractal-shaped orifices for flow measurement improvement. *Flow Measurement and Instrumentation*, 36:14-23.

Flachskampf, F.A., Weyman, A.E., Guerrero, J.L. & Thomas, J.D., 1990. Influence of orifice geometry and flow rate on effective valve area: an in vitro study. *Journal of the American College of Cardiology*, *15*(5), pp.1173-1180.

Haldenwang, R., Sutherland, A.P.N., Fester, V.G., Holm, R. & Chhabra, R.P., 2012. Sludge pipe flow pressure drop prediction using composite power-law friction factor-Reynolds number correlations based on different non-Newtonian Reynolds numbers. *Water SA*, *38*(4) :615-622.

Hobbs, J.M. & Humphreys, J.S., 1990. The effect of orifice plate geometry upon discharge coefficient. *Flow Measurement and Instrumentation*, 1(3) :133-140.

Hollingshead, C.L., Johnson, M.C., Barfuss, S.L. & Spall, R.E., 2011. Discharge coefficient performance of Venturi, standard concentric orifice plate, V-cone and wedge flow meters at low Reynolds numbers. *Journal of Petroleum Science and Engineering, 78*(3-4) :559-566.

Jiang, T., Huang, Z., Li, J., Zhou, Y. & Xiong, C., 2022. Effect of nozzle geometry on the flow dynamics and resistance inside and outside the cone-straight nozzle. *ACS Omega*, *7*(11):9652-9665.

Johansen, F.C., 1930. Flow through pipe orifices at low Reynolds numbers. *Proceedings of the Royal Society of London. Series A, containing Papers of a Mathematical and Physical Character*, *126*(801):31-245.

Kabir, M., 2004. *Flow characteristics of Newtonian and non-Newtonian fluids in a channel with obstruction at the entry* (Doctoral dissertation, CQUniversity, Australia).

Kazemain, S. & Barghchi, M., 2012. Review of soft soils stabilization by grouting and. *Science Research Essays*, 7(24):2104-2111.

Khahledi, M., Haldenwang, R., Chhabra, R. & Fester, V., 2020. Non-Newtonian fluid flow from bottom of tank using orifices of different shapes. *Chemical Engineering Research and Design*, 157:34-45.

Khahledi, M., Haldenwang, RRainer, H., Fester, V. & Chhhabra, R., 2019. Non-Newtonian fluids discharge through circular and square orifices from a tank. *19th International Conference on Transport and Sedimentation of Solid Particles, Cape Town, South Africa*.

Kiaoulias, D.N., Travis, T.A., Moore, J.D. & Risha, G.A., 2019. Evaluation of orifice inlet geometries on single liquid injectors through cold-flow experiments. *Experimental Thermal and Fluid Science, 103* :78-88.

Kim, B. & Park, S., 2019. Effect of orifice inlet roundness on internal flow and external spray characteristics in enlarged nozzle with single-passage. *Experimental Thermal and Fluid Science*, 109 :109875.

Laera, G., Giordano, C., Pollice, A., Saturno, D. & Mininni, G., 2007. Membrane bioreactor sludge rheology at different solid retention times. *Water Research, 41*(18) :4197-4203.

Likitha, J., Savitha, T.M., Karthik, M., Kavya, P. & Usha, G., 2018. CFD analysis on different shapes of concentric orifice plate for turbulent flow. *International Journal of Engineering Research and Technology*, 7(6):421-426.

Linfield, K.W., 2000. *A study of the discharge coefficient of jets from angled slots and conical orifices* (Doctoral dissertation, University of Toronto, Canada).

Liu, H., 2003. *Pipeline engineering*. CRC Press.

Marcinkowski, A. & Dziubiński, M., 2004. Discharge coefficient for discharge of non-Newtonian liquids from vessel. *Chemical and Process Engineering-Inzynieria Chemiczna I Procesowa*, 25:1297–1302.

McNally Institute, B.M., 2010. *Pump, centrifugal pumps, PD pumps, seals and mechanical seals data.* Http://www. Mcnallyinstitute.com/13-html/13-12.html

Metwally, M., 2014. Impacts of short tube orifice flow and geometrical parameters on flow discharge coefficient characteristics, *International Journal of Engineering Research and Technology,* 3(1): 412–419.

Metzner, A.B. & Reed, J.C., 1955. Flow of non- Newtonian fluids—correlation of the laminar, transition, and turbulent- flow regions. *AIChE Journal*, 1(4):434-440.

Mohajane, T.M., 2020. *Effect of round orifice aspect ratios on Non-Newtonian fluid discharge from tanks* (Doctoral dissertation, Cape Peninsula University of Technology).

Mohajane, T.M., Khahledi. M., Haldenwang. R., Fester & Chhabra. R.P. 2019. Effect of round orifice aspect ratio on non-Newtonian fluid discharge from tanks. *19th International Conference on Transportation and Sedimentation of Solid Particles*. 24-27 September, Cape Town, South Africa, pp.129-136.

Morrison, G.L., Deotte, R. E., Moen, M., Hall, K. R. & Holste, J. C., 1990. Beta ratio, dwirl and Reynolds number dependence of wall pressure in orifice flow meters. *Flow Measurement and Instrumentation, 86,* 269-227.

Muñoz-Díaz, E., Solorio-Ordaz, F.J. & Ascanio, G., 2012. A numerical study of an orifice flowmeter. *Flow Measurement and Instrumentation,* 26*:*85-92.

Nasiruddin, S. & Singh, S.N., 2021. Performance evaluation of an innovative design modification of an orifice meter. *Flow Measurement and Instrumentation,* 80*:*101944.

Ntamba, 2011. *Non-Newtonian pressure loss and discharge coefficients for short square-edged orifice plates.* (PhD dissertation, Cape Peninsula University of Technology, Cape Town, South Africa).

Paterson, A. & Cooke, R. 1999. *The design of slurry pipeline systems.* Short course presented at the Cape Technikon, Cape Town.

Panda, S.K., Choudhury, B.K. & Rath, K.C., 2022. A literature review on the orifice as a flow measuring device. *ECS Transactions*, *107*(1):815.

Potanin, A. & Shapley, N.C., 2021. Heel estimate during pressure-driven drainage of gels from tanks. *Chemical Engineering Science, 230:*116158.

Prohaska II, P.D., 2008. *Investigation of the discharge coefficient for circular orifices in riser pipes* (Doctoral dissertation, Clemson University, South Carolina).

Ramamurthi, K. & Nandakumar, K., 1999. Characteristics of flow through small sharp-edged cylindrical orifices. *Flow Measurement and Instrumentation, 10*(3):133-143.

Ramamoorthy, M.V. & Seetharamaiah, K., 1965. Losses in quadrant edge orifice meters. La Houille Blanche, 52(2):129–135. https://doi.org/10.1051/lhb/1965012

Reader-Harris, M., 2015. *Orifice plates and venturi tubes* (pp. 13-14). Basel, Switzerland: Springer International Publishing.

Reader-Harris, M., Barton, N. & Hodges, D. 2012. The effect of contaminated orifice plates on the discharge coefficient. *Flow Measurement and Instrumentation*, *25*: 2–7. http://dx.doi.org/10.1016/j.flowmeasinst.2011.11.003

Sanghani, C.R., Jayani, D.C., Dobariya, C.R., Sabhadiya*, G.K. & Gohil, J.R., 2016. Comparative analysis of different orifice geometries for pressure drop. International Journal of Science Technology & Engineering, 2*(10):494-499.

Sahin, B. & Ceyhan, H., 1996 Numerical and experimental analysis of laminar flow through square-edged orifice with variable thickness. *Transactions of the Institute of Measurement and Control,* 18(4):166–174.

Simpson, A. & Ranade, V.V., 2018. Modelling of hydrodynamic cavitation with orifice: Influence of different orifice designs. *Chemical Engineering Research and Design,* 136*:*698-711.

Singh, R.K., Singh, S.N. & Seshadri, V., 2009. Flow characteristics of double offset s-shaped circular diffusing duct. *International Journal of Fluid Mechanics Research,* 36(4).

Song, Y., Hwang, D. and Ahn, K., 2019. Effect of orifice geometry on column trajectories of liquid jets in crossflows. *International Journal of Aeronautical and Space Sciences*, *20*(1), pp.139-149.

Slatter, P. & Lazarus, J., 1993, September. Critical flow in slurry pipe-lines. Hydrotransport 12. In *12th International Conference on Slurry Handling and Pipeline Transport*. [Memorias] Brugge, Bélgica (pp. 28-30).

Spaur, P.J., 2011. *Investigation of discharge coefficients for irregular orifices*. West Virginia University.

Spencer, R., 2013. Investigation of discharge behaviour from a sharp-edged circular orifice in both weir and orifice flow regimes using an unsteady experimental procedure. (Electronic thesis and dissertation, University of Western Ontario, Canada).

Swamee, P.K. & Swamee, N., 2010. Discharge equation of a circular sharp-crested orifice. *Journal of Hydraulic Research,* 48(1):106–107.

Teoman, B., Potanin, A. & Armenante, P.M., 2022. The discharge of complex fluids through an orifice: a review. *Chemical Engineering Research and Design,* 179:346–364.

Tharakan, T.J. & Rafeeque, T.A., 2016. The role of backpressure on discharge coefficient of sharp edged injection orifices*. Aerospace Science and Technology,* 49:269–275..

Torricelli, E., De motu gravium naturaliter accelerato. *Firenze* (1643) - Torricelli, E., of the naturally accelerated motion of gravity. Florence (1643).

Tomaszewski, A., Przybylinski, T. and Lackowski, M., 2020. Experimental and numerical analysis of multi-hole orifice flow meter: investigation of the relationship between pressure drop and mass flow rate. *Sensors*, *20*(24), p.7281.

Tukiman, M.M., Ghazali, M.N.M., Sadikin, A., Nasir, N.F., Nordin, N., Sapit, A. and Razali, M.A., 2017, September. CFD simulation of flow through an orifice plate. In *IOP Conference Series: Materials Science and Engineering* (Vol. 243, No. 1, p. 012036). IOP Publishing

Tuğçe, Y., 2010. Scrutinazation of flow characteristics through orifices. (Master‘s thesis, Middle East Technical University, Türkiye)

Vemulapalli, S. & Venkata, S.K., 2022. Parametric analysis of orifice plates on measurement of flow: A review. *Ain Shams Engineering Journal*, *13*(3):101639.

Wilkes, J.O., 1999. *Solutions manual for fluid mechanics for chemical engineers*. Prentice Hall PTR.

Yau, K.H., Kua, E.C. and Balvinder, S., 2017, September. Numerical investigation of a thick plate restriction orifice on the pressure drop performance. In *IOP Conference Series: Materials Science and Engineering* (Vol. 243, No. 1, p. 012028). IOP Publishing.

Zakariya, R.A.L., 2017. *Square edge dan quadrant edgequadrant-edged orifice flow meter* (Undergrauate thesis, Sepuluh Nopember Institute of Technology, Indonesia).

Zatloukal, Z. & Šklubalová, Z., 2012. Effect of orifice geometry on particle discharge rate for a flat-bottomed, cylindrical hopper. *Particulate Science and Technology*, *30*(4): 316–328. Doi: 10.1080/02726351.2011.573839.

.

.

Appendices

Appendix A: Loadcell calibration

Table A 1: Loadcell calibration for small weights

Weights	Loadcell Voltage	Voltmeter
kg	V	V
59,24	4,164	4,16
59,38	4,173	4,17
59,42	4,176	4,17
59,38	4,173	4,17
59,14	4,156	4,155
59	4,147	4,147
59,4	4,175	4,17

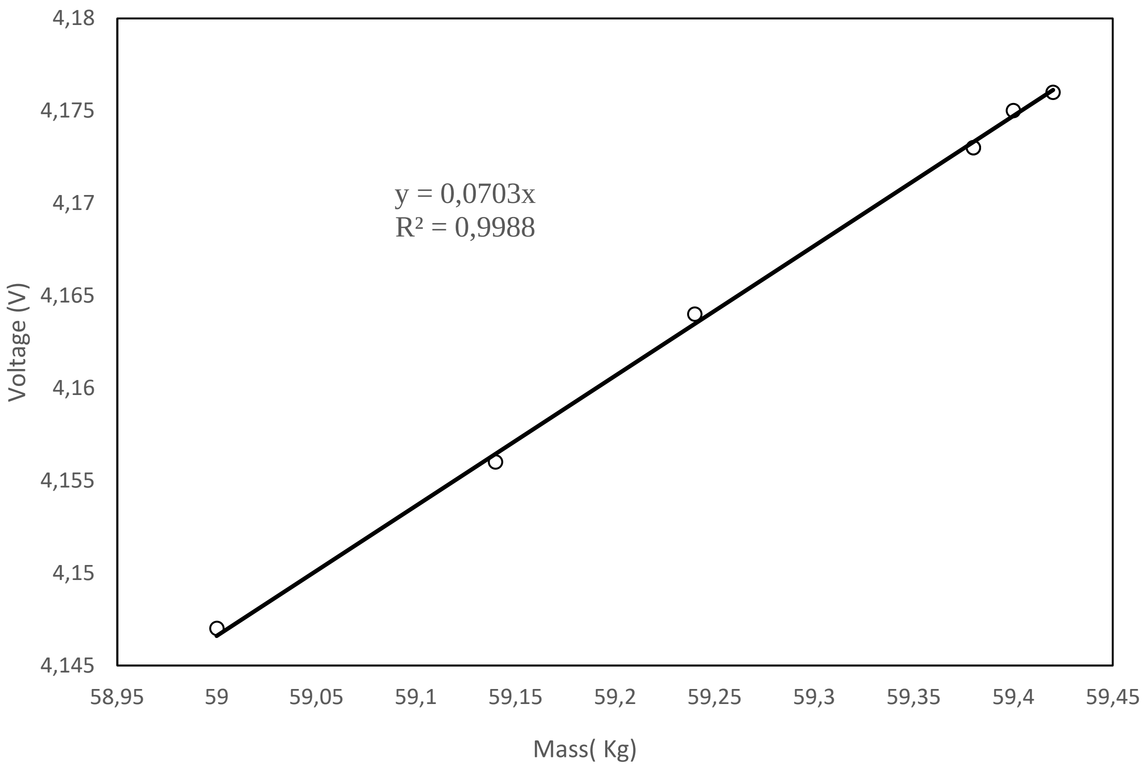

Figure A1: Loadcell calibrations of small weights

Appendix B: Calibration of all the orifices

(Chamfer, quadrant, short square and square bevel back cut edge orifice)

All diameter: 8mm

Liquid : Water	
Orifice : Chamfer edge	
area	0,00005024 m^2
diamneter	0,008m
Tank area	0,16m
Dh	0,008m
Viscosity	0,001 P a.s
Density	1000 Kg /m^3
Gravbitaional acceleration	9,81 m /s^2

Table B 1: loadcell 100 Kg; chamfer edge orifice

Time (s)	Diff Time	Mass in tank (kg)	Height(m)	Diff Height (m)	Flow rate (m^3/s)	Velocity	C_d	Re
162,49	150	63,246	0,395	0,101	0,0001012	2,78	0,72	22278
237,49	225	55,955	0,350	0,147	0,0000952	2,61	0,72	20955
312,49	300	49,080	0,307	0,190	0,0000892	2,45	0,72	19625
387,49	375	42,664	0,267	0,230	0,0000831	2,28	0,72	18298
462,49	450	36,674	0,229	0,267	0,0000771	2,12	0,72	16965
537,49	525	31,116	0,194	0,302	0,0000711	1,95	0,72	15626
612,49	600	25,968	0,162	0,334	0,0000651	1,78	0,73	14275
687,49	675	21,234	0,133	0,364	0,0000591	1,61	0,73	12909
762,49	750	16,904	0,106	0,391	0,0000531	1,44	0,73	11518
837,49	825	13,041	0,082	0,415	0,0000471	1,26	0,74	10116
912,49	900	9,725	0,061	0,436	0,0000411	1,09	0,75	8736
987,49	975	7,071	0,044	0,452	0,0000351	0,93	0,75	7449
1062,49	1050	4,999	0,031	0,465	0,0000291	0,78	0,74	6263
						Av =	0,73	

Liquid : Water	
Orifice :Quadrant edge	
area	0,00005024 m^2
diamneter	0,008m
Tank area	0,16m
Dh	0,008M
Viscosity	0,001 P a.s
Density	1000 Kg /m ^{3}
Gravbitaional acceleration	9,81 m /s^2

Table B 2: Loadcell 100 Kg; quadrant edge orifice

Time (s)	Diff Time	Mass in tank (kg)	Height(m)	Diff Height (m)	Flow rate (m^3/s)	Velocity	C_d	Re
8,32	0	82,276	0,514	0,000	-	0	-	0
58,32	50	75,196	0,470	0,044	0,0001349	3,03	0,88	24292
108,32	100	68,622	0,429	0,085	0,0001286	2,90	0,88	23206
158,32	150	62,370	0,390	0,124	0,0001223	2,76	0,88	22124
208,32	200	56,416	0,353	0,162	0,0001160	2,63	0,88	21041
258,32	250	50,787	0,317	0,197	0,0001097	2,49	0,87	19964
308,32	300	45,470	0,284	0,230	0,0001034	2,36	0,87	18890
358,32	350	40,440	0,253	0,261	0,0000971	2,22	0,87	17814
408,32	400	35,774	0,224	0,291	0,0000908	2,09	0,86	16755
458,32	450	31,380	0,196	0,318	0,0000845	1,96	0,86	15693
508,32	500	27,326	0,171	0,343	0,0000782	1,83	0,85	14644
558,32	550	23,582	0,147	0,367	0,0000719	1,70	0,84	13604
608,32	600	20,144	0,126	0,388	0,0000656	1,57	0,83	12573
658,32	650	17,013	0,106	0,408	0,0000593	1,44	0,82	11555
708,32	700	14,184	0,089	0,426	0,0000530	1,31	0,80	10550
758,32	750	11,670	0,073	0,441	0,0000467	1,19	0,78	9569
808,32	800	9,472	0,059	0,455	0,0000404	1,07	0,75	8622
						Av=	0,85	

Liquid : Water	
Orifice:Short square edge	
Area	0,00005024m^2
Diameter	0,008m
Tank area	0,16m
Dh	0,008M
Viscosity	0,001 P a.s
Density	1000 Kg /m ^{3}
Gravitaional acceleration	9,81 m /s^2

Table B3: Loadcell 250 Kg; short square edge orifice

Time (s)	Diff Time	Mass in tank (kg)	Height(m)	Diff Height (m)	Flow rate (m^3/s)	Velocity	C_d	Re
12,49	0	82,086	0,513	0,0	-	0	-	0
87,49	75,000	75,027	0,469	0,000	0,0000893	3,03	0,59	24265
162,49	150,000	68,502	0,428	0,100	0,0000853	2,89	0,59	23186
237,49	225,000	62,266	0,389	0,100	0,0000812	2,76	0,58	22105
312,49	300,001	56,349	0,352	0,200	0,0000771	2,62	0,58	21029
387,49	375,001	50,726	0,317	0,200	0,0000731	2,49	0,58	19952
462,49	450,001	45,632	0,285	0,200	0,0000690	2,36	0,58	18924
537,49	525,001	40,386	0,252	0,300	0,0000649	2,22	0,58	17803
612,49	600,001	35,671	0,223	0,300	0,0000608	2,09	0,58	16731
687,49	675,001	31,270	0,195	0,300	0,0000568	1,95	0,58	15665
762,49	750,002	27,159	0,170	0,300	0,0000527	1,82	0,57	14599
837,49	825,002	23,362	0,146	0,400	0,0000486	1,69	0,57	13540
912,49	900,002	19,878	0,124	0,400	0,0000446	1,56	0,57	12490
987,49	975,002	16,685	0,104	0,400	0,0000405	1,43	0,56	11443
1062,49	1050,002	13,815	0,086	0,400	0,0000364	1,30	0,56	104122
1137,49	1125,002	11,236	0,070	0,400	0,0000324	1,17	0,55	9390
1212,49	1200,002	8,919	0,056	0,500	0,0000283	1,04	0,54	8366
						Av=	0,57	

Liquid: Water	
Orifice:Square bevel back cut edge	
Area	0,00005024 m^2
Diameter	0,008m
Tank area	0,16m
Dh	0,008m
Viscosity	0,001 P a.s
Density	1000 Kg /m ^{3}
Gravitaional acceleration	9,81 m /s^2

Table B4: Loadcell 250 Kg; square bevel back cut edge edge orifice

Time (s)	Diff Time	Mass in tank (kg)	Height(m)	Diff Height (m)	Flow rate (m^3/s)	Velocity	C_d	Re
12,49	0	82,086	0,513	0,0	-	0	-	0
87,49	75,000	75,027	0,469	0,000	0,0000893	3,03	0,59	24265
162,49	150,000	68,502	0,428	0,100	0,0000853	2,89	0,59	23186
237,49	225,000	62,266	0,389	0,100	0,0000812	2,76	0,58	22105
312,49	300,001	56,349	0,352	0,200	0,0000771	2,62	0,58	21029
387,49	375,001	50,726	0,317	0,200	0,0000731	2,49	0,58	19952
462,49	450,001	45,632	0,285	0,200	0,0000690	2,36	0,58	18924
537,49	525,001	40,386	0,252	0,300	0,0000649	2,22	0,58	17803
612,49	600,001	35,671	0,223	0,300	0,0000608	2,09	0,58	16731
687,49	675,001	31,270	0,195	0,300	0,0000568	1,95	0,58	15665
762,49	750,002	27,159	0,170	0,300	0,0000527	1,82	0,57	14599
837,49	825,002	23,362	0,146	0,400	0,0000486	1,69	0,57	13540
912,49	900,002	19,878	0,124	0,400	0,0000446	1,56	0,57	12490
987,49	975,002	16,685	0,104	0,400	0,0000405	1,43	0,56	11443
1062,49	1050,002	13,815	0,086	0,400	0,0000364	1,30	0,56	104122
1137,49	1125,002	11,236	0,070	0,400	0,0000324	1,17	0,55	9390
1212,49	1200,002	8,919	0,056	0,500	0,0000283	1,04	0,54	8366
						Av=	0,57	

Appendix C: Loadcell calibrations with camera

Table C1: Loadcell calibrations with camera

Frames	Time (s)	Accumulated time(s)	Height difference(m)	Height	Velocity in tank	Flow rate m^3/s	Velocity at the orifice	C_d	Re
40076	0	0	0	0,378	0				
40298	13,87	13,87	0,01	0,388	0,0009	0,000144	2,75	0,96	3104
40477	11,18	27,75	0,02	0,398	0,0009	0,000143	2,79	0,94	3184
40709	14,50	38,93	0,03	0,408	0,0009	0,000143	2,82	0,93	3264
40884	10,93	53,43	0,05	0,428	0,0009	0,000143	2,89	0,91	3424
41079	12,18	64,37	0,06	0,438	0,0008	0,000142	2,93	0,89	3504
41308	14,31	76,56	0,07	0,448	0,0008	0,000142	2,96	0,88	3584
41487	11,18	90,87	0,08	0,458	0,0008	0,000142	2,99	0,87	3664
41670	11,43	102,06	0,09	0,468	0,0008	0,000141	3,03	0,86	3744
41864	12,12	113,50	0,1	0,478	0,0008	0,000141	3,06	0,85	3824
42098	14,62	125,62	0,11	0,488	0,0008	0,000141	3,09	0,84	3904
42279	11,31	140,25	0,12	0,498	0,0008	0,00014	3,12	0,83	3984
42464	11,56	151,56	0,13	0,508	0,0008	0,00014	3,15	0,82	4064
42690	14,12	163,12	0,14	0,518	0,0008	0,00014	3,18	0,81	4144
42887	12,31	177,25	0,15	0,528	0,0008	0,000139	3,21	0,80	4224
43076	11,81	189,56	0,16	0,538	0,0008	0,000139	3,24	0,79	4304
43290	13,37	201,37	0,17	0,548	0,0008	0,000139	3,27	0,78	4384
43480	11,87	214,75	0,18	0,558	0,0008	0,000139	3,30	0,77	4464
43666	11,62	226,62	0,19	0,568	0,0008	0,000138	3,33	0,76	4544
43836	10,62	238,25	0,2	0,578	0,0008	0,000138	3,36	0,75	4624
44072	14,75	248,87	0,21	0,588	0,0008	0,000138	3,39	0,75	4704
44255	11,43	263,62	0,22	0,598	0,0008	0,000137	3,42	0,74	4784
44455	12,50	275,06	0,23	0,608	0,0008	0,000137	3,45	0,73	4864

44675	13,75	287,56	0,24	0,618	0,0008	0,000137	3,482	0,72	4944
44854	11,18	301,31	0,25	0,628	0,0008	0,000136	3,510	0,72	5024
45021	10,43	312,50	0,26	0,638	0,0008	0,000136	3,538	0,71	5104
45203	11,37	322,93	0,27	0,648	0,0008	0,000136	3,565	0,70	5184
45416	13,31	334,31	0,28	0,658	0,0008	0,000135	3,593	0,69	5264
45614	12,37	347,62	0,29	0,668	0,0008	0,000135	3,620	0,69	5344
45784	10,62	360,01	0,3	0,678	0,0008	0,000135	3,647	0,68	5424
45999	13,43	370,62	0,31	0,688	0,0008	0,000135	3,674	0,67	5504
46173	10,87	384,06	0,32	0,698	0,0008	0,000134	3,700	0,67	5584
46340	10,43	394,93	0,33	0,708	0,0008	0,000134	3,727	0,66	5664
							Av =	0,79	

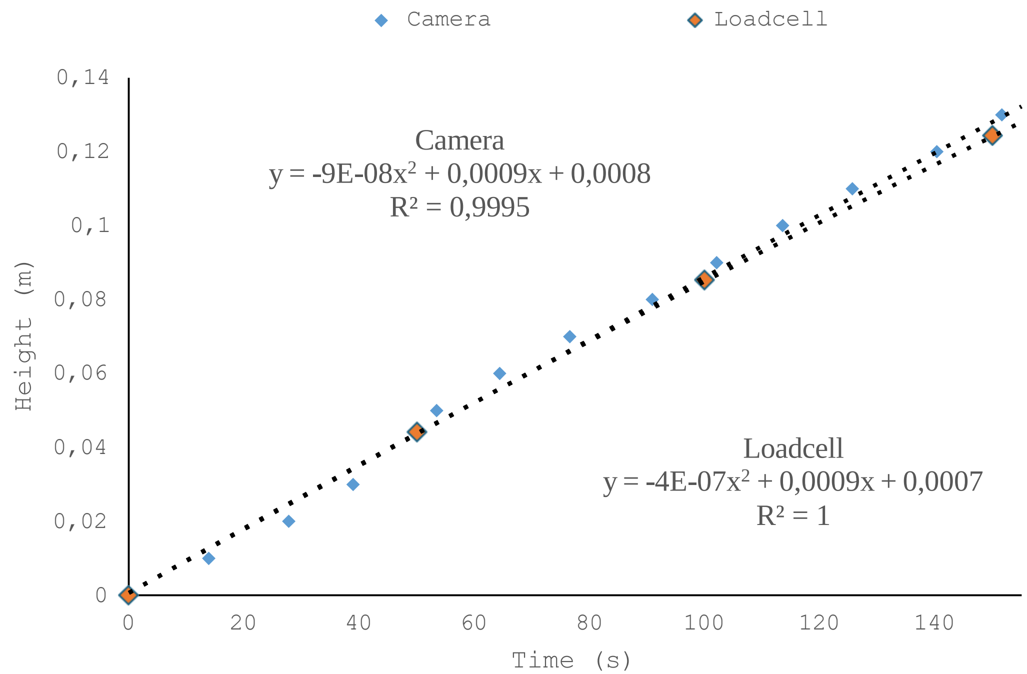

Figure C1: Quadrant edge

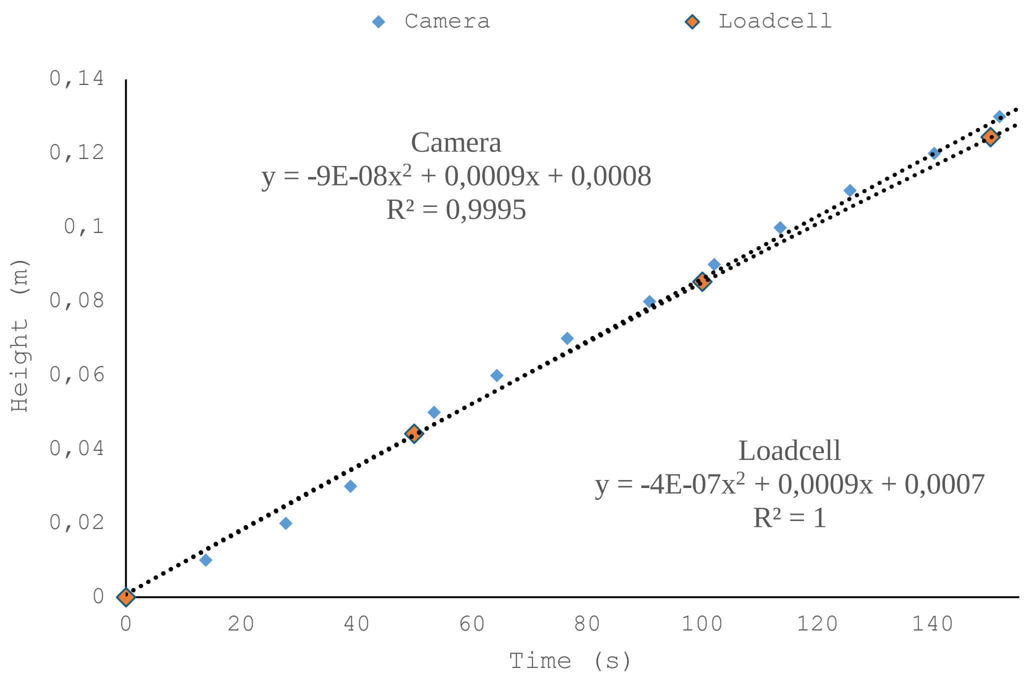

Figure C2: Short square edge

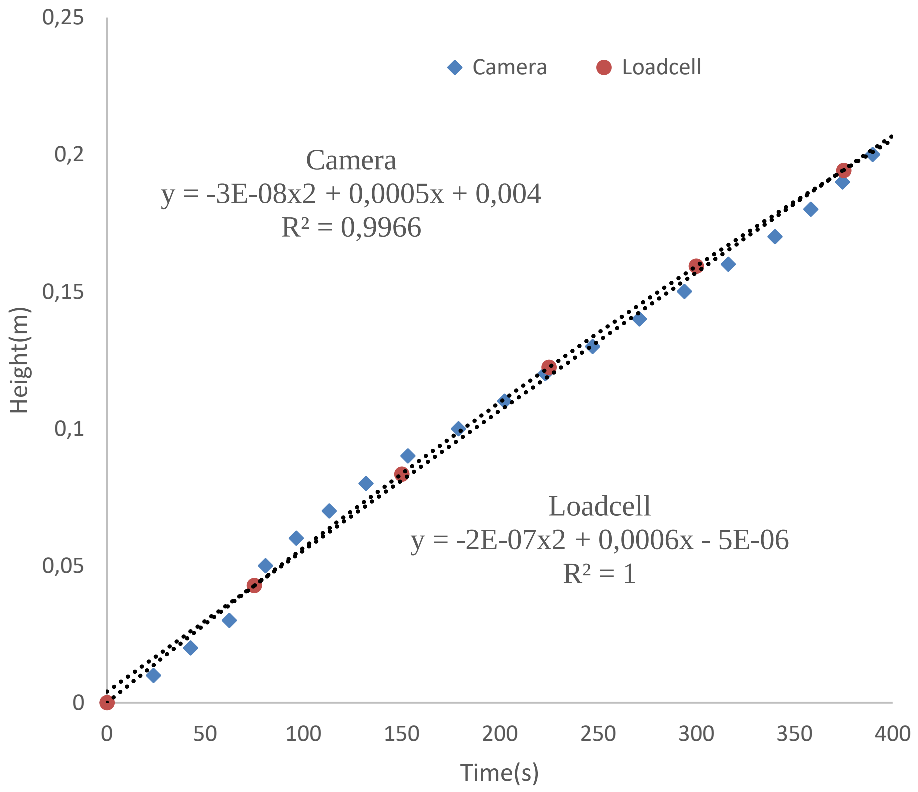

Figure C3: Square bevel back cut edge orifice

Appendix D : 100 % Glycerine discharge; (chamfer, quadrant, short square and square bevel back cut edge orifice)

Appendix D1–D4:100 % Glycerine discharge; (chamfer, quadrant, short square and square bevel back cut edge orifice)

Liquid 100 % glycerine	Temp: 24.5 ℃
Orifice: Chamfer edge	
Area	0,00005024 m^2
Diameter	0,008m
Tank area	0,16m
Dh	0,008m

Viscosity	0,867 Pa.s
Density	1276 Kg / m ^{3}
Gravitaional acceleration	9,81 m ^{2}/s

Table D1: Glycerine solutions: 100% glycerine; chamfer-edge orifice

Time (s)	Diff Time	Mass in tank (kg)	Height(m)	Diff Height (m)	Flow rate (m^3/s)	Velocity	C_d	Re
12,49	0	72,552	0,453	0	-	0	-	0
87,49	75	67,791	0,424	0,029	0,0000593	2,88	0,41	33
162,49	150	63,273	0,395	0,057	0,0000568	2,78	0,41	32
237,49	225	59,000	0,369	0,084	0,0000543	2,68	0,40	31
312,49	300	54,975	0,344	0,109	0,0000517	2,59	0,40	30
387,49	375	51,178	0,320	0,133	0,0000492	2,50	0,39	29
462,49	450	47,604	0,298	0,155	0,0000467	2,41	0,38	28
537,49	525	44,245	0,277	0,176	0,0000441	2,32	0,38	27
612,49	600	41,099	0,257	0,196	0,0000416	2,24	0,37	26
687,49	675	38,150	0,238	0,215	0,0000390	2,16	0,36	25
762,49	750	35,401	0,221	0,232	0,0000365	2,08	0,35	24
837,49	825	32,822	0,205	0,248	0,0000340	2,00	0,34	23
912,49	900	30,422	0,190	0,263	0,0000314	1,93	0,32	22
987,49	975	28,188	0,176	0,277	0,0000289	1,85	0,31	21
1062,49	1050	26,111	0,163	0,290	0,0000263	1,78	0,29	21
1137,49	1125	24,176	0,151	0,302	0,0000238	1,72	0,28	20
1212,49	1200	22,383	0,140	0,313	0,0000213	1,65	0,26	19
1287,49	1275	20,721	0,130	0,323	0,0000187	1,59	0,23	18
1362,49	1350	19,178	0,120	0,333	0,0000162	1,53	0,21	18
						Av=	0,34	

Table D2: Glycerine solutions: 100% glycerine; quadrant edge orifice

Time (s)	Diff Time	Mass in tank (kg)	Height(m)	Diff Height (m)	Flow rate (m^3/s)	Velocity	C_d	Re
16,65	0	75,598	0,472	0	-	0	-	0
116,65	100	69,292	0,433	0,039	0,0000590	2,91	0,40	34
216,65	200	63,422	0,396	0,076	0,0000556	2,78	0,40	32
316,65	300	57,962	0,362	0,110	0,0000523	2,66	0,39	31
416,65	400	52,919	0,331	0,141	0,0000489	2,54	0,38	29
516,65	500	48,233	0,301	0,171	0,0000456	2,43	0,37	28
616,65	600	43,930	0,275	0,197	0,0000422	2,32	0,36	27
716,65	700	39,958	0,250	0,222	0,0000389	2,21	0,35	26
816,65	800	36,326	0,227	0,245	0,0000355	2,11	0,34	24
916,66	900	32,996	0,206	0,266	0,0000322	2,01	0,32	23
1016,66	1000	29,945	0,187	0,285	0,0000288	1,91	0,30	22
1116,66	1100	27,166	0,170	0,302	0,0000255	1,82	0,28	21
1216,66	1200	24,648	0,154	0,318	0,0000221	1,73	0,25	20
1316,66	1300	22,352	0,140	0,332	0,0000188	1,65	0,23	19
						Av=	0,34	

Table D3: Glycerine solutions: 100% glycerine; short square edge orifice

Time (s)	Diff Time	Mass in tank (kg)	Height(m)	Diff Height (m)	Flow rate (m^3/s)	Velocity	C_d	Re
16,65	0	75,598	0,472	0	-	0	-	0
116,65	100	69,292	0,433	0,039	0,0000590	2,91	0,40	34
216,65	200	63,422	0,396	0,076	0,0000556	2,78	0,40	32
316,65	300	57,962	0,362	0,110	0,0000523	2,66	0,39	31
416,65	400	52,919	0,331	0,141	0,0000489	2,54	0,38	29
516,65	500	48,233	0,301	0,171	0,0000456	2,43	0,37	28
616,65	600	43,930	0,275	0,197	0,0000422	2,32	0,36	27
716,65	700	39,958	0,250	0,222	0,0000389	2,21	0,35	26
816,65	800	36,326	0,227	0,245	0,0000355	2,11	0,34	24
916,66	900	32,996	0,206	0,266	0,0000322	2,01	0,32	23
1016,66	1000	29,945	0,187	0,285	0,0000288	1,91	0,30	22
1116,66	1100	27,166	0,170	0,302	0,0000255	1,82	0,28	21
1216,66	1200	24,648	0,154	0,318	0,0000221	1,73	0,25	20
1316,66	1300	22,352	0,140	0,332	0,0000188	1,65	0,23	19
						Av=	0,34	

716,65	700	38,618	0,241	0,226	0,0000391	2,17	0,36	25
816,65	800	34,967	0,219	0,249	0,0000356	2,07	0,34	24
916,66	900	31,642	0,198	0,269	0,0000321	1,96	0,32	23
1016,66	1000	28,618	0,179	0,288	0,0000286	1,87	0,30	22
1116,66	1100	25,870	0,162	0,305	0,0000251	1,78	0,28	21
1216,66	1200	23,383	0,146	0,321	0,0000215	1,69	0,25	20
1316,66	1300	21,162	0,132	0,335	0,0000180	1,61	0,22	19
						Av =	0,34	

Table D4: Glycerine solutions: 100% glycerine; square bevel back cut edge orifice

Time (s)	Diff Time	Mass in tank (kg)	Height(m)	Diff Height (m)	Flow rate (m^3/s)	Velocity	C_d	Re
16,65	0	74,829	0,468	0	-	0	-	0
116,65	100	68,408	0,428	0,040	0,0000602	2,89	0,41	34
216,65	200	62,406	0,390	0,077	0,0000567	2,76	0,41	32
316,65	300	56,847	0,355	0,112	0,0000532	2,64	0,40	31
416,65	400	51,707	0,323	0,144	0,0000497	2,51	0,39	29
516,65	500	46,974	0,294	0,174	0,0000461	2,40	0,38	28
616,65	600	42,615	0,266	0,201	0,0000426	2,28	0,37	26
716,65	700	38,618	0,241	0,226	0,0000391	2,17	0,36	25
816,65	800	34,967	0,219	0,249	0,0000356	2,07	0,34	24
916,66	900	31,642	0,198	0,269	0,0000321	1,96	0,32	23
1016,66	1000	28,618	0,179	0,288	0,0000286	1,87	0,30	22
1116,66	1100	25,870	0,162	0,305	0,0000251	1,78	0,28	21
1216,66	1200	23,383	0,146	0,321	0,0000215	1,69	0,25	20
1316,66	1300	21,162	0,132	0,335	0,0000180	1,61	0,22	19
						Av =	0,34	

Time (s)	**Diff Time**	**Mass in tank (kg)**	**Height(m)**	**Diff Height (m)**	**Flow rate (m^3/s)**	**Velocity**	**C_d**	**Re**
516,65	500	46,367	0,290	0,177	0,0000464	2,38	0,39	28
616,65	600	41,994	0,262	0,204	0,0000427	2,27	0,37	26
716,65	700	38,007	0,238	0,229	0,0000390	2,16	0,36	25
816,65	800	34,386	0,215	0,251	0,0000353	2,05	0,34	24
916,66	900	31,115	0,194	0,272	0,0000316	1,95	0,32	22
1016,66	1000	28,159	0,176	0,290	0,0000279	1,85	0,30	21
1116,66	1100	25,501	0,159	0,307	0,0000242	1,76	0,27	20
1216,66	1200	23,080	0,144	0,322	0,0000204	1,68	0,24	19
1316,66	1300	20,914	0,131	0,336	0,0000167	1,60	0,21	18
1416,66	1400	18,948	0,118	0,348	0,0000130	1,52	0,17	17
						Av=	0,33	

Appendix E: 96 % Glycerine discharge; (chamfer, quadrant, short square and square bevel back cut edge orifice)

Appendix E1–E4: 96 % Glycerine discharge; (chamfer, quadrant, short square and square bevel back cut edge orifice)

Liquid: 96 % glycerine	Temp : 19 ℃
Orifice: Chamfer edge	
Area	0,00005024 m^2
Diameter	0,008m
Tank area	0,16m
Dh	0,008m

Viscosity	0,153 Pa.s
Density	1248 **Kg / m^3**
Gravitaional acc	9,81 **m^2/s**

Table E1: Glycerine solutions: 96 % glycerine; chamfer edge orifice

Time (s)	Diff Time	Mass in tank (kg)	Height(m)	Diff Height (m)	Flow rate (m^3/s)	Velocity	C_d	Re
6,65	0	29,811	0,186	0	-	0	-	0
46,65	40	27,489	0,172	0,014	0,0000554	1,83	0,60	119
86,65	80	25,323	0,158	0,028	0,0000526	1,76	0,59	114
126,65	120	23,232	0,145	0,041	0,0000499	1,68	0,59	110
166,65	160	21,307	0,133	0,053	0,0000471	1,61	0,58	105
206,65	200	19,485	0,122	0,064	0,0000444	1,54	0,57	100
246,65	240	17,810	0,111	0,075	0,0000416	1,47	0,56	96
286,65	280	16,180	0,101	0,085	0,0000389	1,40	0,55	91
326,65	320	14,702	0,092	0,094	0,0000361	1,34	0,54	87
366,65	360	13,327	0,083	0,103	0,0000334	1,27	0,52	83
406,65	400	12,044	0,075	0,111	0,0000306	1,21	0,50	79
446,65	440	10,857	0,068	0,118	0,0000279	1,15	0,48	75
486,65	480	9,789	0,061	0,125	0,0000251	1,09	0,46	71
526,65	520	8,793	0,055	0,131	0,0000224	1,03	0,43	67
566,65	560	7,925	0,050	0,136	0,0000196	0,98	0,40	64
606,65	600	7,099	0,044	0,141	0,0000168	0,93	0,36	60
646,65	640	5,702	0,036	0,150	0,0000141	0,83	0,34	54
						Av =	0,50	

Table E2: Glycerine solutions: 96 % glycerine; quadrant edge orifice

Time (s)	Diff Time	Mass in tank (kg)	Height(m)	Diff Height (m)	Flow rate (m^3/s)	Velocity	C_d	Re
8,32	0	29,633	0,185	0	-	0	-	0
58,32	50	26,860	0,168	0,017	0,0000532	1,81	0,58	118
108,32	100	24,267	0,152	0,033	0,0000499	1,72	0,58	112
158,32	150	21,841	0,137	0,048	0,0000466	1,63	0,57	106
208,32	200	19,615	0,123	0,062	0,0000433	1,55	0,56	101
258,32	250	17,535	0,110	0,075	0,0000400	1,46	0,54	95
308,32	300	15,616	0,098	0,087	0,0000367	1,38	0,53	90
358,32	350	13,913	0,087	0,098	0,0000334	1,30	0,51	85
408,32	400	12,309	0,077	0,108	0,0000301	1,22	0,49	80
458,32	450	10,863	0,068	0,117	0,0000268	1,15	0,46	75
508,32	500	9,608	0,060	0,125	0,0000235	1,08	0,43	70
558,32	550	8,478	0,053	0,132	0,0000202	1,01	0,40	66
						Av=	0,51	

Table E3: Glycerine solutions: 96 % glycerine; short square edge orifice

Time (s)	Diff Time	Mass in tank (kg)	Height(m)	Diff Height (m)	Flow rate (m^3/s)	Velocity	C_d	Re
8,32	0	29,633	0,185	0	-	0	-	0
58,32	50	26,860	0,168	0,017	0,0000532	1,81	0,58	118
108,32	100	24,267	0,152	0,033	0,0000499	1,72	0,58	112
158,32	150	21,841	0,137	0,048	0,0000466	1,63	0,57	106
208,32	200	19,615	0,123	0,062	0,0000433	1,55	0,56	101
258,32	250	17,535	0,110	0,075	0,0000400	1,46	0,54	95
308,32	300	15,616	0,098	0,087	0,0000367	1,38	0,53	90
358,32	350	13,913	0,087	0,098	0,0000334	1,30	0,51	85
408,32	400	12,309	0,077	0,108	0,0000301	1,22	0,49	80
458,32	450	10,863	0,068	0,117	0,0000268	1,15	0,46	75
508,32	500	9,608	0,060	0,125	0,0000235	1,08	0,43	70
558,32	550	8,478	0,053	0,132	0,0000202	1,01	0,40	66
						Av=	0,51	

Table E4: Glycerine solutions: 96 % glycerine; square bevel back cut edge orifice

Time (s)	Diff Time	Mass in tank (kg)	Height(m)	Diff Height (m)	Flow rate (m^3/s)	Velocity	C_d	Re
8,32	0	29,470	0,184	0	-	0	-	0
58,32	50	26,709	0,167	0,017	0,0000528	1,80	0,58	118
108,32	100	24,097	0,151	0,033	0,0000495	1,71	0,57	112
158,32	150	21,712	0,136	0,048	0,0000463	1,63	0,57	106
208,32	200	19,466	0,122	0,062	0,0000431	1,54	0,56	100
258,32	250	17,398	0,109	0,075	0,0000399	1,46	0,54	95
308,32	300	15,505	0,097	0,087	0,0000367	1,37	0,53	89
358,32	350	13,774	0,086	0,098	0,0000334	1,29	0,51	84
408,32	400	12,221	0,076	0,107	0,0000302	1,22	0,49	79
458,32	450	10,783	0,067	0,116	0,0000270	1,14	0,47	75
508,32	500	9,519	0,059	0,124	0,0000238	1,08	0,44	70
558,32	550	8,402	0,053	0,131	0,0000206	1,01	0,40	66
608,32	600	7,403	0,046	0,137	0,0000173	0,95	0,36	62
658,32	650	6,587	0,041	0,143	0,0000141	0,89	0,31	58
						Av =	0,49	

Appendix F: 93 % Glycerine discharge; (chamfer, quadrant, short square and square bevel back cut edge orifice)

Appendix F1–F4 : 93 % Glycerine discharge; (chamfer, quadrant, short square and square bevel back cut edge orifice)

Liquid: 93% glycerine	Temp: 18 ℃
Orifice: Chamfer edge	
Area	0,00005024 m^2
Diameter	0,008m
Tank area	0,16m
Dh	0,008m

Viscosity	0 ,138 Pa.s
Density	1241 **Kg / m ^{3}**
Gravitaional	9,81 **m ^{2}/s**

Table F1: Glycerine solutions: 93 % glycerine; chamfer edge orifice

Time (s)	Diff Time	Mass in tank (kg)	Height(m)	Diff Height (m)	Flow rate (m ^{3}/s)	Velocity	C_d	Re
6,65	0	29,289	0,183	0	-	0	-	0
46,65	40	26,907	0,168	0,014	0,0000570	1,81	0,62	130
86,65	80	24,655	0,154	0,028	0,0000540	1,73	0,62	125
126,65	120	22,560	0,141	0,042	0,0000511	1,66	0,61	119
166,65	160	20,563	0,129	0,054	0,0000481	1,58	0,60	114
206,65	200	18,714	0,117	0,066	0,0000452	1,511	0,59	108
246,65	240	16,982	0,106	0,076	0,0000423	1,44	0,58	103
286,65	280	15,363	0,096	0,087	0,0000393	1,37	0,57	98
326,65	320	13,855	0,087	0,096	0,0000364	1,30	0,56	93
366,65	360	12,472	0,078	0,105	0,0000334	1,23	0,54	88
406,65	400	11,205	0,070	0,113	0,0000305	1,17	0,52	84
446,65	440	10,012	0,063	0,120	0,0000275	1,10	0,49	79
486,65	480	8,947	0,056	0,127	0,0000246	1,04	0,47	75
526,65	520	8,009	0,050	0,133	0,0000216	0,99	0,43	71
566,65	560	7,125	0,045	0,138	0,0000187	0,93	0,40	67
606,65	600	6,351	0,040	0,143	0,0000158	0,88	0,36	63
646,65	640	5,702	0,036	0,147	0,0000128	0,83	0,31	60
						Av =	0,52	

Table F2: Glycerine solutions: 93 % glycerine; quadrant edge orifice

Time (s)	Diff Time	Mass in tank (kg)	Height(m)	Diff Height (m)	Flow rate (m^3/s)	Velocity	C_d	Re
8,32	0	28,872	0,180	0	-	0	-	0
58,32	50	26,028	0,163	0,017	0,0000541	1,78	0,60	128
108,32	100	23,368	0,146	0,034	0,0000506	1,69	0,60	121
158,32	150	20,915	0,131	0,049	0,0000472	1,60	0,59	115
208,32	200	18,664	0,117	0,063	0,0000438	1,51	0,58	108,
258,32	250	16,568	0,104	0,076	0,0000403	1,42	0,56	102
308,32	300	14,655	0,092	0,088	0,0000369	1,34	0,55	96
358,32	350	12,904	0,081	0,099	0,0000335	1,25	0,53	90
408,32	400	11,339	0,071	0,109	0,0000300	1,17	0,51	84
458,32	450	9,946	0,062	0,118	0,0000266	1,10	0,48	79
508,32	500	8,680	0,054	0,126	0,0000232	1,03	0,45	74
558,32	550	7,566	0,047	0,133	0,0000197	0,96	0,41	69
608,32	600	6,617	0,041	0,139	0,0000163	0,90	0,36	64
						Av=	0,52	

Table F3: Glycerine solutions: 93 % glycerine; short square edge orifice

Time (s)	Diff Time	Mass in tank (kg)	Height(m)	Diff Height (m)	Flow rate (m^3/s)	Velocity	C_d	Re
8,32	0	28,306	0,177	0	-	0	-	0
58,32	50	25,531	0,160	0,017	0,0000526	1,76	0,59	127
108,32	100	22,946	0,143	0,033	0,0000493	1,67	0,58	120
158,32	150	20,551	0,128	0,048	0,0000459	1,58	0,58	114
208,32	200	18,343	0,115	0,062	0,0000426	1,49	0,57	107
258,32	250	16,307	0,102	0,074	0,0000392	1,41	0,55	101
308,32	300	14,462	0,090	0,086	0,0000359	1,33	0,54	95
358,32	350	12,766	0,080	0,097	0,0000326	1,25	0,52	90
408,32	400	11,218	0,070	0,106	0,0000292	1,17	0,50	84
458,32	450	9,889	0,062	0,115	0,0000259	1,10	0,47	79
508,32	500	8,655	0,054	0,122	0,0000225	1,03	0,44	74
558,32	550	7,596	0,047	0,129	0,0000192	0,96	0,40	69
608,32	600	6,690	0,042	0,135	0,0000159	0,90	0,35	65
658,32	650	5,923	0,037	0,139	0,0000125	0,85	0,29	61
708,32	700	5,276	0,033	0,143	0,0000092	0,80	0,23	57
758,32	750	4,780	0,030	0,147	0,0000058	0,76	0,15	55
808,32	800	4,533	0,028	0,148	0,0000025	0,74	0,07	53
						Av=	0,43	

Table F4: Glycerine solutions: 93 % glycerine; square bevel back cut edge orifice

Time (s)	Diff Time	Mass in tank (kg)	Height(m)	Diff Height (m)	Flow rate (m^3/s)	Velocity	C_d	Re
8,32	0	28,551	0,178	0	-	0	-	0
58,32	50	25,734	0,161	0,017	0,0000536	1,77	0,60	127
108,32	100	23,079	0,144	0,034	0,0000502	1,68	0,59	121
158,32	150	20,641	0,129	0,049	0,0000468	1,59	0,59	114
208,32	200	18,371	0,115	0,063	0,0000434	1,50	0,57	107
258,32	250	16,317	0,102	0,076	0,0000399	1,41	0,56	101
308,32	300	14,440	0,090	0,088	0,0000365	1,33	0,55	95
358,32	350	12,702	0,079	0,099	0,0000331	1,24	0,53	89
408,32	400	11,170	0,070	0,108	0,0000296	1,17	0,50	84
458,32	450	9,805	0,061	0,117	0,0000262	1,09	0,48	78
508,32	500	8,583	0,054	0,124	0,0000228	1,02	0,44	73
558,32	550	7,520	0,047	0,131	0,0000194	0,96	0,40	69
608,32	600	6,581	0,041	0,137	0,0000159	0,89	0,35	64
658,32	650	5,777	0,036	0,142	0,0000125	0,84	0,30	60
708,32	700	5,148	0,032	0,146	0,0000091	0,79	0,23	57
758,32	750	4,701	0,029	0,149	0,0000056	0,75	0,15	54
						Av=	0,46	

Appendix G : 90 % Glycerine discharge; (chamfer, quadrant, short square and square bevel back cut edge orifice)

Appendix G1–G4 : 90 % Glycerine discharge; (chamfer, quadrant, short square and square bevel back cut edge orifice)

Liquid: 90 % glycerine	Temp: 25 ℃
Orifice: Chamfer edge	
Area	0,00005024 m^2
Diameter	0,008m
Tank area	0,16m
Dh	0,008m

Viscosity	0,077 Pa.s
Density	1234 **Kg / m^3**
Gravitaional acceleration	9,81 **m^2/s**

Table G1: Glycerine solutions: 90 % glycerine; chamfer edge orifice

Time (s)	Diff Time	Mass in tank (kg)	Height(m)	Diff Height (m)	Flow rate (m^3/s)	Velocity	C_d	Re
4,99	0	55,289	0,346	0	-	0	-	0
34,99	30	52,386	0,327	0,018	0,0000959	2,53	0,75	324
64,99	60	49,544	0,310	0,035	0,0000929	2,46	0,75	316
94,99	90	46,787	0,292	0,053	0,0000900	2,39	0,75	307
124,99	120	44,150	0,276	0,069	0,0000870	2,32	0,74	298
154,99	150	41,561	0,260	0,085	0,0000841	2,25	0,74	289
184,99	180	39,102	0,244	0,101	0,0000811	2,18	0,74	280
214,99	210	36,703	0,229	0,116	0,0000781	2,12	0,73	271
244,99	240	34,414	0,215	0,130	0,0000752	2,05	0,73	263
274,99	270	32,202	0,201	0,144	0,0000722	1,98	0,72	254
304,99	300	30,085	0,188	0,157	0,0000692	1,92	0,72	246
334,99	330	28,059	0,175	0,170	0,0000663	1,85	0,71	237
364,99	360	26,095	0,163	0,182	0,0000633	1,78	0,70	229
394,99	390	24,240	0,152	0,194	0,0000604	1,72	0,70	221
424,99	420	22,461	0,140	0,205	0,0000574	1,65	0,69	212
454,99	450	20,802	0,130	0,215	0,0000544	1,59	0,68	204
						Av=	0,72	

Table G2: Glycerine solutions: 90 % glycerine; quadrant edge orifice

Time (s)	Diff Time	Mass in tank (kg)	Height(m)	Diff Height (m)	Flow rate (m^3/s)	Velocity	C d	Re
6,65	0	55,458	0,347	0,000	-	0	-	0
46,65	40	51,581	0,322	0,024	0,0000949	2,51	0,75	322
86,65	80	47,872	0,299	0,047	0,0000909	2,42	0,75	310
126,65	120	44,282	0,277	0,070	0,0000869	2,33	0,74	298
166,65	160	40,900	0,256	0,091	0,0000829	2,23	0,74	287
206,65	200	37,675	0,235	0,111	0,0000789	2,14	0,73	275
246,65	240	34,594	0,216	0,130	0,0000749	2,06	0,72	264
286,65	280	31,707	0,198	0,148	0,0000709	1,97	0,72	252
326,65	320	28,948	0,181	0,166	0,0000668	1,88	0,71	241
366,65	360	26,332	0,165	0,182	0,0000628	1,79	0,70	230
406,65	400	23,895	0,149	0,197	0,0000588	1,71	0,68	219
446,65	440	21,581	0,135	0,212	0,0000548	1,62	0,67	208
						Av =	0,72	

Table G3: Glycerine solutions: 90 % glycerine; short square edge orifice

Time (s)	Diff Time	Mass in tank (kg)	Height(m)	Diff Height (m)	Flow rate (m^3/s)	Velocity	C_d	Re
13,31	0	55,138	0,345	0	-	0	-	0
53,31	40	51,456	0,322	0,023	0,0000906	2,51	0,72	322
93,31	80	47,867	0,299	0,045	0,0000870	2,42	0,71	310
133,31	120	44,448	0,278	0,066	0,0000834	2,33	0,71	299
173,31	160	41,198	0,257	0,087	0,0000798	2,24	0,71	288
213,31	200	38,080	0,238	0,106	0,0000762	2,16	0,70	277
253,31	240	35,121	0,220	0,125	0,0000726	2,07	0,70	266
293,31	280	32,283	0,202	0,142	0,0000690	1,98	0,69	255
333,31	320	29,593	0,185	0,159	0,0000654	1,90	0,68	244
373,31	360	27,062	0,169	0,175	0,0000617	1,82	0,67	233
413,31	400	24,662	0,154	0,190	0,0000581	1,73	0,67	222
453,31	440	22,406	0,140	0,204	0,0000545	1,65	0,65	212
493,31	480	20,306	0,127	0,217	0,0000509	1,57	0,64	202
533,313	520	18,303	0,114	0,230	0,0000473	1,49	0,63	192
						Av =	0,68	

Table G4: Glycerine solutions: 90 % glycerine; square bevel back cut edge orifice

Time (s)	Diff Time	Mass in tank (kg)	Height(m)	Diff Height (m)	Flow rate (m^3/s)	Velocity	C_d	Re
13,31	0	55,807	0,349	0	-	0	-	0
53,31	40	52,011	0,325	0,023	0,0000935	2,52	0,74	323
93,31	80	48,335	0,302	0,046	0,0000897	2,43	0,73	312
133,31	120	44,814	0,280	0,068	0,0000860	2,34	0,73	300
173,31	160	41,453	0,259	0,089	0,0000822	2,25	0,73	289
213,31	200	38,236	0,239	0,109	0,0000785	2,16	0,72	277
253,31	240	35,173	0,220	0,129	0,0000747	2,07	0,72	266
293,31	280	32,276	0,202	0,147	0,0000709	1,98	0,71	255
333,31	320	29,497	0,184	0,164	0,0000672	1,90	0,70	243
373,31	360	26,896	0,168	0,180	0,0000634	1,81	0,70	232
413,31	400	24,419	0,153	0,196	0,0000597	1,73	0,69	221
453,31	440	22,115	0,138	0,210	0,0000559	1,64	0,68	211
						Av=	0,71	

Appendix H : 85 % Glycerine discharge; (chamfer, quadrant, short square and square bevel back cut edge orifice)

Appendix H1–H4 : 85 % Glycerine discharge; (chamfer, quadrant, short square and square bevel back cut edge orifice)

Liquid: 85 % glycerine	Temp: 23 ℃
Orifice: Chamfer edge	
Area	0,00005024 m^2
Diameter	0,008m
Tank area	0,16m
Dh	0,008m

Viscosity	0,055 Pa.s
Density	1200 **Kg / m^3**
Gravitaional	9,81 **m^2/s**

Table H1: Glycerine solutions: 85 % glycerine; chamfer edge orifice

Time (s)	Diff Time	Mass in tank (kg)	Height(m)	Diff Height (m)	Flow rate (m^3 /s)	Velocity	C_d	Re
4,99	0	45,788	0,286	0	-	0	-	0
34,99	30	43,038	0,269	0,017	0,0000890	2,29	0,77	400
64,99	60	40,413	0,253	0,033	0,0000859	2,22	0,77	388
94,99	90	37,876	0,237	0,049	0,0000828	2,15	0,76	376
124,99	120	35,447	0,222	0,064	0,0000797	2,08	0,76	363
154,99	150	33,109	0,207	0,079	0,0000766	2,01	0,76	351
184,99	180	30,883	0,193	0,093	0,0000734	1,94	0,75	339
214,99	210	28,717	0,179	0,106	0,0000703	1,87	0,75	327
244,99	240	26,640	0,166	0,119	0,0000672	1,80	0,74	315
274,99	270	24,682	0,154	0,131	0,0000641	1,73	0,73	303
304,99	300	22,787	0,142	0,143	0,0000610	1,67	0,73	291
334,99	330	21,037	0,131	0,154	0,0000579	1,60	0,72	280
364,99	360	19,337	0,121	0,165	0,0000548	1,53	0,71	268
394,99	390	17,710	0,111	0,175	0,0000517	1,47	0,70	257
424,99	420	16,176	0,101	0,185	0,0000485	1,40	0,69	245
						Av=	0,74	

Table H2: Glycerine solutions: 85 % glycerine; quadrant edge orifice

Time (s)	Diff Time	Mass in tank (kg)	Height(m)	Diff Height (m)	Flow rate (m^3/s)	Velocity	C_d	Re
6,65	0	45,473	0,284	0,000	-	0	-	0
46,65	40	41,886	0,262	0,022	0,0000875	2,26	0,77	404
86,65	80	38,454	0,240	0,044	0,0000833	2,17	0,76	387
126,65	120	35,208	0,220	0,064	0,0000791	2,07	0,76	370
166,65	160	32,117	0,201	0,083	0,0000750	1,98	0,75	353
206,65	200	29,226	0,183	0,102	0,0000708	1,89	0,74	337
246,65	240	26,476	0,165	0,119	0,0000667	1,80	0,74	321
286,65	280	23,897	0,149	0,135	0,0000625	1,71	0,73	305
326,65	320	21,473	0,134	0,150	0,0000583	1,62	0,72	289
366,65	360	19,219	0,120	0,164	0,0000542	1,53	0,70	273
406,65	400	17,123	0,107	0,177	0,0000500	1,44	0,69	258
446,65	440	15,216	0,095	0,189	0,0000459	1,36	0,67	243
486,65	480	13,388	0,084	0,201	0,0000417	1,28	0,65	228
						Av=	0,72	

Table H3: Glycerine solutions: 85 % glycerine; short square edge orifice

Time (s)	Diff Time	Mass in tank (kg)	Height(m)	Diff Height (m)	Flow rate (m^3/s)	Velocity	C_d	Re
13,31	0	45,509	0,284	0	-	0	-	0
53,31	40	42,095	0,263	0,021	0,0000834	2,27	0,73	405
93,31	80	38,819	0,243	0,041	0,0000797	2,18	0,73	389
133,31	120	35,738	0,223	0,061	0,0000759	2,09	0,72	373
173,31	160	32,747	0,205	0,079	0,0000722	2,00	0,72	357
213,31	200	29,940	0,187	0,097	0,0000684	1,91	0,71	341
253,31	240	27,269	0,170	0,113	0,0000647	1,82	0,70	326
293,31	280	24,798	0,155	0,129	0,0000609	1,74	0,70	310
333,31	320	22,408	0,140	0,144	0,0000572	1,65	0,69	295
373,31	360	20,212	0,126	0,158	0,0000534	1,57	0,68	280
413,31	400	18,137	0,113	0,171	0,0000497	1,49	0,66	265
453,31	440	16,215	0,101	0,183	0,0000459	1,41	0,65	251
						Av =	0,70	

Table H4: Glycerine solutions: 85 % glycerine; square bevel back cut edge orifice

Time (s)	Diff Time	Mass in tank (kg)	Height(m)	Diff Height (m)	Flow rate (m^3/s)	Velocity	C_d	Re
13,31	0	45,487	0,284	0	-	0	-	0
53,31	40	41,946	0,262	0,022	0,0000859	2,26	0,75	404
93,311	80	38,594	0,241	0,043	0,0000820	2,17	0,75	387
133,31	120	35,387	0,221	0,063	0,0000781	2,08	0,75	371
173,31	160	32,339	0,202	0,082	0,0000742	1,99	0,74	355
213,31	200	29,447	0,184	0,100	0,0000703	1,90	0,74	338
253,31	240	26,739	0,167	0,117	0,0000664	1,81	0,73	322
293,31	280	24,160	0,151	0,133	0,0000625	1,72	0,72	306
333,31	320	21,729	0,136	0,148	0,0000586	1,63	0,71	291
373,31	360	19,440	0,121	0,162	0,0000547	1,54	0,71	275
413,31	400	17,345	0,108	0,175	0,0000508	1,45	0,69	260
453,31	440	15,387	0,096	0,188	0,0000469	1,37	0,68	244
						Av=	0,73	

Appendix I : 76 % Glycerine discharge; (chamfer, quadrant, short square and square bevel back cut edge orifice)

Appendx I1–I4 : 76 % Glycerine discharge; (chamfer, quadrant, short square and square bevel back cut edge orifice)

Liquid: 76 % glycerine	Temp: 24 ℃
Orifice: Chamfer edge	
Area	0,00005024 m^2
Diameter	0,008m
Tank area	0,16m
Dh	0,008m

Viscosity	0,022 Pa.s
Density	1202 **Kg / m ^{3}**
Gravitaional	9,81 **m ^{2}/s**

Table I1: Glycerine solutions: 76 % glycerine; chamfer edge orifice

Time (s)	**Diff Time**	**Mass in tank (kg)**	**Height(m)**	**Diff Height (m)**	**Flow rate (m^3/s)**	**Velocity**	**C_d**	Re
13,31	0	49,441	0,309	0	-	0	-	0
53,31	40	45,433	0,284	0,025	0,0000983	2,36	0,83	1031
93,31	80	41,598	0,260	0,049	0,0000936	2,258	0,82	987
133,31	120	37,928	0,237	0,071	0,0000889	2,15	0,82	942
173,31	160	34,464	0,215	0,093	0,0000843	2,05	0,82	898
213,31	200	31,191	0,195	0,114	0,0000796	1,95	0,81	854
253,31	240	28,091	0,176	0,133	0,0000750	1,85	0,80	811
293,31	280	25,192	0,157	0,151	0,0000703	1,75	0,80	768
333,31	320	22,485	0,141	0,168	0,0000656	1,66	0,79	725
373,31	360	19,967	0,125	0,184	0,0000610	1,56	0,78	683
413,31	400	17,611	0,110	0,198	0,0000563	1,46	0,76	642
453,31	440	15,419	0,096	0,212	0,0000517	1,37	0,75	601
						Av=	0,80	

Table I2: Glycerine solutions: 76 % glycerine; quadrant edge orifice

Time (s)	Diff Time	Mass in tank (kg)	Height(m)	Diff Height (m)	Flow rate (m^3/s)	Velocity	C_d	Re
6,65	0	49,193	0,307	0,000	-	0	-	0
46,65	40	45,105	0,282	0,026	0,0000990	2,35	0,84	1027
86,65	80	41,244	0,258	0,050	0,0000941	2,24	0,83	982
126,65	120	37,590	0,235	0,073	0,0000893	2,14	0,83	938
166,65	160	34,132	0,213	0,094	0,0000845	2,04	0,82	894
206,65	200	30,822	0,193	0,115	0,0000796	1,94	0,82	849
246,65	240	27,741	0,173	0,134	0,0000748	1,84	0,81	806
286,65	280	24,850	0,155	0,152	0,0000700	1,74	0,80	763
326,65	320	22,160	0,138	0,169	0,0000652	1,64	0,79	720
366,65	360	19,621	0,123	0,185	0,0000603	1,55	0,77	677
						Av =	0,81	

Table I3: Glycerine solutions: 76 % glycerine; short square edge orifice

Time (s)	Diff Time	Mass in tank (kg)	Height(m)	Diff Height (m)	Flow rate (m^3/s)	Velocity	C_d	Re
13,31	0	49,131	0,307	0	-	0	-	0
53,31	40	45,564	0,285	0,022	0,0000875	2,36	0,74	1082
93,31	80	42,169	0,264	0,043	0,0000841	2,27	0,74	1041
133,31	120	38,877	0,243	0,064	0,0000807	2,18	0,74	999
173,31	160	35,727	0,223	0,083	0,0000773	2,09	0,73	958
213,31	200	32,707	0,204	0,102	0,0000738	2,00	0,73	917
253,31	240	29,794	0,186	0,120	0,0000704	1,91	0,73	875
293,31	280	26,993	0,169	0,138	0,0000670	1,81	0,73	833
333,31	320	24,392	0,152	0,154	0,0000636	1,72	0,73	791
373,31	360	21,922	0,137	0,170	0,0000601	1,63	0,73	750
413,31	400	19,616	0,123	0,184	0,0000567	1,55	0,73	710
453,31	440	17,468	0,109	0,197	0,0000533	1,46	0,72	670
493,31		15,465				Av=	0,73	

Table I4: Glycerine solutions: 76 % glycerine; square bevel back cut edge orifice

Time (s)	Diff Time	Mass in tank (kg)	Height(m)	Diff Height (m)	Flow rate (m^3/s)	Velocity	C_d	Re
13,31	0	49,326	0,308	0	-	0	-	0
53,31	40	45,580	0,285	0,023	0,0000929	2,36	0,78	1082
93,31	80	41,934	0,262	0,046	0,0000889	2,26	0,78	1038
133,31	120	38,471	0,240	0,067	0,0000849	2,17	0,78	994
173,31	160	35,138	0,220	0,088	0,0000809	2,07	0,78	950
213,31	200	31,960	0,200	0,108	0,0000769	1,97	0,77	906
253,31	240	28,959	0,181	0,127	0,0000729	1,88	0,77	862
293,31	280	26,130	0,163	0,145	0,0000689	1,79	0,77	819
333,31	320	23,472	0,147	0,161	0,0000649	1,69	0,76	776
373,31	360	20,952	0,131	0,177	0,0000609	1,60	0,76	733
413,31	400	18,595	0,116	0,192	0,0000569	1,51	0,75	691
						Av =	0,77	

Appendix J: 47 % Glycerine discharge; (chamfer, quadrant, short square and square bevel back cut edge orifice)

Appendix J1-J4 : 47 % Glycerine discharge; (chamfer, quadrant, short square and square bevel back cut edge orifice)

Liquid: 47 % glycerine	Temp: 21 ℃
Orifice: Chamfer edge	
Area	0,00005024 m^2
Diameter	0,008m
Tank area	0,16m
Dh	0,008m

Viscosity	0,0073 Pa.s
Density	1136 **Kg / m** $^{\mathbf{3}}$
Gravitaional	9,81 **m** $^{\mathbf{2}}$**/s**

Table J1: Glycerine solutions: 47 % glycerine; chamfer edge orifice

Time (s)	Diff Time	Mass in tank (kg)	Height(m)	Diff Height (m)	Flow rate (m^3/s)	Velocity	C_d	Re
4,15	0	47,463	0,297	0	-	0	-	0
29,15	25	44,867	0,280	0,016	0,0001023	2,34	0,87	2920
54,15	50	42,361	0,265	0,031	0,0000991	2,27	0,87	2837
79,15	75	39,908	0,249	0,047	0,0000960	2,21	0,86	2754
104,15	100	37,568	0,235	0,061	0,0000929	2,14	0,86	2672
129,15	125	35,292	0,221	0,076	0,0000898	2,08	0,86	2589
154,15	150	33,083	0,207	0,089	0,0000866	2,01	0,86	2507
179,15	175	30,938	0,193	0,103	0,0000835	1,94	0,85	2424
204,15	200	28,877	0,180	0,116	0,0000804	1,88	0,85	2342
229,15	225	26,903	0,168	0,128	0,0000773	1,81	0,85	2261
254,15	250	25,000	0,156	0,140	0,0000742	1,75	0,84	2179
279,15	275	23,208	0,145	0,151	0,0000710	1,68	0,84	2100
304,15	300	21,489	0,134	0,162	0,0000679	1,62	0,83	2020
329,15	325	19,813	0,124	0,172	0,0000648	1,55	0,83	1940
354,15	350	18,251	0,114	0,182	0,0000617	1,49	0,82	1862
379,15	375	16,731	0,105	0,192	0,0000585	1,43	0,81	1783
404,15	400	15,319	0,096	0,200	0,0000554	1,37	0,80	1706
429,15	425	13,953	0,087	0,209	0,0000523	1,30	0,80	1628
						Av=	0,84	

Table J2: Glycerine solutions: 47% glycerine; quadrant edge orifice

Time (s)	Diff Time	Mass in tank (kg)	Height(m)	Diff Height (m)	Flow rate (m^3/s)	Velocity	C_d	Re
4,15	0	47,258	0,295	0	-	0	-	0
29,15	25	44,598	0,279	0,016	0,0001037	2,33	0,88	2911
54,15	50	42,069	0,263	0,032	0,0001004	2,27	0,88	2827
79,15	75	39,590	0,247	0,047	0,0000972	2,20	0,88	2742
104,15	100	37,197	0,232	0,062	0,0000939	2,13	0,88	2658
129,15	125	34,863	0,218	0,077	0,0000907	2,06	0,87	2574
154,15	150	32,688	0,204	0,091	0,0000874	2,00	0,87	2492
179,15	175	30,527	0,191	0,104	0,0000842	1,93	0,87	2408
204,15	200	28,459	0,178	0,117	0,0000809	1,86	0,86	2325
229,15	225	26,461	0,165	0,129	0,0000777	1,80	0,86	2242
254,15	250	24,571	0,154	0,141	0,0000744	1,73	0,85	2160
279,15	275	22,753	0,142	0,153	0,0000712	1,67	0,85	2079
304,15	300	21,034	0,131	0,163	0,0000679	1,60	0,84	1999
329,15	325	19,368	0,121	0,174	0,0000646	1,54	0,83	1918
354,15	350	17,778	0,111	0,184	0,0000614	1,47	0,83	1838
379,15	375	16,305	0,102	0,193	0,0000581	1,41	0,82	1760
404,15	400	14,872	0,093	0,202	0,0000549	1,35	0,81	1681
429,15	425	13,535	0,085	0,210	0,0000516	1,28	0,80	1603
						Av =	0,85	

Table J3: Glycerine solutions: 47 % glycerine; short square edge orifice

Time (s)	Diff Time	Mass in tank (kg)	Height(m)	Diff Height (m)	Flow rate (m^3/s)	Velocity	C_d	Re
8,31	0	47,235	0,295	0	-	0	-	0
33,31	25	45,254	0,283	0,012	0,0000776	2,35	0,66	2932
58,31	50	43,353	0,271	0,024	0,0000759	2,30	0,66	2870
83,31	75	41,471	0,259	0,036	0,0000743	2,25	0,66	2807
108,31	100	39,622	0,248	0,047	0,0000726	2,20	0,66	2744
133,31	125	37,831	0,236	0,058	0,0000709	2,15	0,66	2681
158,31	150	36,091	0,226	0,069	0,0000692	2,10	0,66	2618
183,31	175	34,367	0,215	0,080	0,0000676	2,05	0,66	2555
208,31	200	32,716	0,204	0,090	0,0000659	2,00	0,65	2493
233,31	225	31,084	0,194	0,100	0,0000642	1,95	0,65	2430
258,31	250	29,514	0,184	0,110	0,0000626	1,90	0,65	2368
283,31	275	27,947	0,175	0,120	0,0000609	1,85	0,65	2304
308,31	300	26,450	0,165	0,129	0,0000592	1,80	0,65	2242
333,31	325	24,989	0,156	0,139	0,0000575	1,75	0,65	2179
358,31	350	23,531	0,147	0,148	0,0000559	1,69	0,65	2114
383,31	375	22,142	0,138	0,156	0,0000542	1,64	0,65	2051
408,31	400	20,799	0,130	0,165	0,0000525	1,59	0,65	1988
433,31	425	19,486	0,122	0,173	0,0000508	1,54	0,65	1924
458,31	450	18,187	0,114	0,181	0,0000492	1,49	0,66	1859
						Av =	0,65	

Table J4: Glycerine solutions: 47 % glycerine; square bevel back cut edge orifice

Time (s)	Diff Time	Mass in tank (kg)	Height(m)	Diff Height (m)	Flow rate (m^3/s)	Velocity	C_d	Re
8,316683301	0	47,336	0,296	0	-	0	-	0
33,31	25	45,349	0,283	0,012	0,0000794	2,35	0,67	2935
58,31	50	43,358	0,271	0,024	0,0000778	2,30	0,67	2870
83,31	75	41,454	0,259	0,036	0,0000762	2,25	0,67	2806
108,31	100	39,565	0,247	0,048	0,0000747	2,20	0,67	2742
133,31	125	37,708	0,236	0,060	0,0000731	2,15	0,68	2677
158,31	150	35,907	0,224	0,071	0,0000715	2,09	0,68	2612
183,31	175	34,153	0,213	0,082	0,0000699	2,04	0,68	2547
208,31	200	32,413	0,203	0,093	0,0000684	1,99	0,68	2481
233,31	225	30,721	0,192	0,103	0,0000668	1,94	0,69	2416
258,31	250	29,059	0,182	0,114	0,0000652	1,88	0,69	2350
283,31	275	27,439	0,171	0,124	0,0000637	1,83	0,69	2283
308,31	300	25,887	0,162	0,134	0,0000621	1,78	0,69	2218
333,31	325	24,366	0,152	0,143	0,0000605	1,72	0,70	2151
358,31	350	22,887	0,143	0,152	0,0000589	1,67	0,70	2085
383,31	375	21,456	0,134	0,161	0,0000574	1,62	0,70	2019
408,31	400	20,097	0,126	0,170	0,0000558	1,56	0,71	1954
433,31	425	18,753	0,117	0,178	0,0000542	1,51	0,71	1887
458,31	450	17,426	0,109	0,186	0,0000527	1,46	0,72	1819
						Av=	0,69	

Appendix K : 37 % Glycerine discharge; (chamfer, quadrant, short square and square bevel back cut edge orifice)

Appendix K1–K4 : 37 % Glycerine discharge; (chamfer, quadrant, short square and square bevel back cut edge orifice)

Liquid : 37 % glycerine	Temp: 21 ℃
Orifice : Chamfer edge	
Area	0,00005024 m^2
Diamneter	0,008m
Tank area	0,16m
Dh	0,008m

Viscosity	0,005 Pa.s
Density	1130 **Kg / m** $^{\mathbf{3}}$
Gravbitaional	9,81 **m** $^{\mathbf{2}}$**/s**

Table K1: Glycerine solutions: 37 % glycerine; chamfer edge orifice

Time (s)	Diff Time	Mass in tank (kg)	Height(m)	Diff Height (m)	Flow rate (m^3/s)	Velocity	C_d	Re
4,15	0	39,953	0,250	0	-	0	-	0
29,15	25	37,636	0,235	0,014	0,0000922	2,14	0,85	3884
54,15	50	35,357	0,221	0,028	0,0000892	2,08	0,85	3764
79,15	75	33,165	0,207	0,042	0,0000861	2,01	0,85	3646
104,15	100	31,051	0,194	0,055	0,0000831	1,95	0,85	3527
129,15	125	29,032	0,181	0,068	0,0000801	1,88	0,84	3411
154,15	150	27,042	0,169	0,080	0,0000770	1,82	0,84	3292
179,15	175	25,140	0,157	0,092	0,0000740	1,75	0,84	3174
204,15	200	23,348	0,146	0,103	0,0000709	1,69	0,83	3059
229,15	225	21,604	0,135	0,114	0,0000679	1,62	0,83	2942
254,15	250	19,966	0,125	0,124	0,0000648	1,56	0,82	2829
279,15	275	18,381	0,115	0,134	0,0000618	1,50	0,82	2714
304,15	300	16,834	0,105	0,144	0,0000588	1,43	0,81	2597
329,15	325	15,440	0,096	0,153	0,0000557	1,37	0,81	2487
354,15	350	14,100	0,088	0,161	0,0000527	1,31	0,80	2377
379,15	375	12,792	0,080	0,169	0,0000496	1,25	0,79	2264
						Av =	0,83	

Table K2: Glycerine solutions: 37% glycerine; quadrant edge orifice

Time (s)	Diff Time	Mass in tank (kg)	Height(m)	Diff Height (m)	Flow rate (m^3/s)	Velocity	C_d	Re
4,15834165	0	39,803	0,249	0	-	0	-	0
29,15	25	37,398	0,234	0,015	0,0000945	2,14	0,88	3871
54,15	50	35,070	0,219	0,029	0,0000912	2,07	0,88	3749
79,15	75	32,823	0,205	0,043	0,0000879	2,00	0,87	3627
104,15	100	30,680	0,192	0,057	0,0000846	1,93	0,87	3506
129,15	125	28,606	0,179	0,069	0,0000813	1,87	0,86	3386
154,15	150	26,612	0,166	0,082	0,0000780	1,80	0,86	3266
179,15	175	24,712	0,154	0,094	0,0000747	1,74	0,85	3147
204,15	200	22,858	0,143	0,105	0,0000714	1,67	0,85	3026
229,15	225	21,141	0,132	0,116	0,0000681	1,61	0,84	2911
254,15	250	19,480	0,122	0,127	0,0000648	1,54	0,84	2794
279,15	275	17,908	0,112	0,136	0,0000615	1,48	0,83	2679
304,15	300	16,373	0,102	0,146	0,0000583	1,41	0,82	2561
329,15	325	14,982	0,094	0,155	0,0000550	1,35	0,81	2450
354,15	350	13,642	0,085	0,163	0,0000517	1,29	0,80	2338
						Av=	0,85	

Table K3: Glycerine solutions: 37 % glycerine; short square edge orifice

Time (s)	Diff Time	Mass in tank (kg)	Height(m)	Diff Height (m)	Flow rate (m^3/s)	Velocity	C_d	Re
8,31	0	39,840	0,249	0	-	0	-	0
33,31	25	38,049	0,238	0,011	0,0000693	2,16	0,64	3905
58,31	50	36,343	0,227	0,021	0,0000676	2,11	0,64	3816
83,31	75	34,662	0,217	0,032	0,0000660	2,06	0,64	3727
108,31	100	33,036	0,206	0,042	0,0000644	2,01	0,64	3638
133,31	125	31,415	0,196	0,052	0,0000628	1,96	0,64	3548
158,31	150	29,917	0,187	0,062	0,0000612	1,91	0,64	3462
183,31	175	28,404	0,178	0,071	0,0000595	1,86	0,63	3374
208,31	200	26,953	0,168	0,080	0,0000579	1,81	0,63	3286
233,31	225	25,514	0,159	0,089	0,0000563	1,76	0,63	3198
258,31	250	24,137	0,151	0,098	0,0000547	1,72	0,63	3110
283,31	275	22,760	0,142	0,106	0,0000530	1,67	0,63	3020
308,31	300	21,467	0,134	0,114	0,0000514	1,62	0,63	2933
333,31	325	20,178	0,126	0,122	0,0000498	1,57	0,63	2843
358,31	350	18,974	0,119	0,130	0,0000482	1,52	0,63	2757
383,31	375	17,800	0,111	0,137	0,0000465	1,47	0,63	2671
408,31	400	16,651	0,104	0,144	0,0000449	1,42	0,63	2583
433,31	425	15,525	0,097	0,151	0,0000433	1,37	0,62	2494
458,31	450	14,475	0,090	0,158	0,0000417	1,33	0,62	2408
						Av =	0,63	

Table K4: Glycerine solutions: 37 % glycerine; square bevel back cut edge orifice

Time (s)	Diff Time	Mass in tank (kg)	Height(m)	Diff Height (m)	Flow rate (m^3/s)	Velocity	C_d	Re
8,31	0	39,924	0,250	0	-	0	-	0
33,31	25	38,120	0,238	0,011	0,0000716	2,162063	0,66	3909,011
58,31	50	36,365	0,227	0,022	0,0000700	2,11	0,66	3817
83,31	75	34,642	0,217	0,033	0,0000683	2,06	0,66	3726
108,31	100	32,974	0,206	0,043	0,0000667	2,01	0,66	3635
133,31	125	31,287	0,196	0,054	0,0000651	1,95	0,66	3541
158,31	150	29,664	0,185	0,061	0,0000635	1,90	0,66	3448
183,31	175	28,102	0,176	0,073	0,0000619	1,85	0,66	3356
208,31	200	26,601	0,166	0,083	0,0000603	1,80	0,66	3265
233,31	225	25,088	0,157	0,092	0,0000586	1,75	0,67	3171
258,31	250	23,672	0,148	0,101	0,0000570	1,70	0,67	3080
283,31	275	22,249	0,139	0,110	0,0000554	1,65	0,67	2986
308,31	300	20,882	0,131	0,119	0,0000538	1,60	0,67	2893
333,31	325	19,572	0,122	0,127	0,0000522	1,54	0,67	2800
358,31	350	18,310	0,114	0,135	0,0000506	1,49	0,67	2709
383,31	375	17,058	0,107	0,142	0,0000490	1,44	0,67	2614
408,31	400	15,880	0,099	0,150	0,0000473	1,39	0,68	2522
433,31	425	14,714	0,092	0,157	0,0000457	1,34	0,68	2428
458,31	450	13,678	0,085	0,164	0,0000441	1,29	0,68	2341
						Av=	0,67	

Appendix L : 6.6 % CMC discharge; (chamfer, quadrant, short square and square bevel back cut edge orifice)

Appendx L1–L4 : 6.6 % CMC discharge; (chamfer, quadrant, short square and square bevel back cut edge orifice)

Liquid: 6.6 % CMC	Temp: 17 ℃
Orific: Chamfer edge	
Area	0,00005024 m^2
Diameter	0,008m
Tank area	0,16m
Dh	0,008m

Density	1037 **Kg / m^3**
Gravitaional	9,81 **m^2/s**
k	2,406
n	0,593

Table L1: CMC solutions: 6.6 % CMC; chamfer edge orifice

Time (s)	Diff Time	Mass in tank (kg)	Height(m)	Diff Height (m)	Flow rate (m^3/s)	Velocity	C_d	Re_2
8,32	0	36,557	0,228	0	-	0	-	
58,32	50	33,734	0,211	0,017	0,0000531	2,03	0,52	155
108,32	100	31,084	0,194	0,034	0,0000502	1,95	0,51	147
158,32	150	28,595	0,179	0,049	0,0000474	1,87	0,50	138
208,32	200	26,286	0,164	0,064	0,0000445	1,79	0,49	130
258,32	250	24,155	0,151	0,077	0,0000416	1,72	0,48	123
308,32	300	22,151	0,138	0,090	0,0000387	1,64	0,47	115
358,32	350	20,334	0,127	0,101	0,0000358	1,57	0,45	109
408,32	400	18,660	0,117	0,111	0,0000329	1,51	0,43	102
458,32	450	17,124	0,107	0,121	0,0000300	1,44	0,41	96
508,32	500	15,739	0,098	0,130	0,0000271	1,38	0,39	91
558,32	550	14,442	0,090	0,138	0,0000242	1,33	0,36	85
608,32	600	13,305	0,083	0,145	0,0000213	1,27	0,33	80
658,32	650	12,284	0,077	0,151	0,0000184	1,22	0,30	76
708,32	700	11,350	0,071	0,157	0,0000156	1,17	0,26	72
758,32	750	10,524	0,066	0,162	0,0000127	1,136	0,22	68
						Av=	0,41	

Table L2: CMC solutions: 6.6 % CMC; quadrant edge orifice

Time (s)	Diff Time	Mass in tank (kg)	Height(m)	Diff Height (m)	Flow rate (m^3/s)	Velocity	C_d	Re_2
8,32	0	36,251	0,227	0	-	0	-	
58,32	50	33,491	0,209	0,017	0,0000514	2,02	0,51	154
108,32	100	30,928	0,193	0,033	0,0000486	1,94	0,50	146
158,32	150	28,503	0,178	0,048	0,0000459	1,86	0,49	138
208,32	200	26,289	0,164	0,062	0,0000431	1,79	0,48	130
258,32	250	24,211	0,151	0,075	0,0000403	1,72	0,47	123
308,32	300	22,286	0,139	0,087	0,0000375	1,65	0,45	116
358,32	350	20,519	0,128	0,098	0,0000347	1,58	0,44	109
408,32	400	18,895	0,118	0,108	0,0000320	1,52	0,42	103
458,32	450	17,395	0,109	0,117	0,0000292	1,46	0,40	97
508,32	500	16,034	0,100	0,126	0,0000264	1,40	0,37	92
558,32	550	14,824	0,093	0,133	0,0000236	1,34	0,35	87
608,32	600	13,681	0,086	0,141	0,0000208	1,29	0,32	82
658,32	650	12,671	0,079	0,147	0,0000181	1,24	0,29	78
708,32	700	11,767	0,074	0,153	0,0000153	1,20	0,25	74
758,32	750	10,944	0,068	0,158	0,0000125	1,15	0,21	70
						Av=	0,40	

Table L3: CMC solutions: 6.6 % CMC; short square edge orifice

Time (s)	Diff Time	Mass in tank (kg)	Height(m)	Diff Height (m)	Flow rate (m^3/s)	Velocity	C_d	Re_2
8,32	0	35,977	0,225	0	-	0	-	
58,32	50	33,335	0,208	0,016	0,0000494	2,02	0,49	154
108,32	100	30,824	0,193	0,032	0,0000468	1,94	0,48	146
158,32	150	28,499	0,178	0,046	0,0000443	1,86	0,47	138
208,32	200	26,309	0,164	0,060	0,0000418	1,79	0,46	130
258,32	250	24,285	0,152	0,073	0,0000392	1,72	0,45	123
308,32	300	22,397	0,140	0,084	0,0000367	1,65	0,44	116
358,32	350	20,661	0,129	0,095	0,0000341	1,59	0,43	110
408,32	400	19,067	0,119	0,105	0,0000316	1,52	0,41	104
458,32	450	17,597	0,110	0,114	0,0000291	1,46	0,39	98
508,32	500	16,251	0,102	0,123	0,0000265	1,41	0,37	93
558,32	550	15,026	0,094	0,130	0,0000240	1,35	0,35	88
608,32	600	13,909	0,087	0,137	0,0000215	1,30	0,33	83
658,32	650	12,903	0,081	0,144	0,0000189	1,25	0,30	79
708,32	700	12,005	0,075	0,149	0,0000164	1,21	0,27	75
758,32	750	11,181	0,070	0,154	0,0000138	1,17	0,24	71
808,32	800	10,452	0,065	0,159	0,0000113	1,13	0,20	68
858,32	850	9,802	0,061	0,163	0,0000088	1,09	0,16	65 6
						Av=	0,37	

Table L4: CMC solutions: 6.6 % CMC; square bevel back cut edge orifice

Time (s)	Diff Time	Mass in tank (kg)	Height(m)	Diff Height (m)	Flow rate (m^3 /s)	Velocity	C_d	Re_2
8,32	0	36,102	0,226	0	-	0	-	
58,32	50	33,403	0,209	0,016	0,0000502	2,02	0,49	154
108,32	100	30,881	0,193	0,032	0,0000475	1,94	0,49	146
158,32	150	28,460	0,178	0,047	0,0000449	1,86	0,48	138
208,32	200	26,305	0,164	0,061	0,0000422	1,79	0,47	130
258,32	250	24,229	0,151	0,074	0,0000396	1,72	0,46	123
308,32	300	22,341	0,140	0,086	0,0000369	1,65	0,44	116
358,32	350	20,588	0,129	0,096	0,0000342	1,58	0,43	110
408,32	400	18,984	0,119	0,106	0,0000316	1,52	0,41	103
458,32	450	17,528	0,110	0,116	0,0000289	1,46	0,39	98
508,32	500	16,197	0,101	0,124	0,0000263	1,40	0,37	92
558,32	550	15,002	0,094	0,131	0,0000236	1,35	0,35	88
608,32	600	13,917	0,087	0,138	0,0000209	1,30	0,32	83
658,32	650	12,937	0,081	0,144	0,0000183	1,25	0,29	79
708,32	700	12,072	0,075	0,150	0,0000156	1,21	0,26	75
758,32	750	11,299	0,071	0,155	0,0000130	1,17	0,22	72
808,32	800	10,582	0,066	0,159	0,0000103	1,13	0,18	68
858,32	850	9,977	0,062	0,163	0,0000076	1,10	0,14	66
						Av =	0,36	

Appendix M : 6.6 % CMC discharge; (chamfer, quadrant, short square and square bevel back cut edge orifice)

Appendx M1–M4 : 6.6 % CMC discharge; (chamfer, quadrant, short square and square bevel back cut edge orifice)

Liquid: 5.9 % CMC	Temp: 17 ℃
Orifice: Chamfer edge	
Area	0,00005024 m^2
Diameter	0,008m
Tank area	0,16m
Dh	0,008m

Density	1033 Kg / m^3
Gravitaional	9,81 m ^{2}/s
k	0 ,932
n	0,662

Table M1: CMC solutions: 5.9 % CMC; chamfer edge orifice

Time (s)	Diff Time	Mass in tank (kg)	Height(m)	Diff Height (m)	Flow rate (m^3/s)	Velocity	C_d	Re_2
8,32	0	38,046	0,238	0	-	0	-	
58,32	50	34,736	0,217	0,020	0,0000638	2,06	0,61	241
108,32	100	31,604	0,198	0,040	0,0000600	1,96	0,61	226
158,32	150	28,684	0,179	0,058	0,0000562	1,87	0,60	212
208,32	200	25,996	0,162	0,075	0,0000524	1,78	0,58	198
258,32	250	23,481	0,147	0,091	0,0000486	1,69	0,57	185
308,32	300	21,166	0,132	0,105	0,0000448	1,61	0,55	173
358,32	350	19,043	0,119	0,118	0,0000410	1,52	0,53	161
408,36	400	17,073	0,107	0,131	0,0000373	1,44	0,51	150
458,32	450	15,316	0,096	0,142	0,0000335	1,37	0,49	139
508,32	500	13,714	0,086	0,152	0,0000297	1,29	0,46	129
558,32	550	12,269	0,077	0,161	0,0000259	1,22	0,42	120
						Av=	0,54	

Table M2: CMC solutions: 5.9 % CMC; quadrant edge orifice

Time (s)	Diff Time	Mass in tank (kg)	Height(m)	Diff Height (m)	Flow rate (m^3/s)	Velocity	C_d	Re_2
8,32	0	37,392	0,234	0	-	0	-	
58,32	50	34,122	0,213	0,020	0,0000613	2,04	0,60	238
108,32	100	31,094	0,194	0,039	0,0000578	1,95	0,59	224
158,32	150	28,267	0,177	0,057	0,0000543	1,86	0,58	210
208,32	200	25,626	0,160	0,073	0,0000508	1,77	0,57	196
258,32	250	23,204	0,145	0,088	0,0000473	1,68	0,56	184
308,32	300	20,946	0,131	0,102	0,0000438	1,60	0,54	172
358,32	350	18,882	0,118	0,115	0,0000403	1,52	0,53	160
408,32	400	16,969	0,106	0,127	0,0000367	1,44	0,51	149
458,32	450	15,284	0,096	0,138	0,0000332	1,36	0,48	139
508,32	500	13,709	0,086	0,148	0,0000297	1,29	0,46	129
558,32	550	12,316	0,077	0,156	0,0000262	1,22	0,42	120
608,32	600	11,055	0,069	0,164	0,0000227	1,16	0,39	112
658,32	650	9,956	0,062	0,171	0,0000192	1,10	0,35	104
708,32	700	8,965	0,056	0,177	0,0000157	1,04	0,30	97
						Av=	0,49	

Table M3: CMC solutions: 5.9 % CMC; short square edge orifice

Time (s)	Diff Time	Mass in tank (kg)	Height(m)	Diff Height (m)	Flow rate (m^3/s)	Velocit y	C_d	Re_2
8,32	0	36,684	0,229	0	-	0	-	
58,32	50	33,591	0,210	0,019	0,0000590	2,02	0,58	236
108,32	100	30,719	0,192	0,037	0,0000556	1,94	0,57	222
158,32	150	28,008	0,175	0,054	0,0000522	1,85	0,56	209
208,32	200	25,475	0,159	0,070	0,0000488	1,76	0,55	196
258,32	250	23,140	0,145	0,084	0,0000455	1,68	0,54	183
308,32	300	20,951	0,131	0,098	0,0000421	1,60	0,52	172
358,32	350	18,962	0,119	0,110	0,0000387	1,52	0,50	161
408,32	400	17,122	0,107	0,122	0,0000353	1,44	0,48	150
458,32	450	15,469	0,097	0,132	0,0000319	1,37	0,46	140
508,32	500	13,938	0,087	0,142	0,0000285	1,30	0,43	131
558,32	550	12,560	0,078	0,150	0,0000251	1,24	0,40	122
608,32	600	11,346	0,071	0,158	0,0000217	1,17	0,37	114
						Av=	0,50	

Table M4: CMC solutions: 5.9% CMC; square bevel back cut edge orifice

Time (s)	Diff Time	Mass in tank (kg)	Height(m)	Diff Height (m)	Flow rate (m^3/s)	Velocity	C_d	Re_2
8,32	0	36,473	0,228	0	-	0	-	
58,32	50	33,256	0,208	0,020	0,0000609	2,01	0,60	234
108,32	100	30,246	0,189	0,038	0,0000574	1,92	0,59	220
158,32	150	27,442	0,172	0,056	0,0000539	1,83	0,58	206
208,32	200	24,806	0,155	0,072	0,0000504	1,74	0,58	192
258,36	250	22,381	0,140	0,088	0,0000469	1,65	0,56	179
308,32	300	20,144	0,126	0,102	0,0000434	1,57	0,55	167
358,32	350	18,102	0,113	0,114	0,0000399	1,48	0,53	156
408,32	400	16,214	0,101	0,126	0,0000364	1,41	0,51	145
458,32	450	14,513	0,091	0,137	0,0000329	1,33	0,49	134
508,32	500	12,965	0,081	0,146	0,0000294	1,26	0,46	124
558,32	550	11,612	0,073	0,155	0,0000259	1,19	0,43	116
608,32	600	10,379	0,065	0,163	0,0000224	1,12	0,40	107
658,32	650	9,317	0,058	0,169	0,0000189	1,06	0,35	100
708,32	700	8,412	0,053	0,175	0,0000154	1,01	0,30	93
758,32	750	7,623	0,048	0,180	0,0000119	0,96	0,25	87
						Av=	0,48	

Appendix N : 4.8 % CMC discharge; (chamfer, quadrant, short square and square bevel back cut edge orifice)

Appendx N1–N4 : 4.8 % CMC discharge; (chamfer, quadrant, short square and square bevel back cut edge orifice)

Liquid: 4.8. % CMC	Temp: 17 ℃
Orifice: Chamfer edge	
Area	0,00005024 m^2
Diameter	0,008m
Tank area	0,16m
Dh	0,008m

Density	1027 **Kg / m ^{3}**
Gravbitaional	9,81 **m ^{2}/s**
k	0 ,172
n	0,831

Table N1: CMC solutions: 4.8 % CMC; chamfer edge orifice

Time (s)	Diff Time	Mass in tank (kg)	Height(m)	Diff Height (m)	Flow rate (m^3/s)	Velocity	C_d	Re_2
8,32	0	28,438	0,178	0	-	0	-	
58,32	50	25,489	0,159	0,018	0,0000558	1,76	0,63	298
108,32	100	22,753	0,142	0,035	0,0000519	1,67	0,62	279
158,32	150	20,256	0,127	0,051	0,0000481	1,57	0,61	261
208,32	200	17,938	0,112	0,065	0,0000443	1,48	0,59	243
258,32	250	15,844	0,099	0,078	0,0000404	1,39	0,58	226
308,32	300	13,940	0,087	0,090	0,0000366	1,30	0,56	210
358,32	350	12,246	0,077	0,101	0,0000327	1,22	0,53	194
408,32	400	10,711	0,067	0,110	0,0000289	1,14	0,50	180
458,32	450	9,372	0,059	0,119	0,0000251	1,07	0,47	166
508,32	500	8,186	0,051	0,126	0,0000212	1,00	0,42	153
558,32	550	7,208	0,045	0,132	0,0000174	0,94	0,37	142
608,32	600	6,356	0,040	0,138	0,0000136	0,88	0,31	132
						Av=	0,51	

Table N2: CMC solutions: 4.8 % CMC; quadrant edge orifice

Time (s)	Diff Time	Mass in tank (kg)	Height(m)	Diff Height (m)	Flow rate (m^3/s)	Velocity	C_d	Re_2
8,32	0	28,216	0,176	0	-	0	-	
58,32	50	25,347	0,158	0,017	0,0000539	1,76	0,61	297
108,32	100	22,643	0,142	0,034	0,0000503	1,66	0,60	278
158,32	150	20,196	0,126	0,050	0,0000467	1,57	0,59	260
208,32	200	17,943	0,112	0,064	0,0000431	1,48	0,58	243
258,32	250	15,902	0,099	0,076	0,0000395	1,39	0,56	226
308,32	300	14,054	0,088	0,088	0,0000359	1,31	0,54	211
358,32	350	12,383	0,077	0,098	0,0000323	1,23	0,52	195
408,32	400	10,881	0,068	0,108	0,0000287	1,15	0,50	181
458,32	450	9,575	0,060	0,116	0,0000252	1,08	0,46	168
508,32	500	8,432	0,053	0,123	0,0000216	1,01	0,42	156
558,32	550	7,436	0,046	0,129	0,0000180	0,95	0,37	145
608,32	600	6,602	0,041	0,135	0,0000144	0,89	0,32	135
658,32	650	5,884	0,037	0,139	0,0000108	0,84	0,25	126
708,32	700	5,324	0,033	0,143	0,0000072	0,80	0,18	119
						Av=	0,47	

Table N3: CMC solutions: 4.8 % CMC; short square edge orifice

Time (s)	Diff Time	Mass in tank (kg)	Height(m)	Diff Height (m)	Flow rate (m^3/s)	Velocity	C_d	Re_2
8,32	0	27,849	0,174	0	-	0	-	
58,32	50	24,911	0,156	0,018	0,0000562	1,74	0,64	294
108,32	100	22,154	0,138	0,035	0,0000522	1,64	0,63	275
158,32	150	19,627	0,123	0,051	0,0000482	1,55	0,62	256
208,32	200	17,316	0,108	0,065	0,0000442	1,45	0,60	238
258,32	250	15,231	0,095	0,078	0,0000401	1,36	0,58	221
308,32	300	13,355	0,083	0,090	0,0000361	1,27	0,56	204
358,32	350	11,665	0,073	0,101	0,0000321	1,19	0,53	189
408,32	400	10,171	0,064	0,110	0,0000281	1,11	0,50	174
458,32	450	8,880	0,056	0,118	0,0000241	1,04	0,46	161
508,32	500	7,772	0,049	0,125	0,0000200	0,97	0,41	149
558,32	550	6,844	0,043	0,131	0,0000160	0,91	0,35	138
608,32	600	6,058	0,038	0,136	0,0000120	0,86	0,28	129
						Av =	0,51	

Table N4: CMC solutions: 4.8% CMC; square bevel back cut edge orifice

Time (s)	Diff Time	Mass in tank (kg)	Height(m)	Diff Height (m)	Flow rate (m^3/s)	Velocity	C_d	Re_2
8,32	0	27,991	0,175	0	-	0	-	
58,32	50	25,079	0,157	0,018	0,0000557	1,75	0,63	296
108,32	100	22,386	0,140	0,035	0,0000519	1,65	0,62	276
158,32	150	19,867	0,124	0,050	0,0000480	1,56	0,61	258
208,32	200	17,569	0,110	0,065	0,0000441	1,46	0,60	240
258,32	250	15,465	0,097	0,078	0,0000403	1,37	0,58	223
308,32	300	13,557	0,085	0,090	0,0000364	1,28	0,56	206
358,32	350	11,854	0,074	0,100	0,0000325	1,20	0,54	191
408,32	400	10,329	0,065	0,110	0,0000287	1,12	0,51	176
458,32	450	8,992	0,056	0,118	0,0000248	1,05	0,47	162
508,32	500	7,863	0,049	0,125	0,0000209	0,98	0,42	150
558,32	550	6,876	0,043	0,131	0,0000171	0,91	0,37	138
608,32	600	6,085	0,038	0,136	0,0000132	0,86	0,30	129
						Av=	0,52	

Appendix O : 4.8 % CMC discharge; (chamfer, quadrant, short square and square bevel back cut edge orifice)

Appendix O1–O 4: 4.8 % CMC discharge; (chamfer, quadrant, short square and square bevel back cut edge orifice)

Liquid 3.8. % CMC	Temp: 17 ℃
Orifice: Chamfer edge	
Area	0,00005024 m^2
Diameter	0,008m
Tank area	0,16m
Dh	0,008m

Density	1021 **Kg / m** ^{3}
Gravitaional	9,81 **m** ^{2}**/s**
k	0 ,0172
n	0,823

Table O1: CMC solutions: 3.8 % CMC; chamfer edge orifice

Time (s)	Diff Time	Mass in tank (kg)	Height(m)	Diff Height (m)	Flow rate (m^3/s)	Velocity	C_d	Re_2
8,32	0	34,714	0,217	0	-	0	-	
58,32	50	30,887	0,193	0,023	0,0000730	1,94	0,75	861
108,32	100	27,363	0,171	0,045	0,0000680	1,83	0,74	801
158,32	150	24,044	0,150	0,066	0,0000631	1,71	0,73	743
208,32	200	21,029	0,131	0,085	0,0000581	1,601	0,72	686
258,32	250	18,267	0,114	0,102	0,0000531	1,49	0,71	632
308,32	300	15,728	0,098	0,118	0,0000482	1,38	0,69	578
358,32	350	13,479	0,084	0,132	0,0000432	1,28	0,67	528
408,32	400	11,474	0,072	0,145	0,0000382	1,18	0,64	480
458,32	450	9,670	0,060	0,156	0,0000333	1,08	0,61	434
508,32	500	8,129	0,051	0,166	0,0000283	0,99	0,56	392
558,32	550	6,814	0,043	0,174	0,0000233	0,91	0,51	353
608,32	600	5,714	0,036	0,181	0,0000184	0,83	0,44	318
						Av=	0,65	

Table O2: CMC solutions: 3.8 % CMC; quadrant edge orific

Time (s)	Diff Time	Mass in tank (kg)	Height(m)	Diff Height (m)	Flow rate (m^3/s)	Velocity	C_d	Re_2
8,32	0	35,590	0,222	0	-	0	-	
58,32	50	31,719	0,198	0,024	0,0000743	1,97	0,75	874
108,325	100	28,109	0,176	0,046	0,0000692	1,85	0,74	814
158,325	150	24,761	0,155	0,067	0,0000641	1,74	0,73	756
208,32	200	21,692	0,136	0,086	0,0000591	1,63	0,72	699
258,32	250	18,885	0,118	0,104	0,0000540	1,52	0,71	644
308,32	300	16,320	0,102	0,120	0,0000489	1,41	0,69	591
358,32	350	14,015	0,088	0,134	0,0000438	1,31	0,67	540
408,32	400	11,966	0,075	0,147	0,0000388	1,21	0,64	492
458,32	450	10,147	0,063	0,159	0,0000337	1,11	0,60	446
508,32	500	8,567	0,054	0,168	0,0000286	1,02	0,56	404
558,32	550	7,218	0,045	0,177	0,0000236	0,94	0,50	365
						Av=	0,66	

Table O3: CMC solutions: 3.8 % CMC; short square edge orifice

Time (s)	Diff Time	Mass in tank (kg)	Height(m)	Diff Height (m)	Flow rate (m^3/s)	Velocity	C_d	Re_2
8,32	0	35,404	0,221	0	-	0	-	
58,32	50	31,725	0,198	0,022	0,0000706	1,972375	0,71	874,9435
108,32	100	28,297	0,177	0,044	0,0000663	1,86	0,71	817
158,32	150	25,094	0,157	0,064	0,0000620	1,75	0,70	762
208,32	200	22,110	0,138	0,083	0,0000577	1,64	0,70	707
258,32	250	19,358	0,121	0,100	0,0000534	1,54	0,69	653
308,32	300	16,788	0,105	0,116	0,0000491	1,43	0,68	601
358,32	350	14,458	0,090	0,130	0,0000447	1,33	0,67	550
408,32	400	12,302	0,077	0,144	0,0000404	1,22	0,66	500
458,32	450	10,374	0,065	0,156	0,0000361	1,12	0,64	452
508,32	500	8,695	0,054	0,166	0,0000318	1,03	0,61	408
						Av=	0,68	

Table O4: CMC solutions: 3.8% CMC; square bevel back cut edge orifice

Time (s)	Diff Time	Mass in tank (kg)	Height(m)	Diff Height (m)	Flow rate (m^3/s)	Velocity	C_d	Re_2
8,32	0	35,404	0,221	0	-	0	-	
58,32	50	31,725	0,198	0,022	0,0000706	1,97	0,71	874
108,32	100	28,297	0,177	0,044	0,0000663	1,862763	0,71	817
158,32	150	25,094	0,157	0,064	0,0000620	1,754189	0,70	762
208,32	200	22,110	0,138	0,083	0,0000577	1,646595	0,70	707
258,32	250	19,358	0,121	0,100	0,0000534	1,540689	0,69	653
308,32	300	16,788	0,105	0,116	0,0000491	1,434788	0,68	601
358,32	350	14,458	0,090	0,130	0,0000447	1,331523	0,67	550
408,32	400	12,302	0,077	0,144	0,0000404	1,228206	0,66	500
458,32	450	10,374	0,065	0,156	0,0000361	1,127885	0,64	452
508,32	500	8,695	0,054	0,166	0,0000318	1,032587	0,61	408
						Av=	0,68	

Appendix P : 2.4 % CMC discharge; (chamfer, quadrant, short square and square bevel back cut edge orifice)

Appendx P1–P4 : 2.4 % CMC discharge; (chamfer, quadrant, short square and square bevel back cut edge orifice)

Liquid: 2.4 % CMC	Temp: 17 ℃
Orifice: Chamfer edge	
Area	0,00005024 m^2
Diameter	0,008m
Tank area	0,16m
Dh	0,008m

Density	1014 **Kg / m** ^{3}
Gravitaional	9,81 **m** ^{2}**/s**
k	0 ,0071
n	0,944

Table P1: CMC solutions: 2.4 % CMC; chamfer edge orifice

Time (s)	Diff Time	Mass in tank (kg)	Height(m)	Diff Height (m)	Flow rate (m^3/s)	Velocity	C_d	Re_2
8,32	0	34,920	0,218	0	-	0	-	
58,32	50	30,907	0,193	0,025	0,0000775	1,94	0,79	1583
108,32	100	27,180	0,170	0,048	0,0000719	1,82	0,78	1488
158,32	150	23,709	0,148	0,070	0,0000664	1,70	0,78	1394
208,32	200	20,530	0,128	0,089	0,0000609	1,58	0,76	1301
258,32	250	17,621	0,110	0,108	0,0000554	1,46	0,75	1210
308,32	300	14,977	0,094	0,124	0,0000499	1,35	0,73	1119
358,32	350	12,650	0,079	0,139	0,0000444	1,24	0,71	1032
408,32	400	10,562	0,066	0,152	0,0000389	1,138	0,68	947
458,32	450	8,740	0,055	0,163	0,0000334	1,03	0,64	865
508,32	500	7,211	0,045	0,173	0,0000279	0,94	0,59	789
						Av=	0,72	

Table P2: CMC solutions: 2.4 % CMC; quadrant edge orifice

Time (s)	Diff Time	Mass in tank (kg)	Height(m)	Diff Height (m)	Flow rate (m^3/s)	Velocity	C_d	Re_2
8,32	0	34,231	0,214	0	-	0	-	
58,32	50	30,245	0,189	0,024	0,0000764	1,92	0,79	1566,887
108,32	100	26,532	0,166	0,048	0,0000708	1,80	0,78	1471,79
158,32	150	23,107	0,144	0,069	0,0000653	1,68	0,77	1377,664
208,32	200	20,003	0,125	0,088	0,0000597	1,56	0,76	1285
258,32	250	17,160	0,107	0,106	0,0000542	1,45	0,74	1194
308,32	300	14,617	0,091	0,122	0,0000486	1,33	0,72	1106
358,32	350	12,335	0,077	0,136	0,0000431	1,22	0,70	1020
408,32	400	10,339	0,065	0,149	0,0000375	1,12	0,66	937
458,32	450	8,592	0,054	0,160	0,0000320	1,02	0,62	858
508,32	500	7,097	0,044	0,169	0,0000264	0,93	0,56	783
558,32	550	5,865	0,037	0,1778	0,0000209	0,84	0,49	715
						Av=	0,69	

Table P3: CMC solutions: 2.4 % CMC; short square edge orifice

Time (s)	Diff Time	Mass in tank (kg)	Height(m)	Diff Height (m)	Flow rate (m^3 /s)	Velocity	C_d	Re_2
8,32	0	35,805	0,224	0	-	0	-	
58,32	50	32,228	0,201	0,022	0,0000708	1,98	0,71	1615
108,32	100	28,822	0,180	0,043	0,0000667	1,87	0,71	1531
158,32	150	25,617	0,160	0,063	0,0000627	1,77	0,70	1447
208,32	200	22,568	0,141	0,082	0,0000587	1,66	0,70	1362
258,32	250	19,732	0,123	0,100	0,0000546	1,55	0,70	1277
308,32	300	17,052	0,107	0,117	0,0000506	1,44	0,70	1191
358,32	350	14,582	0,091	0,132	0,0000466	1,33	0,69	1105
408,32	400	12,333	0,077	0,146	0,0000426	1,22	0,69	1020
458,32	450	10,303	0,064	0,159	0,0000385	1,12	0,68	936
508,32	500	8,537	0,053	0,170	0,0000345	1,02	0,67	855
558,32	550	7,014	0,044	0,1796	0,0000305	0,92	0,65	779
						Av=	0,69	

Table P4: CMC solutions: 2.4 % CMC; square bevel back cut edge orifice

Time (s)	**Diff Time**	**Mass in tank (kg)**	**Height(m)**	**Diff Height (m)**	**Flow rate (m^3 /s)**	**Velocity**	**C_d**	**Re_2**
8,32	0	33,334	0,208	0	-	0	-	
58,325	50	29,862	0,187	0,021	0,0000683	1,91	0,71	1557
108,325	100	26,547	0,166	0,0421	0,0000642	1,801	0,71	1472
158,32	150	23,460	0,147	0,061	0,0000601	1,69	0,70	1387
208,32	200	20,573	0,129	0,079	0,0000559	1,58	0,70	1303
258,32	250	17,841	0,112	0,096	0,0000518	1,47	0,70	1217
308,32	300	15,319	0,096	0,112	0,0000477	1,37	0,69	1131
358,32	350	13,038	0,081	0,126	0,0000435	1,26	0,69	1047
408,32	400	10,984	0,069	0,1398	0,0000394	1,16	0,68	965
458,326	450	9,113	0,057	0,151	0,0000352	1,057137	0,66	883
508,326	500	7,523	0,047	0,161	0,0000311	0,960449	0,64	805
						Av=	0,69	

Appendix Q :19 % Kaolin discharge; (chamfer, quadrant, short square and square bevel back cut edge orifice)

Appendix Q1–Q4 :19 % Kaolin discharge; (chamfer, quadrant, short square and square bevel back cut edge orifice)

Liquid: 19 % kaolin	Temp: 17 ℃
Orifice: Chamfer edge	
Area	0,00005024 m^2
Diameter	0,008m
Tank area	0,16m
Dh	0,008m

Density	1310 Kg / m ^{3}
Gravitaional	9,81 m ^{2}/s
k	1,295684
n	0,440045
τ (yield stress)	26,29077

Table Q1: Kaolin suspensions: 19 % Kaolin; chamfer edge orifice

Time (s)	**Diff Time**	**Mass in tank (kg)**	**Height(m)**	**Diff Height (m)**	**Flow rate (m^3 /s)**	**Velocity**	**C_d**	**Re_2**
8,32	0	42,282	0,264	0	-	0	-	
58,32	50	37,755	0,236	0,028	0,0000851	2,15	0,79	755
108,32	100	33,645	0,210	0,053	0,0000785	2,03	0,77	683
158,32	150	29,892	0,187	0,077	0,0000720	1,91	0,75	616
208,32	200	26,452	0,165	0,098	0,0000654	1,80	0,72	553
258,32	250	23,387	0,146	0,118	0,0000589	1,69	0,69	497
308,32	300	20,614	0,129	0,135	0,0000524	1,58	0,66	445
358,32	350	18,182	0,114	0,150	0,0000458	1,49	0,61	398
408,32	400	16,085	0,101	0,163	0,0000393	1,40	0,56	358
458,32	450	14,255	0,089	0,175	0,0000327	1,32	0,49	321
508,326	500	12,753	0,080	0,184	0,0000262	1,25	0,42	291
558,326	550	11,541	0,072	0,192	0,0000196	1,18	0,33	267
						Av=	0,62	

Table Q2: Kaolin suspensions: 19 % Kaolin; quadrant edge orifice

Time (s)	**Diff Time**	**Mass in tank (kg)**	**Height(m)**	**Diff Height (m)**	**Flow rate (m^3/s)**	**Velocity**	**C_d**	**Re_2**
8,32	0	41,808	0,261	0	-	0	-	
58,32	50	37,329	0,233	0,027	0,0000848	2,13	0,79	747
108,32	100	33,225	0,208	0,053	0,0000781	2,01	0,77	675
158,32	150	29,487	0,184	0,077	0,0000715	1,90	0,75	609
208,32	200	26,080	0,163	0,098	0,0000648	1,78	0,72	547
258,32	250	23,031	0,144	0,117	0,0000581	1,68	0,69	490
308,32	300	20,323	0,127	0,134	0,0000514	1,57	0,65	439
358,32	350	17,954	0,112	0,149	0,0000447	1,48	0,60	394
408,32	400	15,881	0,099	0,162	0,0000380	1,39	0,54	354
458,32	450	14,141	0,088	0,172	0,0000313	1,31	0,47	319
508,32	500	12,720	0,079	0,181	0,0000246	1,24	0,39	291
558,32	550	11,585	0,072	0,188	0,0000180	1,19	0,30	268
						Av =	0,61	

Table Q3: Kaolin suspensions: 19 % Kaolin; short square edge orifice

Time (s)	Diff Time	Mass in tank (kg)	Height(m)	Diff Height (m)	Flow rate (m^3/s)	Velocity	C_d	Re_2
8,32	0	41,359	0,258	0	-	0	-	
58,32	50	37,163	0,232	0,026	0,0000807	2,13	0,75	745
108,32	100	33,287	0,208	0,050	0,0000748	2,02	0,74	676
158,32	150	29,705	0,186	0,072	0,0000689	1,90	0,72	612
208,32	200	26,426	0,165	0,093	0,0000630	1,80	0,70	553
258,32	250	23,429	0,146	0,112	0,0000570	1,69	0,67	498
308,32	300	20,729	0,130	0,128	0,0000511	1,59	0,64	447
358,32	350	18,301	0,114	0,144	0,0000452	1,49	0,60	401
408,32	400	16,166	0,101	0,157	0,0000392	1,40	0,55	359
458,32	450	14,318	0,089	0,169	0,0000333	1,32	0,50	323
508,32	500	12,817	0,080	0,178	0,0000274	1,25	0,43	293
558,32	550	11,626	0,073	0,185	0,0000214	1,19	0,36	268
608,32	600	10,761	0,067	0,191	0,0000155	1,14	0,27	251
						Av =	0,58	

Table Q4: Kaolin suspensions: 19 % Kaolin; square bevel back cut edge orifice

Time (s)	Diff Time	Mass in tank (kg)	Height(m)	Diff Height (m)	Flow rate (m^3/s)	Velocity	C_d	Re_2
8,32	0	41,984	0,262	0	-	0	-	
58,32	50	37,686	0,236	0,026	0,0000824	2,14	0,76	754
108,32	100	33,721	0,211	0,051	0,0000763	2,03	0,75	684
158,32	150	30,025	0,188	0,074	0,0000701	1,91	0,73	618
208,32	200	26,687	0,167	0,095	0,0000639	1,80	0,70	558
258,32	250	23,645	0,148	0,114	0,0000577	1,70	0,67	502
308,32	300	20,948	0,131	0,131	0,0000515	1,60	0,64	451
358,32	350	18,517	0,116	0,146	0,0000453	1,50	0,60	405
408,32	400	16,431	0,103	0,159	0,0000391	1,41	0,55	364
458,32	450	14,650	0,092	0,170	0,0000329	1,34	0,49	329
508,32	500	13,167	0,082	0,180	0,0000267	1,27	0,42	300
558,32	550	11,943	0,075	0,187	0,0000205	1,21	0,34	275
608,32	600	11,025	0,069	0,193	0,0000143	1,16	0,25	256
						Av=	0,57	

Appendix R: 15 % Kaolin discharge; (chamfer, quadrant, short square and square bevel back cut edge orifice)

Appendix R1–R4 : 15 % Kaolin discharge; (chamfer, quadrant, short square and square bevel back cut edge orifice)

Liquid: 15 % kaolin	Temp: 17 ℃
Orifice: Chamfer edge	
Area	0,00005024 m^2
Diameter	0,008m
Tank area	0,16m
Dh	0,008m

Density	1246 **Kg / m** **3**
Gravitaional	9,81 **m** ^{2}**/s**
k	0,132
n	0,663
τ (yield stress)	12,84

Table R1: Kaolin suspensions: 15 % Kaolin; chamfer edge orifice

Time (s)	Diff Time	Mass in tank (kg)	Height(m)	Diff Height (m)	Flow rate (m^3/s)	Velocity	C_d	Re_2
8,325	0	44,965	0,281	0	-	0	-	
58,325	50	39,909	0,249	0,031596842	0,0000956	2,212211	0,86	1400,805
108,325	100	35,213	0,220	0,06094734	0,0000889	2,077985	0,85	1268,549
158,32	150	31,070	0,194	0,086	0,0000822	1,95	0,84	1148 4
208,32	200	27,190	0,170	0,111	0,0000755	1,82	0,82	1032
258,32	250	23,522	0,147	0,134	0,0000688	1,69	0,81	918
308,32	300	20,221	0,126	0,154	0,0000621	1,57	0,79	813
358,32	350	17,267	0,108	0,173	0,0000554	1,45	0,76	715
408,32	400	14,693	0,092	0,189	0,0000487	1,34	0,72	627
458,32	450	12,414	0,078	0,203	0,0000420	1,23	0,68	546
508,32	500	10,477	0,065	0,215	0,0000353	1,13	0,62	475
						Av=	0,77	

Table R2: Kaolin suspensions: 15 % Kaolin; quadrant edge orifice

Time (s)	Diff Time	Mass in tank (kg)	Height(m)	Diff Height (m)	Flow rate (m^3/s)	Velocity	C_d	Re_2
8,32	0	44,644	0,279	0	-	0	-	
58,32	50	39,594	0,247	0,031	0,0000971	2,20	0,88	1427
108,32	100	34,877	0,218	0,061	0,0000900	2,06	0,87	1288
158,32	150	30,556	0,191	0,088	0,0000829	1,93	0,85	1157
208,32	200	26,589	0,166	0,112	0,0000757	1,80	0,83	1033
258,32	250	23,005	0,144	0,135	0,0000686	1,67	0,81	918
308,32	300	19,772	0,124	0,155	0,0000615	1,55	0,79	810
358,32	350	16,891	0,106	0,173	0,0000544	1,43	0,75	712
408,32	400	14,347	0,090	0,189	0,0000472	1,32	0,71	622
458,32	450	12,140	0,076	0,203	0,0000401	1,22	0,65	541
508,32	500	10,307	0,064	0,214	0,0000330	1,124	0,58	472
558,32	550	8,813	0,055	0,223	0,0000259	1,03	0,50	414
						Av=	0,75	

Table R3: Kaolin suspensions: 15 % Kaolin; short square edge orifice

Time (s)	Diff Time	Mass in tank (kg)	Height(m)	Diff Height (m)	Flow rate (m^3/s)	Velocity	C_d	Re_2
8,32	0	43,588	0,272	0	-	0	-	
58,32	50	39,337	0,246	0,026	0,0000856	2,19	0,78	1419
108,32	100	35,240	0,220	0,052	0,0000805	2,07	0,77	1299
158,32	150	31,341	0,196	0,076	0,0000754	1,96	0,77	1181
208,32	200	27,664	0,173	0,099	0,0000702	1,84	0,76	1067
258,32	250	24,259	0,152	0,120	0,0000651	1,72	0,75	959
308,32	300	21,079	0,132	0,140	0,0000600	1,60	0,74	854
358,32	350	18,194	0,114	0,158	0,0000548	1,49	0,73	757
408,32	400	15,555	0,097	0,175	0,0000497	1,38	0,72	665
458,32	450	13,180	0,082	0,190	0,0000446	1,27	0,70	580
508,32	500	11,157	0,070	0,202	0,0000395	1,16	0,67	504
558,32	550	9,438	0,059	0,213	0,0000343	1,07	0,64	438
						Av=	0,73	

Table R4: Kaolin suspensions: 15 % Kaolin; square bevel back cut edge orifice

Time (s)	Diff Time	Mass in tank (kg)	Height(m)	Diff Height (m)	Flow rate (m ^{3} /s)	Velocity	C_d	Re_2
8,32	0	44,456	0,278	0	-	0	-	
58,32	50	40,111	0,251	0,027	0,0000872	2,21	0,78	1442
108,32	100	35,976	0,225	0,053	0,0000820	2,10	0,78	1321
158,32	150	32,022	0,200	0,077	0,0000767	1,98	0,77	1202
208,32	200	28,297	0,177	0,100	0,0000714	1,86	0,76	1087
258,32	250	24,766	0,155	0,123	0,0000662	1,74	0,76	975
308,32	300	21,559	0,135	0,143	0,0000609	1,62	0,75	870
358,32	350	18,592	0,116	0,161	0,0000556	1,50	0,73	770
408,32	400	15,919	0,099	0,178	0,0000504	1,39	0,72	678
458,32	450	13,563	0,085	0,193	0,0000451	1,28	0,70	594
508,32	500	11,523	0,072	0,205	0,0000398	1,18	0,67	518
558,32	550	9,779	0,061	0,216	0,0000346	1,09	0,63	452
						Av =	0,73	

Appendix S : 12 % Kaolin discharge; (chamfer, quadrant, short square and square bevel back cut edge orifice

Appendix S-S4 : 12 % Kaolin discharge; (chamfer, quadrant, short square and square bevel back cut edge orifice)

Liquid: 12 % kaolin	Temp: 16 ℃
Orifice: Chamfer edge	
Area	0,00005024 m^2
Diameter	0,008m
Tank area	0,16m
Dh	0,008m

Density	1193 **Kg / m** ^{3}
Gravitaional	9,81 **m** ^{2}**/s**
k	0,055
n	0,731
τ (yield stress)	0,55

Table S1: Kaolin suspensions: 12 % Kaolin; chamfer edge orifice

Time (s)	Diff Time	Mass in tank (kg)	Height(m)	Diff Height (m)	Flow rate (m^3 /s)	Velocity	C_d	Re_2
6,65	0	49,674	0,310	0	-	0	-	
46,65	40	45,339	0,283	0,027	0,0001068	2,35	0,90	3195
86,65	80	41,168	0,257	0,053	0,0001013	2,24	0,90	3001
126,65	120	37,207	0,233	0,077	0,0000958	2,13	0,89	2811
166,65	160	33,489	0,209	0,101	0,0000902	2,02	0,89	2626
206,65	200	29,981	0,187	0,123	0,0000847	1,91	0,88	2444
246,65	240	26,721	0,167	0,143	0,0000792	1,81	0,87	2268
286,65	280	23,656	0,148	0,162	0,0000737	1,70	0,86	2095
326,65	320	20,826	0,130	0,180	0,0000682	1,59	0,85	1929
366,65	360	18,206	0,114	0,196	0,0000627	1,49	0,83	1767
406,65	400	15,817	0,099	0,211	0,0000571	1,39	0,82	1612
446,65	440	13,651	0,085	0,225	0,0000516	1,29	0,79	1465
486,65	480	11,719	0,073	0,237	0,0000461	1,19	0,77	1325
						Av=	0,85	

Table S2: Kaolin suspensions: 12 % Kaolin; quadrant edge orifice

Time (s)	Diff Time	Mass in tank (kg)	Height(m)	Diff Height (m)	Flow rate (m^3 /s)	Velocity	C_d	Re_2
8,32	0	46,655	0,292	0	-	0	-	
58,32	50	41,395	0,259	0,032	0,0001006	2,25	0,89	3119
108,32	100	36,527	0,228	0,063	0,0000937	2,11	0,88	2881
158,32	150	32,028	0,200	0,091	0,0000867	1,98	0,87	2650
208,32	200	27,870	0,174	0,117	0,0000798	1,84	0,86	2426
258,32	250	24,085	0,151	0,141	0,0000728	1,71	0,84	2212
308,32	300	20,613	0,129	0,162	0,0000659	1,58	0,83	2004
358,32	350	17,499	0,109	0,182	0,0000590	1,46	0,80	1806
408,32	400	14,714	0,092	0,199	0,0000520	1,34	0,77	1618
458,32	450	12,243	0,077	0,215	0,0000451	1,22	0,73	1439,893
						Av =	0,83	

Table S3: Kaolin suspensions: 12 % Kaolin; short square edge orifice

Time (s)	Diff Time	Mass in tank (kg)	Height(m)	Diff Height (m)	Flow rate (m^3 /s)	Velocity	C_d	Re_2
8,32	0	43,588	0,272	0	-	0	-	
58,32	50	39,337	0,246	0,026	0,0000856	2,19	0,78	3019
108,32	100	35,240	0,220	0,052	0,0000805	2,07	0,77	2816
158,32	150	31,341	0,196	0,076	0,0000754	1,96	0,77	2614
208,32	200	27,664	0,173	0,099	0,0000702	1,84	0,76	2415
258,32	250	24,259	0,152	0,120	0,0000651	1,72	0,75	2222
308,32	300	21,079	0,132	0,140	0,0000600	1,60	0,74	2032
358,32	350	18,194	0,114	0,158	0,0000548	1,49	0,73	1851
408,32	400	15,555	0,097	0,175	0,0000497	1,38	0,72	1676
458,32	450	13,180	0,082	0,190	0,0000446	1,27	0,70	1508
508,32	500	11,157	0,070	0,202	0,0000395	1,16	0,67	1357
558,32	550	9,438	0,059	0,213	0,0000343	1,07	0,64	1220
						Av=	0,73	

Table S4: Kaolin suspensions: 12% Kaolin; square bevel back cut edge orifice

Time (s)	Diff Time	Mass in tank (kg)	Height(m)	Diff Height (m)	Flow rate (m^3 /s)	Velocity	C_d	Re_2
8,32	0	48,047	0,300	0	-	0	-	
58,32	50	43,822	0,274	0,026	0,0000843	2,31	0,72	3233
108,32	100	39,765	0,249	0,051	0,0000805	2,20	0,73	3040
158,32	150	35,867	0,224	0,076	0,0000766	2,09	0,73	2847
208,32	200	32,129	0,201	0,099	0,0000728	1,98	0,73	2655
258,32	250	28,532	0,178	0,121	0,0000690	1,87	0,73	2463
308,32	300	25,134	0,157	0,143	0,0000652	1,75	0,74	2272
358,32	350	21,924	0,137	0,163	0,0000614	1,63	0,75	2083
408,32	400	18,921	0,118	0,182	0,0000576	1,52	0,75	1897
458,32	450	16,139	0,101	0,199	0,0000538	1,40	0,76	1715
508,32	500	13,599	0,085	0,215	0,0000500	1,29	0,77	1539
558,32	550	11,359	0,071	0,229	0,0000462	1,18	0,78	1373
608,32	600	9,357	0,058	0,241	0,0000423	1,07	0,79	1214
						Av =	0,75	

Appendix T : 9 % Kaolin discharge; (chamfer, quadrant, short square and square bevel back cut edge orifice)

Appendix T1–T4 : 9 % Kaolin discharge; (chamfer, quadrant, short square and square bevel back cut edge orifice)

Liquid: 9 % kaolin	Temp: 16 ℃
Orifice: Chamfer edge	
Area	0,00005024 m^2
Diameter	0,008m
Tank area	0,16m
Dh	0,008m

Density	1149 **Kg / m ^{3}**
Gravitaional	9,81 **m ^{2}/s**
k	0,013518481
n	0,884992897
τ (yield stress)	2,434686819

Table T1: Kaolin suspensions: 9 % Kaolin; chamfer edge orifice

Time (s)	Diff Time	Mass in tank (kg)	Height(m)	Diff Height (m)	Flow rate (m^3/s)	Velocity	C_d	Re_2
8,32	0	53,229	0,333	0	-	0	-	
58,32	50	47,817	0,299	0,033	0,0001051	2,42	0,86	3412
108,32	100	42,804	0,268	0,065	0,0000990	2,29	0,86	3183
158,32	150	37,943	0,237	0,095	0,0000930	2,15	0,86	2950
208,32	200	33,405	0,209	0,123	0,0000869	2,02	0,85	2721
258,32	250	29,223	0,183	0,150	0,0000809	1,89	0,85	2499
308,32	300	25,336	0,158	0,174	0,0000748	1,76	0,84	2280
358,32	350	21,779	0,136	0,196	0,0000687	1,63	0,84	2068
408,32	400	18,471	0,115	0,217	0,0000627	1,50	0,83	1858
458,32	450	15,495	0,097	0,235	0,0000566	1,37	0,82	1655
508,32	500	12,838	0,080	0,252	0,0000506	1,25	0,80	1461
558,32	550	10,489	0,066	0,267	0,0000445	1,13	0,78	1276
						Av=	0,84	

Table T2: Kaolin suspensions: 9% Kaolin; quadrant edge orifice

Time (s)	Diff Time	Mass in tank (kg)	Height(m)	Diff Height (m)	Flow rate (m^3 /s)	Velocity	C_d	Re_2
8,325	0	54,037	0,338	0	-	0	-	
58,32	50	48,267	0,302	0,036	0,0001113	2,43	0,91	4055
108,32	100	42,848	0,268	0,069	0,0001043	2,29	0,91	3794
158,32	150	37,814	0,236	0,101	0,0000974	2,15	0,90	3539
208,32	200	33,132	0,207	0,130	0,0000904	2,01	0,89	3287
258,32	250	28,809	0,180	0,157	0,0000834	1,87	0,88	3041
308,32	300	24,805	0,155	0,182	0,0000764	1,74	0,87	2797
358,32	350	21,175	0,132	0,205	0,0000695	1,61	0,86	2561
408,32	400	17,864	0,112	0,226	0,0000625	1,48	0,84	2330
458,32	450	14,904	0,093	0,244	0,0000555	1,35	0,82	2106
508,32	500	12,282	0,077	0,260	0,0000485	1,22	0,79	1890
						Av =	0,87	

Table T3: Kaolin suspensions: 9 % Kaolin; short square edge orifice

Time (s)	Diff Time	Mass in tank (kg)	Height(m)	Diff Height (m)	Flow rate (m^3 /s)	Velocity	C_d	Re_2
8,32	0	53,909	0,337	0	-	0	-	
58,32	50	49,687	0,311	0,026	0,0000828	2,46	0,67	4121
108,32	100	45,635	0,285	0,051	0,0000796	2,36	0,67	3930
158,32	150	41,759	0,261	0,075	0,0000765	2,26	0,67	3740
208,32	200	38,004	0,238	0,099	0,0000733	2,15	0,68	3549
258,32	250	34,421	0,215	0,121	0,0000701	2,05	0,68	3358
308,32	300	31,002	0,194	0,143	0,0000669	1,94	0,68	3168
358,32	350	27,714	0,173	0,163	0,0000638	1,84	0,69	2976
408,32	400	24,572	0,154	0,183	0,0000606	1,73	0,69	2783
458,32	450	21,605	0,135	0,201	0,0000574	1,62	0,70	2590
508,32	500	18,813	0,118	0,219	0,0000542	1,51	0,71	2398
558,32	550	16,302	0,102	0,235	0,0000510	1,41	0,72	2214
608,32	600	13,933	0,087	0,249	0,0000479	1,30	0,73	2028
658,32	650	11,764	0,074	0,263	0,0000447	1,20	0,74	1845
708,32	700	9,766	0,061	0,275	0,0000415	1,09	0,76	1664
						Av=	0,70	

Table T4: Kaolin suspensions: 9 % Kaolin; square bevel back cut edge orifice

Time (s)	Diff Time	Mass in tank (kg)	Height(m)	Diff Height (m)	Flow rate (m^3 /s)	Velocity	C_d	Re_2
8,32	0	53,754	0,336	0	-	0	-	
58,32	50	49,434	0,309	0,026	0,0000844	2,46	0,68	4109
108,32	100	45,290	0,283	0,052	0,0000812	2,35	0,69	3913
158,32	150	41,308	0,258	0,077	0,0000779	2,25	0,69	3718
208,32	200	37,510	0,234	0,101	0,0000747	2,14	0,69	3523
258,32	250	33,880	0,212	0,124	0,0000715	2,03	0,70	3329
308,32	300	30,397	0,190	0,145	0,0000682	1,93	0,70	3133
358,32	350	27,056	0,169	0,166	0,0000650	1,82	0,71	2936
408,32	400	23,835	0,149	0,186	0,0000618	1,70	0,72	2736
458,32	450	20,806	0,130	0,205	0,0000585	1,59	0,73	2536
508,32	500	17,989	0,112	0,223	0,0000553	1,48	0,74	2339
558,32	550	15,374	0,096	0,239	0,0000520	1,37	0,75	2143
608,32	600	13,022	0,081	0,254	0,0000488	1,26	0,77	1953
658,32	650	10,893	0,068	0,267	0,0000456	1,15	0,78	1768
708,32	700	8,964	0,056	0,279	0,0000423	1,04	0,80	1586
						Av =	0,73	

Appendix U : 6% Bentonite discharge; (chamfer, quadrant, short square and square bevel back cut edge orifice)

Appendix U1–U4 : 6% Bentonite discharge; (chamfer, quadrant, short square and square bevel back cut edge orifice)

Liquid: 6 % bentonite	Temp: 20 ℃
Orifice Chamfer edge	
Area	0,00005024 m^2
Diameter	0,008m
Tank area	0,16m
Dh	0,008m

Density	1037 Kg / m^3
Gravitaional	9,81 m ^{2}/s
k	0,0172
n	1
τ (yield stress)	7,040

Table U1: Bentonite suspensions: 6 % Bentonite; chamfer edge orifice

Time (s)	Diff Time	Mass in tank (kg)	Height(m)	Diff Height (m)	Flow rate (m^3/s)	Velocity	C_d	Re_2
6,65	0	14,763	0,092	0	-	0	-	
46,65	40	13,192	0,082	0,009	0,0000360	1,27	0,56	463
86,65	80	11,869	0,074	0,018	0,0000316	1,20	0,52	434
126,65	120	10,695	0,067	0,025	0,0000273	1,14	0,47	406
166,65	160	9,672	0,060	0,031	0,0000230	1,08	0,42	381
206,65	200	8,857	0,055	0,036	0,0000186	1,04	0,36	360
246,65	240	8,174	0,051	0,041	0,0000143	1,00	0,28	342
286,65	280	7,728	0,048	0,043	0,0000100	0,97	0,20	330
326,65	320	7,403	0,046	0,045	0,0000056	0,95	0,12	321
366,65	360	7,242	0,045	0,047	0,0000013	0,94	0,03	316
						Av =	0,33	

Table U2: Bentonite suspensions: 6% Bentonite; quadrant edge orifice

Time (s)	Diff Time	Mass in tank (kg)	Height(m)	Diff Height (m)	Flow rate (m^3/s)	Velocity	C_d	Re_2
4,15	0	14,791	0,092	0	-	0	-	
29,15	25	13,783	0,086	0,006301939	0,0000370	1,30	0,57	626
54,15	50	12,892	0,081	0,011869078	0,0000343	1,25	0,54	605
79,15	75	12,078	0,075	0,016957783	0,0000316	1,21	0,52	586
104,15	100	11,340	0,071	0,021569366	0,0000288	1,17	0,49	568
129,15	125	10,673	0,067	0,025	0,0000261	1,14	0,45	551
154,15	150	10,029	0,063	0,029	0,0000234	1,10	0,42	534
179,15	175	9,473	0,059	0,033	0,0000206	1,07	0,38	519
204,15	200	9,004	0,056	0,036	0,0000179	1,05	0,34	506
229,15	225	8,583	0,054	0,038	0,0000152	1,02	0,29	494
254,15	250	8,235	0,051	0,040	0,0000124	1,00	0,25	484
279,15	275	7,961	0,050	0,042	0,0000097	0,98	0,20	476
304,15	300	7,748	0,048	0,044	0,0000070	0,97	0,14	469
329,15	325	7,564	0,047	0,045	0,0000042	0,96	0,09	464
354,15	350	7,464	0,047	0,045	0,0000015	0,95	0,03	461
						Av=	0,34	

Table U3: Bentonite suspensions: 6% Bentonite; short square edge orifice

Time (s)	Diff Time	Mass in tank (kg)	Height(m)	Diff Height (m)	Flow rate (m^3/s)	Velocity	C_d	Re_2
4,15	0	14,250	0,089	0	-	0	-	
29,15	25	13,284	0,083	0,006	0,0000377	1,27	0,59	615
54,15	50	12,367	0,077	0,011	0,0000346	1,23	0,56	593
79,15	75	11,578	0,072	0,016	0,0000316	1,19	0,53	574
104,15	100	10,807	0,068	0,021	0,0000285	1,15	0,49	554
129,15	125	10,105	0,063	0,025	0,0000254	1,11	0,45	536
154,15	150	9,521	0,060	0,029	0,0000224	1,08	0,41	520
179,15	175	8,986	0,056	0,032	0,0000193	1,04	0,37	505
204,15	200	8,540	0,053	0,035	0,0000162	1,02	0,32	493
229,15	225	8,209	0,051	0,037	0,0000132	1,00	0,26	483
254,15	250	7,909	0,049	0,039	0,0000101	0,98	0,20	474
279,15	275	7,679	0,048	0,041	0,0000070	0,97	0,14	467
304,15	300	7,495	0,047	0,042	0,0000040	0,95	0,08	462
329,15	325	7,430	0,046	0,042	0,0000009	0,95	0,02	460
						Av =	0,34	

Table U4: Bentonite suspensions: 6% Bentonite; square bevel back cut edge orifice

Time (s)	Diff Time	Mass in tank (kg)	Height(m)	Diff Height (m)	Flow rate (m^3/s)	Velocity	C_d	Re_2
4,15	0	14,738	0,092	0	-	0	-	
29,15	25	13,770	0,086	0,006	0,0000381	1,29	0,58	626
54,15	50	12,864	0,080	0,011	0,0000353	1,25	0,56	605
79,15	75	12,013	0,075	0,017	0,0000325	1,21	0,53	584
104,15	100	11,216	0,070	0,022	0,0000296	1,17	0,50	565 1
129,15	125	10,535	0,066	0,026	0,0000268	1,13	0,47	547
154,15	150	9,872	0,062	0,030	0,0000240	1,10	0,43	530
179,15	175	9,312	0,058	0,033	0,0000212	1,06	0,40	514
204,15	200	8,834	0,055	0,036	0,0000184	1,04	0,35	501
229,15	225	8,390	0,052	0,039	0,0000156	1,01	0,31	488
254,15	250	8,042	0,050	0,041	0,0000128	0,99	0,26	478
279,15	275	7,772	0,049	0,043	0,0000100	0,97	0,20	470
304,15	300	7,573	0,047	0,044	0,0000072	0,96	0,15	464
329,15	325	7,475	0,047	0,045	0,0000044	0,95	0,09	461
354,15	350	7,378	0,046	0,045	0,0000015	0,95	0,03	458
						Av =	0,35	

Appendix V : 5.4% Bentonite discharge; (chamfer, quadrant, short square and square bevel back cut edge orifice)

Appendix V1–V4: 5.4% Bentonite discharge; (chamfer, quadrant, short square and square bevel back cut edge orifice)

Liquid: 5.4 % bentonite	Temp: 20 ℃
Orifice: Chamfer edge	
Area	0,00005024 m^2
Diamneter	0,008m
Tank area	0,16m
Dh	0,008m

Density	1033 **Kg / m** ^{3}
Gravitaional	9,81 **m** ^{2}**/s**
k	0,013
n	1
τ (yield stress)	2,827

Table V1: Bentonite suspensions: 5.4 % Bentonite; chamfer edge orifice

Time (s)	Diff Time	Mass in tank (kg)	Height(m)	Diff Height (m)	Flow rate (m^3/s)	Velocity	C_d	Re_2
8,32	0	33,702	0,211	0	-	0	-	
58,32	50	29,710	0,186	0,024	0,0000762	1,90	0,79	1089
108,32	100	26,046	0,163	0,047	0,0000703	1,78	0,78	1012
158,32	150	22,690	0,142	0,068	0,0000644	1,66	0,77	938
208,32	200	19,628	0,123	0,087	0,0000585	1,55	0,75	864
258,32	250	16,854	0,105	0,105	0,0000526	1,43	0,73	793
308,32	300	14,385	0,090	0,120	0,0000467	1,32	0,70	725
358,32	350	12,185	0,076	0,134	0,0000408	1,22	0,66	659
408,32	400	10,296	0,064	0,146	0,0000349	1,12	0,62	598
458,32	450	8,684	0,054	0,156	0,0000290	1,03	0,56	541
508,32	500	7,350	0,046	0,164	0,0000231	0,94	0,48	491
						Av=	0,68	

Table V2: Bentonite suspensions: 5.4% Bentonite; quadrant edge orifice

Time (s)	Diff Time	Mass in tank (kg)	Height(m)	Diff Height (m)	Flow rate (m^3 s)	Velocity	C_d	Re_2
6,65	0	34,920	0,218	0	-	0	-	
46,65	40	31,632	0,198	0,020	0,0000793	1,96	0,80	1251
86,65	80	28,550	0,178	0,039	0,0000745	1,87	0,79	1189
126,65	120	25,665	0,160	0,057	0,0000697	1,77	0,78	1127
166,65	160	22,985	0,144	0,074	0,0000649	1,67	0,77	1067
206,65	200	20,477	0,128	0,090	0,0000601	1,58	0,76	1007
246,65	240	18,167	0,114	0,104	0,0000553	1,49	0,74	948
286,65	280	16,099	0,101	0,117	0,0000505	1,40	0,72	893
326,65	320	14,126	0,088	0,129	0,0000457	1,31	0,69	836
366,65	360	12,412	0,078	0,140	0,0000409	1,23	0,66	784
406,65	400	10,853	0,068	0,150	0,0000362	1,15	0,62	733
446,65	440	9,499	0,059	0,158	0,0000314	1,07	0,58	686
486,65	480	8,296	0,052	0,166	0,0000266	1,00	0,52	641
526,65	520	7,292	0,046	0,172	0,0000218	0,94	0,46	601
566,65	560	6,470	0,040	0,177	0,0000170	0,89	0,38	566
						Av =	0,66	

Table V3: Bentonite suspensions: 5.4% Bentonite; short square edge orifice

Time (s)	Diff Time	Mass in tank (kg)	Height(m)	Diff Height (m)	Flow rate (m^3/s)	Velocity	C_d	Re_2
6,65	0	33,226	0,208	0	-	0	-	
46,65	40	30,425	0,190	0,017	0,0000696	1,93	0,72	1227
86,65	80	27,740	0,173	0,034	0,0000661	1,84	0,71	1172
126,65	120	25,180	0,157	0,050	0,0000626	1,75	0,71	1116
166,65	160	22,722	0,142	0,065	0,0000591	1,66	0,70	1061
206,65	200	20,419	0,128	0,080	0,0000556	1,58	0,70	1005
246,65	240	18,245	0,114	0,093	0,0000522	1,49	0,69	950
286,65	280	16,183	0,101	0,106	0,0000487	1,40	0,69	895
326,65	320	14,339	0,090	0,118	0,0000452	1,32	0,68	842
366,65	360	12,580	0,079	0,129	0,0000417	1,24	0,67	789,
406,65	400	11,021	0,069	0,138	0,0000382	1,16	0,65	738
446,65	440	9,606	0,060	0,147	0,0000347	1,08	0,64	689
486,65	480	8,379	0,052	0,155	0,0000312	1,01	0,61	644
526,65	520	7,340	0,046	0,161	0,0000278	0,94	0,58	603
566,65	560	6,467	0,040	0,167	0,0000243	0,89	0,54	566
						Av=	0,66	

Table V4: Bentonite suspensions: 5.4% Bentonite; square bevel back cut edge orifice

Time (s)	Diff Time	Mass in tank (kg)	Height(m)	Diff Height (m)	Flow rate (m^3/s)	Velocity	C_d	Re_2
6,65	0	34,077	0,213	0	-	0	-	
46,65	40	31,240	0,195	0,017	0,0000706	1,95	0,72	1244
86,65	80	28,543	0,178	0,034	0,0000671	1,87	0,71	1189
126,65	120	25,945	0,162	0,050	0,0000635	1,78	0,71	1133
166,65	160	23,458	0,147	0,066	0,0000599	1,69	0,70	1078
206,65	200	21,096	0,132	0,081	0,0000563	1,60	0,70	1022
246,65	240	18,872	0,118	0,095	0,0000528	1,52	0,69	967
286,65	280	16,817	0,105	0,107	0,0000492	1,43	0,68	912
326,65	320	14,937	0,093	0,119	0,0000456	1,35	0,67	860
366,65	360	13,177	0,082	0,130	0,0000421	1,27	0,66	808
406,65	400	11,605	0,073	0,1401	0,0000385	1,19	0,64	758
446,65	440	10,193	0,064	0,149	0,0000349	1,11	0,62	710
486,65	480	8,927	0,056	0,157	0,0000314	1,04	0,60	665
						Av =	0,68	

Appendix W : 3.6% Bentonite discharge; (chamfer, quadrant, short square and square bevel back cut edge orifice)

Appendix W1–W4: 3.6% Bentonite discharge; (chamfer, quadrant, short square and square bevel back cut edge orifice)

Liquid: 3. 6 % bentonite	Temp: 20 ℃
Orifice: Chamfer edge	
Area	0,00005024 m^2
Diameter	0,008m
Tank area	0,16m
Dh	0,008m

Density	1022 Kg / m^3
Gravitaional	9,81 m ^{2}/s
k	0,007
n	1
τ (yield stress)	0,186

Table W1: Bentonite suspensions: 3.6 % Bentonite; chamfer edge orifice

Time (s)	Diff Time	Mass in tank (kg)	Height(m)	Diff Height (m)	Flow rate (m^3/s)	Velocity	C_d	Re_2
8,32	0	34,193	0,214	0	-	0	-	
58,32	50	30,073	0,188	0,025	0,0000789	1,920348	0,82	2080,337
108,32	100	26,276	0,164	0,049	0,0000730	1,79503	0,81	1942,831
158,32	150	22,770	0,142	0,071	0,0000671	1,67	0,80	1806
208,32	200	19,569	0,122	0,091	0,0000611	1,54	0,79	1672
258,32	250	16,668	0,104	0,109	0,0000552	1,42	0,77	1541
308,32	300	14,078	0,088	0,125	0,0000492	1,31	0,75	1414
358,32	350	11,771	0,074	0,140	0,0000433	1,20	0,72	1291
408,32	400	9,743	0,061	0,152	0,0000373	1,09	0,68	1172
458,32	450	7,996	0,050	0,163	0,0000314	0,99	0,63	1059
508,32	500	6,580	0,041	0,172	0,0000255	0,89	0,56	959
						Av =	0,73	

Table W2: Bentonite suspensions: 3.6% Bentonite; quadrant edge orifice

Time (s)	Diff Time	Mass in tank (kg)	Height(m)	Diff Height (m)	Flow rate (m^3/s)	Velocity	C_d	Re_2
6,65	0	33,673	0,210	0	-	0	-	
46,65	40	30,338	0,190	0,020	0,0000803	1,92	0,83	2116
86,65	80	27,224	0,170	0,040	0,0000754	1,82	0,82	2005
126,65	120	24,313	0,152	0,058	0,0000705	1,72	0,81	1894
166,65	160	21,598	0,135	0,075	0,0000656	1,62	0,80	1786
206,65	200	19,057	0,119	0,091	0,0000607	1,52	0,79	1677
246,65	240	16,741	0,105	0,105	0,0000558	1,43	0,78	1572
286,65	280	14,616	0,091	0,119	0,0000509	1,33	0,76	1469
326,65	320	12,678	0,079	0,131	0,0000460	1,24	0,73	1368
366,65	360	10,920	0,068	0,142	0,0000411	1,15	0,71	1269
406,65	400	9,376	0,059	0,151	0,0000362	1,07	0,67	1176
446,65	440	8,027	0,050	0,160	0,0000313	0,99	0,63	1088
486,65	480	6,835	0,043	0,167	0,0000264	0,91	0,57	1004
						Av =	0,74	

Table W3: Bentonite suspensions: 3.6% Bentonite; short square edge orifice

Time (s)	Diff Time	Mass in tank (kg)	Height(m)	Diff Height (m)	Flow rate (m^3/s)	Velocity	C_d	Re_2
6,65	0	34,925	0,218	0	-	0	-	
46,65	40	32,230	0,201	0,01684642	0,0000670	1,988004	0,67	2181,73
86,65	80	29,627	0,185	0,033	0,0000643	1,90	0,67	2091
126,65	120	27,112	0,169	0,048	0,0000615	1,82	0,67	2001
166,65	160	24,696	0,154	0,063	0,0000588	1,74	0,67	1909
206,65	200	22,356	0,140	0,078	0,0000560	1,65	0,67	1817
246,65	240	20,174	0,126	0,092	0,0000533	1,57	0,67	1726
286,65	280	18,107	0,113	0,105	0,0000505	1,49	0,68	1635
326,65	320	16,145	0,101	0,117	0,0000478	1,40	0,68	1544
366,65	360	14,294	0,089	0,128	0,0000450	1,32	0,68	1452
406,65	400	12,562	0,079	0,139	0,0000423	1,24	0,68	1362
446,65	440	10,920	0,068	0,150	0,0000395	1,15	0,68	1269
486,65	480	9,434	0,059	0,159	0,0000368	1,07	0,68	1180
						Av =	0,68	

Table W4: Bentonite suspensions: 3.6% Bentonite; square bevel back cut edge orifice

Time (s)	Diff Time	Mass in tank (kg)	Height(m)	Diff Height (m)	Flow rate (m^3/s)	Velocity	C_d	Re_2
6,65	0	33,850	0,212	0	-	0	-	
46,65	40	31,161	0,195	0,016	0,0000661	1,95	0,67	2145
86,65	80	28,591	0,179	0,032	0,0000633	1,87	0,67	2054
126,65	120	26,135	0,163	0,048	0,0000605	1,79	0,67	1964
166,65	160	23,742	0,148	0,063	0,0000578	1,70	0,67	1872
206,65	200	21,488	0,134	0,077	0,0000550	1,62	0,67	1781
246,65	240	19,345	0,121	0,090	0,0000522	1,54	0,67	1690
286,65	280	17,295	0,108	0,103	0,0000494	1,45	0,68	1598
326,65	320	15,353	0,096	0,115	0,0000467	1,37	0,68	1505
366,65	360	13,543	0,085	0,126	0,0000439	1,28	0,68	1414
406,65	400	11,864	0,074	0,137	0,0000411	1,20	0,68	1323
446,65	440	10,312	0,064	0,147	0,0000384	1,12	0,68	1234
486,65	480	8,943	0,056	0,155	0,0000356	1,04	0,68	1149
						Av =	0,68	

Appendix X: Editing certificate

Ricky Woods Academic Editing Services

Editing Certificate

Ricky Woods Academic Editing Services
Cell: +27 (0)83 3126310
Email: rickywoods604@gmail.com

To Whom It May Concern

Cape Peninsula University of Technology

Editing of Master's Dissertation

I, Marietjie Alfreda Woods, hereby certify that I have completed the editing and correction of the dissertation: **The effect of orifice edge geometry on the discharge of non-Newtonian liquids from a tank** by **Ninelle Samia Mampouya**. This was submitted in fulfilment of the requirements of the degree **Master of Engineering** at the **Cape Peninsula University of Technology.** I believe that the dissertation meets with the grammatical and linguistic requirements for a document of this nature. The following aspects were covered in the process of the editing:

- A full language edit, including grammar, spelling, concord and clumsy expression;
- Reference formatting was checked, according to Harvard, as stipulated by CPUT and used by the student;
- Heading styles and captions were standardised;
- Formatting and pagination was checked;
- Table of Contents and Lists of Figures and Tables were checked.

Name of Editor: Marietjie Alfreda (Ricky) Woods

Qualifications: BA (Hons) (Wits); Copy-editing and Proofreading (UCT); Editing Principles and Practice (UP); Accredited Text Editor (English) (PEG)

10 January 2025

Professional EDITORS Guild 30+ Est 1993
Promoting excellence in editing

Ricky Woods
Full Member
Accredited Text Editor (English)

Membership number: WOO003
Membership year: March 2024 to February 2025

+27 83 312 6310
rickywoods604@gmail.com
https://rickywoods604.wixsite.com/website

www.editors.org.za